C.1

RESPONSE OF PILE FOUNDATION UNDER SIMULATED EARTHQUAKE LOADING

By

Huaren Dou

B. Eng. Dalian Institute of Technology, China, 1983

M. Eng. Dalian Institute of Technology, China, 1986

A THESIS SUBMITTED IN PARTIAL FULFILLMENT OF

THE REQUIREMENTS FOR THE DEGREE OF

MASTER OF APPLIED SCIENCE

in

THE FACULTY OF GRADUATE STUDIES

CIVIL ENGINEERING

We accept this thesis as conforming

to the required standard

THE UNIVERSITY OF BRITISH COLUMBIA

September 1991

In presenting this thesis in partial fulfilment of the requirements for an advanced degree at the University of British Columbia, I agree that the Library shall make it freely available for reference and study. I further agree that permission for extensive copying of this thesis for scholarly purposes may be granted by the head of my department or by his or her representatives. It is understood that copying or publication of this thesis for financial gain shall not be allowed without my written permission.

Department of Civil Engineering

The University of British Columbia
Vancouver, Canada

Date Sept. 10, 1991

Abstract

An extensive series of small scale model tests on single piles embedded in sand were carried out using the hydraulic gradient similitude (HGS) technique simulating earthquake loading. The dynamic loading was applied using the shake table at the University of British Columbia. The HGS method employs a high hydraulic gradient across the sand sample to increase the effective stresses in the model simulating full scale stress conditions in the field. Since the soil behaviour is stress level dependent, the HGS technique is considered to provide a realistic simulation of the full scale pile foundation behaviour.

Free vibration tests were performed to study the natural frequency response of soil-pile system, and the behaviour of the system stiffness and damping at different soil stress levels. The boundary effects are evaluated and discussed. The dynamic behaviour of pile response and soil-pile interaction were investigated over a range of shaking intensities at various exciting frequencies. The dynamic p-y curves were derived from the test data and found to be highly nonlinear and hysteretic at shallow depth. Approximate linear elastic p-y response occurs at greater depth. The test results show an insignificant and negligible influence of loading cycles for dense sand. The backbone p-y curves for sand recommended by the American Petroleum Institute (API) were computed and compared with the experimental data, and were seen to be in poor agreement. The near field hysteretic damping was estimated from the p-y hysteretic loops.

The tests create a data base against which the theoretical and numerical approaches can be assessed. Predictions of the response of pile and superstructure to dynamic loading were made using different procedures of constructing p-y curves. The analyses show, generally, a reasonable agreement with test data.

Table of Contents

List of Tables

List of Figures

Acknowledgement

The author wishes to express his gratitude to his research supervisor, Professor Peter M. Byrne, for his support, encouragement, patience, and valuable discussions throughout this research. The author would also like to thank Professors R.G. Campanella and Y.P. Vaid for their help with the equipment, and Professor W.D. Liam Finn for reviewing the manuscript and making helpful suggestions.

The assistance of the Civil Engineering Workshop with test equipment is gratefully acknowledged. The helpful discussions with his colleagues, especially Li Yan and Ralph Kuerbis are also greatly appreciated.

The financial support provided by the Natural Science and Engineering Research Council of Canada, which made this study possible, is gratefully acknowledged.

Finally, the author wishes to thank his wife Hong and his parents for their love, support, and understanding over the course of this research. This thesis is dedicated to them.

Chapter 1

Introduction

1.1 Introduction

Piles have been used for many years, but in the last two decades, have been the subject of a considerable interest and research. In recent years, the concentration of studies has focused on the dynamic response of pile foundations to seismic and earthquake loading because the pile foundations are more extensively employed for the support of structures, such as onshore and offshore engineering, nuclear powerplants. In addition, pile foundations have suffered severe failure and damage (Fukuka, 1966; Margason, 1975; Sugimura, 1981; Mizuno, 1987) during earthquakes in the past decades. Analytical and numerical methods for the analysis and design of piles under dynamic loading have developed very rapidly in the past twenty years. These methods provided a much sounder theoretical basis for pile design than the equivalent cantilever concept and other traditional empirical approaches which dominated this field for decades. However, because of the scarcity of experimental data on well documented pile response in the field under various dynamic loading conditions, particularly, under real earthquake occurrences, the actual behaviour and performance of pile foundation under seismic loading is still poorly understood. Thus model tests have frequently been performed to study the seismic response of pile foundations, and these tests provide a data base against which analytical approaches may be verified.

The shake table has been so far the most commonly used equipment for examining

earthquake effects on soil and soil-structure systems. However, its application to soil-structure interaction, especially to pile foundations, is severely limited essentially due to the small size of model which results in relatively low stress level in the soil under the condition of conventional 1 g gravitational field. Since the stress-strain response of soil is highly stress level dependent, the behaviour of the prototype will be quite different from that of model. Thus small-scale model tests in a normal gravitational acceleration field often fail to reveal some important phenomena that may exist at the prototype stress level. As a result, that type of modelling test is not appropriate.

It is desirable to carry out a small-scale model test at field stress level conditions so as to overcome the stress similitude problem stated above. At present, one method of modelling field behaviour is the use of dynamic centrifuge testing technique, which can induce stresses and strains in the model in the same order of magnitude as those typically encountered in the field. In centrifuge modelling, a small model of 1/n scale of the assumed prototype is tested under an "ng" acceleration field generated by centripetal acceleration. This escalated gravitational field produces the same self-weight stresses as those that exist in the full scale structure at corresponding points. The simulation of prototype behaviour is assumed based upon modelling laws (Roscoe, 1968; Scott, 1978; Schofield, 1981). Although the principles employed in centrifuge technique are simple, its application to simulating the prototype behaviour involves certain difficulties in practice. Quite often, a complete similitude relation and various prototype soil conditions can not be fully satisfied and simulated by the centripetal acceleration alone (Whitman and Arulanandan, 1985; Cheney, 1985; Tan and Scott, 1985). This is also an expensive approach, requiring costly equipment and well trained personnel to operate the system. In addition, the application of seismic loading during centrifugal flight is not that easy, involving specially built facilities (Whitman, 1984). Therefore, the existing body of test data available on dynamic response of piles needs to be expanded in order to validate

numerical approaches.

Instead of the centrifuge technique, an inexpensive alternative method for performing model tests on conventional shake table but at field (full scale) stress level is presented in this thesis. This method, called the Hydraulic Gradient Similitude (HGS) method (Zelikson, 1969, 1978, 1988; Yan and Byrne, 1989; Yan, 1990; Yan et al. 1991), employs a high hydraulic gradient which causes a seepage force within the granular soil to create a high body force. This body force results in a high stress level simulating the field conditions. The HGS modelling technique are herein used to study the response of pile and soil-pile interaction under simulated earthquake loading. The testing principles and its applications to seismic pile response will be discussed in detail later.

1.2 Scope of Study

The interest in soil-structure interaction is rapidly growing in the field of earthquake engineering. With this growing interest comes an increased need for adequate physical data to substantiate newly developed analytical theories. It is shown in this thesis that the hydraulic gradient modelling technique can be used to provide a well controlled experimental environment in which such physical data can be generated.

Hydraulic gradient model tests were carried out using single piles embedded in sand deposit and subjected to simulated earthquake (sinusoidal) loading. The study mainly consists of the series of free vibration tests and the series of forced vibration tests on piles. Data were obtained for different shaking intensities and HGS scale factors and then compared with the predictions of pseudo dynamic and dynamic analyses using the program LATPILE and theoretical methods.

An extensive series of HGS model tests were carried out using shaking table at the University of British Columbia. Three series of free vibration tests were performed to

study the natural frequency response of soil-pile system, and behaviour of the stiffness and damping of the system. The dynamic modelling laws were also verified. Three series of forced vibration tests were also carried out on single piles embedded in sand, subjected to moderate to strong shaking intensities under different HGS scale factors to study the behaviour of superstructure response, pile response and the soil-pile interactions. The soil-pile interaction p-y curves were computed for a variety of tests over several cycles of shaking.

1.3 Organization of Thesis

The thesis describes model tests carried out to simulate soil-pile response to earthquake loading. The hydraulic gradient method was used in the model to increase the effective body forces and the shake table was used to simulate earthquake loading. The thesis is comprised of 6 chapters as follow:

Chapter 1 gives a background introduction and scope of this research work.

A review of dynamic pile response to lateral loading is presented in Chapter 2. The experimental studies and numerical analysis are discussed .

In Chapter 3, the hydraulic gradient similitude principles, the testing procedures and experimental programs are described. The boundary effects are discussed.

The test results are presented in Chapter 4. The experiments include the series of free vibrations and the series of forced vibrations in which the experimental p-y curves are compared with those recommended by the API code (1987).

Chapter 5 presents theoretical and numerical predictions of the observed superstructure and pile responses. Nonlinear numerical analysis with p-y curves determined by the API procedure and linear elastic model are carried out and the results compared to the experimental data.

Finally, in Chapter 6, summary and general conclusions are made, and suggestions are given for future research.

Chapter 2

Review of Pile Response to Dynamic Lateral Loading

In this Chapter, the current studies of single pile response subjected to dynamic lateral loading are reviewed. The analytical approaches, experimental research as well as the field observations are discussed. The review is primarily on the study of pile response to lateral dynamic loading in sand.

2.1 Single Pile Response to Cyclic Lateral Loading – Experiments

2.1.1 Full-Scale Testing

Most of the field pile loading tests were carried out using a hydraulic actuator and reaction piles to apply the cyclic lateral loading at the pile head. In those tests, the amplitudes of lateral pile motion were sufficient to induce significant non-linearity in the soil adjacent to the pile (the near field). The full scale field tests have been carried out to study the dynamic nature of pile foundation response by a number of researchers (Matlock, 1970; Reese et al., 1974; Reese, 1979; Scott et al., 1982; Blaney and O'Neill, 1986; Han and Novak, 1988). These studies have shown that non-linear soil-pile interaction significantly influences pile head response. Particularly, the reduction in measured natural frequency and increase in system damping with increasing dynamic load level have been observed, indicating a strain softening system whose stiffness and hysteretic damping characteristics are load level dependent.

Near field soil response in saturated medium dense to dense sands has been described

by Ting (1987) in an analysis of full scale shaker tests. Ting's analysis indicates significant soil non-linearity occurs in the near field p-y response at shallow depths as a result of strain softening, soil-pile interface gaping and pore pressure build-up which caused transient liquefaction of the sand. The latter was substantiated by the presence of sand boils around the pile. At greater depths, near linear soil-pile interaction p-y response was observed.

Cox et al.(1974) reported their lateral monotonic and cyclic loading tests on single instrumented piles embedded in sand, on the basis of which the early p-y curve construction method was proposed by Reese et al. (1974). The single tests under displacement controlled two-way cyclic loading was conducted by Brown et al.(1987) for piles embedded about 10 pile diameter deep in sand overlaying a stiff clay deposit. This study showed that, unlike in the case of stiff clay, piles embedded in sand were not significantly affected by the number of loading cycles.

The comprehensive full scale tests are still needed to allow for a systematic fundamental study. However, Running this type of experiments are expensive and time consuming. Therefore, model tests on pile foundations are often carried out to simulate the prototype conditions for generation of the experimental data base.

2.1.2 Model Testing

In the past, most model tests were performed under normal gravitational field condition. Such tests were not effective in predicting the full scale pile response because of lack of similitude in soil stress level, since the soil stress-strain behaviour is highly stress level dependent. Recently, centrifugal modelling and hydraulic gradient modelling techniques have been applied to study the dynamic behaviour of pile foundations under field stress condition so as to avoid the problems encountered under 1 g gravity condition.

A number of researchers have carried out model pile dynamic tests using cyclic lateral

loading at the pile head. The behaviour of soil-pile interaction non-linearity has been studied in these modelling tests (Scott, 1979; Scott et al. 1982; Barton, 1982; Prevost and Abodel-Ghaffar, 1982; Yan, 1990). These studies, similar to full scale experiments, have demonstrated that non-linear soil-pile interaction considerably affect pile head response. Namely, the measured natural frequency decreases and the system damping increases respectively as dynamic load magnitude increases. This implies that system stiffness and hysteretic damping are load level dependent and the system suffers a strain softening.

Barton's centrifuge tests (1982), where the full scale pile tests at Mustang Island (Cox et al. 1974) were simulated, showed that during the initial half cycle of load, sand near the head of the pile undergoes shear and rupture as the pile pushes into it. Behind the pile, the soil cannot sustain tensile stresses and so the pile breaks away leaving a cavity which can stand for short periods of time due to the transient suction created in the sand. On reversal of the loading direction, with free water present, the previously ruptured material now becomes liquefied and flows into the cavity around the pile. The fluidized sand later becomes compacted as the pile moves across in the reversed direction. With subsequent cycles more material flows down around the pile and becomes densified at some depth below the surface. The result is that the lateral response becomes stiffer with number of cycles until a steady state is reached. Reese et al. (1974) full scale pile loading tests also showed the stabilization of pile head deflection after a number of cycles of loading. The combined processes of soil-water flow and densification result in the pile being pushed in the direction corresponding to the initial direction of loading. After the load is removed, the pile remains in a distinctly distorted shape and residual bending moments are induced. It is noted that Barton's tests (1982) were carried out in dense saturated sand so that the sand response would be expected to be dilative, allowing the sand response to stabilize after a number of loading cycles.

The soil resistance-deflection response for cyclic lateral loading of piles behaves usually

with the following characteristics. At soil surface to around 1 pile diameter depth, there is an area of rupture and erosion with a no tension cavity. Below this depth is a region of plastic yielding with a soil-pile interface gaping development. At greater depths the soil response is nearly linear elastic due to a relatively small lateral pile displacement. These behaviours are confirmed by the present studies (Chapter 4)

2.2 Field Pile Response During Earthquake Loading – Observations

Pile supported structures have suffered severe damage during past major earthquakes such as the Niigata and Alaska earthquakes of 1964, the San Francisco earthquake of 1906 (Kagawa,1980), the Mexico City earthquake of 1985 and the Loma Prieta earthquake of 1989. A number of pile foundations for bridge structures, for instance, were damaged during these earthquakes. Liquefaction was the major cause of this damage, which resulted in failure and slides of the foundation soils that caused intolerably large displacements of pile foundations. The buckling failure of steel pipe piles supporting the piers of the Showa River Bridge during the Niigata earthquake was reportedly due to the resonance of the bridge as a result of soil-pile-structure interaction. Under pile resonant condition, large lateral pile displacements occurred which led the simple supported spans to fall off the piers of the Showa River Bridge. The pile damage during earthquakes up to 1983 has been reported by a couple of researchers (Kishida, 1966; Ross et al., 1969; Margason, 1975; Sugimura, 1981 and Mizuno, 1987). Unfortunately, there is no instrumented pile response to strong earthquake loading recorded. From the available pile damage reports, it is observed that the damage to piles may result from a few causes such as vibration effects, liquefaction, and embankment movements.

There have been several case histories published in recent years documenting the field response of pile foundations to low level earthquake shaking, in which the free field

surface accelerations were less than around 0.1 g (Sugimura, 1977; Esashi and Yoshida, 1980; Hamada and Ishida, 1980; Oda et al., 1980; Ohira et al., 1984 and Abe et al., 1984). The available instrumental data cover soil conditions over a broad range. Some parameters have been measured at various depths such as pile accelerations, pile bending and axial strains, free field accelerations, and shear wave velocity distributions. Pile response during earthquake shaking occurs over a broad range of frequencies with peak responses corresponding to the natural frequencies of the pile-superstructure system and of the free field. This reflects the combined influence of structure inertia forces and free field ground motions on pile bending.

2.3 Single Pile Response to Dynamic Loading – Analysis

A number of analytical and numerical approaches to the analysis of pile dynamic behaviour have been developed. These approaches provided a much sounder theoretical basis for pile design than the equivalent cantilever concept or other purely empirical methods which dominated the field for decades. The response of single piles to earthquake loading has been modelled theoretically by the following approaches: (a) elastic continuum models applicable to low level excitation, (b) finite element methods, and (c) non-linear lumped mass models with empirically or analytically derived Winkler type springs and viscous dashpots.

Elastic continuum models was first formulated by Tajimi (1966) for solution of the horizontal response of an end bearing pile in a homogeneous layer. Since 1970's, a significant advance has been made in solving the problem of an elastic beam vibrating in a homogeneous or non-homogeneous elastic isotropic continuum subjected to dynamic pile head loadings by Novak, Nogami and their co-workers (Novak, 1974; Nogami and Novak, 1977; Novak and Nogami, 1977; Novak and Aboul-Ella, 1978; Novak et al., 1978;

Poulos and Davis, 1980; Novak and Sheta, 1980 and 1982). In 1974, Novak developed a very simple approach based on plane strain soil reactions, which can be interpreted as dynamic Winkler medium or a plain strain, complex compliance spring attached directly to the pile. This spring is similar to the standard spring but is frequency dependent and complex, i.e. it has a stiffness part as well as the damping part. This solution identified dimensionless parameters of the problem, produced a number of design charts and tables for dynamic stiffness and damping of piles, and indicated the effect of the pile static load on the horizontal pile characteristics. Material damping was later included in closed form expressions for the soil reactions in Novak et al. (1978). A more rigorous solution, similar to that of Tajimi (1966), was formulated for the horizontal response by Novak and Nogami (1977). This approximate solution offered a basic insight into the behaviour of the soil-pile system.

The principal problem in using these approaches is the selection of appropriate equivalent elastic moduli compatible with strains occurring around the pile during shaking. Thus, much of the attention is focused on the pile complex dynamic stiffnesses, i.e. impedance functions because they have a strong influence on the response of pile supported buildings and structures. The impedance functions are defined as amplitudes of harmonic forces (or moments) that have to be applied to the pile head in order to generate a harmonic motion with a unit amplitude in the specified direction. These are often used as foundation spring and dashpot parameters in an uncoupled analysis of a superstructure subjected to the free field surface motions induced by the earthquake. Novak and Nogami's (1977) theoretical solutions indicated a few interesting features of the pile impedances: Pile dynamic stiffness varies little with frequency, except for very heavy piles or very weak soils for which it diminishes with frequency in a parabolic manner; for end-bearing piles vibrating below the fundamental frequency of the soil layer, the geometric damping is absent because no progressive waves are generated in an elastic medium, just

as with shallow foundations, leaving soil and pile material damping as the only sources of energy dissipation. Apart from this low frequency region, a fully embedded slender pile, not supporting any additional mass, is usually overdamped and consequently does not exhibit any marked resonance peak in dynamic tests.

More rigorous solutions were obtained by a few researchers. For the horizontal response of infinitely long pile, Koberi et al.(1977) formulated a solution in the form of infinite series of multiple integral. More recent analyses based on the solution of the governing equations of a three dimensional continuum were made by Sen et al. (1985) and Pak and Jennings (1987). All vibration modes were investigated by Rajapakse and Shah (1987a, 1987b and 1989). The later authors evaluated the accuracy of some of the existing solutions and concluded that continuum models based on harmonic line loads may not be accurate enough and generated an extensive set of charts for impedances of floating piles.

The finite element method is an efficient numerical technique in solving the problem of soil-pile system. A significant improvement in this model was formulated by Roesset and his co-workers (Blaney et al., 1976; Roesset and Angelides, 1979) who placed the consistent frequency dependent boundary, derived by Kausel et al. (1975), directly to the pile or outside the cylindrical finite element zone around the pile. This approach was then used by Krishnan et al. (1983) and by Gazetas (1984) in their extensive parametric studies. In his dynamic elastic finite element analyses, Gazetas (1984) has studied the influence of kinematic interaction on differences in pile acceleration at the ground surface relative to that in the free field, and concludes that the effects of kinematic interaction are relatively minor for excitation frequencies up to about 1.5 times that fundamental frequency of the free field. Similar conclusions have been made by Waas and Hartman (1984). Provided the free field surface motions are dominated by frequencies in this range, the neglect of kinematic interaction in an uncoupled superstructure analysis appears to

be valid. The neglect of kinematic interaction generally results in an overestimate of dynamic pile cap motions transmitted to the superstructure. Using plane strain soil reactions with the appropriate low frequency corrections, Novak (1974) derived pile head impedance functions for a homogeneous elastic medium. Nogami and Novak (1977) derived similar pile head impedances using the plane displacement soil reactions. The latter was compared with three dimensional, elastic finite element solutions for the case of pile head loading (Kuhlemeyer, 1979; Blaney et al., 1976). The results were found to be similar, suggesting that plain strain models of soil response can provide reasonably accurate predictions of pile head impedance. It is apparent that the use of plane strain soil reactions allows specification of non-uniform moduli along the pile since soil response at one depth depends only on soil properties at that depth. This technique has been adopted to formulate a simple and very versatile solution, particularly well suited for high frequencies, by Novak and Aboul-Ella (1978). They extended the plane strain approach to include layered media and incorporated it in an efficient computer program PILAY to compute pile head impedance. This program is extensively used in the elastic analysis of pile response to low amplitude vibration. Roesset et al. (1986) also found the plane strain approach to work very well for high frequencies. For very low frequencies, an adjustment to the plane strain soil reaction is made for the vertical and horizontal directions as discussed in Novak and El Sharnouby (1983) and implemented in the code PILAY. The plane strain approach works well for high frequencies because, in a layer, elastic waves tend to propagate more and more horizontally as the frequency increases, like in a wave guide.

Work of Novak and Nogami (1977) has been extended by Kagawa and Kraft (1980a) to the case in which pile is excited by seismic base motion. This work examined whether neglect of the free field ground motions in solving the dynamic equations of motion of the pile has a significant effect on the computed dynamic soil reactions. Homogeneous, elastic

soil response was assumed and soil reactions around the perimeter of the pile determined by solving simultaneously Navier's equations of motion for a viscoelastic medium and the dynamic equations of beam flexure. The solution included soil inertia terms involving the input base accelerations, which have been neglected in the work of Novak and Nogami.

Kagawa and Kraft simplified the problem by making an assumption that soil displacements due to the lateral pile motion occur in a horizontal plane. The plane displacement solutions were found to be in good agreement with three dimensional finite element solutions where vertical displacements are considered (Kagawa and Kraft, 1980b). The plane displacement solution shows that the elastic soil stiffness at a point has some dependence on pile curvature since gradients of lateral displacement in the vertical direction are considered. This has been expressed by Kagawa and Kraft in terms of a dependence on the relative soil-pile stiffness, K_r, defined as $K_r = EI/E_s r_0^4$ where EI is the flexural rigidity of pile, E_s is the equivalent elastic Young's modulus of the soil and r_0 is the pile radius. A similar three dimensional effect has been examined by Poulos (1980) for the case of static lateral pile head loading.

The results of Kagawa and Kraft indicate that the method of pile loading can have an effect on the lateral soil response and provide a theoretical basis for estimating the importance of relative soil-pile stiffness, ratio of pile length to diameter and excitation frequency on dynamic elastic compliance. It is noted that the lateral soil compliances can be assumed to remain constant during shaking using equivalent elastic soil parameters or could be varied for each time step during a step by step integration of equations of motion of the pile. The results of Kagawa and Kraft also postulate that the elastic dynamic stiffness is reasonably independent of frequency in the low frequency range. They note that during an earthquake, the frequency of most interest for onshore and offshore pile supported structures is about 0.1 to 2 Hz, which corresponds to the likely range of structural fundamental frequencies, although typical earthquake records include

frequency components up to about 25 Hz. Therefore, we are most concerned with soil-pile interaction during low frequency shaking.

The theories discussed so far are essentially linear and thus quite adequate for small displacements. At large displacements, piles behave in a nonlinear manner because of soil nonlinearity at high strain, pile separation (gapping), slippage and friction. To incorporate these factors into a continuum theory is extremely difficult and therefore, lumped mass models are most often used when nonlinear analysis is required. Such models (Penzien, 1970; Arnold et al., 1977; Matlock et al., 1978; Bea et al., 1984; Nogami and Chen, 1987) feature nonlinear springs and nonlinear dampers along the pile, gaps and coulomb friction blocks. The stiffness of these springs represents the combined stiffness of the strain softened, near field soil and the exterior free field soil whose properties are governed by the intensity of the earthquake ground motion. The soil stiffness for a particular depth is defined by a nonlinear soil resistance versus lateral pile deflection relationships known as p-y curve recommended in the literature. Matlock et al.(1978) formulated a model for analysis of dynamic pile response where it is possible to simulate the load-unload response of the soil to the lateral pile motions as shaking proceeds. This was coded in the computer program SPASM to model single pile response to earthquake loading, in which the change in soil stiffness during loading and unloading is simulated by computing the tangent soil stiffness along the input p-y curve compatible with the computed lateral deflection. The gaps in the soil-pile interface are also simulated in the SPASM. It is noted that hysteretic damping in the near field soil is automatically accounted for by using a tangent soil stiffness approach.

The p-y curves can be specified in mathematical formation for clay as well as sand in both static and cyclic loading conditions (American Petroleum Institute, 1978; Gazioglu and O'Neill, 1984; Murchison and O'Neill, 1984). These recommendations come from the experimental results of full scale pile head loading. The cyclic p-y curves derived

from simulated wave loading on piles represent an envelope of soil reaction-deflection behaviour after shaking but are often used as backbone p-y curves in earthquake analysis of single piles. The assumption in their use implies that the pile response is dominated by the effects of loading at the pile head and that the lateral soil response is reasonably independent of frequency in the low frequency range. Nogami and Chen (1987) suggested a procedure where the input low frequency p-y curves, derived from full scale experimental measurements or non-linear finite element analysis, can be adjusted to account for higher frequency loading. The procedure involves decomposing the input p-y curves into their static near field and free field components, with the free field properties derived from an appropriate free field response analysis.

The most commonly used is the recommendations of the American Petroleum Institute for constructing p-y curves among the empirically based p-y curves suggested in the literature. The API recommendations of p-y relationships for sand is an adoption of the procedures proposed by Murchison and O'Neill (1984), where the lateral soil resistance versus pile deflection relationships are non-linear and may be approximated at any specific depth z by the following single analytical expression:

$$p = \eta A p_u tanh[(\frac{n_h z}{\eta A p_u})y] \tag{2.1}$$

where n_h is initial modulus of subgrade reaction determined from Figure 2.1, η is a factor accounting for pile shape effect, A refers to a factor to account for cyclic or static loading condition evaluated by:

$A = 0.9$ (for cyclic loading)

$A = (3.0 - 0.8\frac{z}{D}) \geq 0.9$ (for static loading)

and p_u is ultimate lateral bearing capacity at depth z, given by the smallest value of following equations (Bogard and Matlock, 1980):

$$p_{us} = (C_1 z + C_2 D)\gamma' z \tag{2.2}$$

$$p_{ud} = C_3 D \gamma' z \tag{2.3}$$

in which C_1, C_2 and C_3 are coefficients determined from figure 2.2 as function of internal friction angle of sand, D refers to average pile diameter from surface to depth and γ' is effective unit weight of soil.

The validity of the API procedure for earthquake analysis of single piles has not been verified. Kagawa and Kraft (1980a, 1981) also proposed that backbone p-y curves be constructed using more fundamental soil parameters with a mathematical form based on the hyperbolic or Ramberg-Osgood equation. These equations are defined from (a) the initial slope of the p-y curve using the measured low strain stiffness properties of the soil and results from elastic analysis of dynamic pile response, and (b) the ultimate lateral resistance of the soil to a translating pile derived from the theory of plasticity and based on the shear strength properties of the soil. Unload-reload p-y response is generally modelled assuming Masing behaviour. Similar approaches could be applied based on in-situ determination of soil properties from pressuremeter tests (Atukorala et al., 1986).

2.4 Summary

The preceding review has summarized a number of computational approaches used to analyze the response of pile foundations to dynamic lateral loading. The behaviour of soil-pile interaction during dynamic loading were also discussed. There are also instrumental records available which illustrate pile foundation response to low level earthquake excitation. The data from instrumented pile foundations are not available for strong

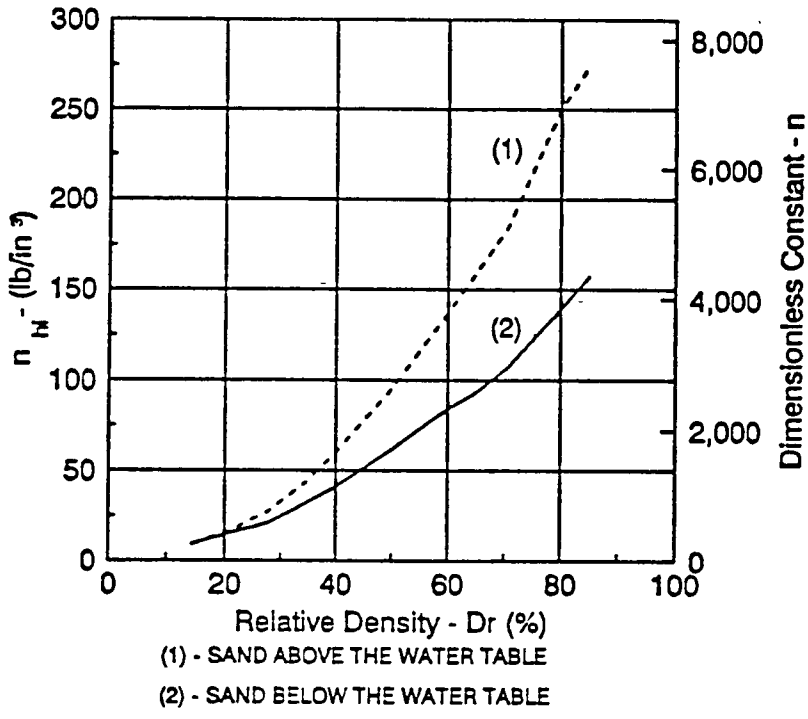

Figure 2.1: n_h vs. relative density (after Murchison and O'Neill, 1984)

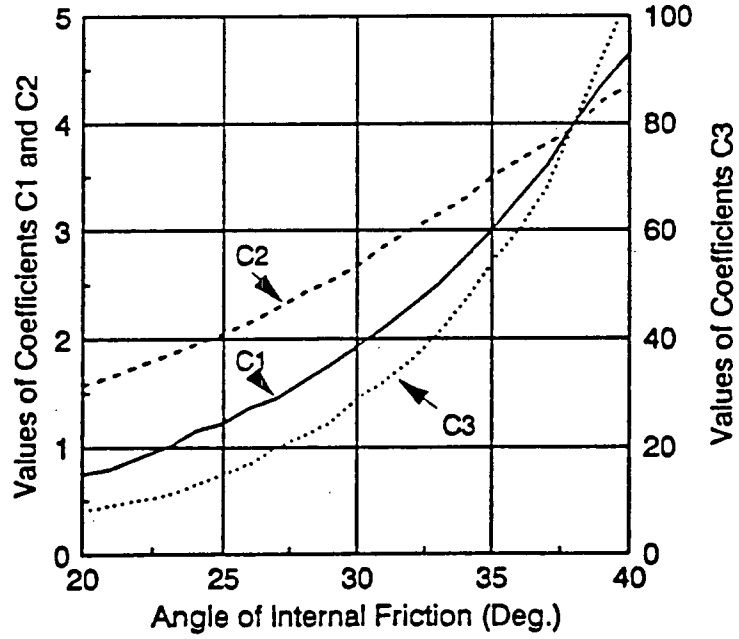

Figure 2.2: Coefficients for p_u (after Murchison and O'Neill, 1984)

earthquakes so that it has not yet been possible to examine those analytical procedures which propose to account for soil nonlinearity.

To enrich the existing data base, the hydraulic gradient similitude tests were carried out using single piles embedded in dense sand and subjected to simulated earthquake loading. The experiments were performed under the condition in which in-situ soil stress is simulated. The analytical method can then be evaluated by comparison with the experimental data. The test procedures are described in Chapter 3. The experimental results are presented in Chapter 4.

Chapter 3

Test Procedures and Program

This chapter describes experimental procedures used to perform model pile testing on Hydraulic Gradient Similitude (HGS) Shake Table at the University of British Columbia. The testing principles and modelling laws of hydraulic gradient similitude method are stated. The testing principles of this type was first introduced by Zelikson(1969). It was applied to the model tests of anchor and certain pile problems (Zelikson, 1978 and 1988). The hydraulic gradient model tests were compared with centrifuge testing results in relevant aspects of application (Zelikson, et al. 1982; Zelikson and Leguay, 1986; Yan and Byrne, 1989; Yan, 1990; Yan et al. 1991) and similar results were observed.

3.1 The Principles of H.G.S. Modelling

Small scaled models of large objects are used in many disciplines of engineering and science to study physical phenomena. In geotechnical engineering, model tests are often employed to investigate the complex nature of soil response and soil-structure interaction under a controlled condition. Scaled models of the geotechnical structures under normal 1 g gravity, however, seriously lack similitude because the stress levels in the model do not match those in the full scale prototype. One may obtain prototype stress levels in the model by placing the model in an increased stress field. Similar to the centrifuge modelling technique, the HGS method is just another way of increasing soil stresses in the model. The only difference is that the body force of the model soil is effectively increased by the seepage force through the porous material rather than by the centripetal

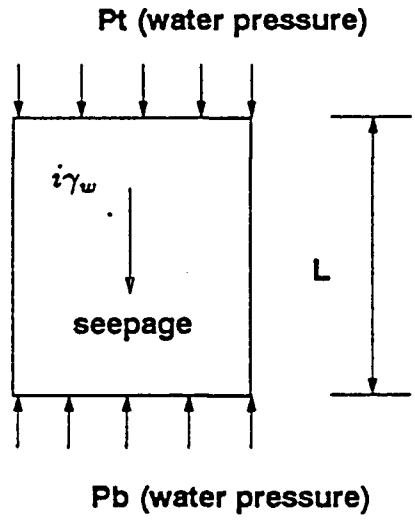

Figure 3.1: A stress increased soil element in the HGS tests

acceleration acting on the centrifuge bucket. This has the advantage that the models with escalated stress field can be mounted on the usual shake table and readily subjected to prescribed input excitation, unlike seismic centrifuge testing in which the seismic input has to be supplied within the high stress environment during the centrifugal flight.

For a model scale-reduced by a factor of 1/n of the prototype structure subjected to a controlled downward hydraulic gradient throughout the model, as shown in Figure 3.1, seepage force increases the unit volume body force of a soil element by an amount of $i\gamma_w$. This is equivalent to an increase of the unit weight of material by $i\gamma_w$. Thus the effective unit weight, γ_m, of the model soil is:

$$\gamma_m = i\gamma_w + \gamma' \tag{3.1}$$

Where i is the applied downward hydraulic gradient, γ_w is the unit weight of water if water is used in the test, and γ' is the submerged unit weight of soil. Hence, the vertical

effective stress in the model soil is increased at a depth, z, below the surface and is given as:

$$\sigma_v^{'} = \gamma_m \cdot z \tag{3.2}$$

and the hydraulic gradient similitude scale factor, N, is defined as:

$$N = \frac{\gamma_m}{\gamma_p} = \frac{i\gamma_w + \gamma^{'}}{\gamma_p} \tag{3.3}$$

in which γ_p is the effective unit weight of the soil in the prototype, which could be either total or submerged unit weight depending upon the ground water conditions in the prototype soil. Therefore, when the 1/n scaled model test is performed under a hydraulic gradient scale factor N=n, the stresses caused by the self-weight of soils at corresponding points of model and prototype will be the same, as shown below:

$$\begin{aligned} (\sigma_v)_m &= \gamma_m z_m \\ &= (N\gamma_p)(\frac{z_p}{n}) \\ &= (\sigma_v)_p \end{aligned} \tag{3.4}$$

where z_m and z_p are the model and prototype depths, and $(\sigma_v)_m$ and $(\sigma_v)_p$ are the effective vertical self-weight stresses at the corresponding points of model and prototype soil elements, respectively. This indicates that the stresses in model and prototype is identical, i.e., the scale factor for stress is unity. If the soil tested in the model is the same as that in the prototype and the same stress path is followed in the model and prototype, the strains in the model and prototype is the same (Roscoe, 1968), i.e., the scale factor for strain is also unity, while the displacement of the prototype is larger than the model by the factor n=N. Hence, the modelling laws for hydraulic gradient similitude

Table 3.1: Scaling Relations for Centrifuge and Hydraulic Gradient Tests

Quantity	Full Scale	Model at N g's
Linear Dimension	1	$1/N$
Area	1	$1/N^2$
Volume	1	$1/N^3$
Stress	1	1
Strain	1	1
Force	1	$1/N^2$
Acceleration	1	N
Velocity	1	1
Time - In Dynamic Terms	1	$1/N$
Time - In Diffusion Cases	1	$1/N^2$
Frequency in Dynamic Problems	1	N

tests are expected to be the same as those for centrifuge tests. The modelling laws are summarized in Table 3.1 (Scott, 1978).

In dynamic problems, if the prototype motion is considered as a harmonic motion:

$$x_p = A_p \sin(\omega t_p)$$

$$\frac{dx_p}{dt_p} = A_p \omega \cos(\omega t_p)$$

$$\frac{d^2x_p}{dt_p^2} = -A_p \omega^2 \sin(\omega t_p) \tag{3.5}$$

Where ω is the prototype frequency of excitation, A_p, $A_p\omega$, and -$A_p\omega^2$ are the displacement, velocity, and acceleration magnitudes, respectively. The model must experience the prototype strain (x_p/L_p), hence the motion a model scaled geometrically by a factor $1/N$ must experience is:

$$x_m = (A_p/N) \sin(N\omega t_m)$$

$$\frac{dx_m}{dt_m} = A_p\omega\cos(N\omega t_m)$$

$$\frac{d^2x_m}{dt_m^2} = -NA_p\omega^2\sin(N\omega t_m) \tag{3.6}$$

Where A_p/N, $A_p\omega$, and $-NA_p\omega^2$ are the displacement, velocity and acceleration magnitudes respectively in the model. Obviously, the model frequencies and accelerations are higher than the prototype ones by the factor N, and velocities are unchanged. Consequently, time in the model is $1/N$ times that in the prototype. A detailed description of the ideal requirements for modelling laws is reported by Schofield (1981).

It should be emphasized that, although it is desirable to assess the method wherever possible by direct comparison with field tests (Lyndon and Schofield, 1978), this is not necessary in every situation. In the actual testing, the scaling laws related to the problems studied have to be verified experimentally, as many factors may not be scaled due to technical limitations. It is possible to provide indirect evidence of the validity of the modelling laws by using the "modelling of models" technique, in which an assumed prototype behaviour is simulated with different scaled models under different stress fields. In this thesis , the above technique has been used to examine the HGS modelling laws for testing dynamic pile response.

3.2 Description of UBC−HGS Testing Device

A schematic layout of the hydraulic gradient similitude test device at the University of British Columbia (UBC−HGS) (Yan, 1990) is shown in Figure 3.2. The device consists of five major components as follows:

1. Soil container and air pressure chamber;
2. Water supply and circulation system;

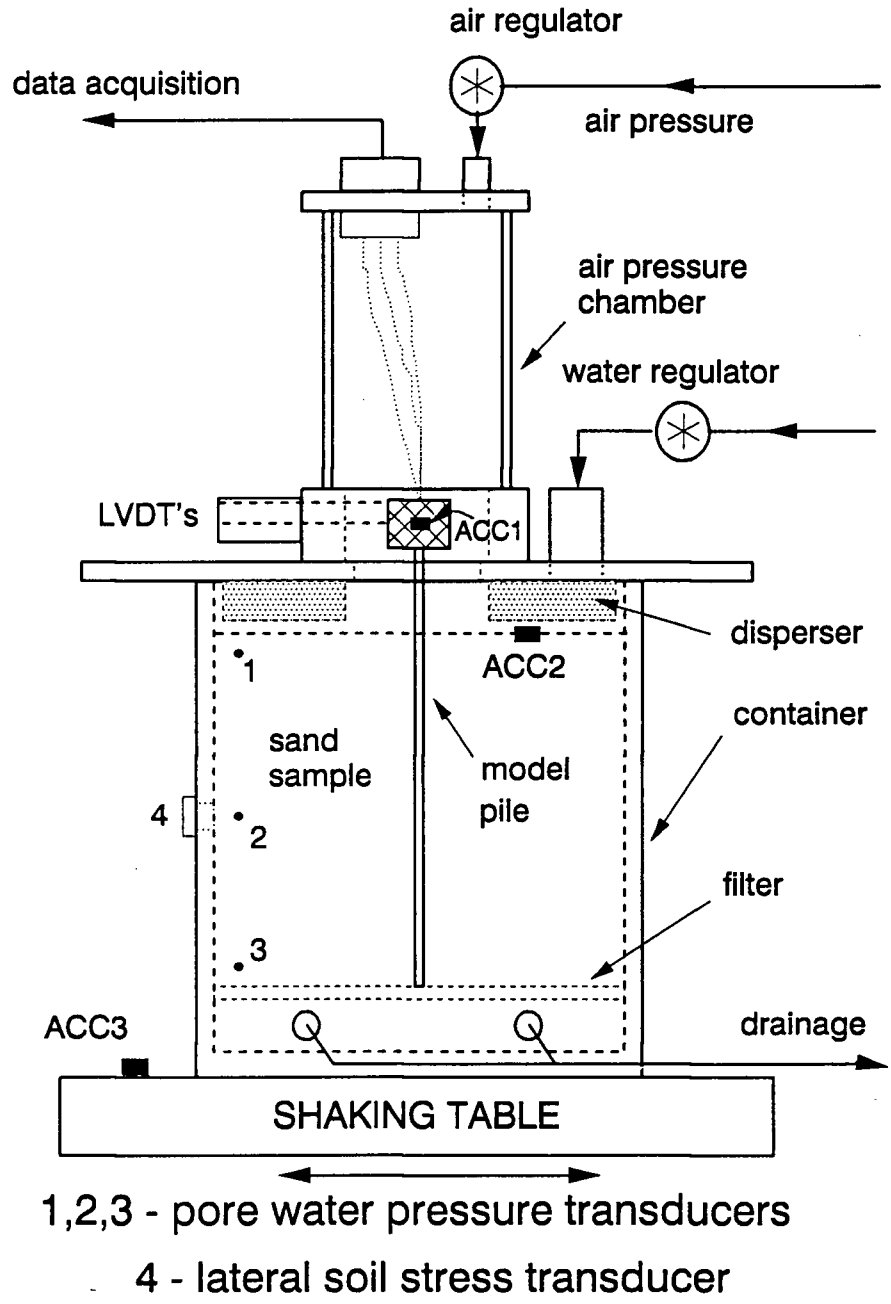

Figure 3.2: Schematic of UBC–HGS Testing Device

3. Air pressure supply system;
4. Loading system and
5. Data acquisition and control system.

The soil container in which the model piles and sand were placed is a rectangular box with inside cross section dimension of 404 × 190 mm and a depth of 400 mm. The box is made of 19.05 mm thick welded aluminum plates anodized with hard coatings. The maximum hydraulic gradient may be applied to increase the soil body force by 100 times. The corresponding maximum air pressure applied is about 350 kPa within the enclose system.

A filter at the bottom of soil container, supported on a grid of perforated aluminum strips about 25.4 mm (1 in) thick, retains the sand deposit and cellular chambers provided allows water to freely flow before draining out of the soil container. The filter consists of a 6.35 mm thick perforated aluminum plate overlain by a series of stainless steel sieves including #10, #140 and #200 mesh sieves. The sand used was re-sieved and only the portion retained in sieve #140 was used in the test.

The soil container lid is 19.1 mm thick, and a plexiglass cylinder resting on an annular block on the lid function as air chamber. The air pressure is supplied from an entry at the cap on the plexiglass cylinder. Several special pressure tight electrical plugs are installed on the cap to connect the instrumentation wires leading to the data acquisition unit.

The water is constantly supplied by the pump through a 25.4 mm I.D. entry hole at one side of the lid. During the test, the water table was kept around 25.4 mm above the sand surface but below the lid level.

The water pump is used for water circulation which is a centrifugal type with a capacity of 24 US GPM at a total pressure head of 30.5 m (100 ft), manufactured by Monarch Industries Ltd. It has a 1.5 horse power built-in motor. Plastic hoses are used to connect the pump with HGS device.

Currently, the load can be applied to the pile in soil container either from pile head or excitation base facility. For lateral pile head loading, with a double acting air piston mounted on the soil container lid, a one-way or two-way force controlled cyclic load can be applied through a loading bushing to the pile head inside the air chamber. The applied load is measured by a low capacity load cell mounted between the piston rod and the loading ram. For seismic loading tests, the seismic input base excitation may be applied through the conventional shake table on which the HGS device is mounted, and model tests are performed as usual shaking table tests.

A frictionless air leaking bearing system is used for LVDT (displacement transducer) cores. Two LVDT's are placed on the soil container lid. The LVDT's measures pile head deflections from outside the air chamber.

3.3 UBC Shake Table Characteristics

Model pile tests were carried out using the shake table in the Soil Dynamics Laboratory at the University of British Columbia. It measures 1.8 m by 2.7 m (6 ft by 9 ft). The principles of shake table operation are described below.

The table, 17.1 cm deep, is made up of welded aluminum with about 1 cm plates top and bottom separated by 5.1 $\times$ 15.2 cm hollow rectangular tubing in a grid pattern to provide stiffness, weighing about 450 kg. The essential feature of the table is that it be very stiff in order to transmit uniform base accelerations and be very light in order to make optimum use of the loading ram. The table is mounted on a set of 4 horizontal, V-slotted needle bearings (manufactured by Schneeberger, Switzerland) which allow only one degree of motion. the table motions are input using a hydraulic shaker which is comprised of a piston-cylinder, a servo-valve, a fluid pump and a driving electric motor. Hydraulic fluid (oil) is pressurized and pumped into the cylinder through a servo-valve

which regulates the flow of oil to the piston and thereby controls its motion. The servo-valve is moved by means of a linear torque motor, which is driven by an external electrical excitation. The excitation is applied through an MTS controller which is driven by a sine wave function generator or other computer controlled input. An LVDT (displacement transducer), which is housed within the hydraulic ram, monitors the displacement of the piston and transmits the signal back into the controller which represents the actual movement of the ram and therefore the table. The input signal is compared to the feedback signal from the LVDT, and the difference of the two signals is transmitted to the electronic controlled servo-valve located in the hydraulic ram. The electronic valve responds by allowing the ram to move in such a manner as to make the feedback signal equal to the input signal. The MTS control system generate a continuous single-direction shaking of the table and are capable of inputting a wide variety of sinusoidal or random earthquake motions into a test model.

Hydraulic actuators are most suitable for heavy load testing and can be operated over a range of frequencies. Large displacements (stroke) are possible only at low frequencies. Although any general excitation may be input into the controller, faithful reproduction of these signals is actually impossible because of distortion and higher order harmonics introduced by the high noise levels that are common in hydraulic systems.

Ambient vibrations recorded by the table accelerometer when the hydraulic pump pressure was at its maximum are shown in Figure 3.3. The acceleration data was recorded using a high speed data acquisition system which interfaced with an IBM PC microcomputer, described in Appendix A. A sampling rate of 1000 Hz per channel was used for this series of tests so that frequencies of up to 500 Hz could be reliably discerned. Fourier spectrum computed from the recorded accelerations is shown in Figure 3.3b. The figure shows that the table hydraulic system creates low amplitude acceleration of up to 0.005 g, and contain a number of higher frequency components. Where the frequency content

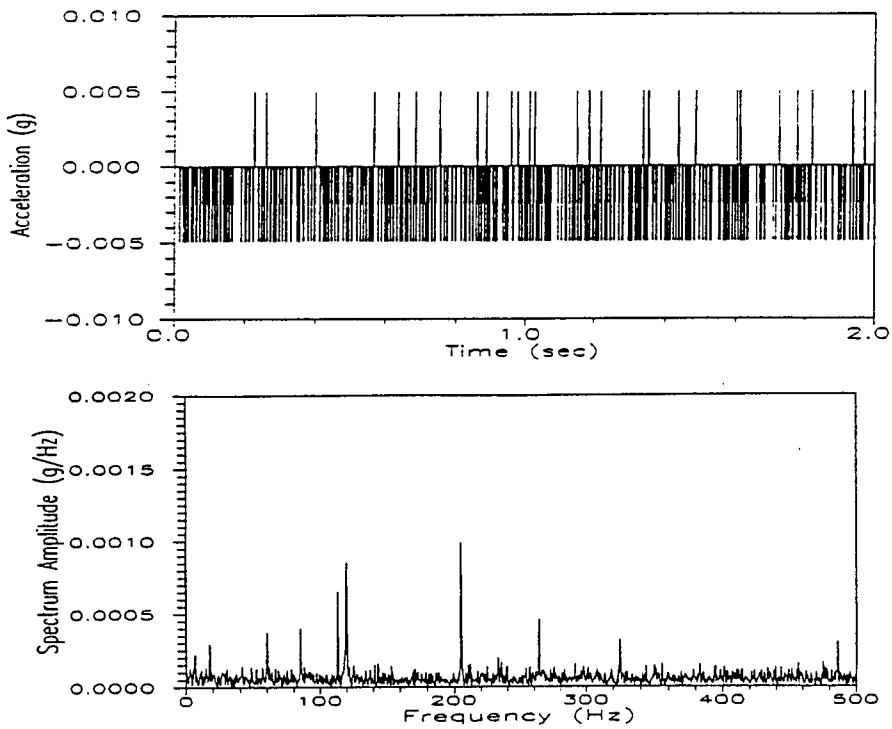

Figure 3.3: Shake table pump vibration

of the pump vibration matches the natural frequencies of the sand, whose fundamental frequency has been found to be in the range of 60 to 160 Hz, amplified accelerations at the soil surface have been observed. The first mode, frequency of the model pile, on the other hand, lies in the range of 7 to 20 Hz (see Chapter 3). It has been found that the high frequency accelerations contained in the pump vibration are not significantly amplified by the pile since they are well removed from its resonant frequency.

The shake table input was calibrated using sinusoidal base motion over a rang of input frequencies varying from 5 to 70 Hz. For a given input frequency, the peak table accelerations were measured against the amplitudes of the table displacement (span) using a storage oscilloscope. The feedback control system was fine tuned using the procedures described in the table operation manual so that the shape of the input sine wave was optimized.

Typical sinusoidal base motions produced by shake table at an input frequency of 10

Table 3.2: Physical Properties of Model Piles

Diam.(mm)	6.35 (instrum.)	9.525	12.7
Wall Thick.(mm)	0.81	1.27	1.27
Length (mm)	424.0	424.0	424.0
Mass (g)	20.3	38.3	53.4
$\bar{m}$(g/mm)	0.0479	0.0901	0.1259
EI($N \cdot mm^2$)	4.03×10^6	19.56×10^6	52.05×10^6

Hz (sampling rate of 1000 Hz per channel) are shown in Figure 3.4. The average peak accelerations of 0.5 g and 0.2 g are shown in Figures 3.4a and 3.4c, respectively. Fourier spectra computed from the recorded base accelerations are shown in Figures 3.4b and 3.4d, respectively. The figure shows that higher frequency overtones are present in the table input and these are more pronounced for lower intensities of shaking.

3.4 Pile Characteristics and Model Layout

Model piles are made of 6061-T6 aluminum tubing. Three models with diameters 6.35 mm (1/4 in), 12.70 mm (1/2 in) and 9.53 mm (3/8 in) are used for studying laterally loaded pile problem subject to pile head perturbation and ground motion excitation.

A summary of the physical properties of these three piles is given in Table 3.2. The flexural rigidities (EI) of the piles were measured using transverse dead loading of the pile while they were clamped at one end and free at the other. From the measurements of pile deflection versus applied transverse load, the pile EI values were computed based on static beam bending theory.

Among three piles, only one pile with 6.35 mm outside diameter (O.D.) and 0.81 mm wall thickness was instrumented with 8 pairs of 120 Ω foil type strain gauges mounted on the outside of the pile to measure the bending strains (moments) at the locations shown

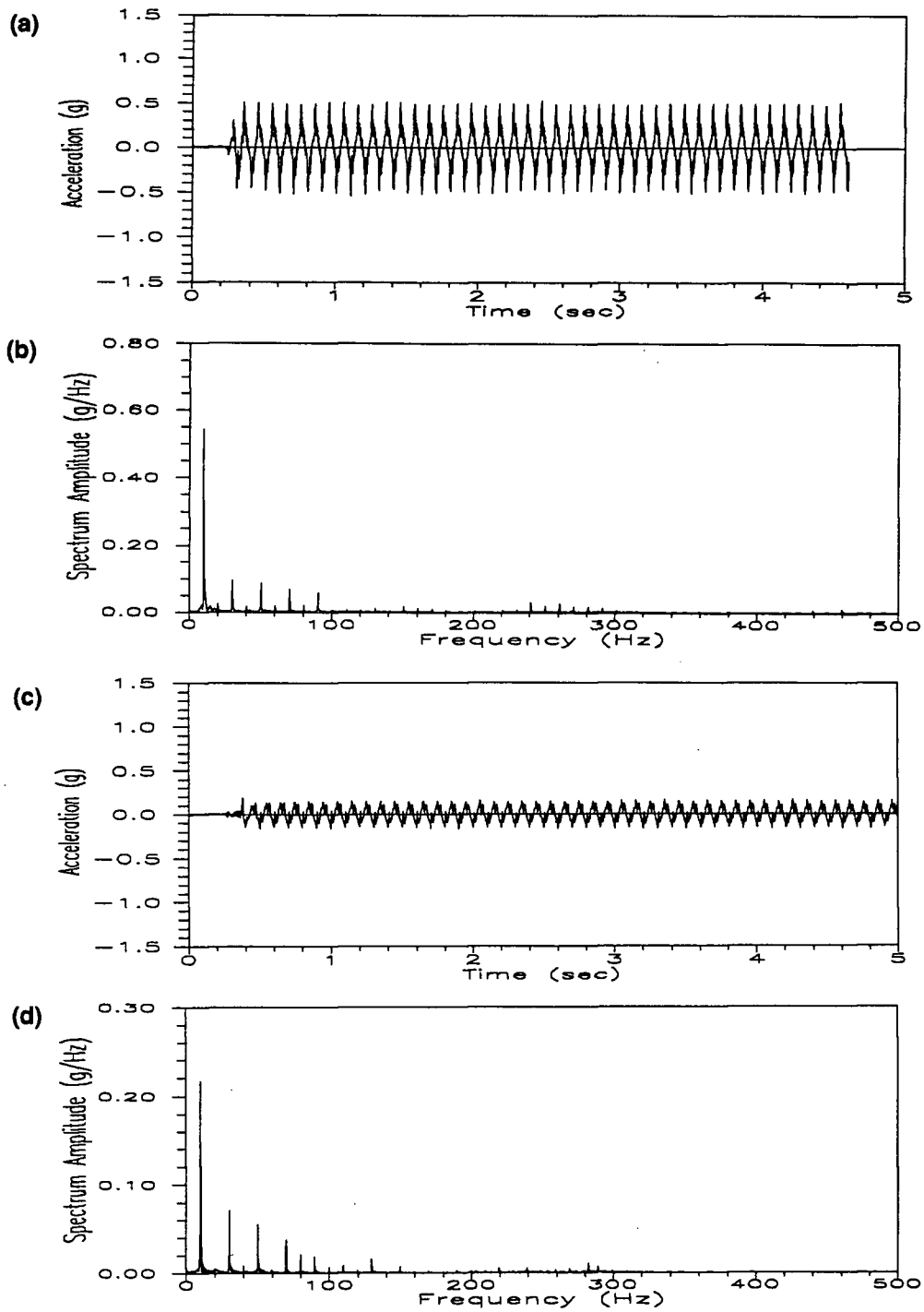

Figure 3.4: Typical sinusoidal input base motions recorded using a sampling rate of 1000 Hz per channel (a) high intensity shaking accelerations, (b) high intensity shaking Fourier spectrum, (c) moderate intensity shaking accelerations, (d) moderate intensity shaking Fourier spectrum.

in Figure 3.5.

The strain gauges are spaced at 20, 15, 20, 20, 30, 40, 60 mm down the pile. The electrical lead wires from the gauges are brought up the inside of the pile through holes drilled through the tube wall. The wires are then passed through a slot in the pile head mass, and connected to the bridge completion and amplifier circuitry.

A rigid pile head mass with a weight of 7.90 N was clamped to the head of the pile to simulate the effect of a superstructure. The mass geometry is 50.8 mm in height and 50.8 mm in diameter. A sensitive ± 10 g, miniature accelerometer (Appendix A) and two displacement transducers (LVDT's) were mounted on the pile head mass to measure accelerations and displacements of the mass. The accelerometer was placed at the centre of gravity of the mass, and the LVDT's were spacing 20 mm. Displacements were measured with respect to the moving base of the soil container. The rotation of the mass may be calculated from the two displacement measurements and the vertical separation distance between the LVDT's.

3.5 Instrumentation and Measurement Resolution

The Pile foundation models were instrumented with strain gauges, accelerometers and LVDT's, as shown in Figures 3.5. A description of the instrumentation, calibration procedures, and the data acquisition systems used during testing may be found in Appendices A.

Before testing, a series of checks were run to determine the amplitudes of instrument line noise which affect the resolution with which the engineering parameters of interest (i.e. bending moment, acceleration and displacement) can be measured. The line noise is due to a number of factors including inadequate grounding or shielding of lend wires and power supplies, and in the case of the LVDT's, internal signal conditioning circuitry

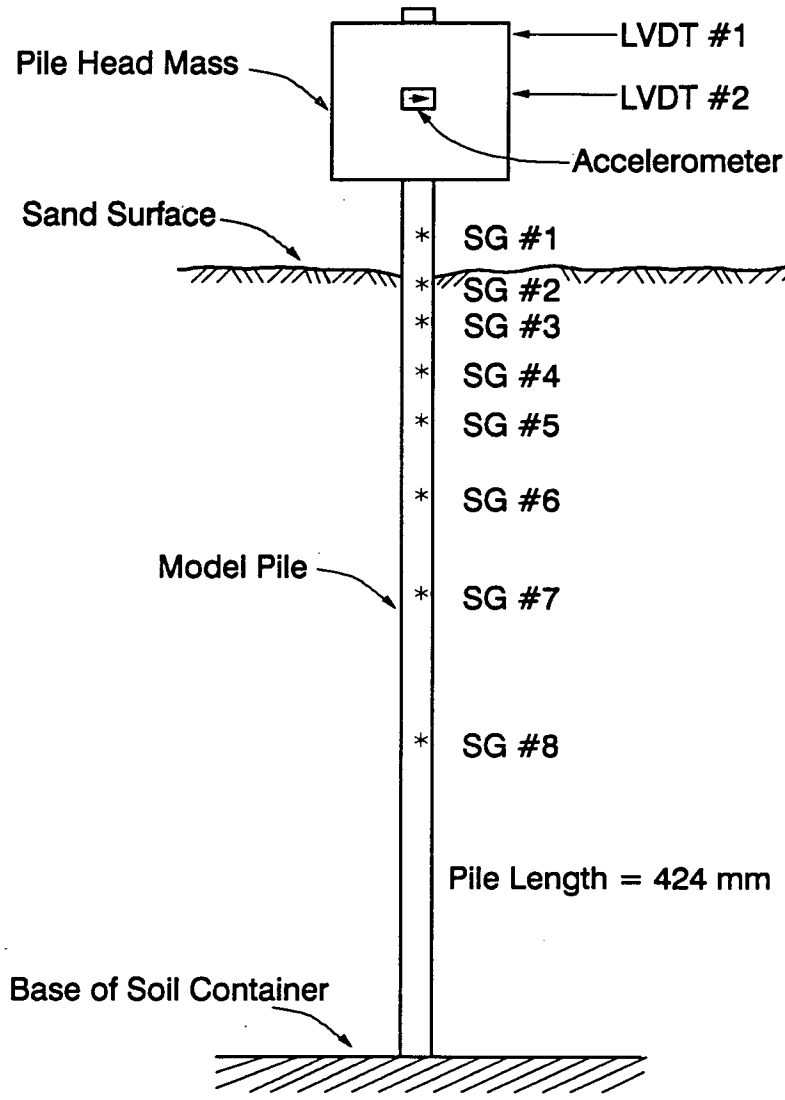

Figure 3.5: Model pile layout

Table 3.3: Instrument Noise Levels

Instrument	Noise Level
Bending Strain Gauges	± 2 - 6 N.mm
Accelerometers	± 0.01 g
LVDT #1	± 0.02 mm
LVDT #2	± 0.02 mm
Pore Pressure Transducer	± 0.2 kPa

designed to convert AC to DC voltage output.

Experimental observations and analysis of the lateral vibration response of the pile have shown that the pile vibrates primarily in its first mode at frequencies of 15 to 18 Hz, corresponding to HGS scale factors of 30 to 60. Tests have shown that the majority of line noise from the transducers is at much higher frequency than the pile natural frequency. Line noise from the accelerometers is of the order of 0.01 g and the noise from the strain gauges is in an order of 2 to 6 $N \cdot mm$, and may be neglected. The electronic noise from the LVDT's occurs over a broad range of frequencies, therefore, a 100 Hz low pass filter was applied to LVDT outputs to improve the signal to noise ratio. The noise level, expressed in terms of engineering quantities of interest, are given in Table 3.3

3.6 Foundation Sand Characteristics

The sand chosen for the model tests is a uniform rounded Ottawa sand. Its mineral composition is primarily quartz with a specific gravity of 2.67 and a constant volume friction angle, ϕ_{cv} of 31°. Its grain size distribution is shown in Figure 3.6, which indicates an average particle size D_{50} of 0.16 mm, and a coefficient of uniformity D_{60}/D_{10} of 1.5. It should be kept in mind that only sand retained on the sieve#140 was used for the test. Pile tests were carried out in dense sand only (Dr=75%). Reference maximum and

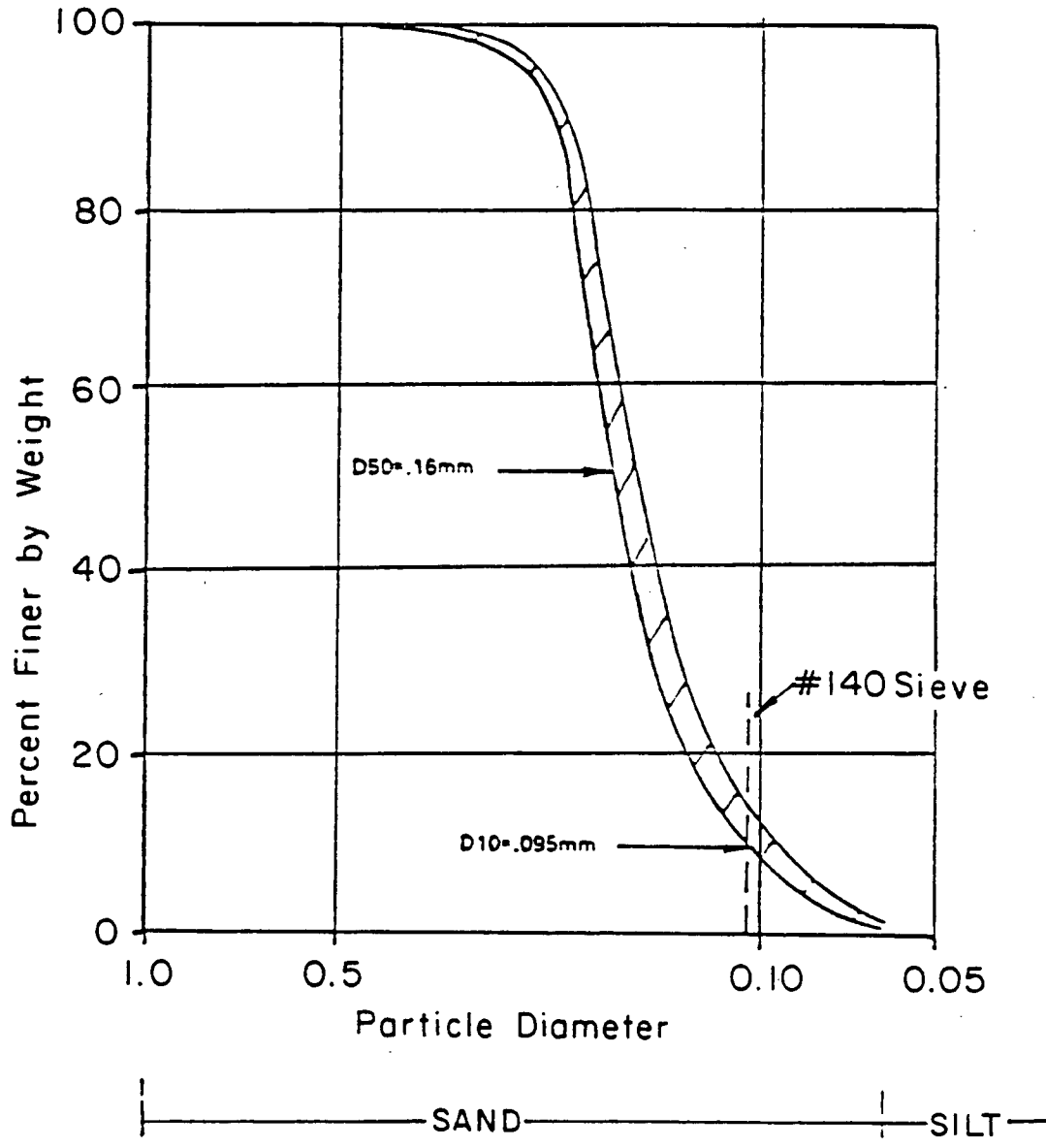

Figure 3.6: Grain size distribution of fine Ottawa sand

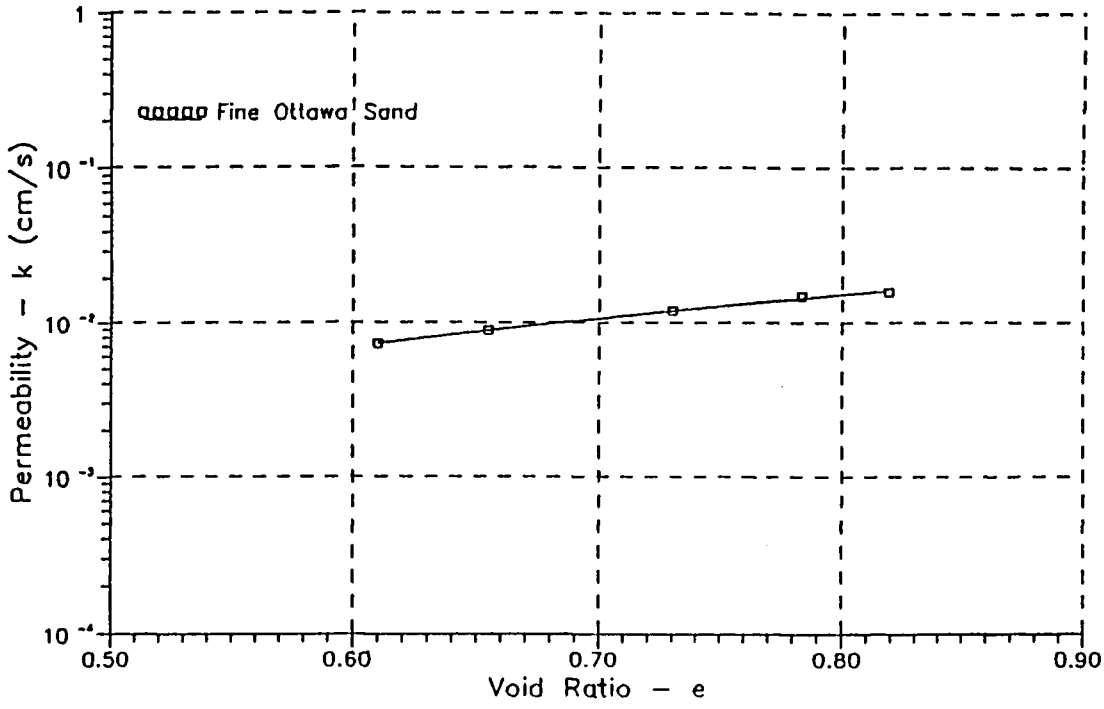

Figure 3.7: Variation of permeability vs. void ratio

minimum void ratios of 0.88 and 0.58 were determined according to ASTM standard (1972). The variation or permeability (k) versus void ratio (e) of the sand used was determined by the variable head method (Lambe, 1951) and is shown in Figure 3.7.

Conventional drained triaxial compression tests were carried out to determine the hyperbolic soil parameters of the soil tested based on the procedure suggested by Duncan et al.(1980). Confining stresses used in the triaxial tests were in the range of 20 to 200 kPa. At low stress levels, stress corrections for membrane forces were made by the methods proposed by Fukushima and Tatsuoka (1984) and Kuerbis (1988). A summary of the soil parameters estimated is given in Table 3.4.

Table 3.4: Hyperbolic Soil Parameters from Drain Triaxial Tests

Sands	K_e	n	K_b	m	R_f	ϕ_1	$\Delta\phi$	ϕ_{cv}	K_o
$D_r = 30\%$	600	0.88	470	0.25	0.95	32	0.0	31	0.5
$D_r = 75\%$	1600	0.67	600	0.05	0.70	39	4.0	31	0.4

K_e = Young's modulus number.
n = Young's modulus exponent.
K_b = bulk modulus number.
m = bulk modulus exponent.
R_f = failure stress ratio.
ϕ_1 = mobilized friction angle at a confining pressure of atmosphere.
$\Delta\phi$ = decrease in mobilized friction angle for a tenfold increase in confining stress.
ϕ_{cv} = constant volume friction angle.
K_o = pressure coefficient at rest = $(1 - \sin\phi)$ for the testing condition.

3.7 Sand Foundation Preparation and Test Procedure

3.7.1 Reconstitution of Sand Foundation

A level sand foundation was prepared in the soil container bolted to the shake table. The soil preparation method employed in this study was the "quick sand" technique developed by Yan and Byrne (1989).

During sample preparation, the top cap platform and air chamber cylinder were all removed, and replaced by an open-ended plexiglass extension box. The drainage lines from the bottom water circulation chamber were closed and water was filled up to the top of extension box. A given weight of dry sand was then rained through the water uniformly. After the water table was lowered down to the sand surface, a controlled upward seepage gradient was applied by pumping water into the sample from the bottom, causing the sand to expand and to form a loose slurry state. Typically, the sand sample during the slurry state would expand up to 60% of its original volume.

The upward gradient was then turned off and the sand particles started to settle

down under their gravity. The sand used was uniform, and no segregation was observed. As the sedimentation was in process, the sample was densified through tapping the base and sides of the soil container with a soft hammer. The water table was lowered down again when the soil surface descended down to the top end of the container. Tapping was carried out until a given sample density was reached, which is controlled by measuring the average sand surface height against a reference height. Then the upper extension box was removed, and sample preparation is complete. The above preparation approach was used to form and reform soil deposit for each test. The uniform sand foundation can then be obtained with stress-strain response similar to samples formed by the water pluviation method (Vaid and Negussey, 1986). The in-situ measurements of the maximum shear modulus, G_{max}, of the model soils within the HGS device have been made by Yan (1990).

3.7.2 Pile Installation

After the sand foundation was formed at a given density, an accelerometer was placed at the surface of the sand a distance of 101 mm (16 pile diameters) from the centre of the single pile to measure the free field surface accelerations. Another accelerometer was placed on the base of the soil container to measure input accelerations from the MTS controller.

Instrumented pile was pushed into the sand deposit by hand through a pile driving guide which made the model pile be driven at the centre of the soil container and be in line with the LVDT's measurement cores. The distance between the centre of the pile and the boundary of soil container perpendicular to the direction of shaking was 32 pile diameters. The model piles were close-ended at the tip, and driven to the bottom of sand deposit, resting on the filter surface with an embedment length of 322 mm. Thus, the model piles simulated full displacement end bearing piles.

Pushing the pile into the soil foundation disturbs the near field soil and also affects the

initial soil properties and density. The technique for driving model piles into a prepared foundation under high hydraulic gradient to simulate full scale pile driving condition was not available while performing the present series of tests. Thus the model piles were pushed into the sand under normal stress conditions.

Robinsky and Morrison (1964) performed a series of model pile installation studies in sand at 1 g stress condition. The sand displacement and compaction around model friction piles were observed by means of radiography technique, and found to be dependent upon the pile property, soil stress level and soil density, The envelope of soil displacement due to pile installation extends 3 to 4 pile diameters from the sides of piles in loose sand, and 4.5 to 5.5 pile diameters in dense sand. The shape of this envelope resembles on elongated bulb, its diameter decreases significantly near the ground level due to the free surface boundary and low confining stress. Thus, the stress field created by hydraulic gradient in the tests may be affected by the disturbed soils caused by the pile driving. However, for the laterally loaded pile tests, its effect is not significant because flexible pile response is dominated by soil reactions in the upper part of the sand where installation induced stress changes are minimum. The observation by Robinsky and Morrison also indicated that the soil compaction due to pile installation is less severe for close-ended pipe piles than for cone tip or tapered piles.

In the centrifugal modelling, many tests were performed on piles installed at 1 g stress condition (Scott, 1977 and Barton, 1982). Recently, techniques have been developed to drive the model piles into a prepared foundation while in flight on the centrifuge (Oldham, 1984; Ko et al., 1984 and Craig, 1984, 1985). Their studies show that pile behaviour under axial loading is significantly affected by the stress level at pile installation. But the effect of the stress level is much less important on laterally loaded pile response. This is because the pile behaviour under lateral loading is controlled by soil reaction in the upper levels where stress changes caused by pile installation are lowest. Furthermore the nature of

lateral pile loading modifies the soil stress regime around the pile to a much greater extent than in axial loading. It is postulated that installation effects are gradually erased with increasing number of lateral load cycles. Based on the above considerations, the procedure of installing pile under the normal stress condition and then performing pile loading tests at a higher stress level was applied in this thesis. After pile installation the distance between the soil surface and upperside of the pile head mass was measured. One accelerometer and two LVDT measurement cores were also attached to the pile head mass to measure the head acceleration and deflections. The air pressure chamber was thereafter installed and all the instrumentation wires connected to the data acquisition unit.

3.7.3 Soil loading Process and Seismic Loading on Pile

After enclosing the whole testing device, the soil loading process began by applying air pressure in the air chamber and in the mean time pumping the water into the sand container. During this process, the micro-computer with a monitoring program was used to monitor the hydraulic gradient in the sand until a given hydraulic gradient was reached.

Thereafter, for the forced vibration tests, a sinusoidal excitation was input through the shake table which the HGS device was mounted on to simulate earthquake motion.

3.7.4 Test Repeatability

Repeatability of test results is an important requirement for the consistency of conclusions to be derived from the test results. Rigorously identical model preparation and testing conditions are key to achieving repeatable test results. Good repeatability of test results for pile frequency testing are accomplished and shown in Table 3.5.

Table 3.5: Evaluation of Test Repeatability

Model Pile Diam. (mm)	Cap Mass (g)	H.G.S. N	1st Freq.(Hz) Test #1	1st Freq.(Hz) Test #2
12.7	2654.4	24	13.89	13.89
12.7	2654.4	36	17.00	17.30

3.7.5 Experimental Program

The experimental program falls into three categories:

First, three series of free vibration tests on single piles (see Chapter 4) were performed to study the behaviour of the pile natural frequency and soil damping under different stress level (H.G.S.scale factor N). Furthermore, the hydraulic gradient modelling laws were verified for seismic laterally loaded piles using "modelling of models" technique.

Secondly, free field experiments were conducted to examine the accelerations in the soil sample and characteristics of the free field response during a simulated earthquake.

Thirdly, three series of forced vibration tests were carried out under a sequence of excitation frequencies, different stress levels and different excitation intensities to study the response of superstructure and pile, and soil-pile interactions.

3.8 Discussion of Boundary Effect

An important consideration in dynamic modelling is the presence of an artificial boundary on soil system due to the containment walls. Coe (1985) and Coe et al. (1985) have demonstrated the existence of standing waves due to wave reflection at the centrifuge bucket walls during dynamic excitation. Nevertheless, in many of the investigations in dynamic centrifuge modelling (Morris, 1981; Bolton and Steedman, 1982; Ortiz, et al. 1983; Belton and Steedman, 1984 and Finn, et al. 1986), nothing was done to attenuate

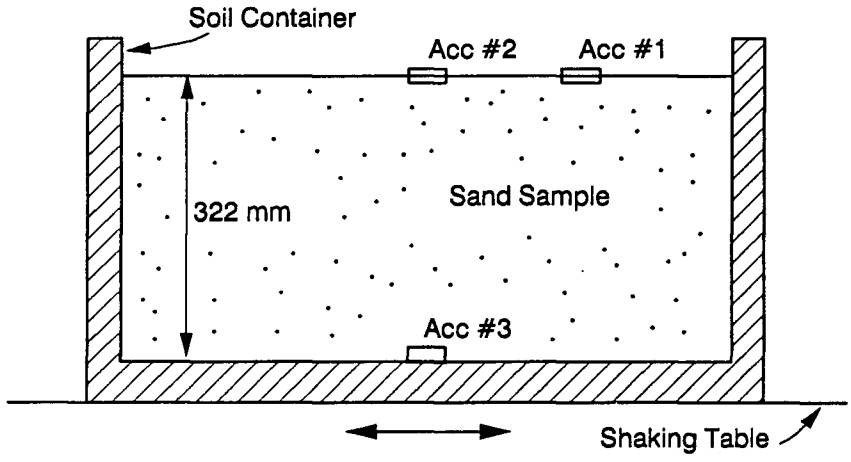

Figure 3.8: Accelerometer configuration for free field experiments

wave reflections in the experimental system. Recently, an effort was made to better simulate the free field response during earthquake loading by placing appropriate energy absorptive material (soft material) on the model boundary (Coe, 1985; Weissman and Prevost, 1989) averting wave reflections. In this thesis, the effectiveness and limitation of this method are examined in light of experimental observation and numerical analysis.

3.8.1 Experimental Evaluation of Boundary Effect

The behaviour of a soil deposit in the HGS testing device is examined under the simulated earthquake loading by the experimentation under HGS scale factor of 60. A 322.0 mm deep soil stratum is prepared using the method as described in this chapter earlier and instrumented with accelerometers as shown in Figure 3.8. The accelerations on the free field (at centre of the soil surface and soil surface to the right of centre) and input base excitation are measured. The experiments are only carried out under rigid boundary conditions that there is no soft material placed on the container walls to model

a horizontal stratum of infinite extent since it is found that the soft boundary is not sufficient to simulate the simple shear mode of soil motion, on the contrary, it introduces active soil failures at the boundaries when the stress in the soil deposit is increased by the hydraulic gradient, thus violating zero strain boundary conditions before earthquake loading.

Figures 3.9 and 3.10 show an example of the acceleration measured by each of the transducers (Figure 3.8) followed by their corresponding Fourier Transforms, in which the input exciting frequency is 10 Hz. It is evident from the free field measurements (Figure 3.9) that the simulated earthquake motion is amplified as it travels towards the soil surface. The peak to peak amplitude of the acceleration is amplified by 1.7 times from the base motion (Figure 3.9a) to the soil surface (Figure 3.9b). The Fourier Transforms (Figures 3.10a and b) show that the spectrum amplitudes at input dominant 10 Hz frequency are essentially the same. This implies that the response of soil deposit is similar to the excitation base motion at lower frequency ranges in terms of amplitude where concerned. The fundamental frequency of the soil layer tested in the horizontal direction is about 161 Hz (model scale) and is far higher than the frequency of interest. It is observed that the input base signal is not purely clean at 10 Hz and does contain the other frequency contents between 30 and 500 Hz resulting from the system noise. Figure 3.10b illustrates that the acceleration on the soil surface is amplified with respect to the base of the soil deposit at higher frequency range of 380 to 480 Hz which corresponds to a higher order resonant frequency of the soil layer. The amplification of the surface acceleration at higher frequency component obviously contributes to the overall magnitude of the acceleration which results in a increase in the average peak value of the soil surface acceleration (Figure 3.9b).

A comparison of the two signals recorded at different locations on the soil surface

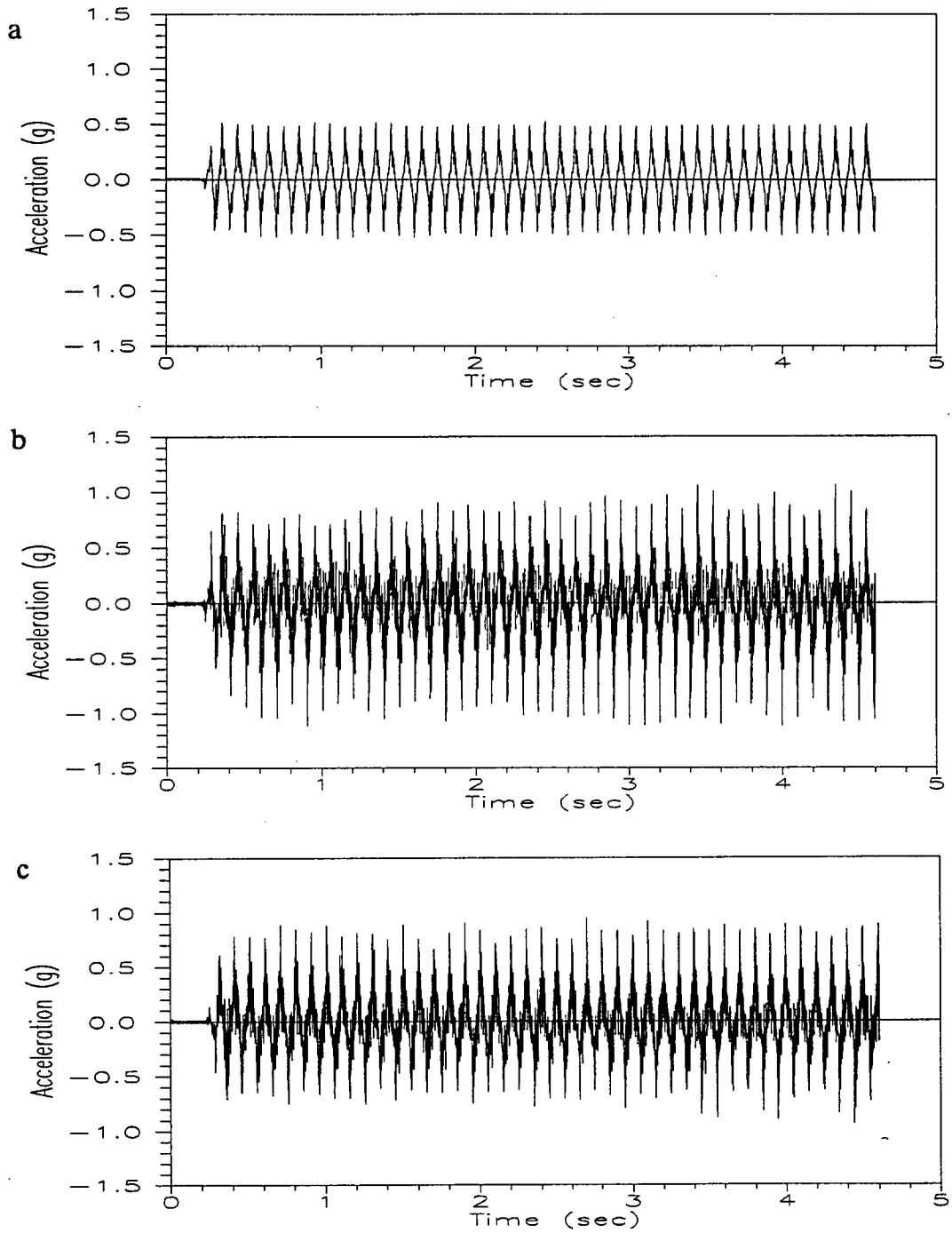

Figure 3.9: Soil layer acceleration time histories for experimental evaluation of boundary. (a) input base; (b) centre of soil surface; (c) soil surface to the right of centre

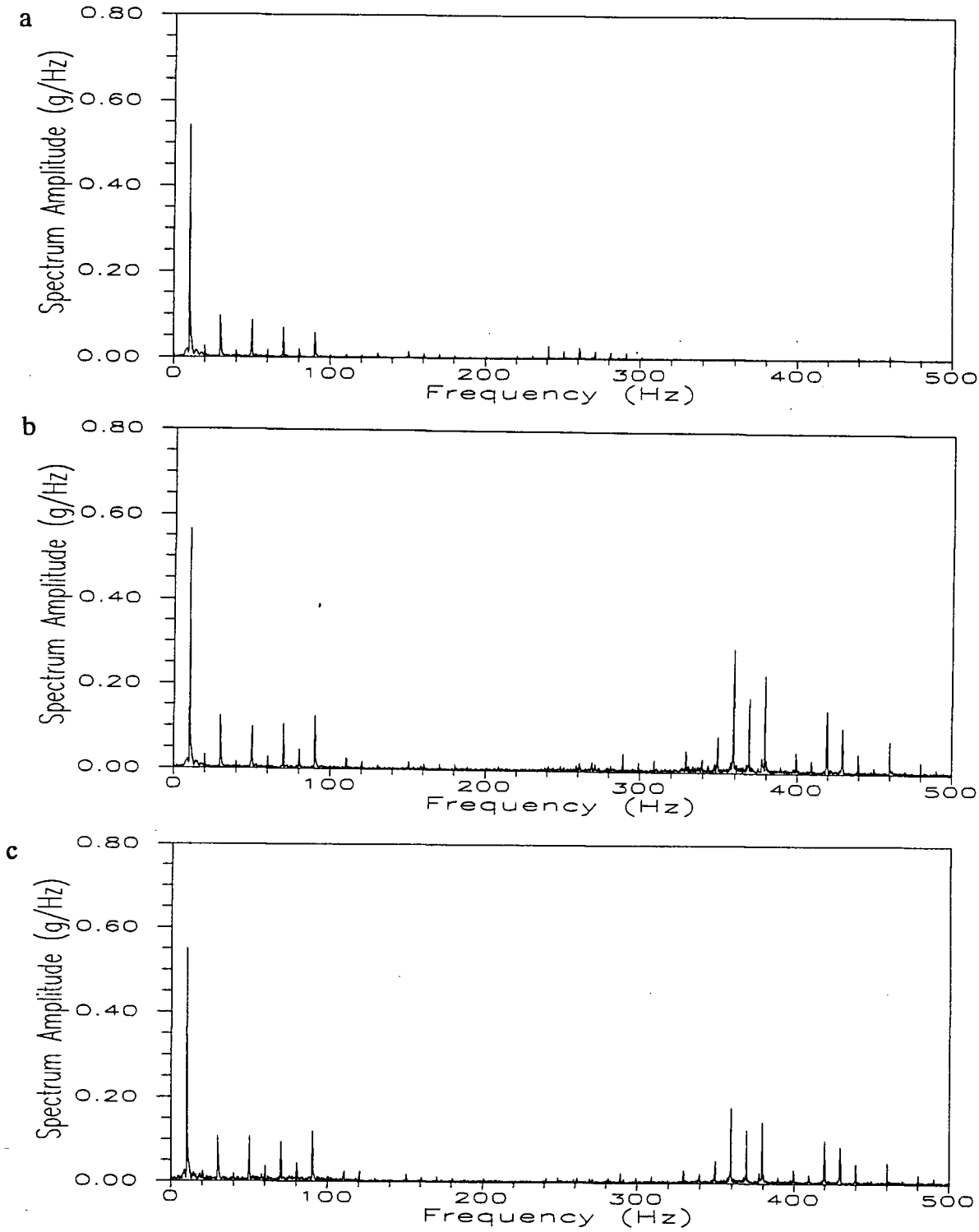

Figure 3.10: Fourier Transforms of soil layer accelerations. (a) input base; (b) centre of soil surface; (c) soil surface to the right of centre

should provide an indications of how well the system is modelling a homogeneous horizontal stratum of infinite lateral extent. Ideally, vertically incident shear waves should yield the same acceleration at all points on the surface of a uniform soil layer. The acceleration at the soil surface to the left of the centre (Figure 3.9c) is slightly smaller in amplitude but otherwise very similar to the acceleration measured at the centre (Figure 3.9b). The discrepancy between the acceleration at these two points is due to the fact that the off-centre point is closer to the rigid container wall which undergoes the same vibration as input base motion. The distance between the two accelerometer is 32 pile diameters used in the soil-pile interaction experiments described in Chapter 4. The acceleration is, therefore, fairly uniform for a region well beyond the position of the pile. Thus, wave reflections almost do not occur at the boundary walls when the vibration ranged lower frequencies far from soil natural frequency.

3.8.2 Numerical Analysis of Boundary Effect

As described in Section 3.8.1, the effectiveness of the soft material installed on the HGS soil container wall could not be evaluated directly using experimental method because it causes active soil failure before starting the dynamic tests. Therefore, it turns to numerical approach to assess the effectiveness of the soft boundary and effect of testing device boundary. The computer program FLUSH is applied to achieve these objectives.

Numerical analyses are carried out in three cases, i.e., soil deposit with rigid boundaries, soil deposit with soft boundaries and simulated free field condition where transmitting boundaries are employed to absorb wave energy radiating. In the case of soft boundaries, Two 30 mm thick layers of clay-like material are simulated to be placed on the container walls, which may accommodate a large lateral deformation to model the free field condition. For all the cases, the control motions are the same (Figure 3.11a) and input through the base of the soil deposit.

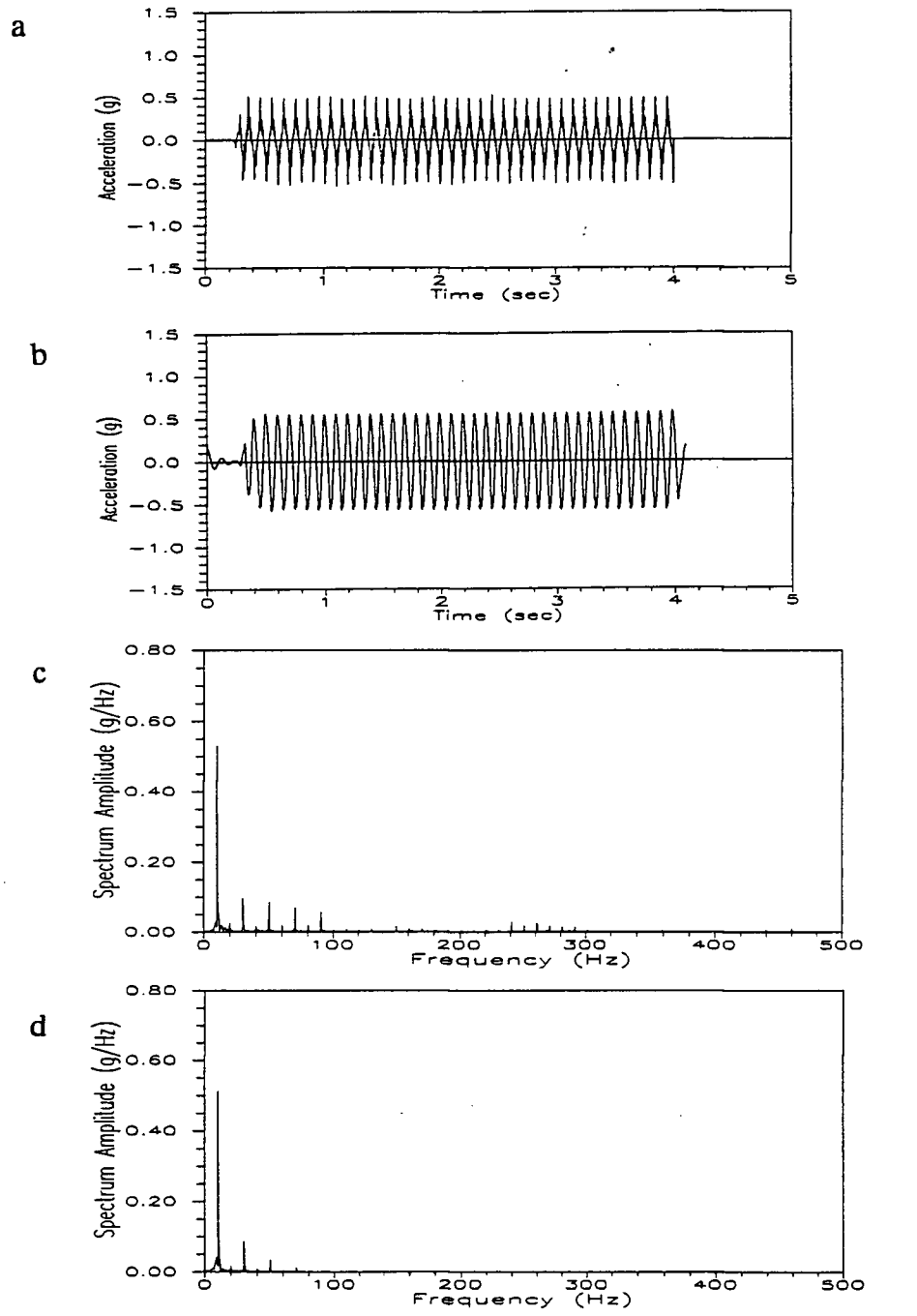

Figure 3.11: Computed acceleration time histories and their corresponding Fourier Transforms for infinite soil stratum: (a)base control motion acceleration; (b) soil surface acceleration; (c) FFT of base acceleration; (d) FFT of soil surface acceleration

Figure 3.11 shows the input control motion at the base and computed free field surface acceleration response both in time domain and frequency domain for simulated infinite soil layer with transmitting boundaries. It can be seen that the base excitation are almost identical with the response of free field surface in terms of peak average accelerations and Fourier spectrum amplitude at about 10 Hz. The acceleration of the soil surface is a little amplified by a factor of 1.14 with respect to the base acceleration of 0.50 g through the soil deposit. The high frequency components of base motion are filtered out via the soil deposit (Figure 3.11b and d) and the Fourier amplitudes of acceleration at range of frequency of interest are basically unchanged between base and free field motions. This indicate again, similar to experiment, that the response of soil stratum is essentially similar to base excitation motion in light of spectrum amplitude at lower frequency range.

The responses of soil deposit in HGS test device are analyzed using FLUSH with two types of constraints, i.e. soft boundaries and rigid ones. Figure 3.12 illustrates the response behaviour of sand within the device with 30 mm thick soft material on the constrained boundary. It is clearly depicted from the figures that the high frequency energy of base excitation (Figure 3.11a and c) is absorbed by the soft boundaries (Figure 3.12). The peak average amplitude of acceleration of soil surface is reduced to 0.4 g from 0.5 g of base through travelling the soil deposit. Nevertheless, the Fourier amplitude at exciting frequency is amplified to 0.74 g/Hz from 0.53 g/Hz of base which implies that the soil response is primarily contributed from the energy at frequency of 10 Hz. Accelerations at centre and off-centre of soil surface (Figure 3.12a, c and b, d) are identical in peak average value, and negligibly different in terms of Fourier amplitudes. This implies that the uniformity of accelerations on soil surface is well satisfied.

The behaviour of amplification of soil in the HGS test device with rigid constraint boundaries is shown in Figure 3.13. It demonstrates that the overall average peak amplitude of acceleration of the soil surface (Figure 3.13a) has no amplification to the base

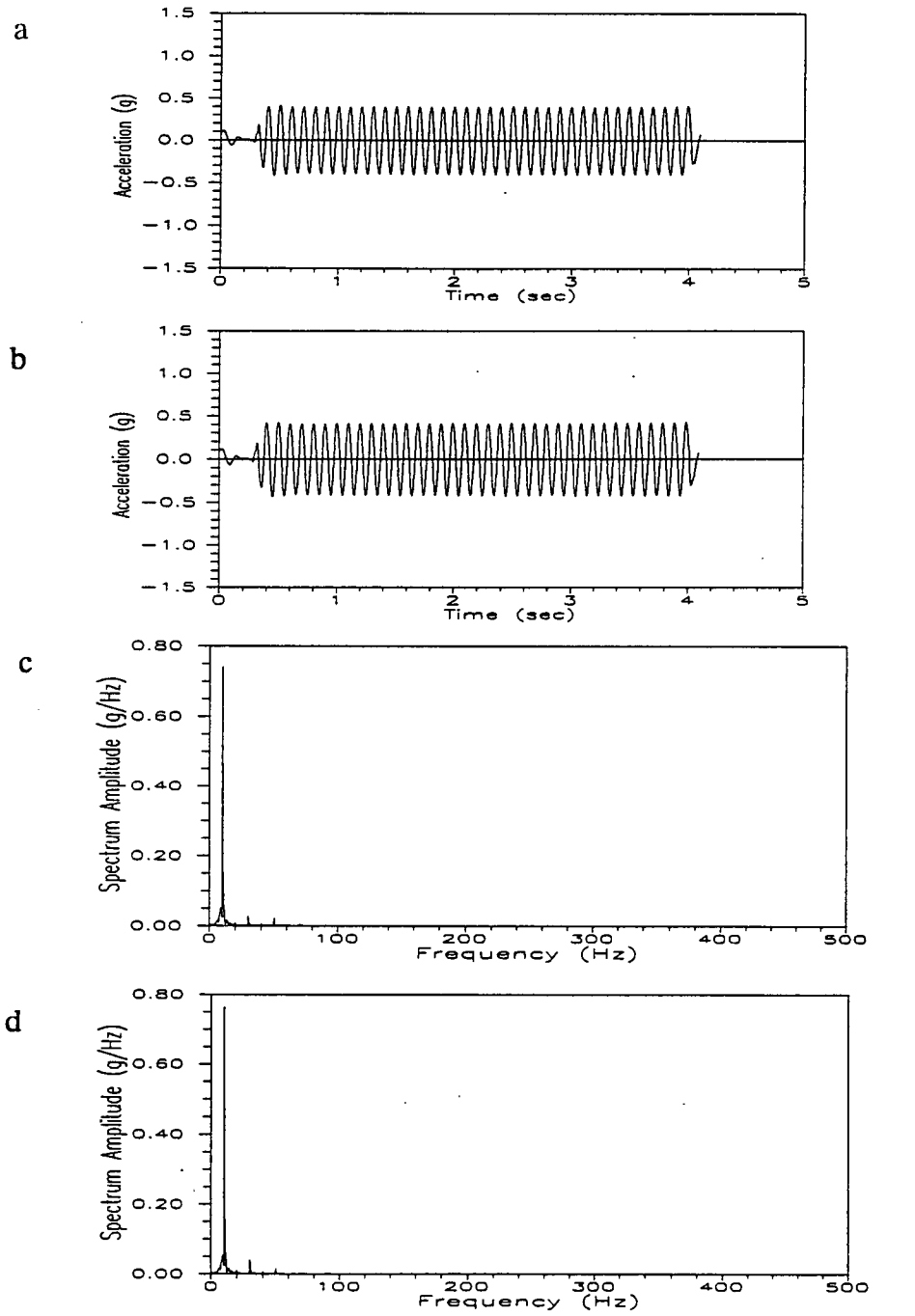

Figure 3.12: Computed acceleration time histories and their corresponding Fourier transforms for soil deposit with soft boundaries: (a)centre acceleration of soil surface; (b) acceleration of soil surface to the right of centre; (c) FFT of centre acceleration; (d) FFT of off-centre acceleration

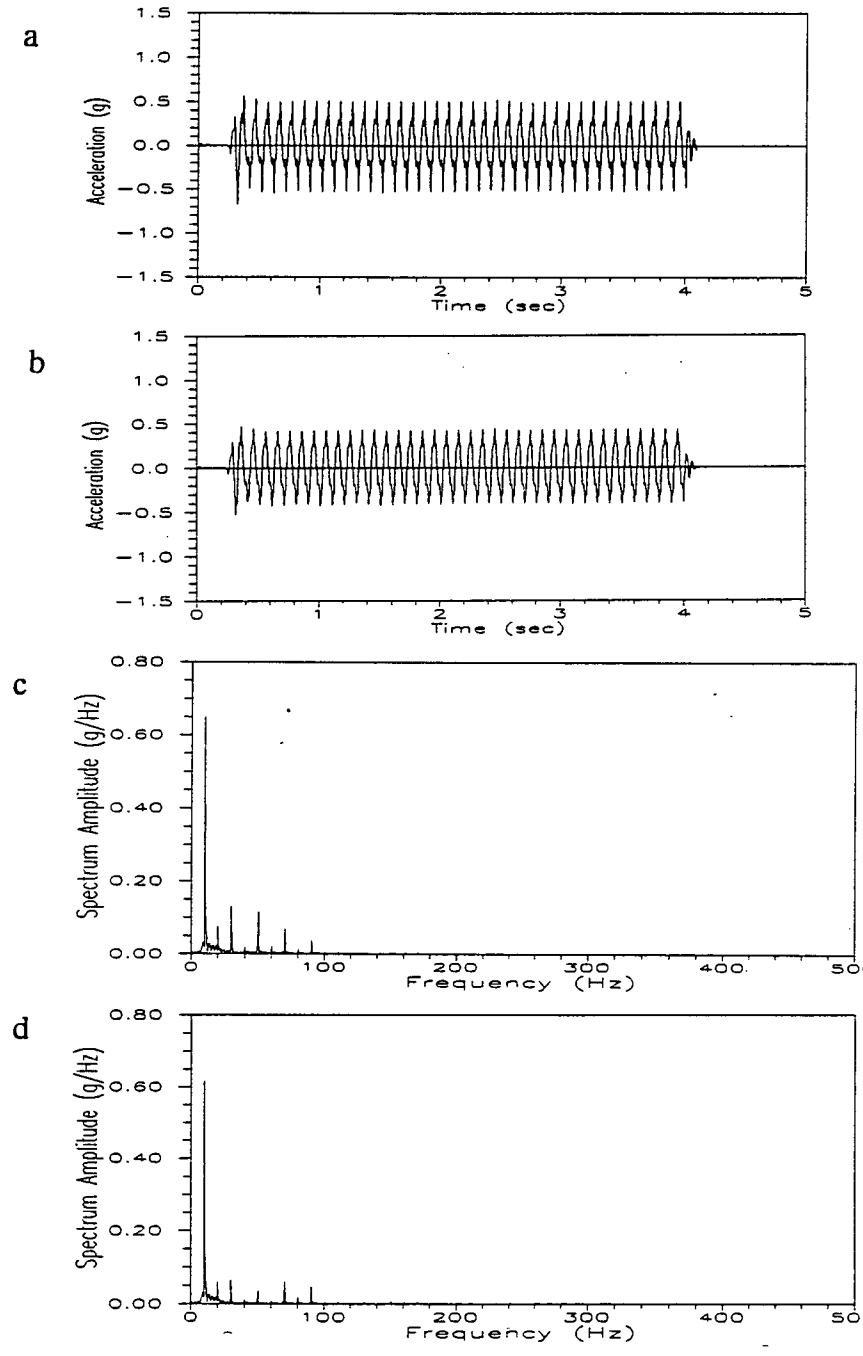

Figure 3.13: Computed acceleration time histories and their corresponding Fourier transforms for soil deposit with rigid boundaries: (a) acceleration at centre of soil surface; (b)acceleration at the right of centre of soil surface; (c) FFT of centre acceleration; (d) FFT of off-centre acceleration

Table 3.6: Summary of Characteristics of Boundary Evaluation

Bound. Cond.	Base $\ddot{x}_{bs}$	Centre $\ddot{x}_{cl}$	Off-Centre $\ddot{x}_{oc}$	$\ddot{x}_{cl}/\ddot{x}_{bs}$	FFT of $\ddot{x}_{bs}$	FFT of $\ddot{x}_{cl}$	FFT of $\ddot{x}_{oc}$
Free Field	0.5	0.57	0.57	1.14	0.53	0.52	0.52
Soft	0.5	0.40	0.40	0.80	0.53	0.74	0.77
Rigid	0.5	0.50	0.42	1.00	0.53	0.65	0.62
Rigid-Exp.	0.5	0.85	0.80	1.70	0.53	0.56	0.55

excitation of 0.5 g, but the spectral amplitude is amplified by a factor of 1.22 to the base at 10 Hz frequency. The high frequency components are damped out through the soil layer, however, unlike the case of soft boundaries the components 30 Hz and 90 Hz still exist with no amplification. The comparison of the accelerations at centre and off-centre of soil surface, similar to the result of experiments (Section 3.8.1), gives a rational uniformity of acceleration on the surface (Figure 3.13a, c and b, d) although the one at off-centre is slightly smaller than that at the centre.

The characteristics of the analyses and experiments on evaluation of boundary conditions are summarized in Table 3.6. Analytical results and experimental observations suggest that the soft material on the sides of the container walls are not efficient in simulating the free field situation (Table 3.6), but causes active soil failure within the container under high hydraulic gradient. It may be concluded that the soil response with rigid boundaries is closer to that in free field condition. The experimental results with rigid boundaries show that the soil response is only amplified within high frequency ranges which are far beyond the exciting frequencies and not in the ranges of interest. So the HGS device reasonably provide a high stress level which match the field conditions.

Chapter 4

Test Results

4.1 Introduction

In this chapter, the test results on model piles are presented in terms of free vibrations and forced vibrations, using the technique of hydraulic gradient similitude modelling. The single piles with a mass on top were embedded in a dense sand foundations and the natural frequency and the damping behaviour of soil-pile system was investigated under various soil stress levels from the free vibration tests. Three series of forced vibration tests on a given model pile were then carried out under different stress level subjected to moderate to strong base excitation. The dynamic response of the superstructure and pile are presented herein. Cyclic p-y curves were also developed from the test data to study the nature of soil-pile interaction for various input excitations, compared with the backbone p-y curves for sand recommended by the API code (1987)

4.2 Free Vibration Tests

4.2.1 Introduction

This section describes the results of tests performed to determine the fundamental natural frequencies of the model piles. It is necessary to know the natural frequencies of the soil-pile-mass system in order to determine whether a resonance condition could develop during shaking. Resonance occurs if the frequency of the input base motion matches the fundamental frequency of the pile and results in significant pile flexure.

While higher mode vibration contributes to the overall pile response, theoretical analysis and the experimental data have shown that first mode vibration dominates. Therefore, experiments herein to define the fundamental frequencies of the model piles have been emphasized.

The natural frequencies of the soil-pile system and those of the free field are generally very different. The natural frequency of the soil-pile system depends upon the structural properties of the pile, the pile head mass and the lateral stiffness of the near field soil, while the natural frequencies of the free field depend on the soil layer thickness and stiffness values.

4.2.2 Test Procedures

The free vibration tests on model piles were performed in dense sand foundation. The technique of sand foundation preparation has been described in Section 3.7. After the preparation of the sand foundation at relative density D_r= 75%, the model pile was pushed into the sand deposit at the centre of the soil container with the help of a pile driving guide. The pile was driven to the bottom of the sand deposit with embedded length of 322.0 mm.

After necessary instrumentation wire connections and enclosure of the whole testing device, sand foundation was subjected to hydraulic gradient loading process until the given gradient was reached. Then, a series of free vibration tests on the model piles were carried out with "ring down" test in which the pile head was displaced a certain amount by pushing it and then released quickly so that the pile underwent free vibration. Pile head cap acceleration and lateral displacement were measured, respectively by a miniature accelerometer at the mass centre and two LVDT's. The miniature accelerometer was capable of measuring acceleration of $\pm$10 g.

4.2.3 Outline of Experiments

The experimental program was designed to examine the dynamic properties and the stiffness of pile foundations under various factors of influence, which may affect the pile response to seismic lateral loading. The results are interpreted in terms of pile head response to an initial perturbation at pile head, system stiffness and damping, and verification of modelling laws.

The free vibration testing includes three series of experiments on the behaviour of model pile response and experiments on the verification of modelling laws.

(1) The First Series of Free Vibration Texts

In this series, a model pile (pile 1)with diameter 6.35 mm was tested, with a simulated superstructure mass cap weighing 805.57 g clamped at the pile head, under a series of hydraulic gradient similitude scale factors (N). Initial displacement of perturbation at the head was 4 mm.

(2) The Second Series of Free Vibration Texts

In order to evaluate the effect of the amplitude of initial perturbation, i.e. strain level, on the behaviour of pile response, the initial displacement of 0.2 mm was applied to the same pile (pile 1) and set-up as that in the first series. The only difference from 1st series is nothing but initial lateral displacement amplitude.

(3) The Third Series of Free Vibration Texts

This series of tests were performed to estimate the influence of stiffness of the pile on the characteristics of the pile response. Another model pile (pile 2) of 9.525 mm in diameter were tested under the same testing condition as 1st series.

The characteristics of the above three series of tests are summarized in Table 4.1.

(4) Experiments of Verification of Modelling Law

This part of the testing was aimed to experimentally examine the dynamic modelling

Table 4.1: Summary of Three Series of Free Vibration Tests

Series No.	Pile No.	HGS N	Diam. (mm)	EI ($N \cdot mm^2$)	Cap Mass (g)	Initial Displ.(mm)
1	1	1-70	6.35	4.03×10^6	805.570	4
2	1	1-70	6.35	4.03×10^6	805.570	2
3	2	1-70	8.525	19.56×10^6	1119.825	4

Table 4.2: Verification of Modelling Law

Prototype Scale(mm)	N	Model Pile Diam.(mm)	Cap Mass(g)	Model Eccn.(mm)	Cap Size(mm) (Ht.×Diam.)	Initial Disp.(mm)
D_p=304.8	24	12.7	2654.4	97.900	76.2 × 76.2	6.60
(12 in)	32	9.525	1119.825	73.425	57.15 × 57.15	4.95
E_p=2349.6	48	6.35	331.8	48.950	38.1 × 38.1	3.30
D_p=457.2	36	12.7	2654.4	88	76.2 × 76.2	5.60
(18 in)	48	9.525	1119.825	66	57.15 × 57.15	4.20
E_p=3168.0	72	6.35	331.8	44	38.1 × 38.1	2.80

Note:
(i) Initial displacements (X_0) were applied laterally to the centre of pile head mass;
(ii) Subscripts m and p express "model" and "prototype" scales respectively;
(iii) N indicates the HGS scale factor.

laws indirectly. The "modelling of models" technique was used as described in Chapter 3. Three model piles were tested under different scale factors to simulate the same prototype. The testing characteristics of verifying modelling laws are given in Table 4.2.

4.2.4 Variation of Soil-Pile Stiffness with Soil Stress Level

The free vibration tests described in this section were carried out using single piles embedded in dense sand. Three different series were performed at different hydraulic gradients for all series, the sand deposit was 322 mm in height and had an average void ratio of 0.655, corresponding to an average relative density of 75%; the distance between

the soil surface and the centre of gravity of the pile head mass (eccentricity or pile head stick-up) was 50.4 mm. The tests were carried out by displacing the pile head mass laterally and then releasing it from its initial displaced position, setting it into free vibration. In Series I and Series III, the pile heads were subjected to the same initial lateral displacement of 4 mm, but in Series II, the pile head was subjected to 2 mm of displacement.

Figures 4.1a, 4.1c and 4.2a show typical pile head acceleration responses for Series I, series II and series III, respectively, at N=30. These are typical responses of underdamped system. The vibrations continued for more than seven cycles. The fundamental natural frequencies of soil-pile system can be determined from the time between acceleration peaks. For the tests shown in Figures 4.1a , 4.1c and 4.2a, the frequencies are 16.6, 17.6 and 23 Hz, respectively. The natural frequencies were also obtained from the Fourier spectra and, as shown in Figures 4.1b, 4.1d and 4.2b, are 16.6, 17.6 and 23 Hz, respectively, in agreement with those obtained from the pile head acceleration response.

Each series of pile free vibration tests were carried out over a range in hydraulic gradients but at the same initial lateral displacement to evaluate the variation of the natural frequencies with the stress level. Figure 4.3 shows the relation between natural frequency, f_n, of the pile and HGS scale factor, N, for the three series of free vibration tests. The data show that the natural frequency of the pile increases linearly with the hydraulic gradient in log-log space with a slope 0.25, which implies that $f_n = cN^{0.25}$, where c is a constant. This pattern was followed by all three series of tests, which confirms the usual result from resonant column tests. The similar result was found on centrifuge modelling tests for cocking towers by Morris (1981).

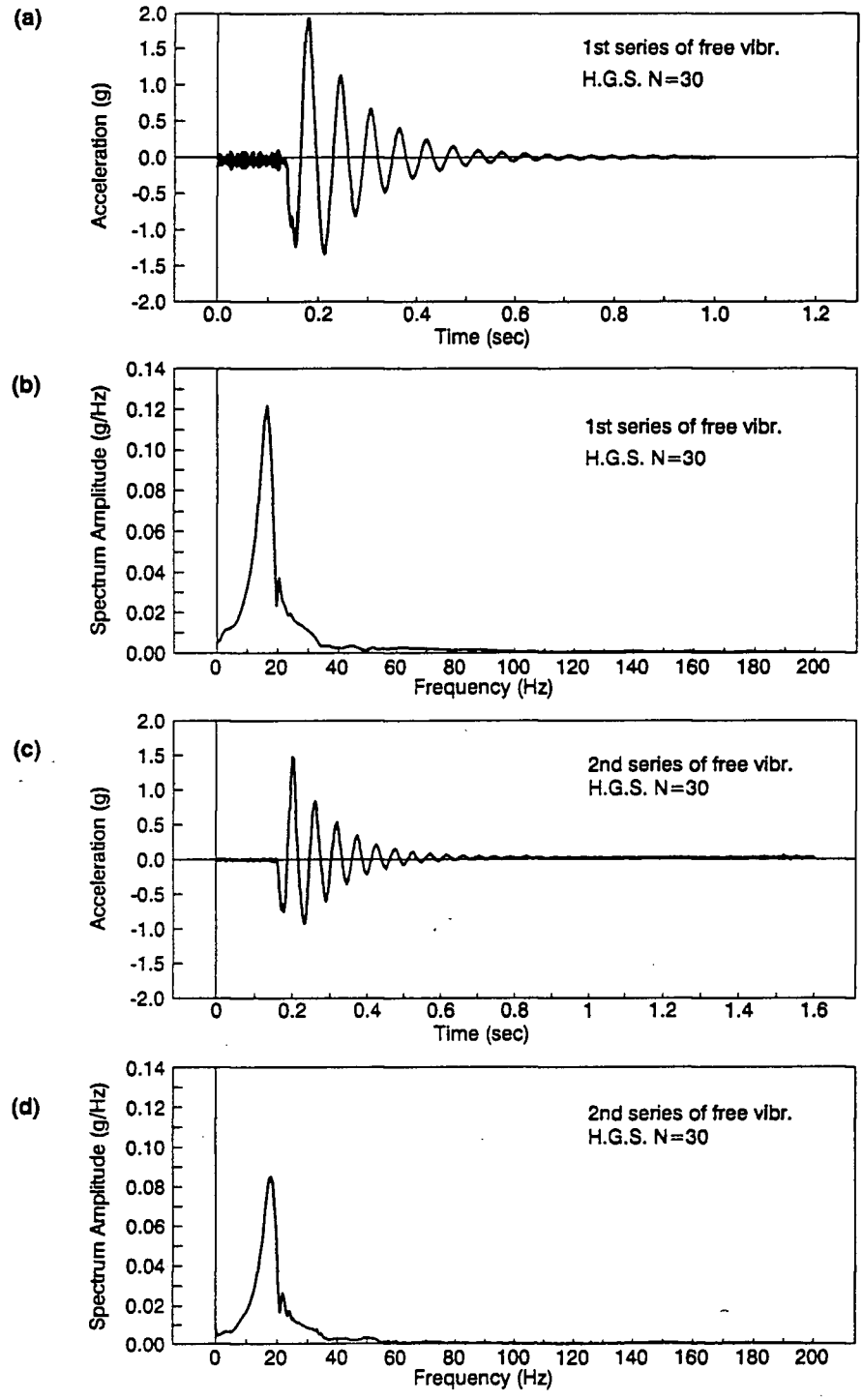

Figure 4.1: Typical example of free vibration tests - Series I and II (a) and (c) pile head acceleration response (b) and (d) Fourier spectra of the accelerations

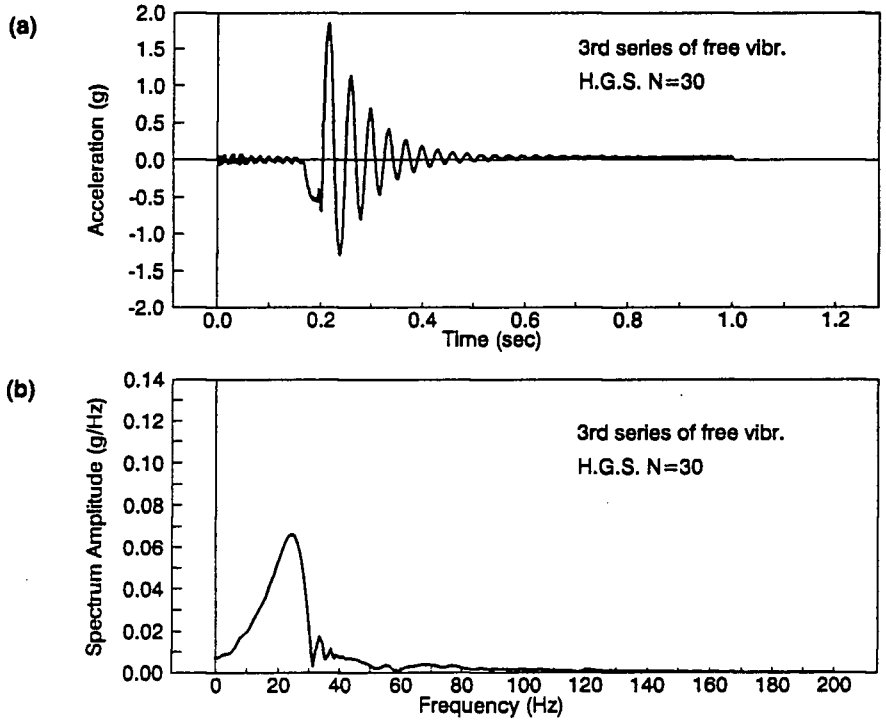

Figure 4.2: Typical example of free vibration tests-Series III (a) pile head acceleration response (b) Fourier spectrum of the accelerations

Figure 4.3a also shows that the initial displacement magnitude (or strain level) effect on the natural frequencies of the same pile-soil system. It is clearly shown that the pile-soil system subjected to a higher lateral displacement has a lower frequency (or stiffness) than that subjected to a lower one. A reduction of 50% in the initial displacement causes an increase of 10% in the natural frequency. During pushing at the pile head, a complex strain field is set up around the pile which alters the insitu moduli. The insitu shear moduli control the lateral stiffness of the soil adjacent to the pile and are strain level dependent. The higher shear strain or amplitude of the pile vibration causes higher reduction of the shear moduli, and further a higher reduction of soil stiffness. Thus, the natural frequencies of the pile will depend on the amplitudes of the pile vibration where measured. The result suggests that at the same stress level (i.e. same N), A higher amplitude of the vibration results in a lower natural frequency of the pile.

a

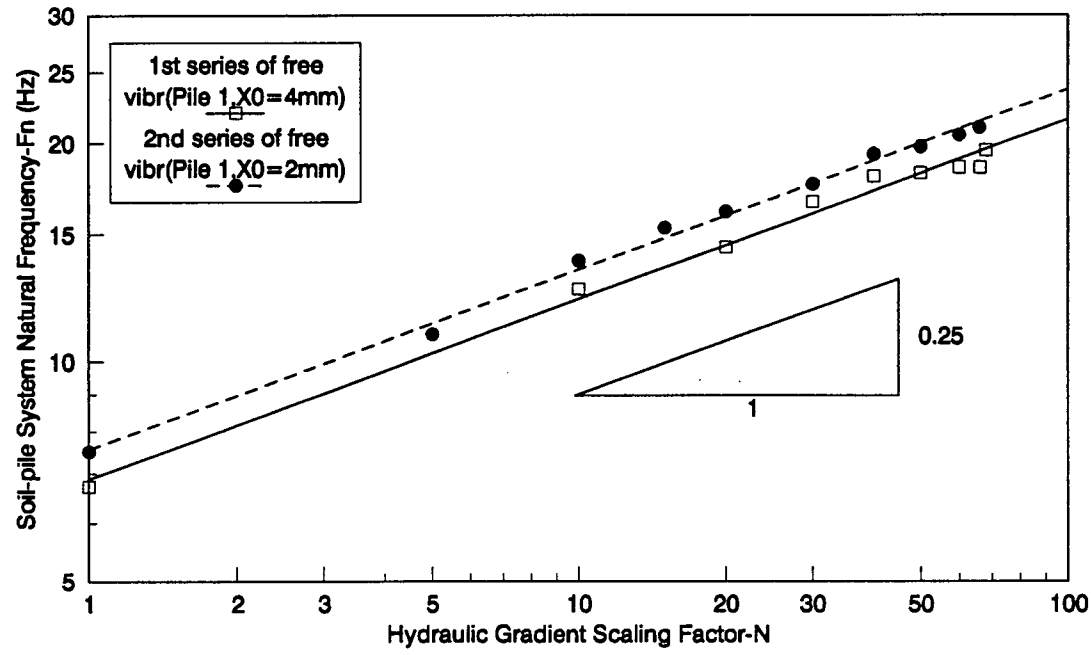

b

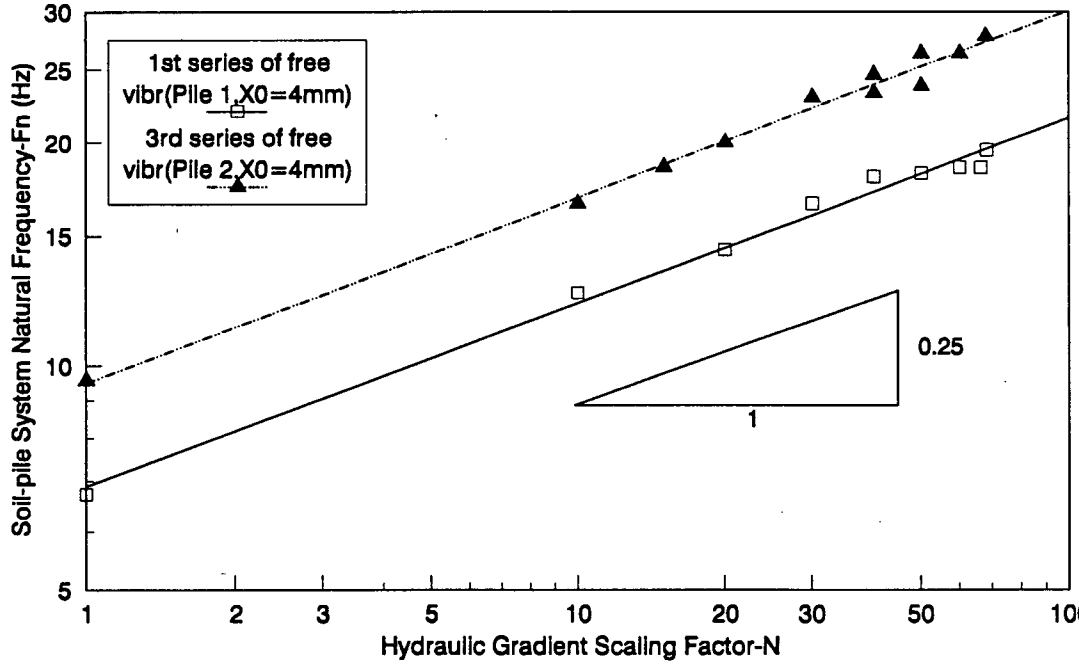

Figure 4.3: Variation of pile natural frequency with soil stress level

The influence of the pile stiffness on its natural frequency was tested and shown in Figure 4.3b. The figure demonstrates that the stiffer pile has a higher natural frequency. The flexural rigidity of pile 2 is about 4.8 times that of pile 1, and the frequency is about 1.4 times that of pile 1 at a certain stress level.

If the natural frequency of the piles is normalized with respect to the first natural frequency of the soil deposit, i.e. $(f_n)_{soil} = V_s/4H$, where V_s and H are the shear wave velocity and depth of soil deposit, respectively. The normalized pile natural frequency appears to be independent of the soil stress level, as shown in Figure 4.4.

As described in Section 4.2.1, the single piles tested primarily vibrates at its first mode. Based on the observation and findings of the tests, the pile of free vibration may be simplified as a cantilever which is free with a lumped mass at the head and fixed at a certain depth of sand foundation. The depth (length) between the centre of lumped mass and fixed end is referred to as "equivalent length" of the pile. Then, the theory of elastic beam was applied to compute the equivalent length of the piles from measured frequency and physical properties of the piles, as given in Equation 4.1:

$$L_e = (\frac{3EI}{4\pi^2 f_n^2 M})^{1/3} \tag{4.1}$$

Where EI and f_n refers to pile rigidity and natural frequency, respectively, M is pile head cap mass.

Figure 4.5 gives the variation of the equivalent length of the piles with soil stress level. It is seen that the equivalent lengths of the piles decrease with stress due to an increase in soil stiffness. Furthermore, the data indicate that the equivalent length decrease slowly at the portion of higher stress level, and finally may reach a ultimate value, depending on

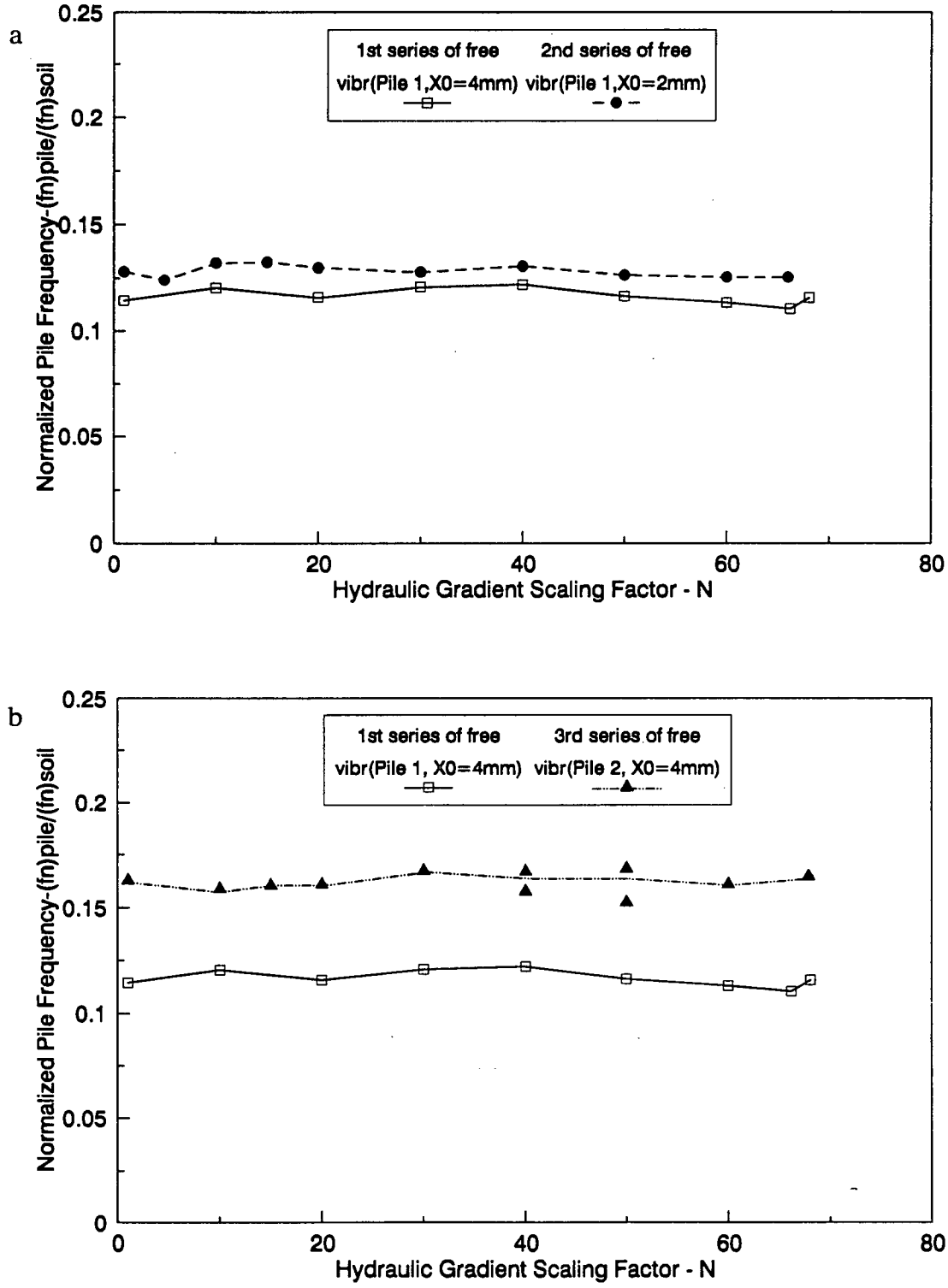

Figure 4.4: Variation of normalized pile natural frequency with soil stress level

the soil stiffness. For the tests of same pile (Series I and Series II) undergoing different initial lateral deflections (Figure 4.5a), the higher deflection results in a longer equivalent length at the same stress level. And Figure 4.5b shows that the pile with higher stiffness, subjected to the same initial lateral deflection (X_0 = 4 mm), has a longer equivalent length than that with lower stiffness (Series I and III). The maximum equivalent lengths are 203, 189 and 243 mm, respectively for Series I, Series II and Series III.

4.2.5 Damping Behaviour of Soil-Pile System

The decay in the acceleration amplitude results from the soil-pile system damping such as shown in Figure 4.1a. An equivalent viscous damping of the system can be obtained from the oscillatory decay following initial perturbation by logarithmic decrement method of the amplitude.

Figure 4.6 shows the equivalent viscous damping of the soil-pile system. It is shown that the damping is nearly independent of soil stress levels, but appears to be dependent on vibration amplitude. A large vibration amplitude induces a higher damping at the first cycle than a small amplitude at the sixth cycle as suggested from the three series of tests. The average damping ratios for different cycles are summarized in Table 4.3. The damping ratios at the first cycles are observed to be 1.4 to 1.6 times that at the sixth cycles. The damping ratio ranges from 5.5% to 9.1% for the material tested, depending upon the deflection level and the pile stiffness.

The equivalent damping obtained from the logarithmic decrement of amplitude represents the total damping, i.e. material damping and radiation damping, of the system. The strong dependency of the measured damping on the vibration amplitude suggests that the major component of the measured damping results from material damping rather than radiation damping, i.e. the overall damping is dominated by material damping. The theoretical studies (Nogami and Novak, 1977) have shown that material damping is the

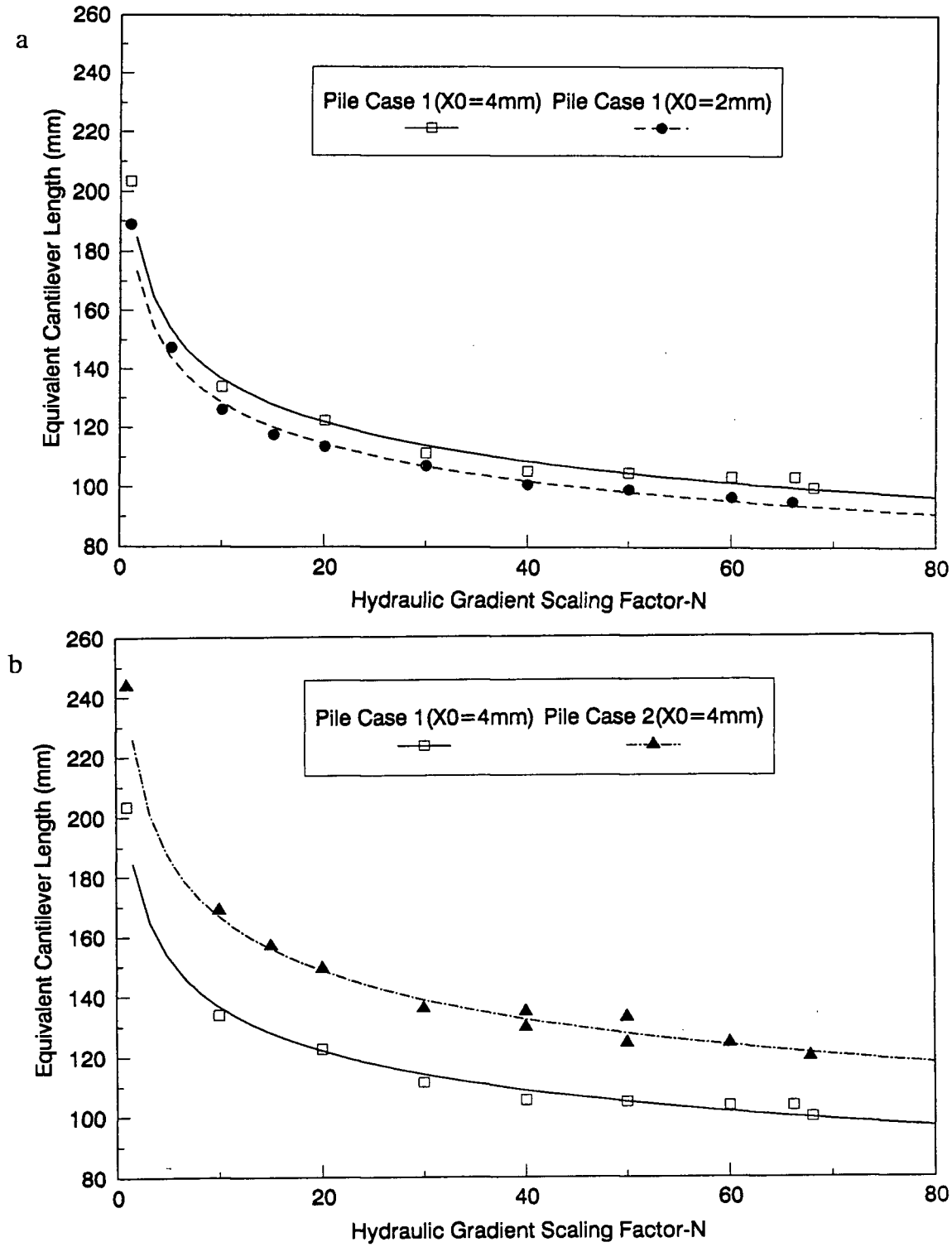

Figure 4.5: Vibration of pile equivalent length with soil stress

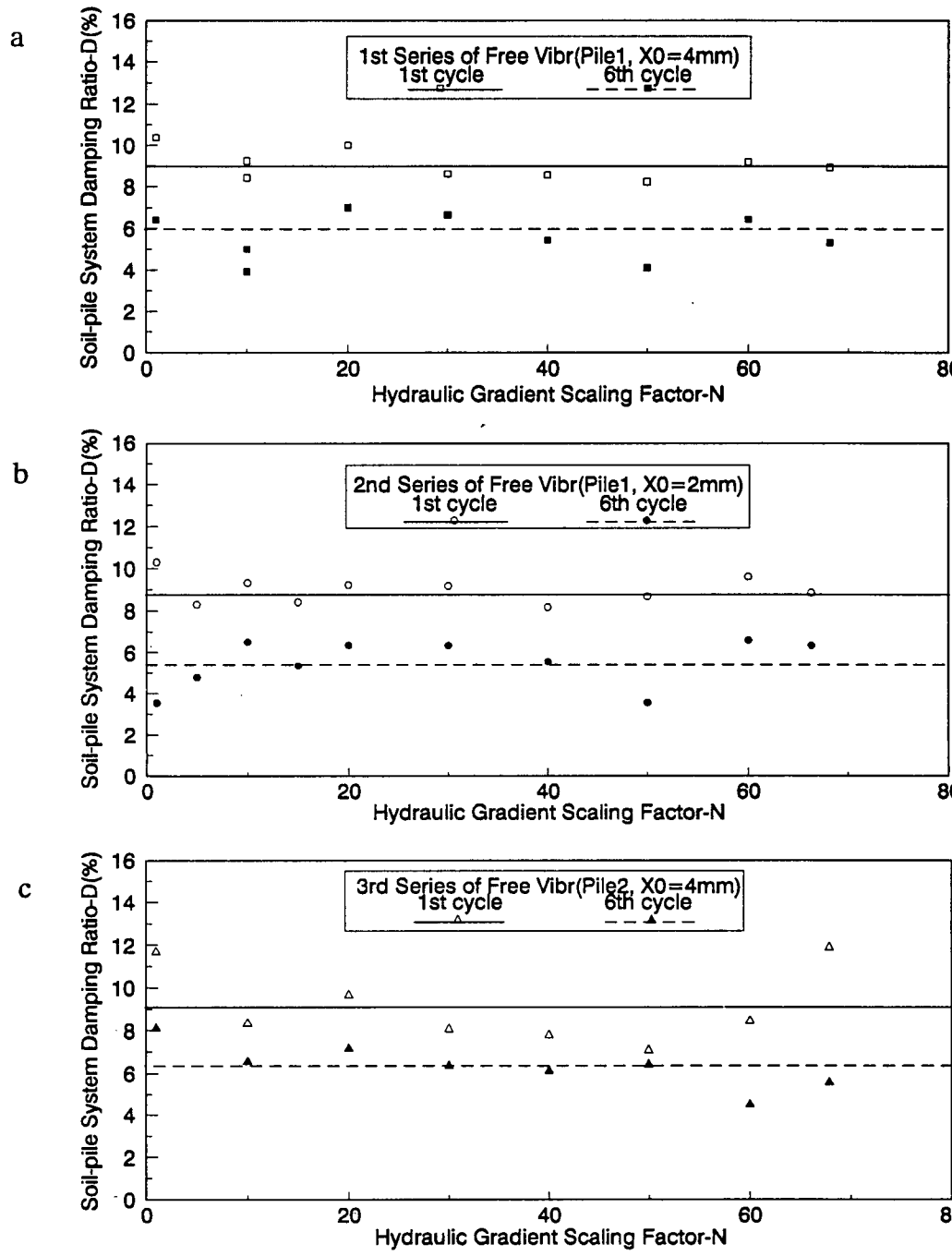

Figure 4.6: Soil stress level effect on equivalent viscous damping ratio

Table 4.3: Average Damping Ratios at Different Cycles

Series No.	D(%) at 1st Cycle	D(%) at 6th Cycle	EI ($N \cdot mm^2$)	Init. Disp. X_0 (mm)
I	9.0	6.0	4.03×10^6	4
II	8.9	5.5	4.03×10^6	2
III	9.1	6.4	19.56×10^6	4

major source of system damping when pile is vibrated in a frequency lower than the natural frequency of the soil deposit, as is the case for these tests (Figure 4.4). In the absence of radiation damping, the rigid boundary would have little effect on the free vibration test results.

4.2.6 Verification of the Modelling Laws

A hydraulic gradient model test, like centrifugal modelling, may be regarded as an experiment on models at full-scale stress level without a specific prototype, with which a numerical approach is to be assessed. A given prototype condition can be modelled with different geometric models at certain corresponding scale factors. Therefore, although it is impossible to verify the modelling laws by comparing the quantity of model piles with equivalent full-size structures, it is possible to evaluate the method by modelling the same full-scale structure (prototype) at different scales and checking the coincidence of the predicted full-scale results, referred to as modelling of models. The hydraulic gradient modelling laws for dynamic laterally loaded pile tests are described in Table 3.1 (Section 3.1).

Three geometrically similar piles of different sizes were made in the ratio 1:1.5:2 and tested under free vibration in terms of natural frequency, so as to verify the modelling relations. These three models were tested in the scaled parameters of a 6.35 mm diameter

pile at N=48, a 9.525 mm diameter pile at N=32, and a 12.7 mm diameter pile at N=24. Each model pile was then modelling the same prototype pile of diameter 304.8 mm (12 in). Another prototype pile with diameter 457.2 mm (18 in) was also modeled as listed in Table 4.2. According to the modelling laws, the natural frequency of a model $(f_n)_m$, at a modelling scale of N, has a relation with the natural frequency of the prototype structure $(f_n)_p$ such as:

$$(f_n)_m = N(f_n)_p \tag{4.2}$$

which implies that the frequencies of the models are linearly proportional to the HGS scale factor N as $(f_n)_p$ is constant. Therefore, if the model frequencies of the same prototype are plotted versus the scale factor N, they should form a straight line through the origin.

Figure 4.7 shows the testing results, and in both cases a straight line passing through the origin was obtained, which confirms that the modelling laws in HGS tests are satisfied.

Some experimental error would be expected because the piles were not, as a matter, perfectly geometrically similar due to the factors of identical size of accelerometers and basically the same proximity of the size of the container in all cases, thus the boundary conditions were not scaled in exactly correct proportion. However, the experimental results of the satisfication of modelling laws indicate that these effects appear to be very small.

4.3 Forced Vibration Tests

4.3.1 Introduction and Experimental Program

In this section, an experimental study of dynamic pile response, using hydraulic gradient shaking table techniques, is presented. The single instrumented pile was embedded in a dense sand deposit with relative density of 75% and then subjected to moderate and

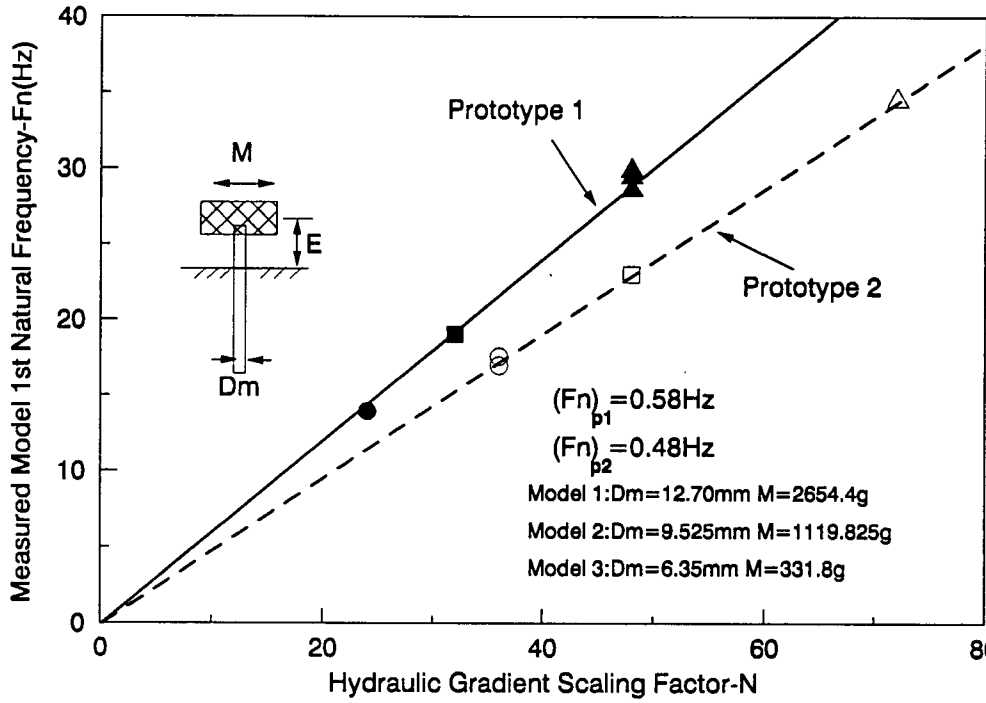

Figure 4.7: Verification of HGS modelling law

strong sinusoidal base shaking with a set of input frequencies under a given hydraulic gradient. The behaviours of the superstructure and pile response as well as soil-pile interactions were studied in order to better understand the pile foundation response under earthquake loading, and to enrich a data base with which the current analytical approaches can be assessed. The cyclic p-y curves were then developed from the test data to evaluate the nature of soil-pile interaction for various tests.

Sand sample preparation and experimental setup were already described in Chapter 3. During the tests, pile head acceleration and lateral displacements were measured, respectively, by a miniature accelerometer at the head mass centre and two LVDT's. Acceleration of free field and input base excitation were also measured. In addition, the strain gauges installed on the pile measured the bending moment distribution along the pile at any instant time.

In the experimental program of forced vibration tests, three series of tests were preformed. For all forced vibrations, the same model pile of 6.35 mm diameter with a simulated superstructure mass, weighing 805.57 g, clamped at the pile head having eccentricity of 57.6 mm to the soil surface was used. Void ratio (or relative density) changes in the dense sand tested were found to be negligible. The pertinent test characteristics of all series are summarized in Tables 4.4, 4.5 and 4.6.

Series I were carried out with an expected base excitation of peak average acceleration of 0.5 g, herein referred to as strong excitation under HGS scale factor, N, of 60. In this case, the natural frequency of the model pile is about 17.54 Hz determined from a free vibration test.

Series II were also performed with an expected base excitation of peak average acceleration of 0.5 g, but under HGS scale factor of 30. Moreover, the natural frequency of the model pile is around 15.75 Hz for this series.

Series III were conducted with an expected base excitation of peak average acceleration of 0.2 g, herein referred to as a moderate excitation, under HGS scale factor of 60. The natural frequency of the model pile is the same for this series as for series I.

Through the above three series tests, the behaviours of the pile foundation response were extensively investigated under different effect factors such as, excitation frequencies, excitation intensities, and stress level. The results are given and discussed in the following sections.

4.3.2 Superstructure Response

(A) Acceleration and Displacement

Experiments on seismic response of soil-pile-structure system were broadly carried out, involving three series as depicted in Table 4.4, 4.5 and 4.6. However, in this thesis,

Table 4.4: Series I Forced Vibration (N=60, Strong Excitation)

Test No.	Input Freq.(Hz)	$\ddot{x}_{bs}$ (g)	$\ddot{x}_{ff}$ (g)	$\ddot{x}_{hd}$ (g)
1	5	0.457	0.520	0.536
2	10	0.472	0.669	0.673
4	14	0.485	0.616	0.956
5	16	0.454	0.541	1.414
7	17.54	0.493	0.560	1.700
8	20	0.505	0.545	1.441
11	22	0.410	0.420	1.030
12	26	0.490	0.580	0.712
15	30	0.661	0.985	1.112
17	40	0.411	0.592	0.685
21	50	0.494	0.690	1.413

only some examples of typical response history of accelerations and displacements at pile head mass are given for three series.The input base, free field and pile head accelerations measured for tests I-4, I-7, I-15, II-10 and III-7 are shown in Figures 4.8 to 4.17 together with their corresponding Fourier Transforms. It should be noted that the input exciting frequencies for tests I-4, I-7 and I-15 are less than, nearly equal, and greater than the natural frequency, about 17.54 Hz, of the soil-pile system, respectively. For test II-10 and III-7, the forcing frequencies are the same as the natural frequencies, about 15.75 Hz and 17.54 Hz, of the pertinent models, respectively.

From Figures 4.8 to 4.10 for Series I, it is seen that the sinusoidal input motion is reasonably symmetric and dominated by a corresponding input exciting frequency component of 14 Hz, 17.54 Hz and 30 Hz respectively. Minor high frequency contents are also present. Following several cycles of low amplitude vibration the input acceleration achieved a steady state response averaging 0.485 g, 0.493 g and 0.661 g, respectively.

Free field surface accelerations are seen to in phase with the base accelerations and

Table 4.5: Series II Forced Vibration (N=30, Strong Excitation)

Test No.	Input Freq.(Hz)	$\ddot{x}_{bs}$ (g)	$\ddot{x}_{ff}$ (g)	$\ddot{x}_{hd}$ (g)
2	5	0.490	0.588	0.593
4	10	0.495	0.540	0.542
6	12	0.475	0.771	0.788
8	14	0.515	0.646	1.415
10	15.75	0.486	0.710	1.641
11	18	0.497	0.548	1.778
12	20	0.487	0.558	1.214
13	22	0.524	0.506	1.036
14	24	0.465	0.628	1.050
15	26	0.480	0.737	0.400
16	28	0.448	0.744	0.440
17	30	0.505	0.930	0.562
18	34	0.483	0.748	0.504
19	40	0.471	0.584	0.664
20	44	0.502	0.612	1.114
21	50	0.494	0.712	0.780
21	60	0.442	0.660	0.354
23	70	0.480	0.811	0.427

Table 4.6: Series III Forced Vibration (N=60, Strong Excitation)

Test No.	Input Freq.(Hz)	$\ddot{x}_{bs}$ (g)	$\ddot{x}_{ff}$ (g)	$\ddot{x}_{hd}$ (g)
1	5	0.204	0.307	0.310
2	10	0.155	0.206	0.231
4	14	0.192	0.276	0.446
5	16	0.246	0.313	0.712
7	17.54	0.286	0.326	1.472
8	20	0.059	0.124	0.227
10	22	0.093	0.126	0.129
11	26	0.184	0.187	0.190
12	30	0.190	0.242	0.375
13	40	0.163	0.194	0.317
14	45	0.202	0.293	0.545
15	50	0.180	0.236	0.723
16	55	0.180	0.220	0.480
17	60	0.121	0.148	0.266
18	70	0.218	0.266	0.164

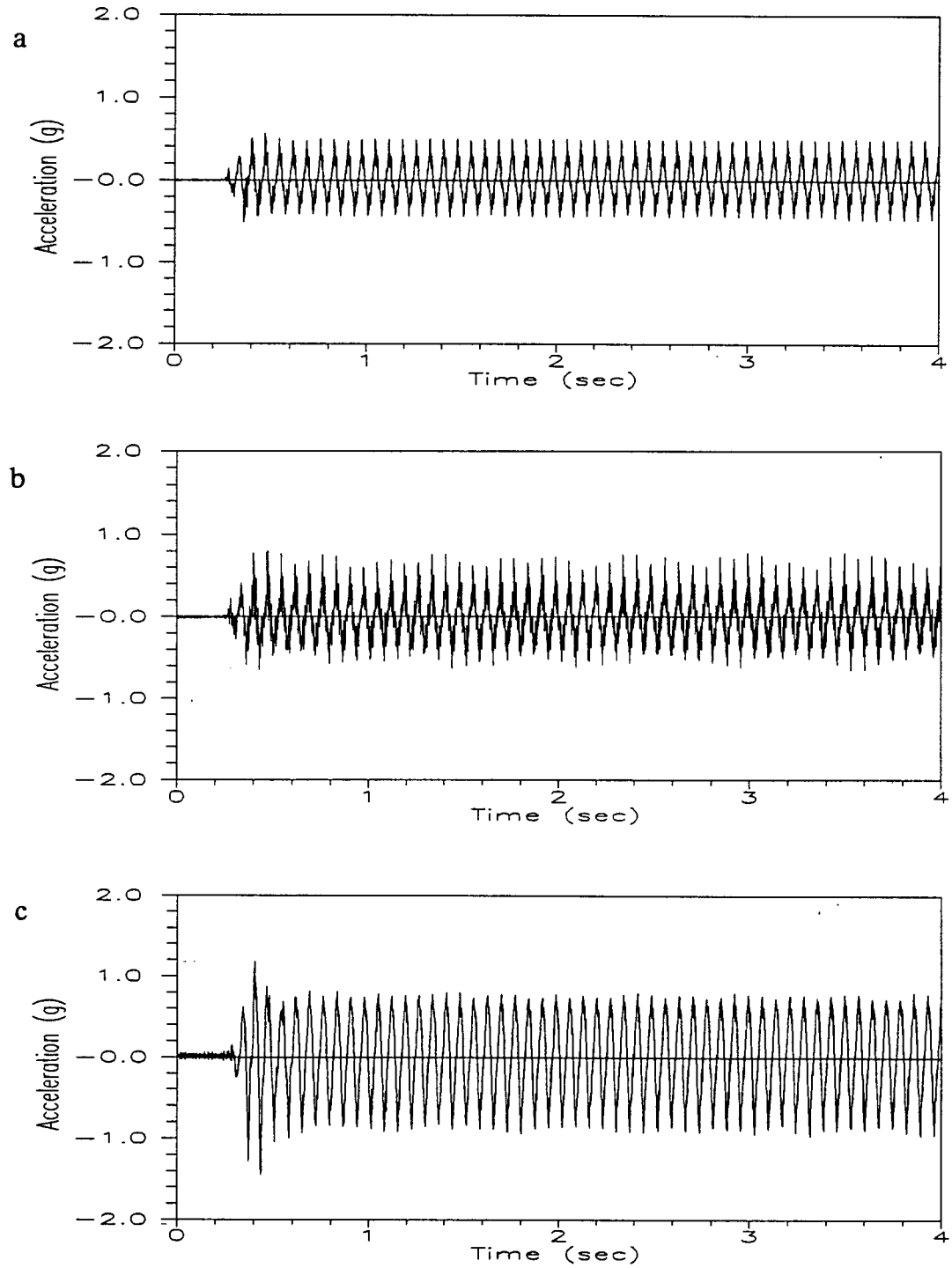

Figure 4.8: Measured accelerations: test I-4 (a) input base (b) free field (c) pile head mass

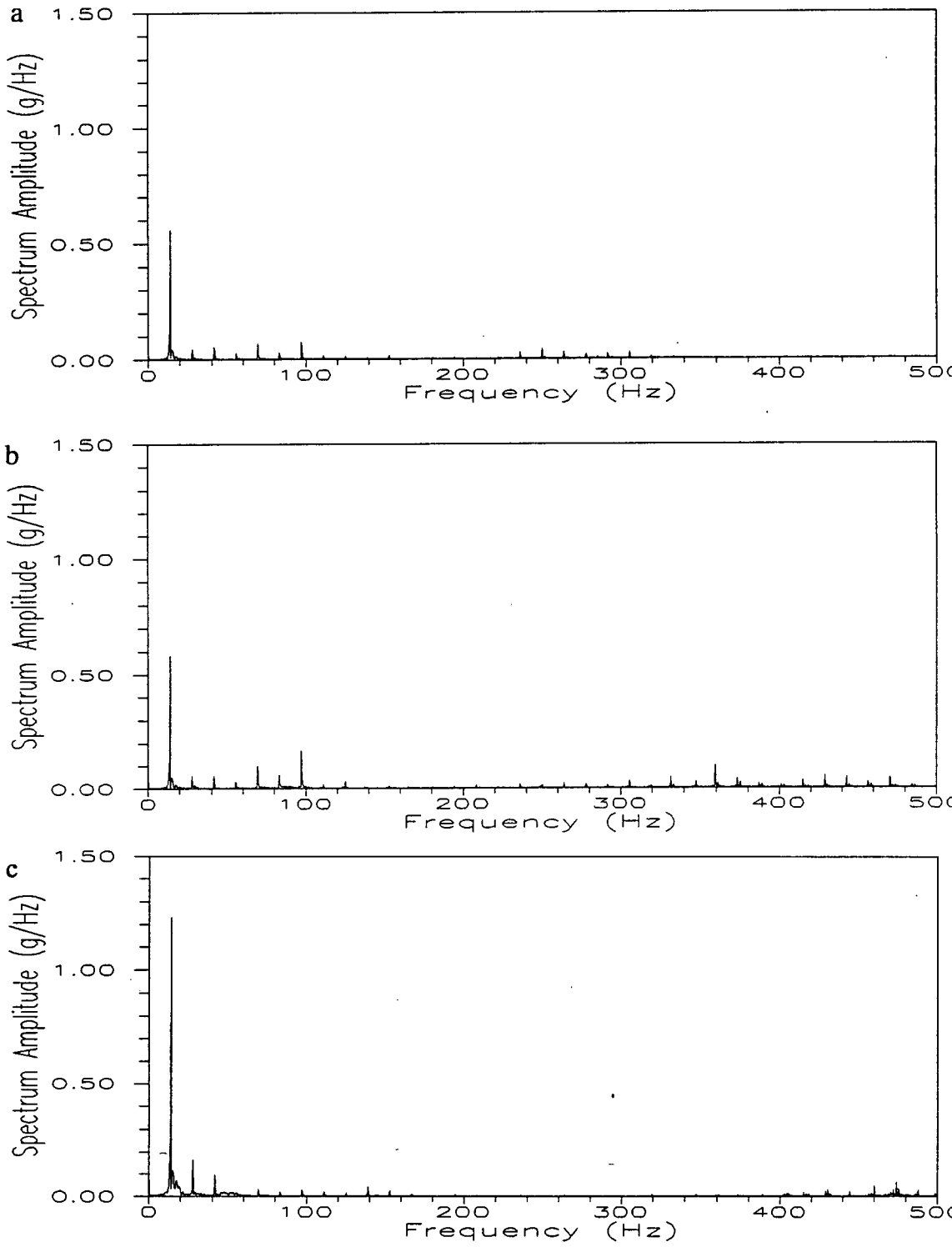

Figure 4.9: Fourier transforms of accelerations: test I-4 (a) input base (b) free field (c) pile head mass

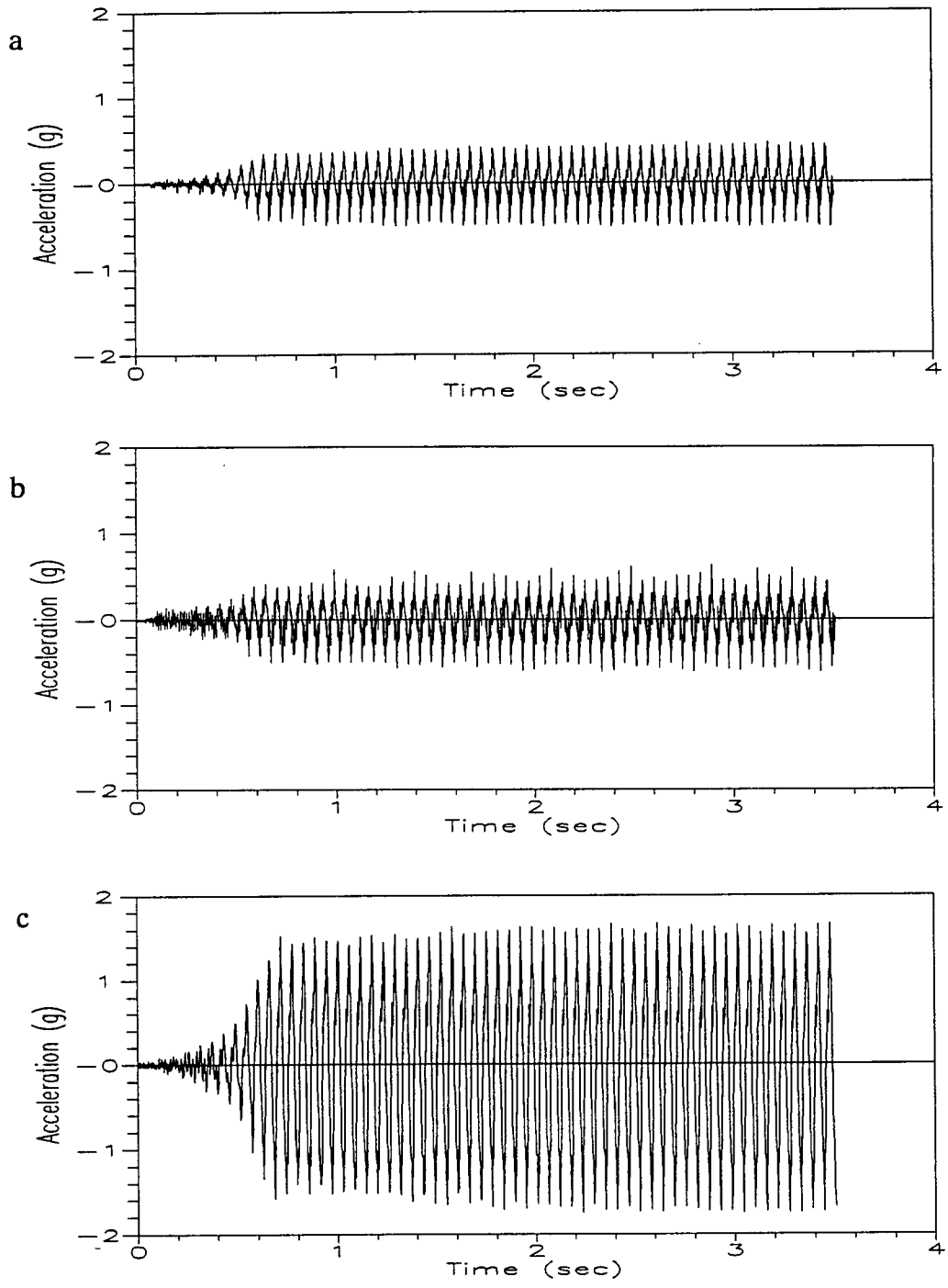

Figure 4.10: Measured accelerations: test I-7 (a) input base (b) free field (c) pile head mass

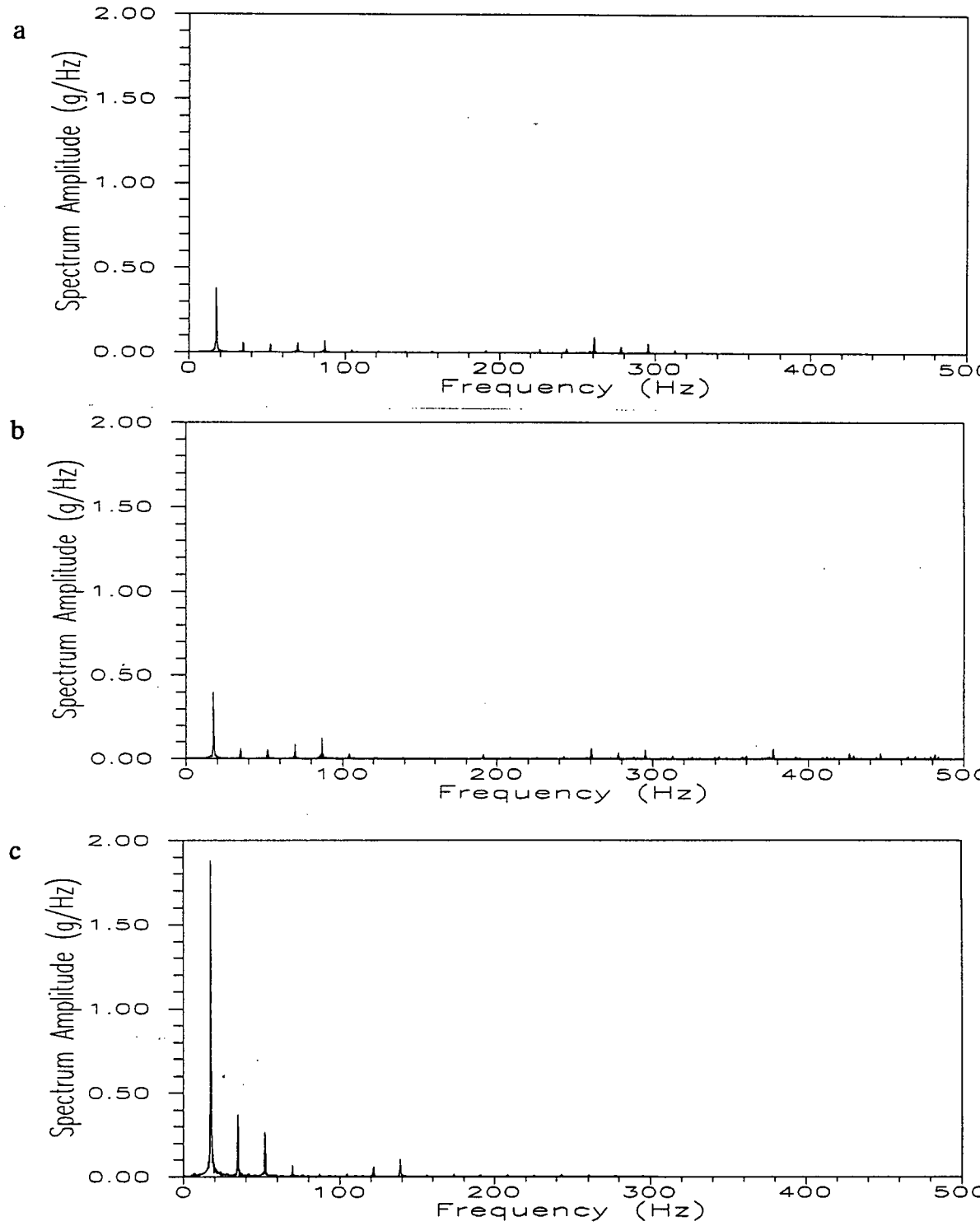

Figure 4.11: Fourier transforms of accelerations: test I-7 (a) input base (b) free field (c) pile head mass

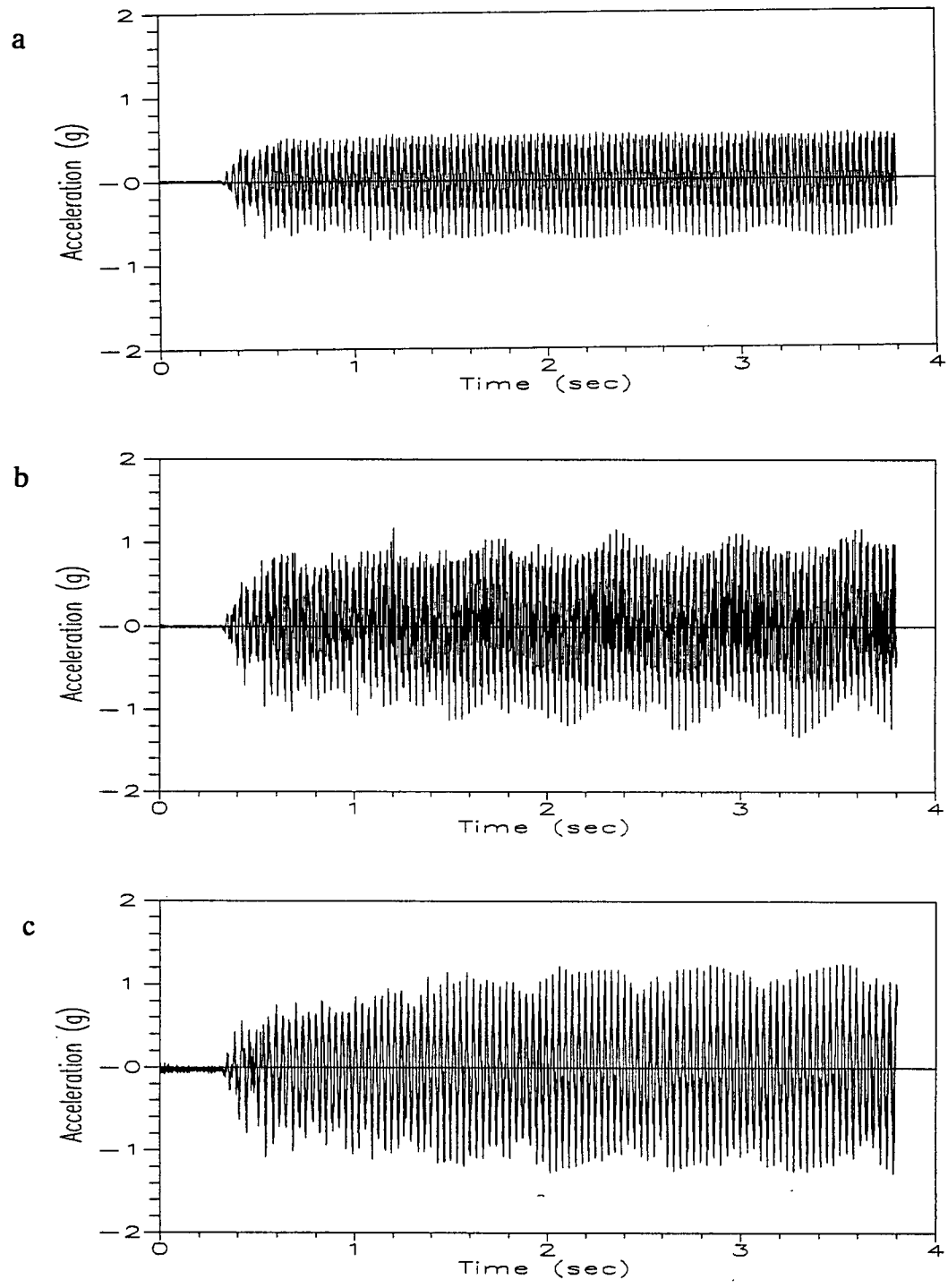

Figure 4.12: Measured accelerations: test I-15 (a) input base (b) free field (c) pile head mass

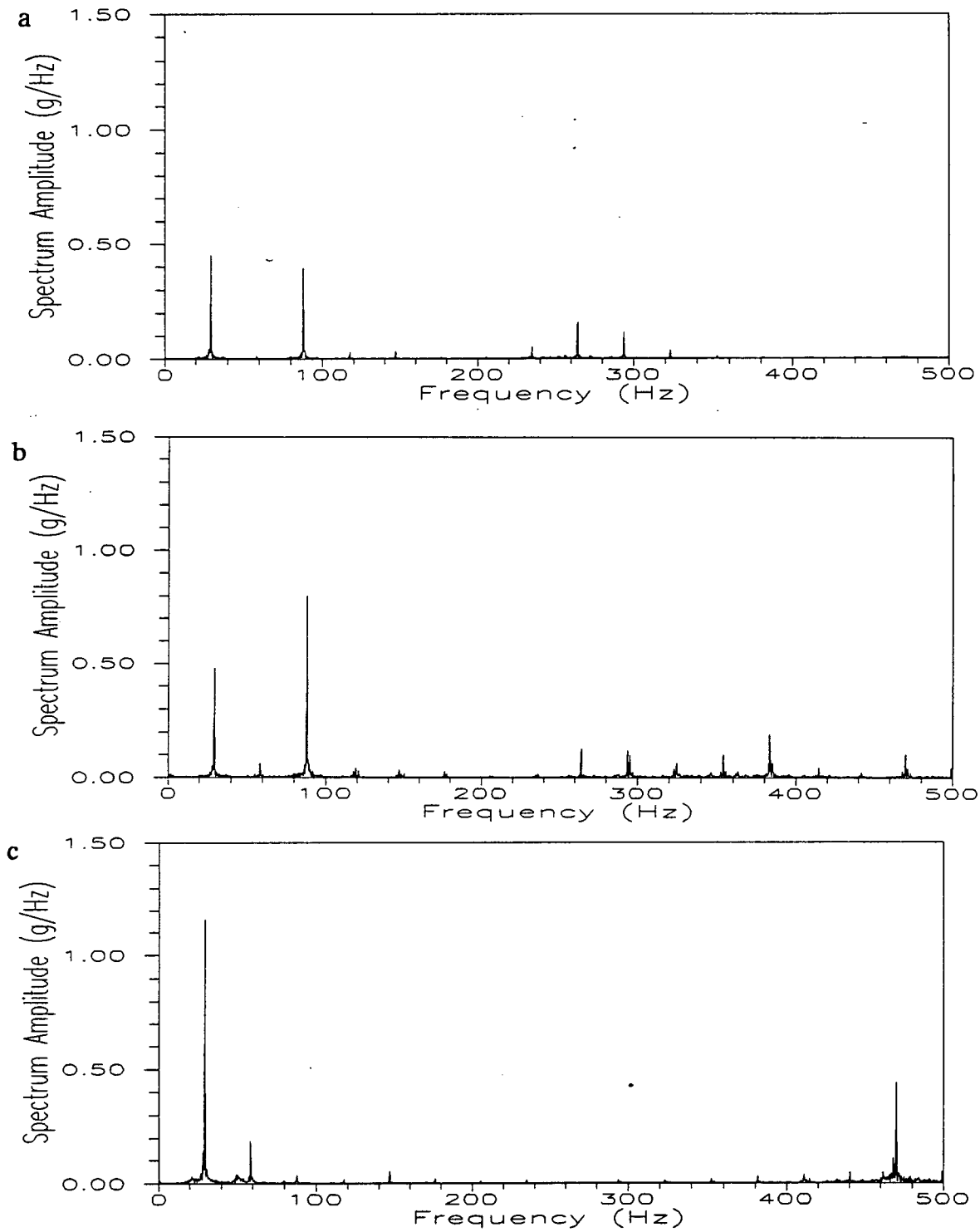

Figure 4.13: Fourier transforms of accelerations: test I-15 (a) input base (b) free field (c) pile head mass

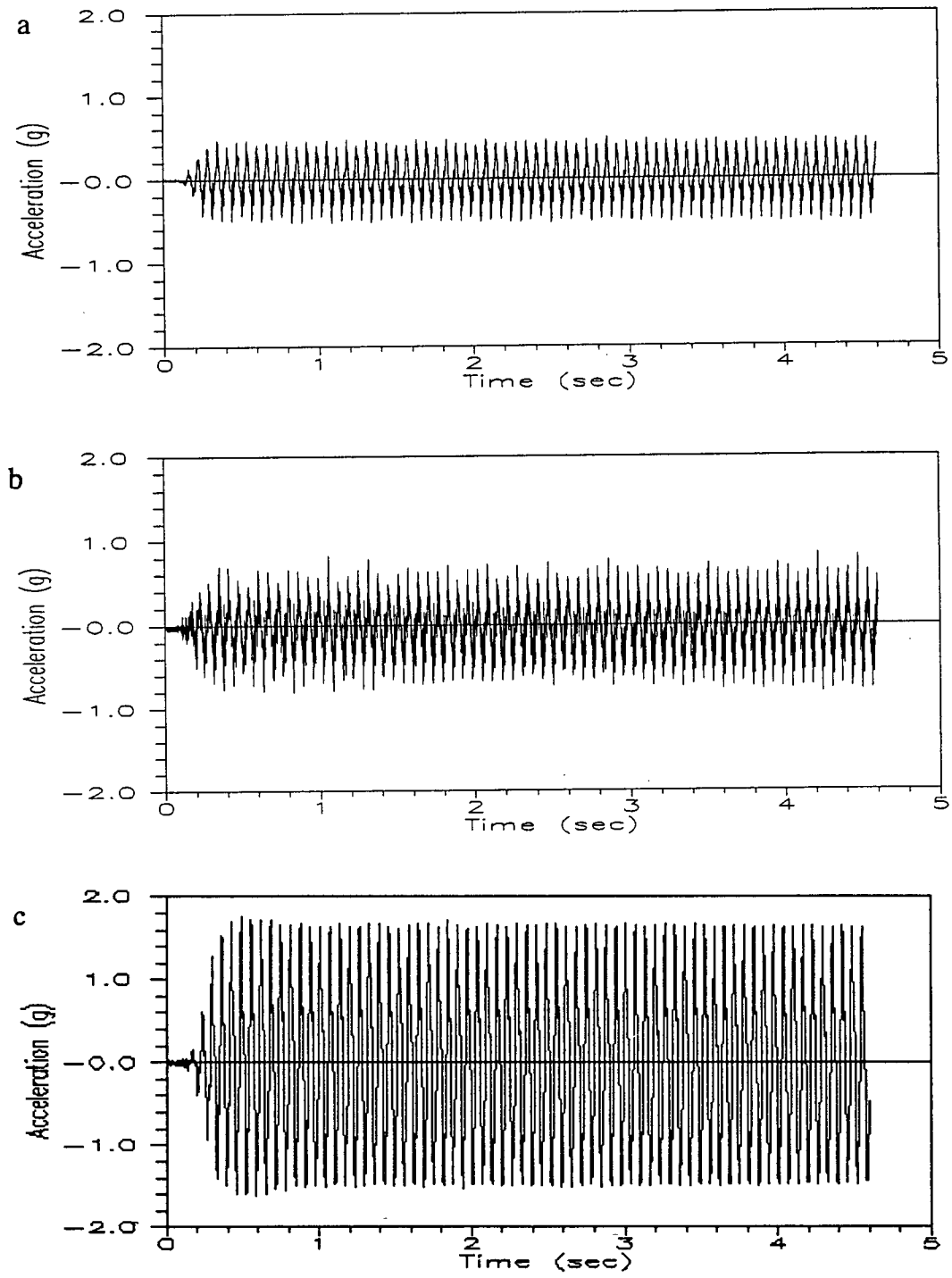

Figure 4.14: Measured accelerations test: II-10 (a) input base (b) free field (c) pile head mass

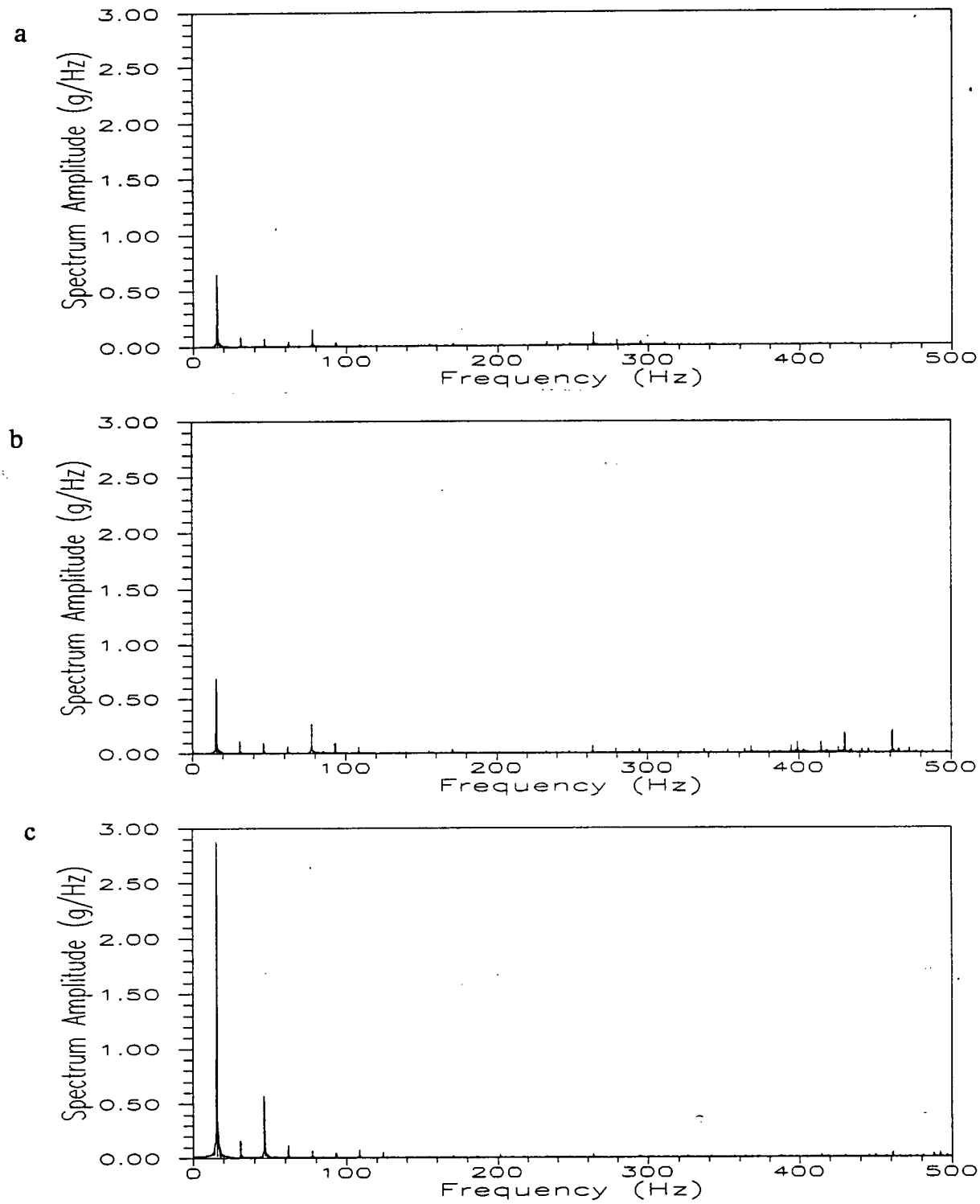

Figure 4.15: Fourier transforms of accelerations: test II-10 (a) input base (b) free field (c) pile head mass

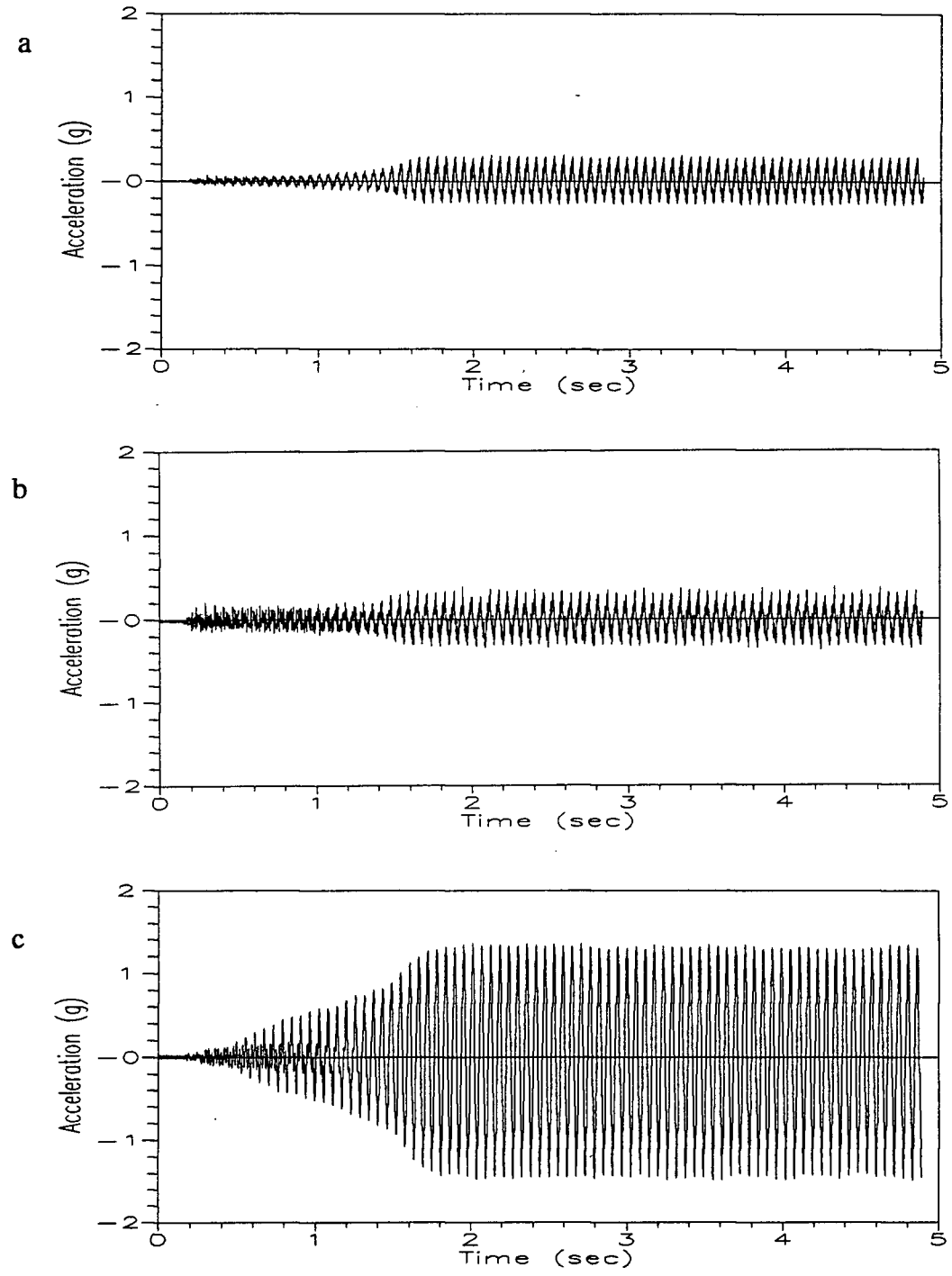

Figure 4.16: Measured accelerations: test III-7 (a) input base (b) free field (c) pile head mass

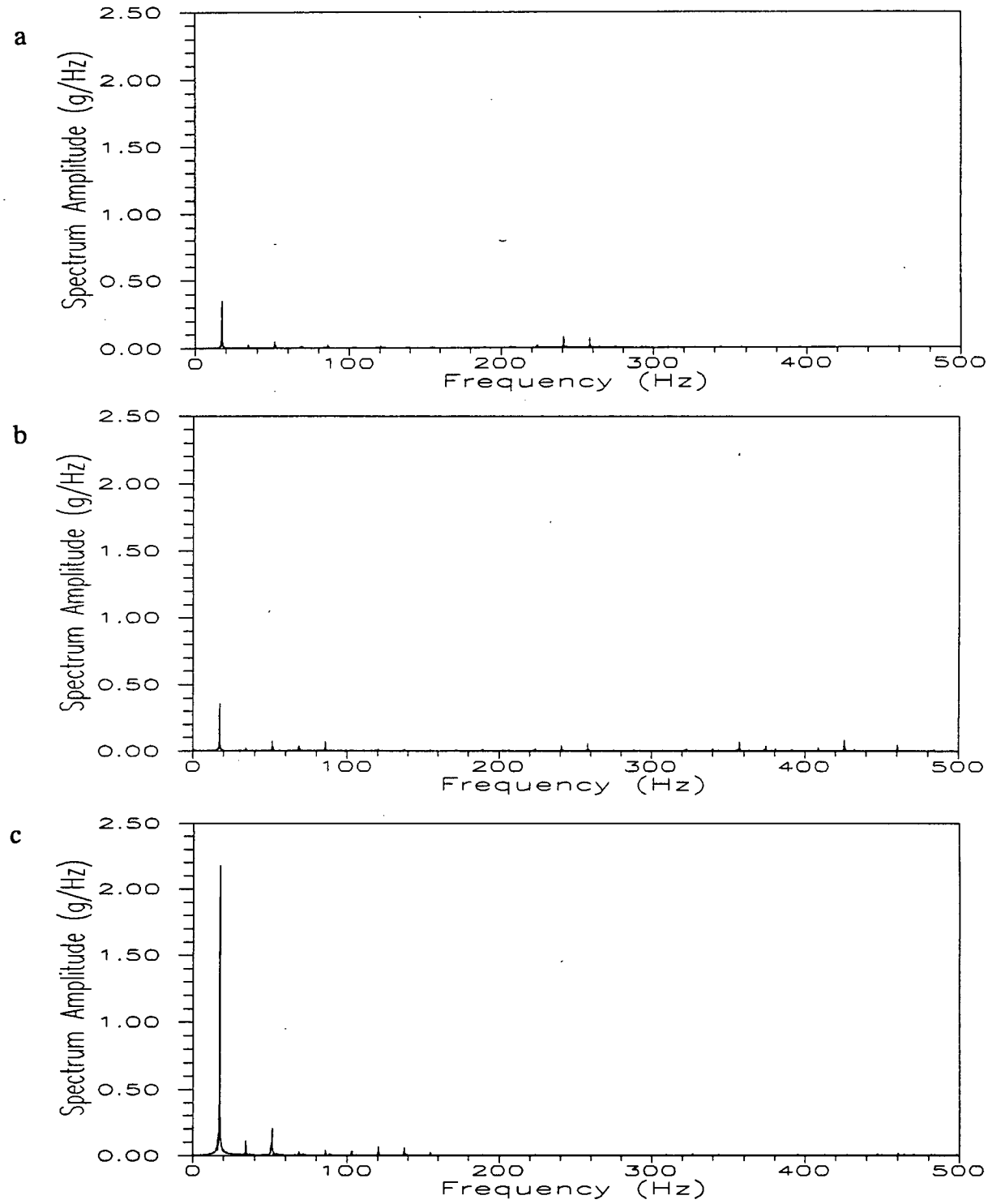

Figure 4.17: Fourier transforms of accelerations: test III-7 (a) input base (b) free field (c) pile head mass

were amplified through the sand by very small factors of 1.27, 1.13 and 1.49, respectively, to levels of approximately 0.616 g, 0.56 g and 0.985 g during steady state excitation.

Following the initial several cycles of small amplitude input excitation, pile head accelerations averaging 0.956 g, 1.707 g and 1.112 g were measured in the steady state region of response for tests I-4, I-7 and I-15, respectively. The data show that pile head accelerations were amplified to a different extent relative to the free field surface accelerations, depending upon the exciting frequency and resonant frequency. The other tests performed is characterized in Table 4.4, 4.5, and 4.6.

The time histories of pile head displacements recorded by LVDT#2 near the centre of gravity of the pile cap mass are shown in Figures 4.18 and 4.19 for tests I-4, I-7, I-15, II-10 and III-7, respectively. For tests I-4, I-7 and I-15, the maximum recorded displacement during steady state are 0.06, 0.14 and 0.02 pile diameters respectively. It was observed that an initial transient phase of displacement response existed when the forcing frequency was not close to resonance. For tests II-10 and III-7, the pile head displacements averaged 0.20 and 0.15 pile diameters during steady state vibration, respectively.

(B) Frequency Response Curves

Typical response curves of acceleration amplitude ratios (amplification factor) versus frequency ratios are depicted in Figure 4.20 for three series of forced vibration tests. In these tests the ratio of pile head mass (superstructure) acceleration amplitude over free field acceleration amplitude gives the amplification factor (relative to soil surface). The frequency ratio is the ratio of the exciting frequency over the model natural frequency. The first mode resonance is easily discernible. An indication of second mode response is also apparent.

The results show that the resonant (natural) frequencies increase with increasing stress levels and decreasing shaking intensities (Figure 4.20). This also confirms the

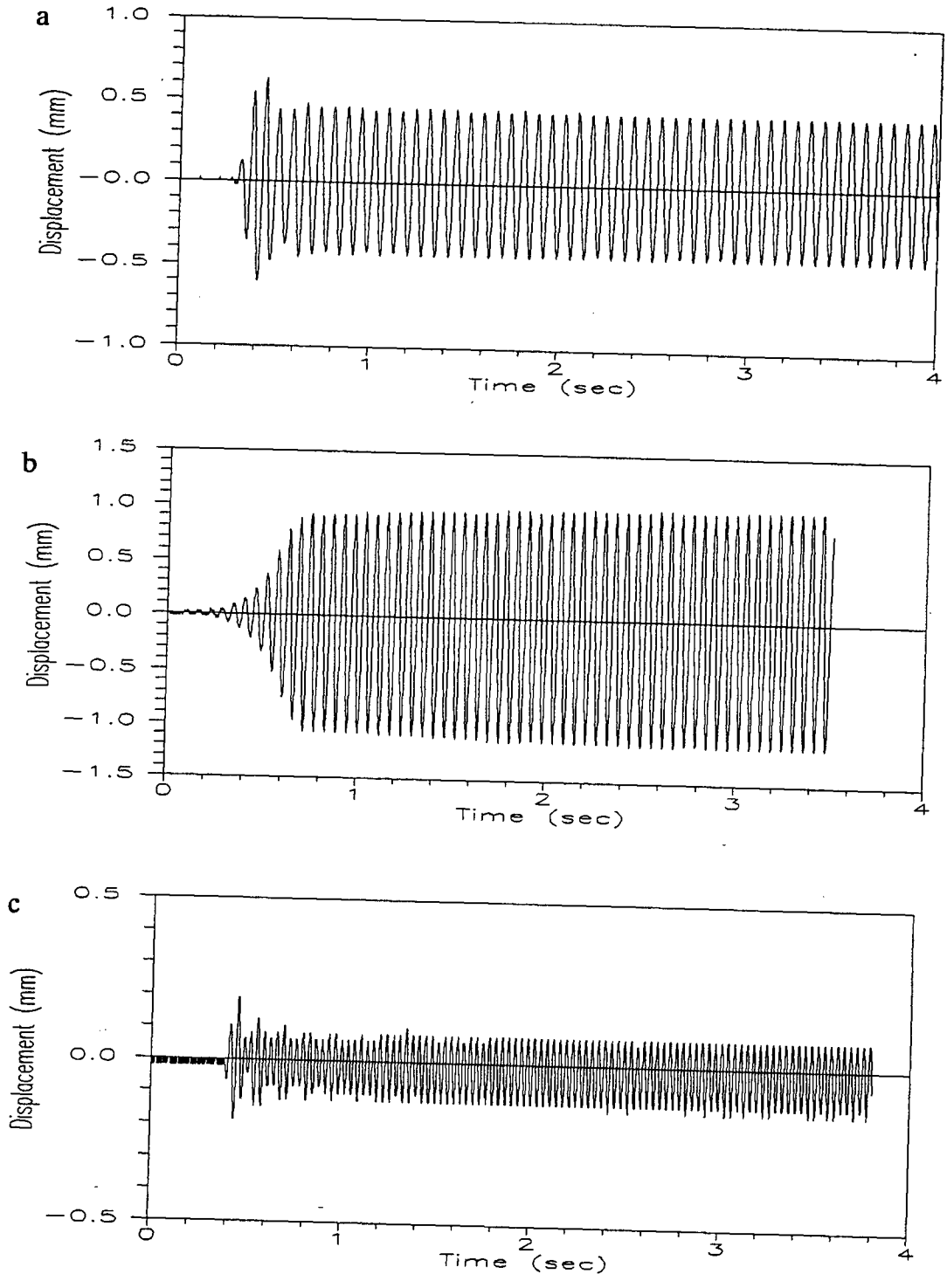

Figure 4.18: Pile head mass displacements (a) test I-4 (b) test I-7 (c) test I-15

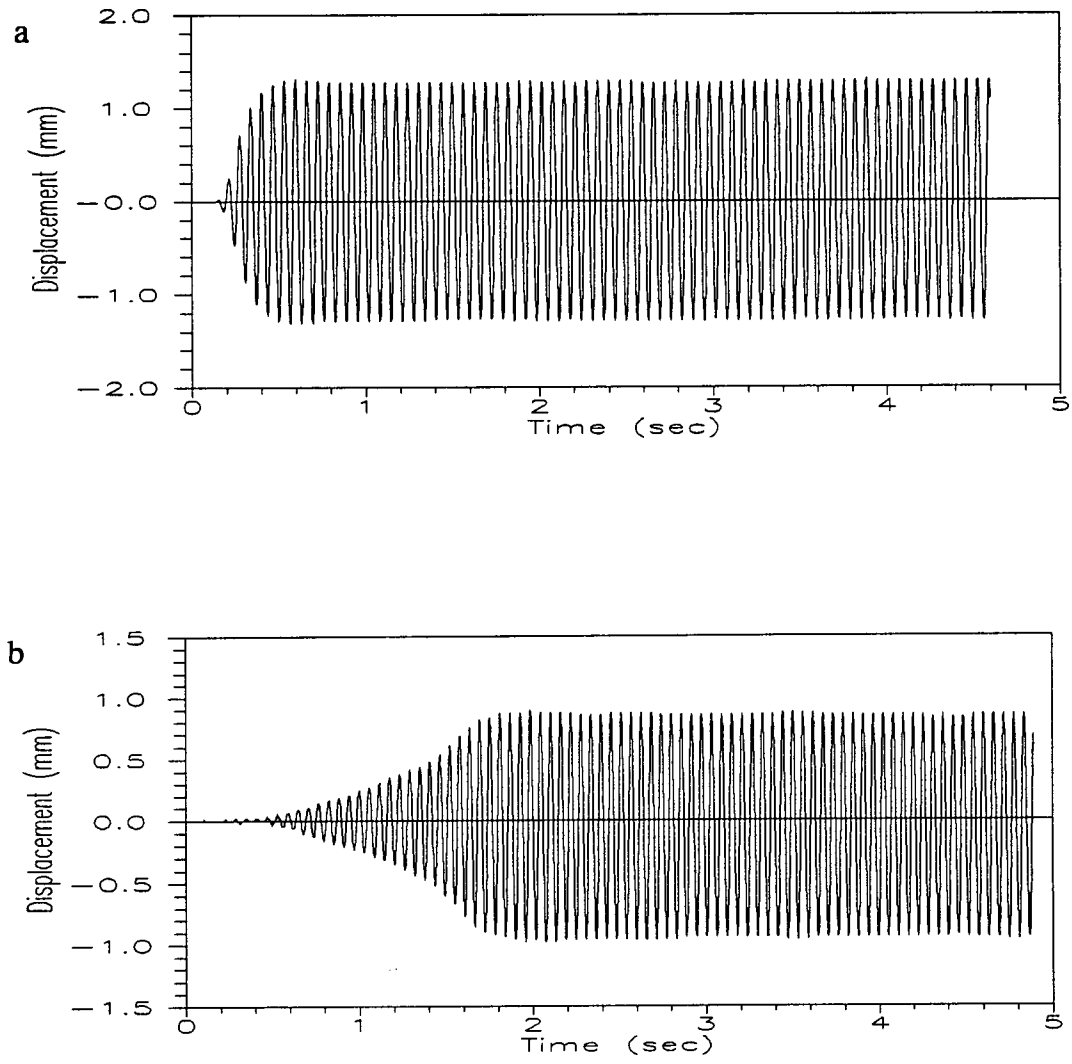

Figure 4.19: Pile head mass displacements (a) test II-10 (b) test III-7

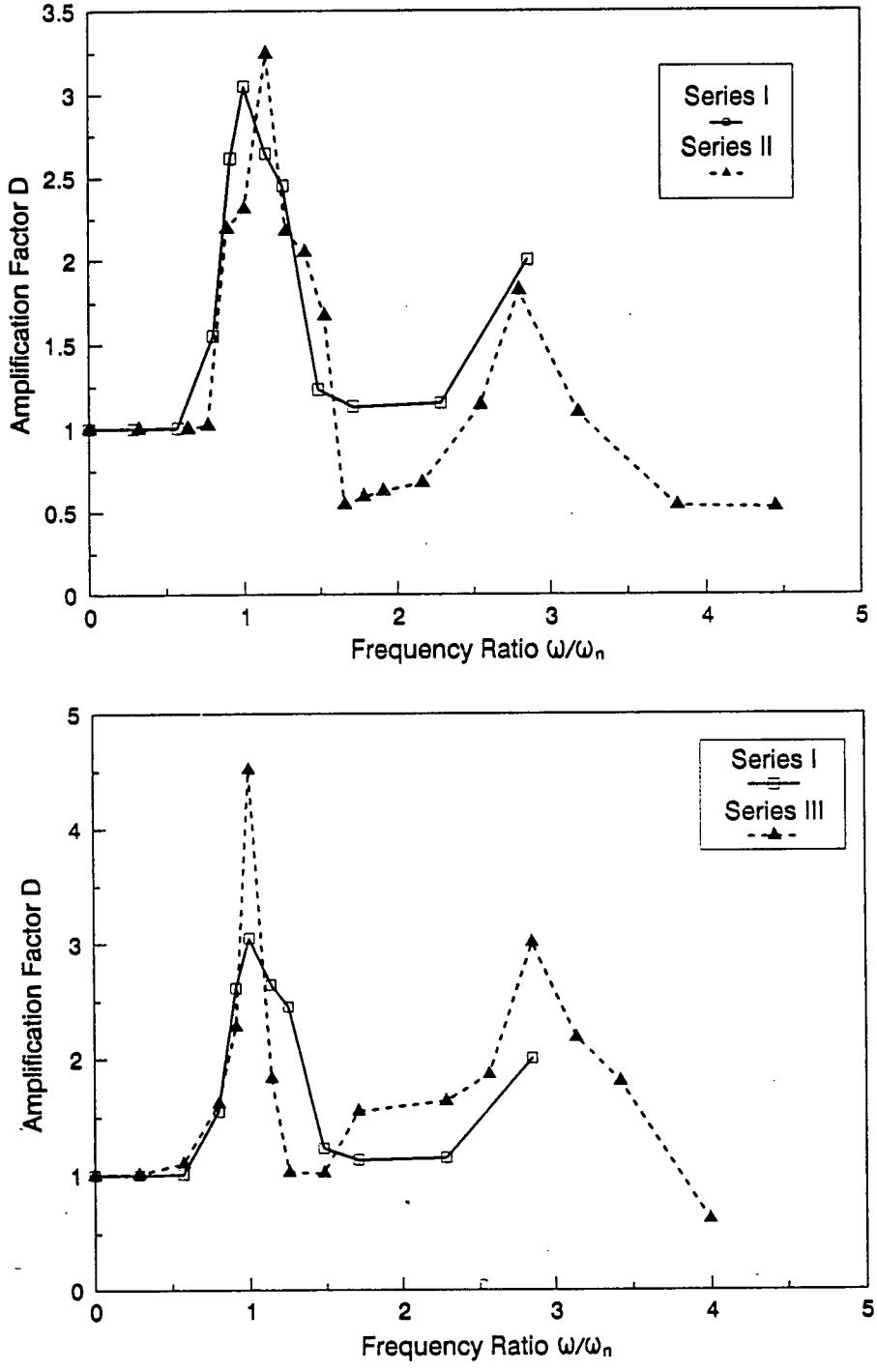

Figure 4.20: Amplitude vs. frequency response curve

results of the free vibration tests. The amplification factors at resonance are very close for series I and for series II, and are 3.05 and 3.24, respectively. But for series I and III (Figure 4.20b), the amplifications of the amplitudes are quite different due to the different excitation intensities. The amplification factor for series III is about 1.48 times that for series I, which indicates that low level excitation results in a higher pile head amplification.

(C) Pile Head Stiffness

Figure 4.21 shows the variation of pile head effective stiffness with its deflections. Here, The effective stiffness is defined as the force amplitude required to produce a unit pile head deflection amplitude. The dynamic lateral stiffness of the pile-soil system decreases with increasing deflection amplitude, and appears to be slightly greater for high soil stress level (series I) than for the low one (series II). The pile head stiffness for test series III were not computed since these tests were performed at high soil stress levels using low shaking intensity, thus the pile head deflections are very small and may not be reliably discerned except close to resonance.

Also, it is portrayed that the stiffness is dependent upon the input excitation intensity, higher for moderate shaking at the same stress level.

4.3.3 Behaviour of Pile Response

Time histories of pile bending moment measured at various points along the pile are shown in Figure 4.22 and 4.23 only for tests I-4 and I-7. These are examples of typical history curves of bending moments, whose exciting frequencies are less than, and close to resonance. The time history of bending moment variation at any one depth has the same frequency content as the pile head acceleration and corresponds with the forcing frequency. The peak bending moments occurring in the pile do not appear to change with number of loading cycles, which is also seen from Figure 4.24b.

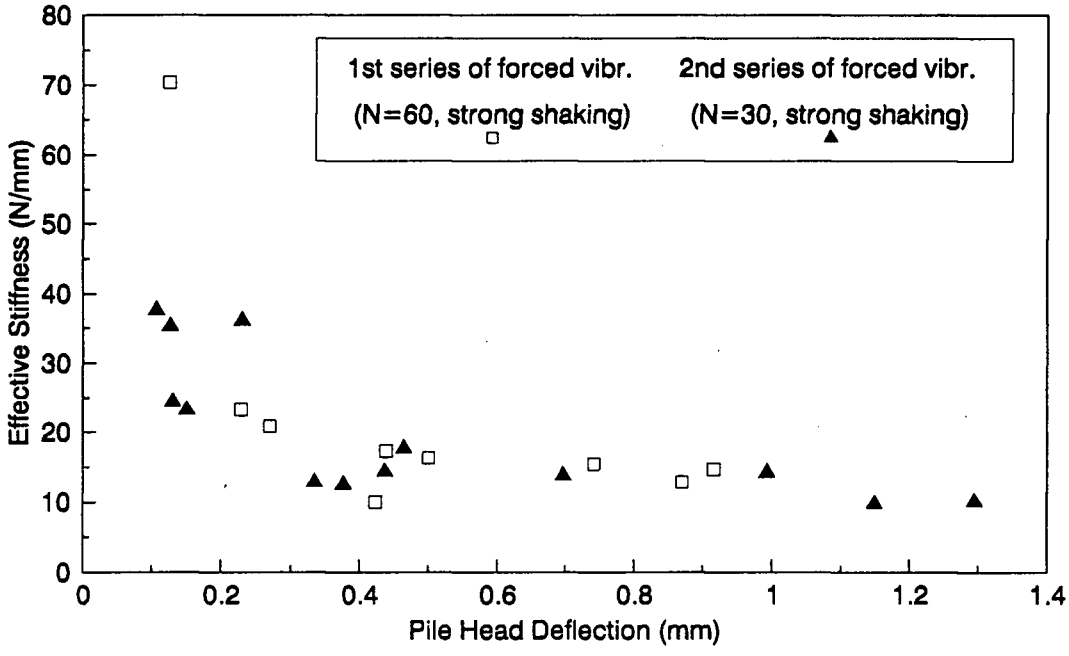

Figure 4.21: Effective stiffness vs. pile head deflection

Figure 4.24 shows the peak bending moment distributions along the pile for different loading cycles during steady state excitation for tests I-4 and I-7. These bending moment distributions are very similar to the observations from centrifuge tests (Finn and Gohl, 1987). The moments are seen to increase to a maximum value at strain gauge#3, located about 3.6 pile diameters below the soil surface, and then decrease to zero at greater depth. This suggests that the pile may be considered long in the sense that the lower parts of the pile do not affect the pile head response to the inertia loads applied at the pile head. The variation of observed bending moments along the pile (Figure 4.24) delineates that all points along the pile experience the same sign of bending moment at any instant in time with the exception of strain gauge#6 which shows a negligible small moment of opposite sign. This shows that the free headed pile is vibrating in its fundamental mode.

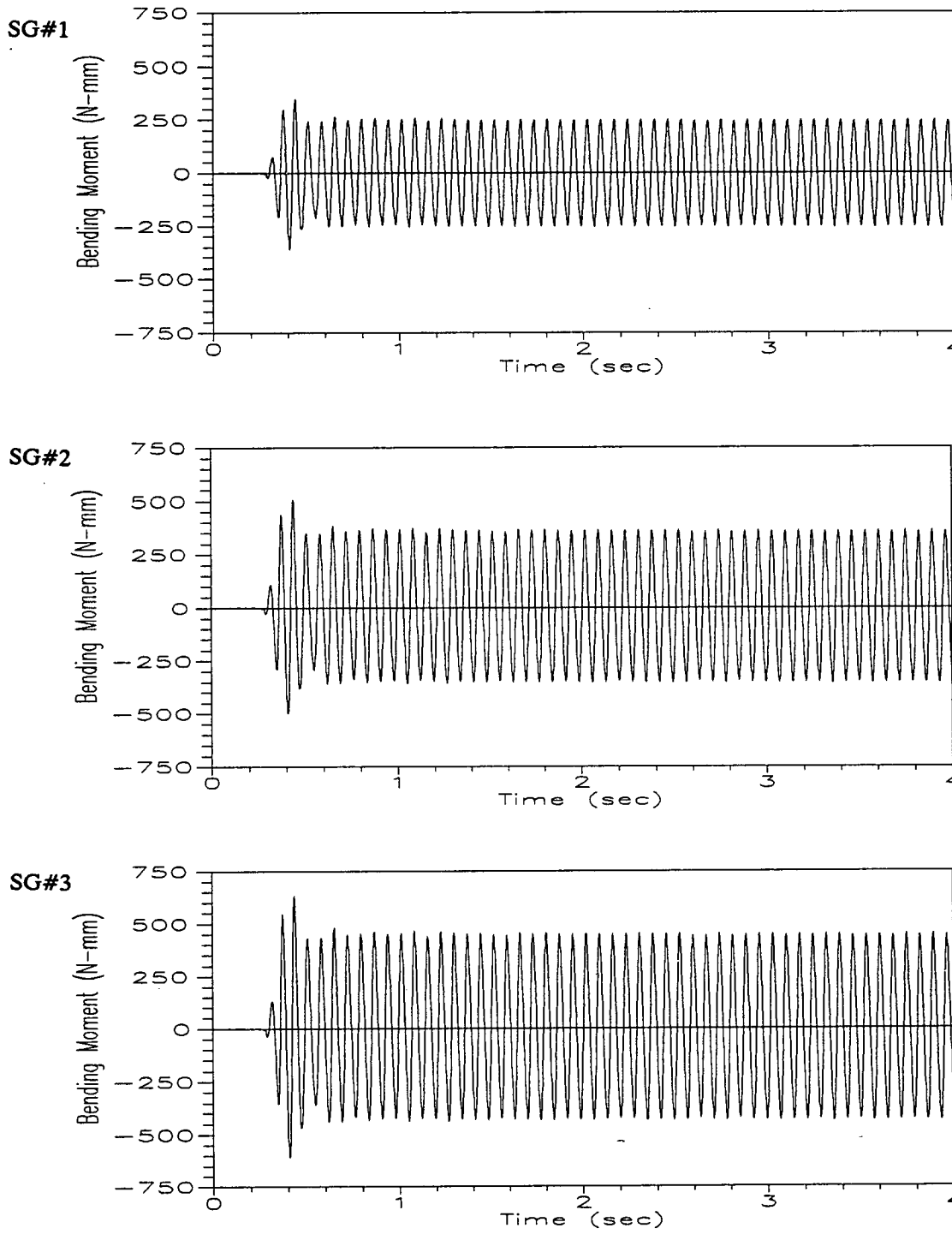

Figure 4.22: Time histories of bending moment-test I-4

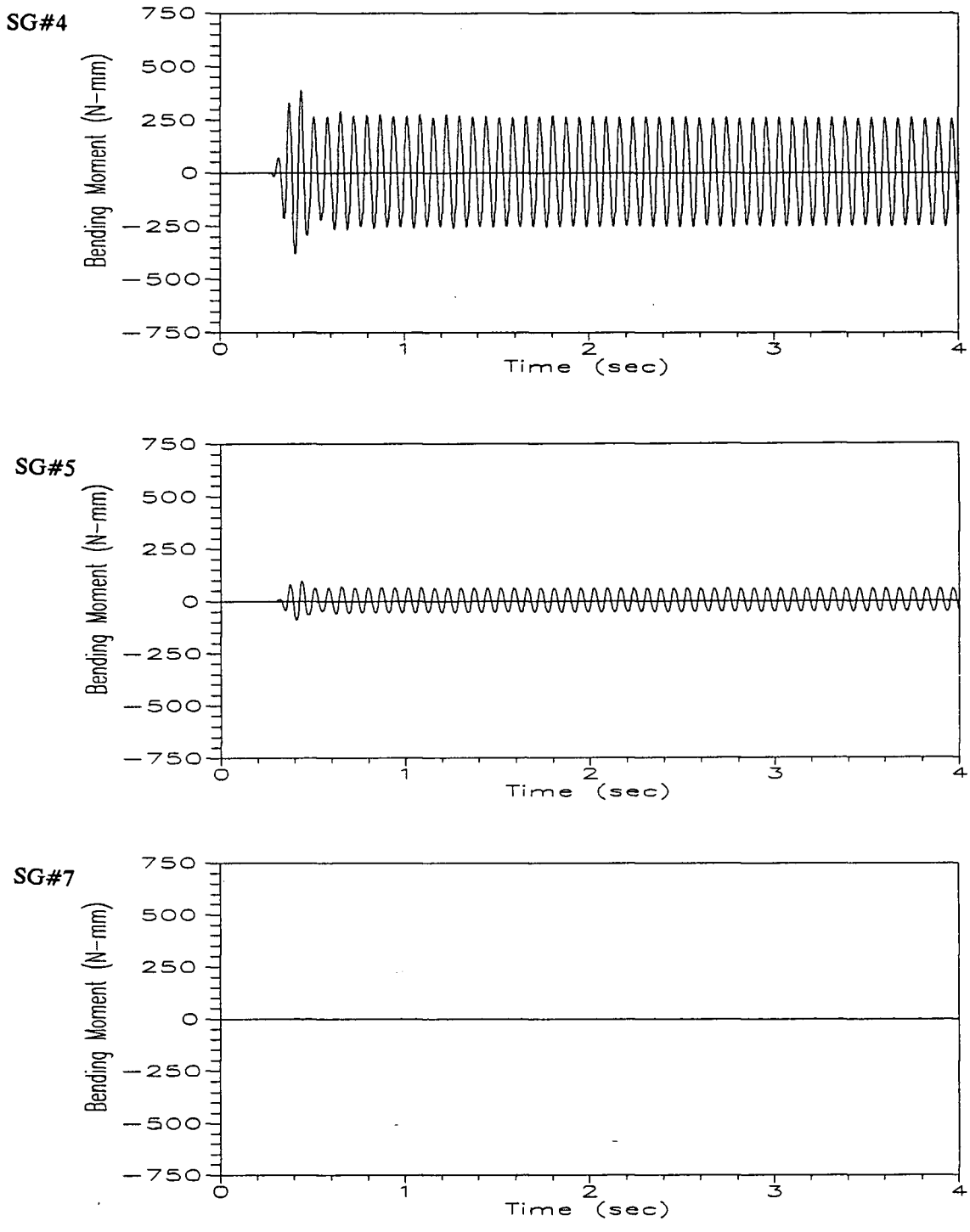

Figure 4.22: Time histories of bending moment-test I-4

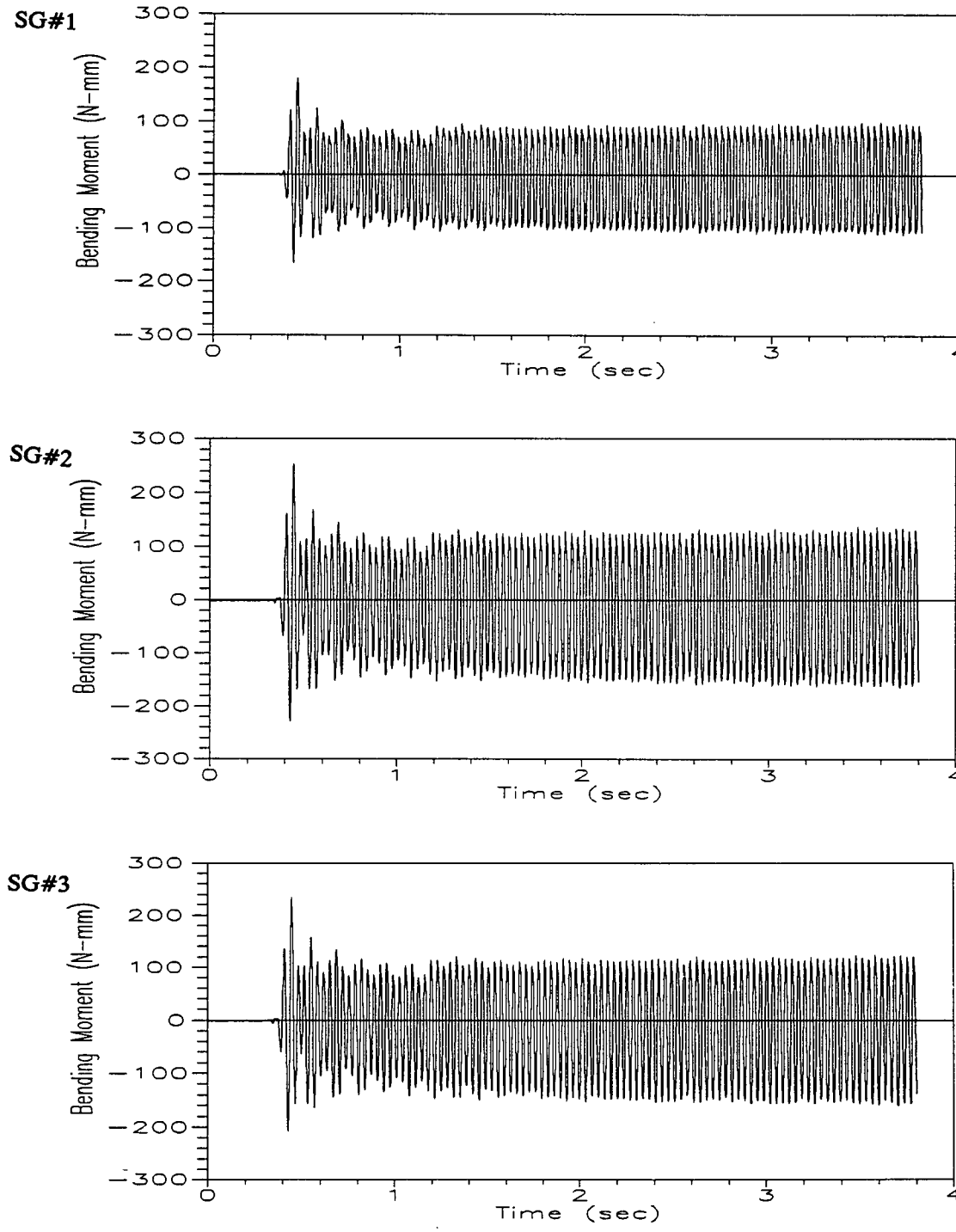

Figure 4.23: Time histories of bending moment-test I-7

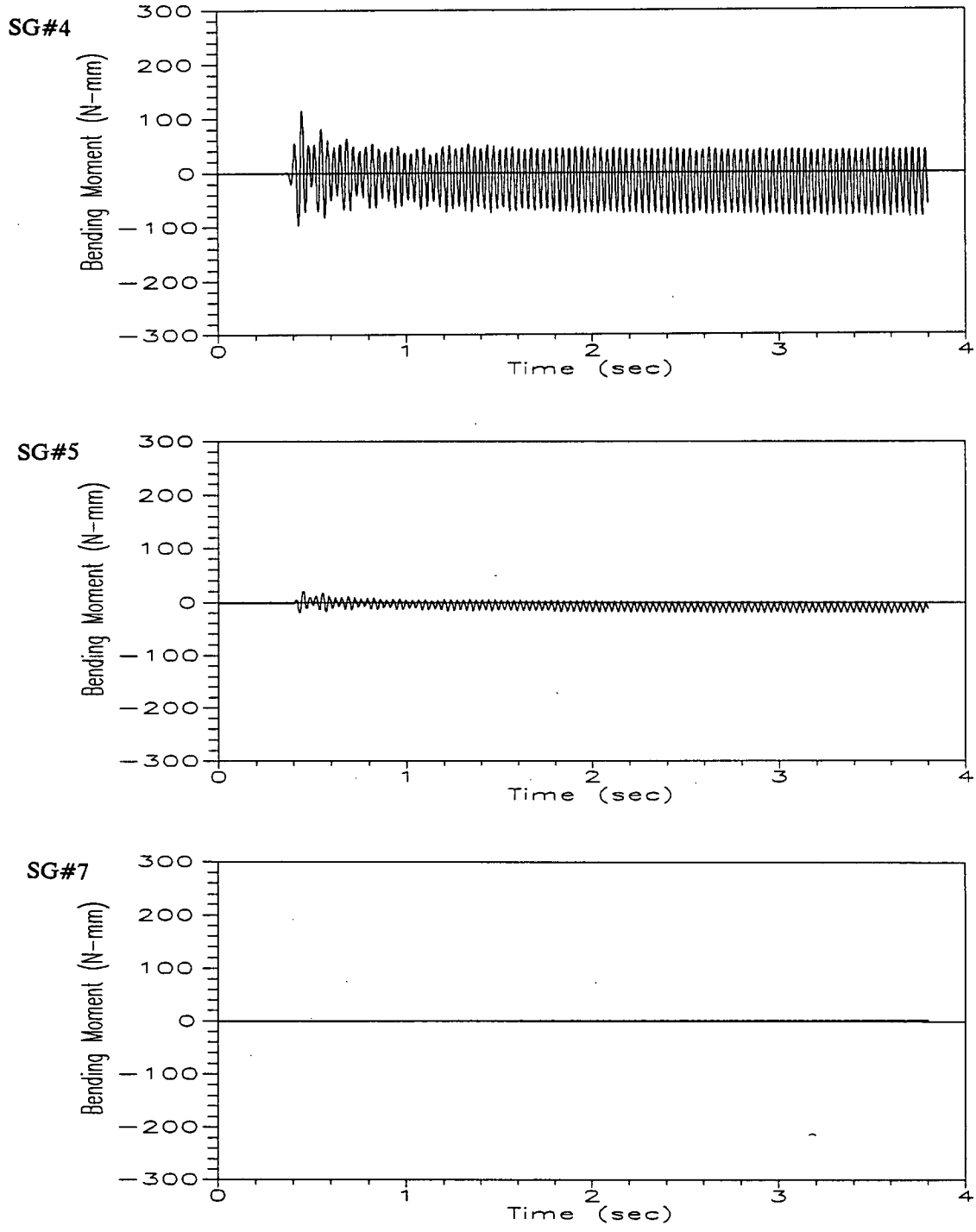

Figure 4.23: Time histories of bending moment-test I-7

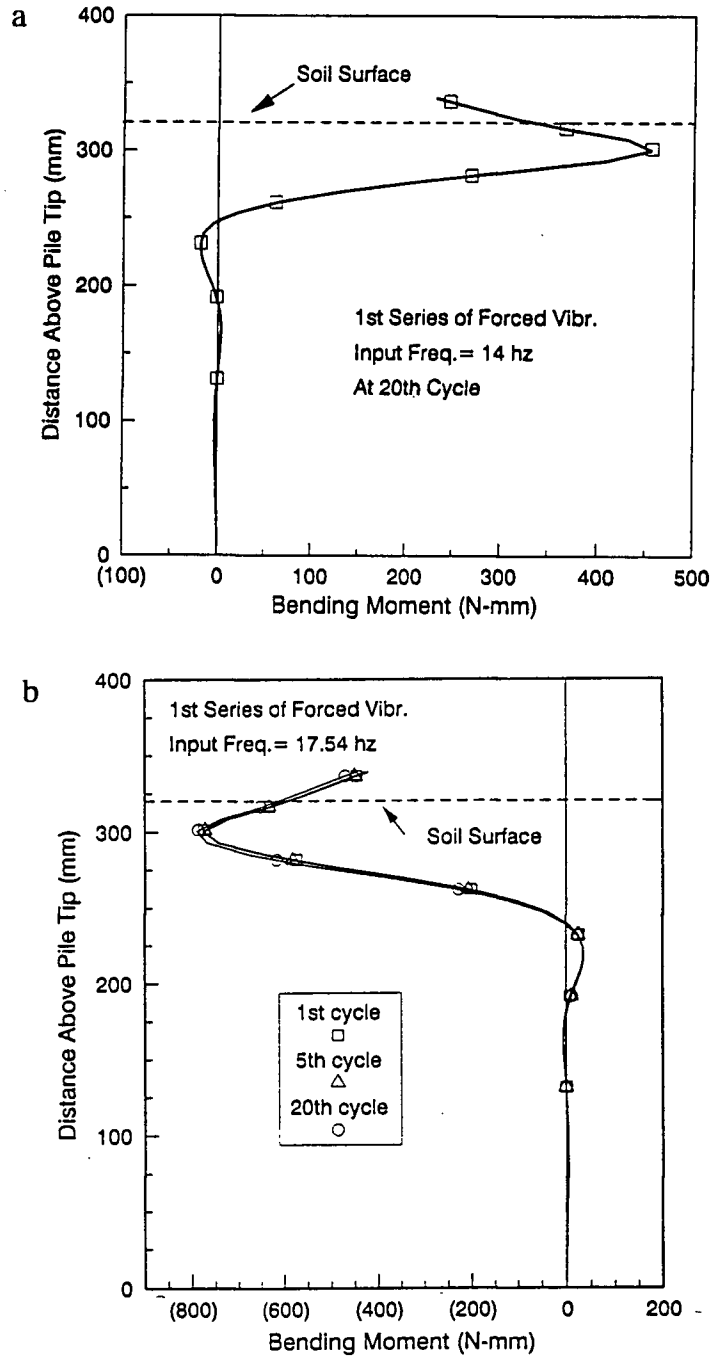

Figure 4.24: Bending moment distribution during steady state excitation (a) test I-4 (b) test I-7

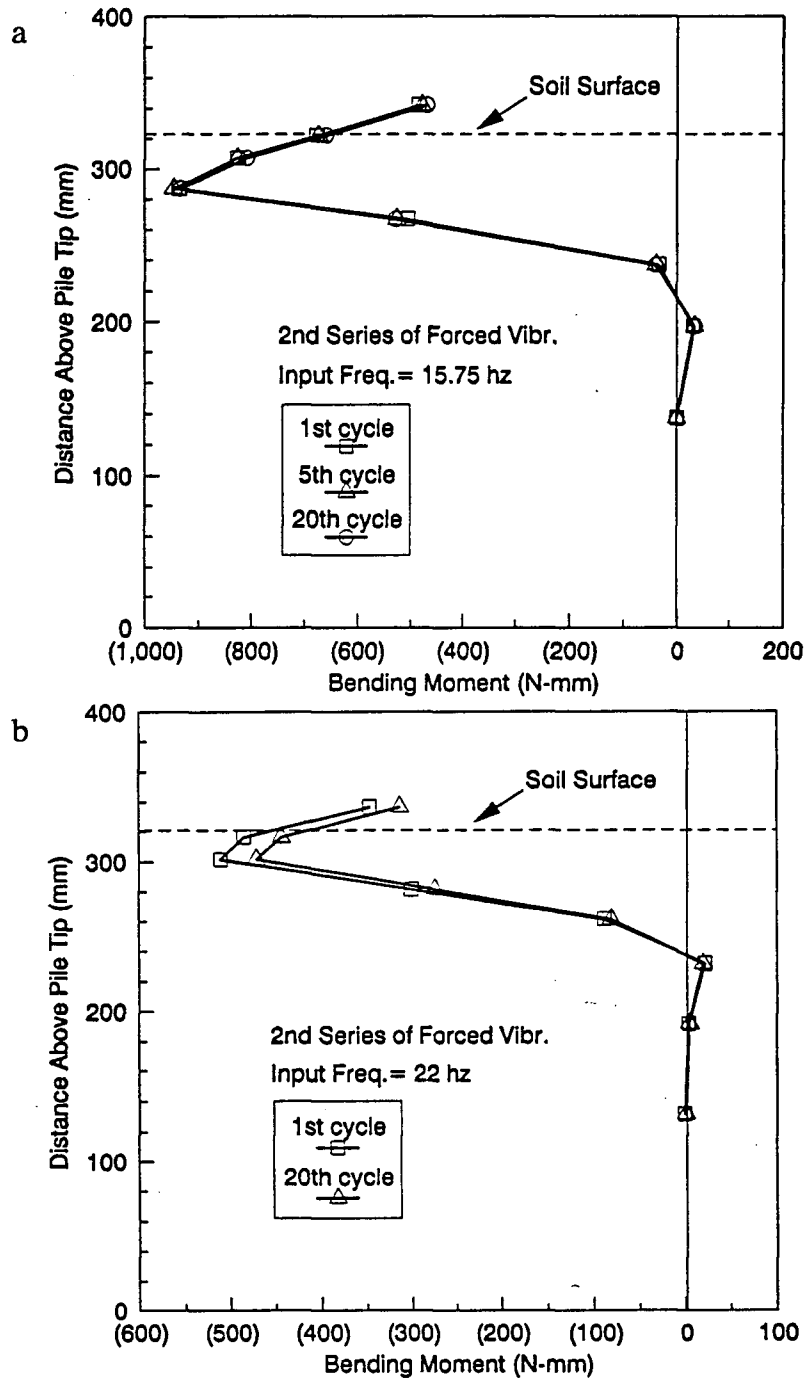

Figure 4.25: Bending moment distribution during steady state excitation (a) test II-10 (b) test II-13

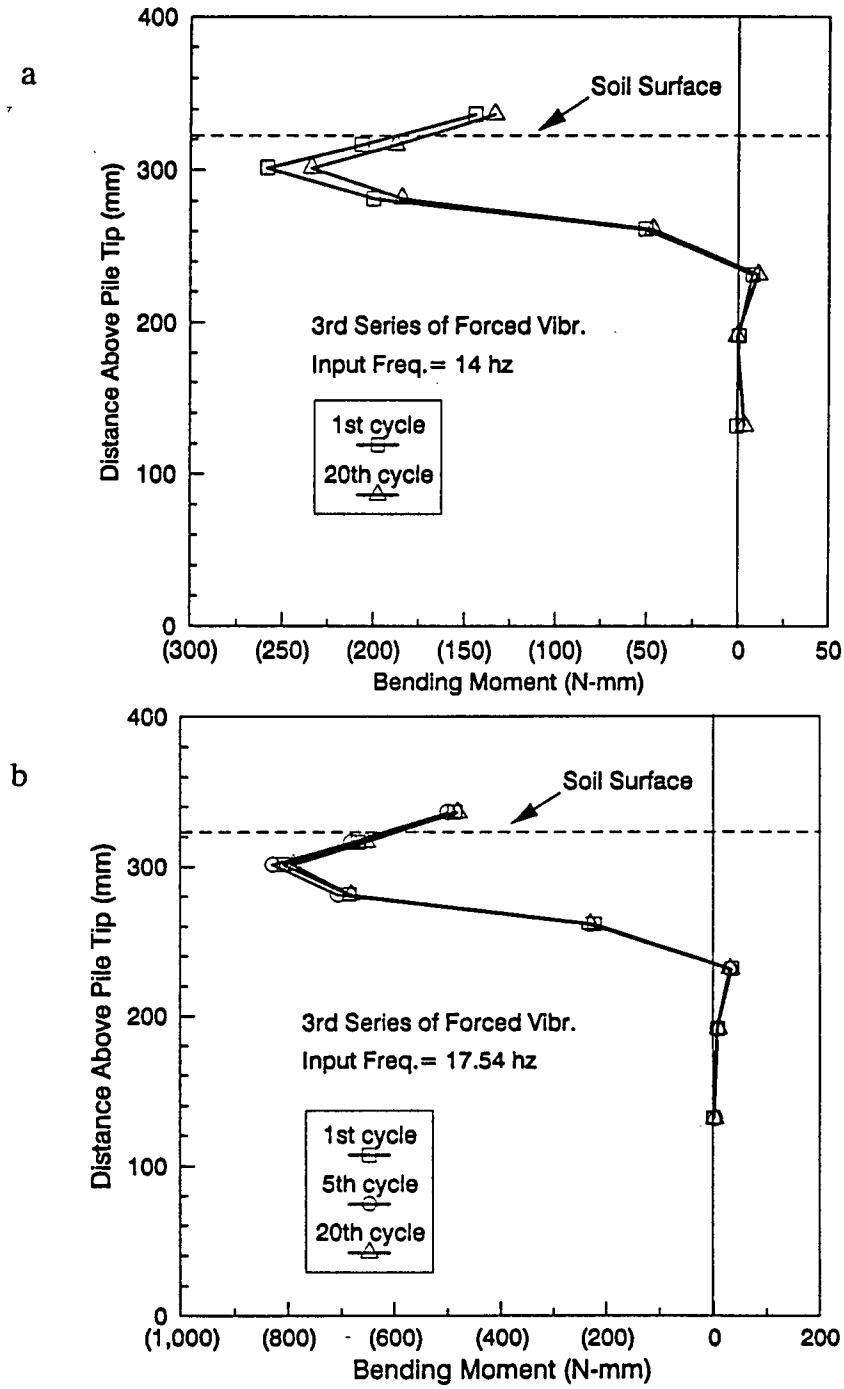

Figure 4.26: Bending moment distribution during steady state excitation (a) test III-4 (b) test III-7

Bending moment distributions measured during tests II-10 and II-13, and III-4 and III-7 are shown in Figures 4.25 and 4.26, respectively. These show the similar general behaviour described for tests I-4 and I-7. But for test II-10 (Figure 4.25a), maximum bending moments occur at approximately the 6.8 pile diameter depth. Comparing the depth of maximum bending moment observed in tests I-4 and I-7 (Figure 4.24) having similar shaking intensity, it may be seen that the lower soil stress level used in test II-10 relative to that used in test I-7 has given rise to an increase in the depth of maximum bending.

Comparisons of pile bending moment distribution measured under different exciting frequencies, i.e. induced different inertia lateral loads, are displayed in Figures 4.27 for different soil stress level and excitation intensities, respectively. It is consistently seen that the maximum bending moment occur at resonant cases for all three series of tests, caused by the greater inertia forces induced. Also, as inertia load increases, it is evidently observed that the maximum bending moment moves progressively deeper below the soil surface and increase substantially in magnitude.

4.3.4 Soil-Pile Interaction

(A) Introduction

The nature of interaction between the soil and the pile during simulated earthquake loading was investigated in terms of cyclic p-y curves derived from the testing data according to the procedures described in Appendix B. The method uses a cubic spline fitting to the discrete bending moments measured along the pile so as to specify the unknown soil reaction distribution along the pile through a double numerical differentiation of bending moments. At the ground surface, the net soil resistance p is set into zero as

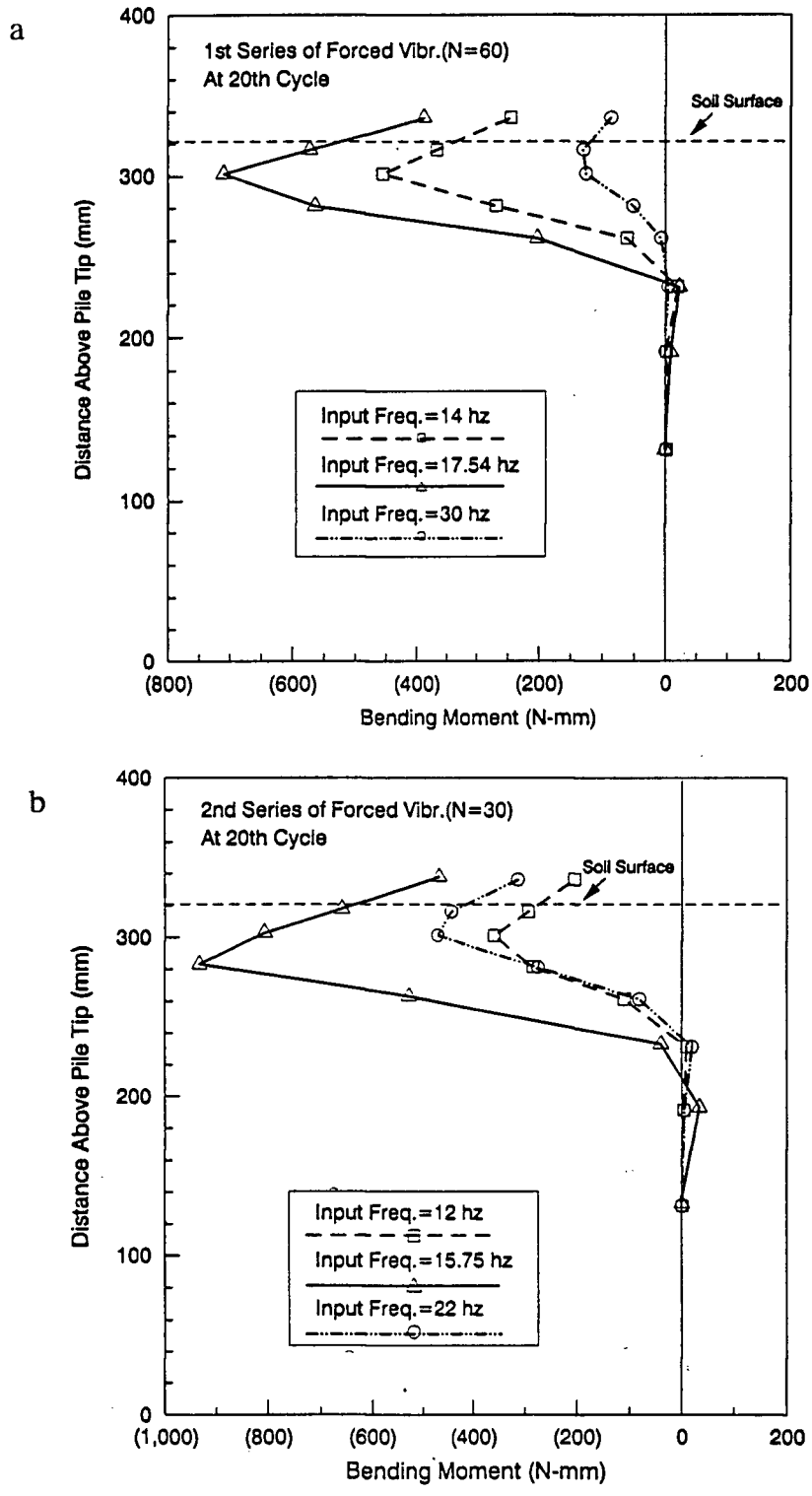

Figure 4.27: Bending moment at different exciting frequencies (a) series I (b) series II

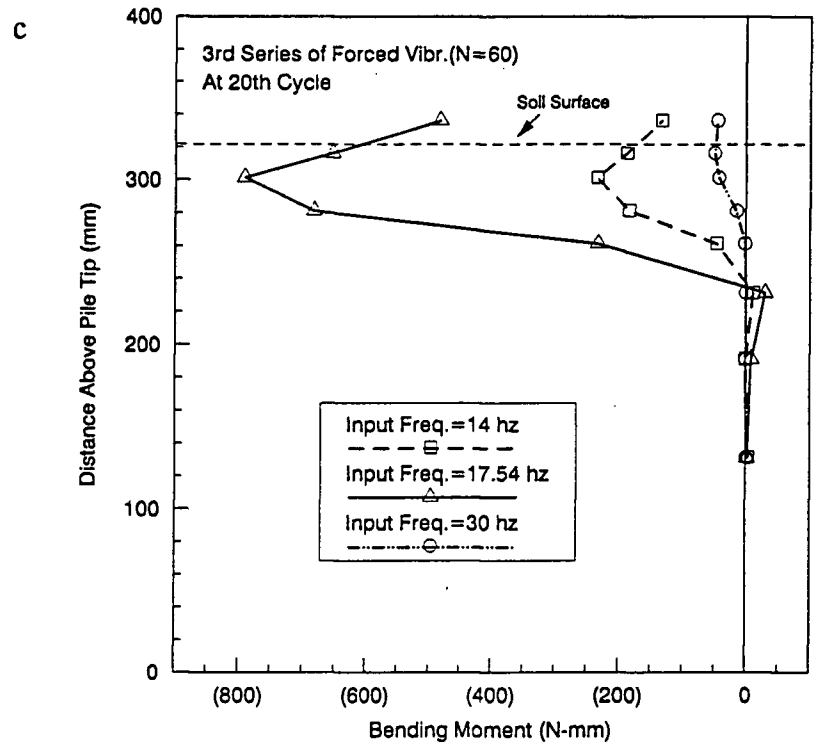

Figure 4.27: Bending moment at different exciting frequencies (c) series III

a constraint.

Lateral pile deflections along the pile were evaluated also by fitting a piecewise cubic spline through the measured bending moments and then double integrating the cubic spline. The accuracy of the numerical integration was checked by computing deflections at the top of the pile head mass where displacements were measured. Discrepancies of 0.008-0.015 mm (at model scale) occurred due to the limited number of bending moment data points employed in the cubic spline fit and inherent measurement error. Therefore, computed deflections were scaled a constant amount along the pile such that a match of the measured pile head deflection was achieved.

The lateral pile deflections are computed with respect to the moving base. These are not necessarily the same as the relative deflection between the pile and the free field, which is the form the p-y curves should be expressed in for earthquake loading. The

experimental data shows that bending moments greater than about the 12 pile diameter depth are very small, suggesting that pile curvatures due to the free field ground motions are similarly small. Furthermore, it will be shown that measured bending moment distributions along the pile are well predicted when only structural inertia forces are considered to contribute to pile bending (see Chapter 5). Computed pile head deflections due to the pile head inertia forces, which represent pile deflections relative to the free field displacements, also agree closely with pile head deflections measured relative to the moving rigid base. Hence, for all practical purposes, the measured bending moment data can be used to develop the relationship between soil resistance (p), and displacement (y) relative to free field.

The p-y curves from test data are compared to the backbone cyclic p-y curves recommended by the American Petroleum Institute (API) (1987). The generation procedure of p-y curves using API code (1987) has been reviewed in Chapter 2. The p-y relationship is expressed by a hyperbolic tangent function (Eq.2.1) at any specific depth. The "$n_h z$" defines the initial slope of the p-y curve, where n_h is an initial modulus of subgrade reaction. The ultimate soil resistance is estimated from the smallest value given by Equations 2.2 and 2.3. For the saturated sand in test at relative density of 75%, the API p-y curves were computed using a peak friction angle of 39°, obtained from triaxial test measurements, and an n_h value of 32464 kN/m^3 for saturated dense sand.

It should be noted that all p-y curve data presented in the present section are in prototype scale. In the following, only some examples of typical p-y responses will be presented, the more may be found in Appendix C.

(B) Strong Shaking Under High Soil Stress Condition

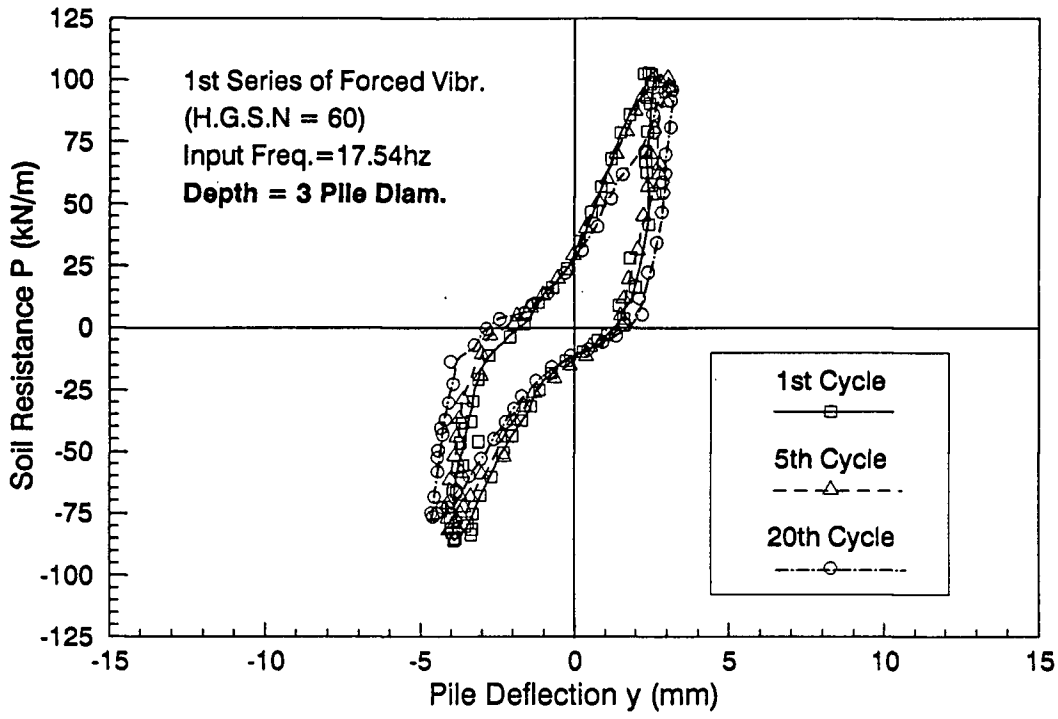

Figure 4.28: Cyclic p-y curves at different loading cycles at 3 pile diameter depth - test I-7

Series I of Forced Vibration Tests were performed using strong excitation under hydraulic gradient scale factor of 60. The experimental dynamic p-y curves computed for different loading cycles at different depths will be presented herein for tests I-7 and I-4.

Cyclic p-y curves computed from test I-7 are shown in Figure 4.28 to 4.29. Figure 4.28 shows the p-y curves computed at the 3 pile diameter depth for three different loading cycles. The effect of loading cycles on the cyclic p-y curves was not clearly observed from this specific test since the three p-y curves are nearly identical with the same secant lateral stiffness, defined as the slope of the line passing through the end points of hysteresis loop. This indicates the dense sand tested were not significantly densified during the test.

Figure 4.29 shows that the computed p-y curves for test I-7 during steady state up to about the 4 pile diameter depth are non-linear and exhibit hysteresis loops with typical of an inelastic, damping system. The p-y response is linear beyond about the 5 pile

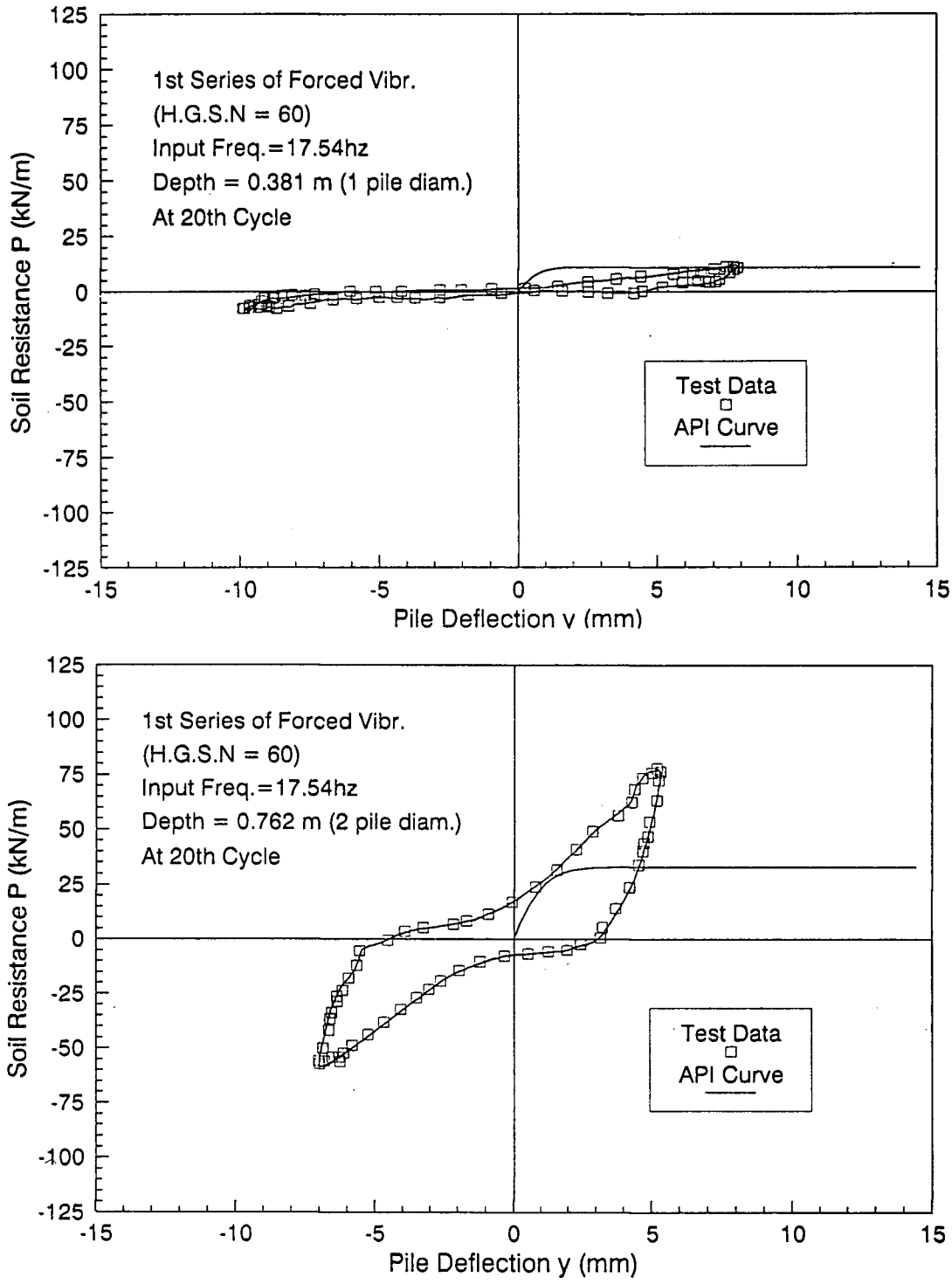

Figure 4.29: Cyclic p-y curves at 1 to 2 pile diameter depths during steady state shaking and comparison with API curves - test I-7

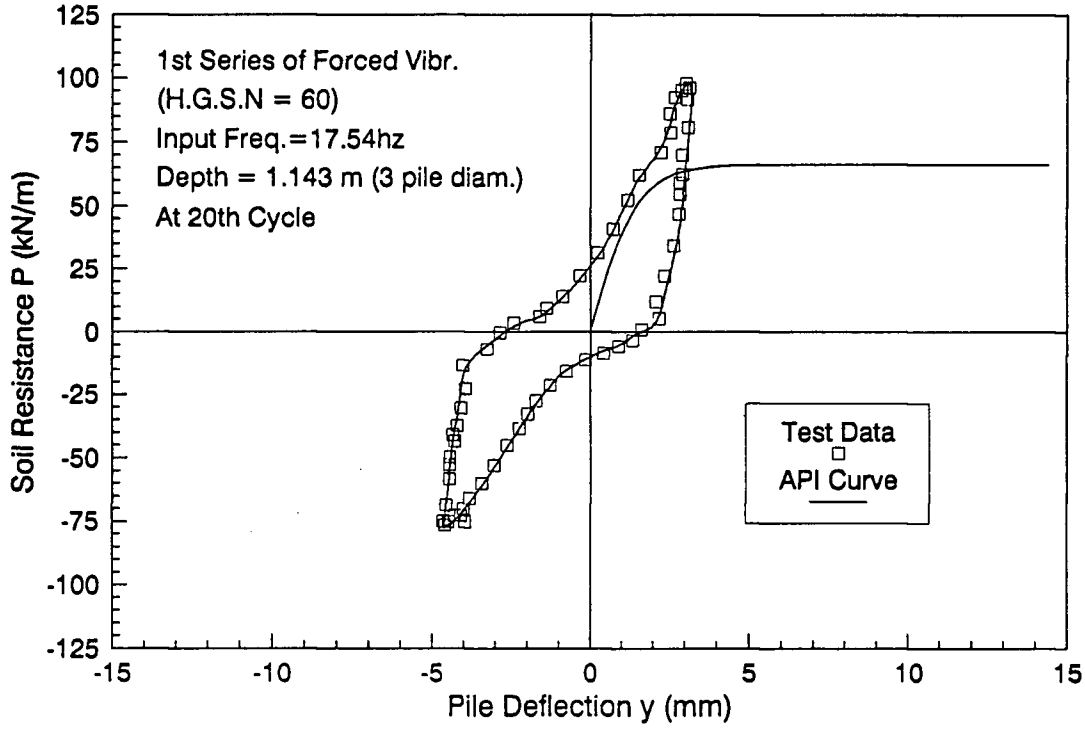

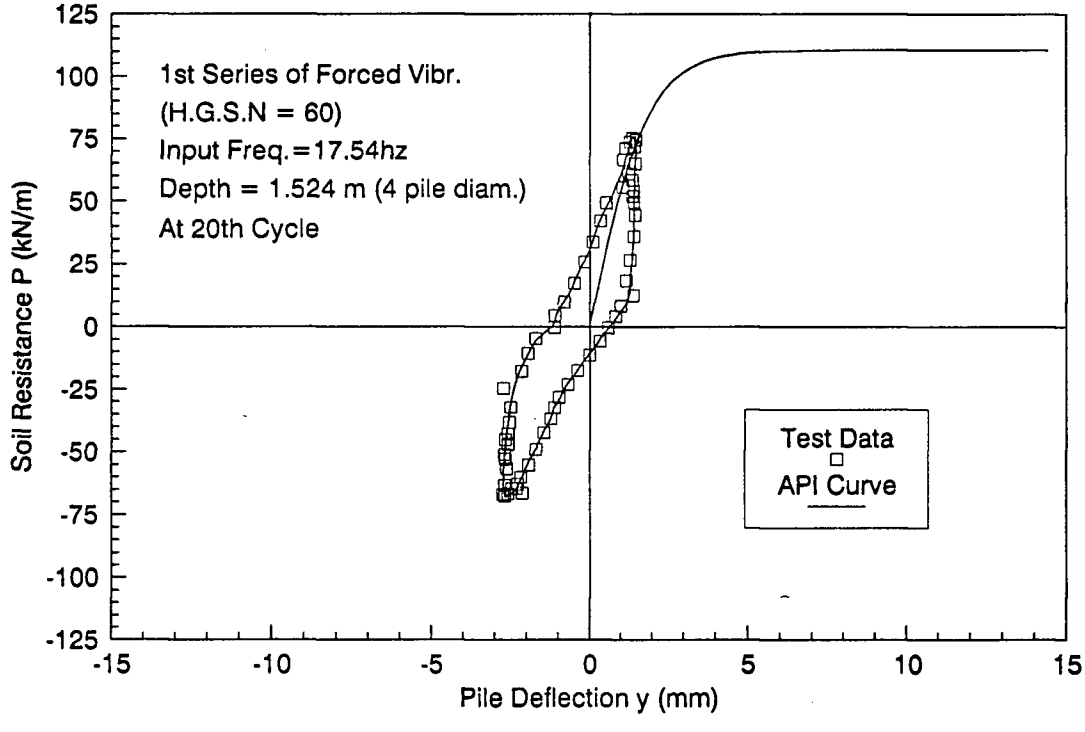

Figure 4.29: Cyclic p-y curves at 3 to 4 pile diameter depths during steady state shaking and comparison with API curves - test I-7

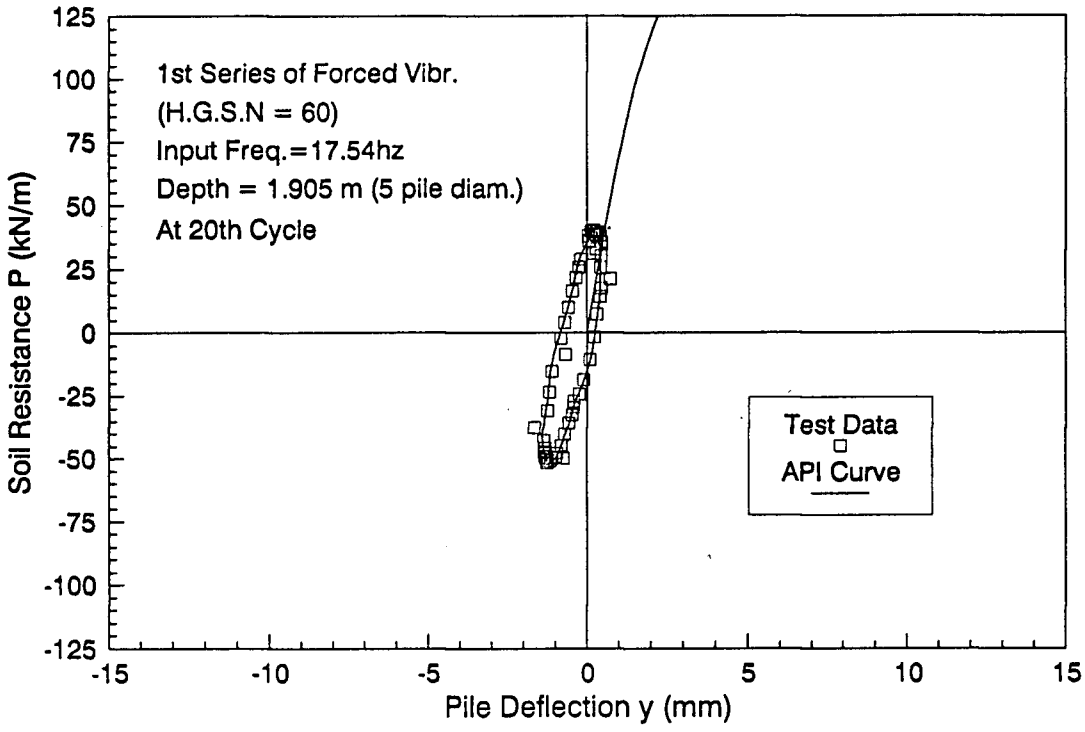

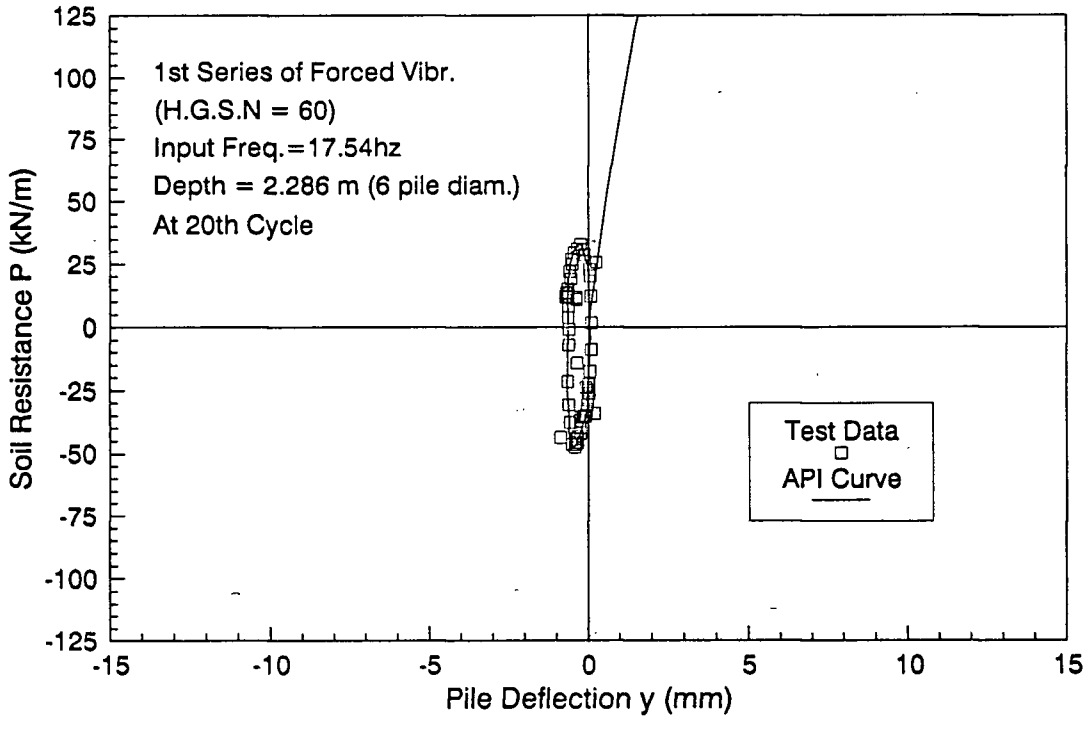

Figure 4.29: Cyclic p-y curves at 5 to 6 pile diameter depths during steady state shaking and comparison with API curves - test I-7

diameter depth. The curves are very flat near the surface and become stiffer with depth as the soil confining stress increases, in another words, the secant lateral soil stiffness for a certain cycle of shaking are seen to increase with depth. Gapping between the sand and the pile are observed at shallow depth, as shown in Figure 4.29. The soil-pile interaction curve at 1 pile diameter depth is very flat with negligible soil resistance, indicating the development of soil gap around the pile at this depth. The phenomenon of gapping occurred for a depth of 2 pile diameters.

The cyclic p-y curves computed using the API code are also shown in the Figures. The API p-y curves provide a poor match of the experimental ones, especially at shallow depths. The comparison shows that the API curves are considerably softer than that induced from the experiments up to the 3 pile diameter depth except 1 pile diameter depth. This indicates that effective lateral soil stiffness would be underestimated by API code (1987) for shallow depths. However, at greater depths the API curve slope approaches the secant slope of the experimental curve. Thus the API curves seem to give a reasonable estimate of the lateral soil stiffness below the 4 pile diameter depth.

The cyclic p-y curves computed for test I-4 are shown in Figures 4.30. The p-y curves were computed for the initial cycle of transient excitation when maximum pile response occurred and were then compared with the curves evaluated for steady state vibration. The p-y curves have been computed up to the 4 pile diameter depth, since below this depth lateral pile deflections could not be reliably discerned. During the initial transient excitation (1st cycle), relatively large lateral pile deflections occurred. The test p-y curves are non-linear and exhibit hysteretic behaviour. No signs of gapping at the soil-pile interface are evident from the curves. The lateral pile deflections are clearly less during steady state than during the initial transient phase. The p-y response is approximately linear past the 4 pile diameter depth. The depth where linear p-y relationship occurred is shallower for test I-4 than for test I-7, owing to smaller inertia forces at the pile head

for test I-4.

Cyclic p-y curves based on the API procedures are also shown in Figure 4.30. The API curves are again seen to generally underpredict the lateral soil reactions.

Figure 4.31 portrays the effect of inertial loading amplitude on the p-y response for tests I-4, I-7 and I-15 at the 3 pile diameter depth. It is seen that test I-7, at resonance frequency of 17.54 Hz, suffers a large pile lateral deflection as a result of considerable inertia load occurring. The p-y response is softer, i.e. lateral soil stiffness is smaller than the other case shown. It is also observed that the p-y behaviour for test I-7 is significantly non-linear, hysteretic and highly damped. However, for the other two cases, the p-y curve is much stiffer, closer to linear response, resulting from their smaller inertia forces.

(C) Strong Shaking Under Low Soil Stress Condition

This series of tests (series II) were carried out using strong shaking at a lower soil stress level than series I to study the effect of the stress on the soil-pile system response. To examine this effect, typical of p-y responses from tests II-10 and II-13 will be shown.

Figure 4.32 illustrates cyclic p-y curves computed at the 3 pile diameter depth for initial transient and steady state loading cycles for test II-10, which is close to resonant case with input exciting frequency of 15.75 Hz. It is seen that the loading cycle had no influence on the p-y response for this test, and the two p-y behaviours are nearly identical. There was no sign of soil hardening with load cycles.

Cyclic p-y curves have been computed for test II-10 during steady state shaking and are shown for the 1 to 5 pile diameter depths in Figure 4.33. The experimental curves are non-linear and hysteretic up to about the 5 pile diameter depth, indicating a highly damped system. The p-y response, however, become stiffer with depth. The secant

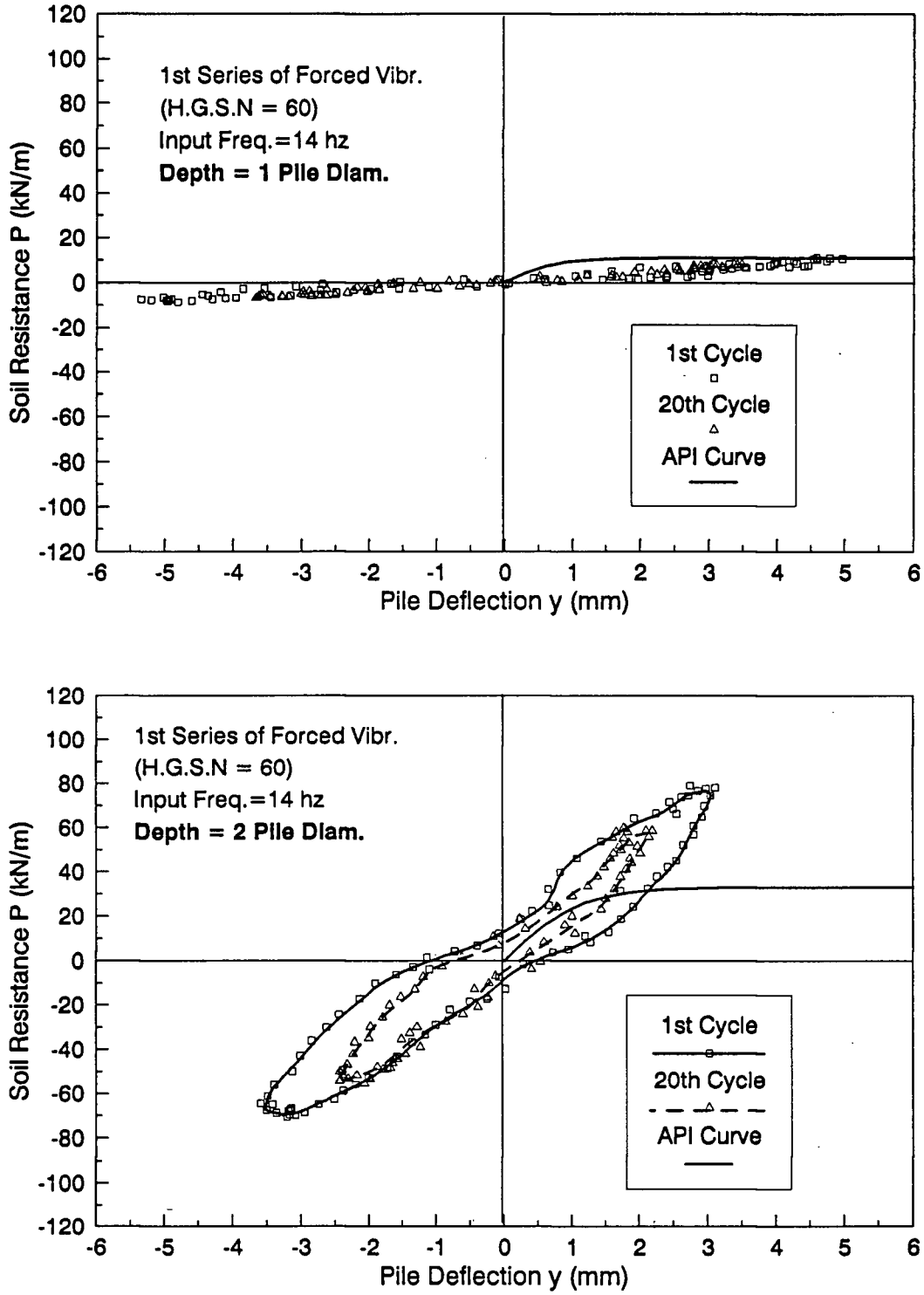

Figure 4.30: Cyclic p-y curves at 1 to 2 pile diameter depth for different cycles and comparison with API curves - test I-4

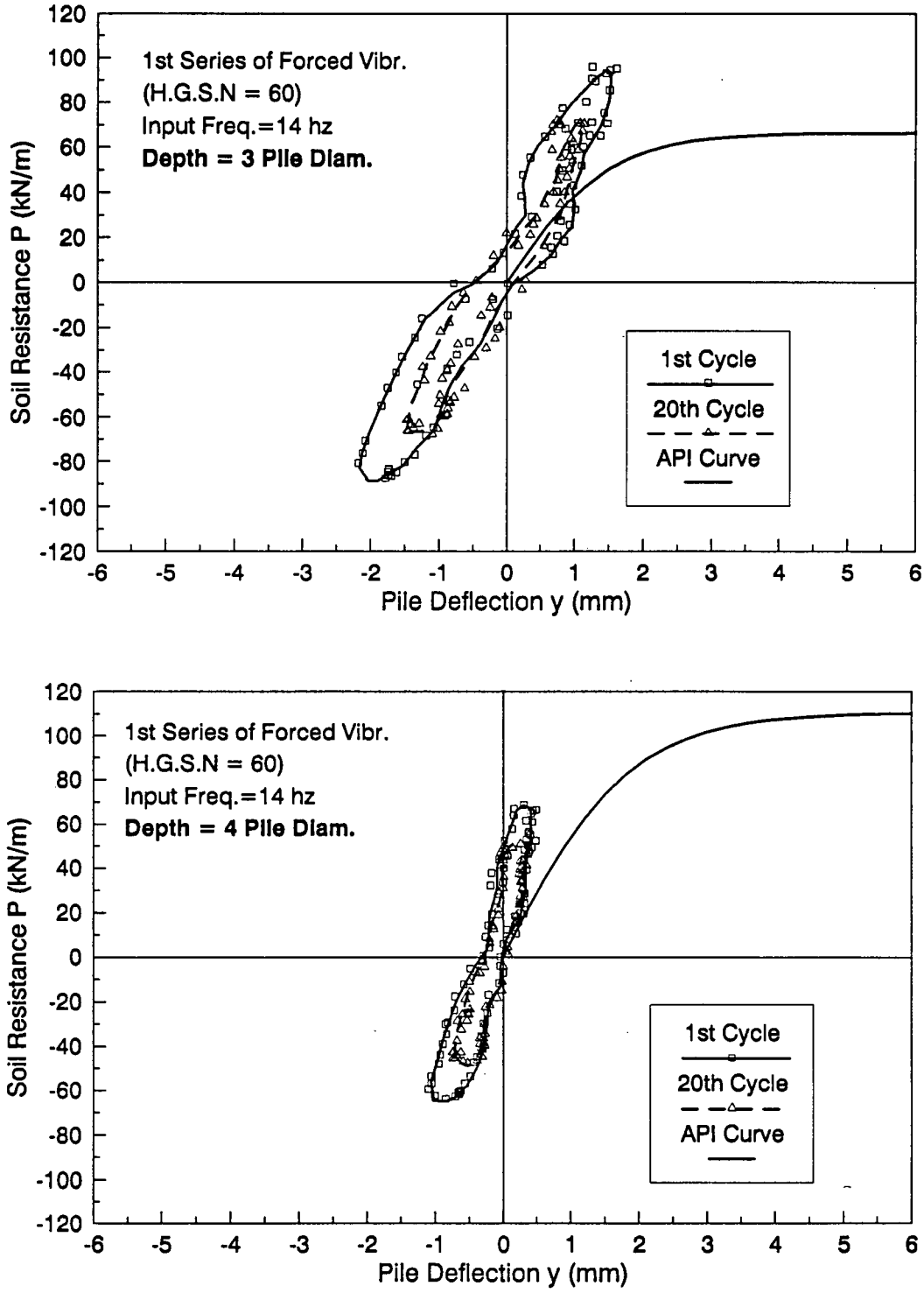

Figure 4.30: Cyclic p-y curves at 3 to 4 pile diameter depth for different cycles and comparison with API curves - test I-4

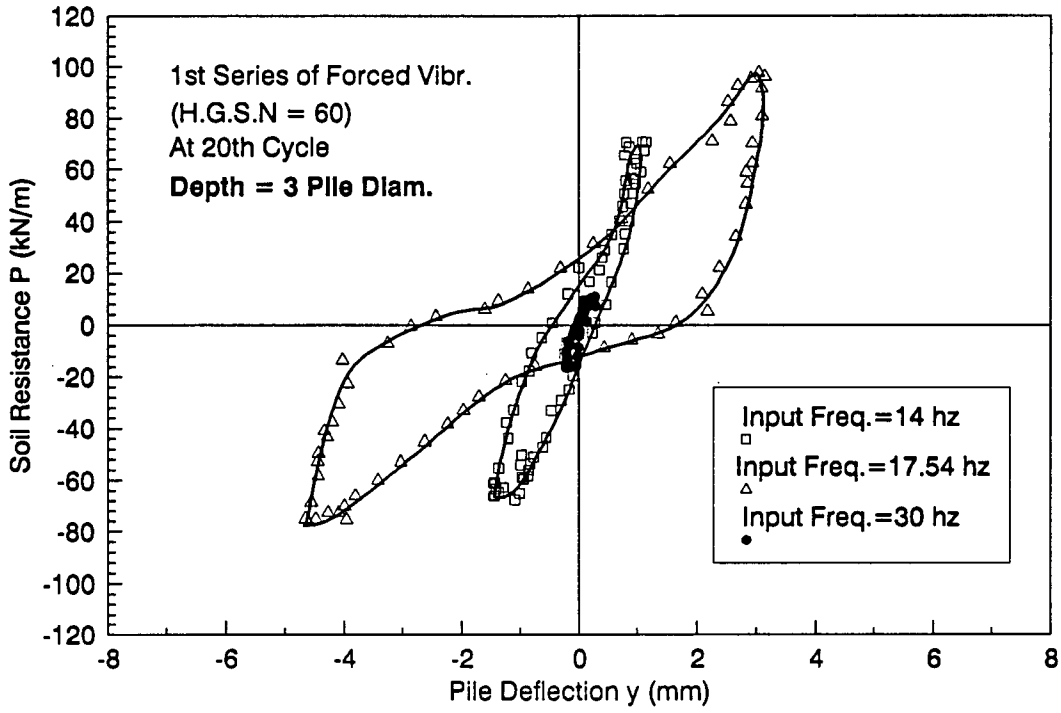

Figure 4.31: Comparison of p-y curves at different inertia loading levels at 3 pile diameter depths - test series I

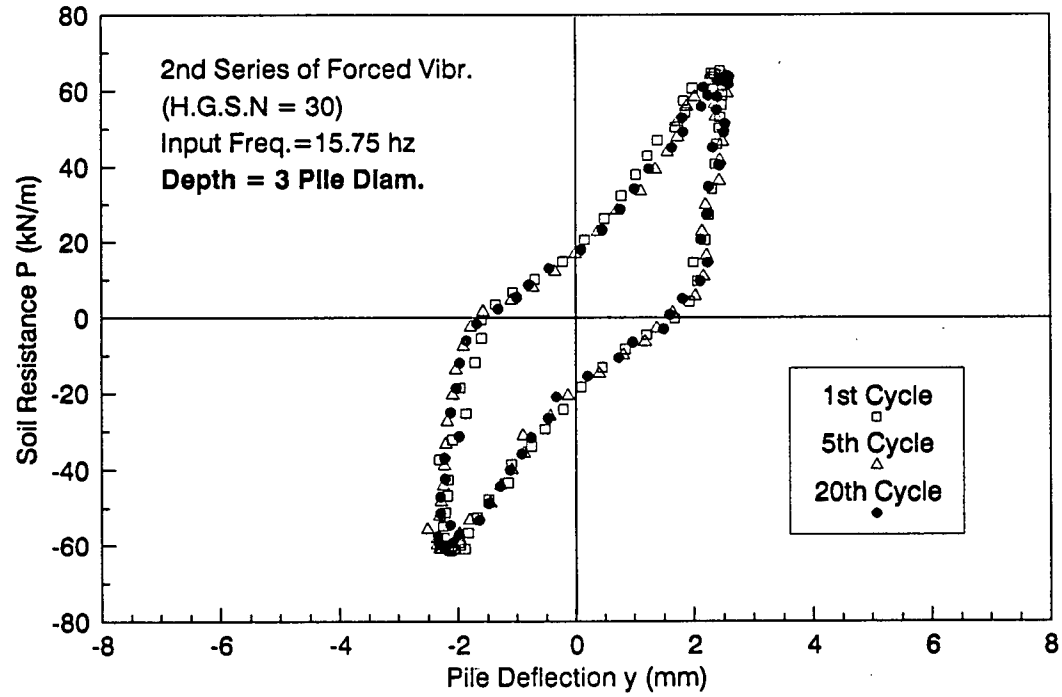

Figure 4.32: Cyclic p-y curves at different loading cycles at 3 pile diameter depths - tests II-10

lateral soil stiffness also increase with depth. The gapping may have occurred at the soil-pile interface at around 1 pile diameter depth, since the p-y response at this depth is very soft and flat with negligible soil resistance.

The API p-y curves are also shown on the Figures. The comparison clearly shows that the API curves are substantially softer than those derived from the experiments. This suggests again that the lateral soil stiffness would be underpredicted using the API code procedures. It is more pronounced at shallow depth.

Similar data are also potted in Figures 4.34 and 4.35 for test II-13. For the initial transient cycle and steady state cycle, the p-y curves at the 3 pile diameter are shown in Figure 4.34, which are not sufficiently different to suggest that significant cyclic densification has occurred. The smaller amplitude of inertia force, resulting from a smaller magnification to base excitation, gave rise to a smaller lateral pile deflections and higher stiffness. The API curves consistently underestimate the lateral soil reactions.

Figure 4.36 delineates the influence of the inertia load amplitude on the p-y response for tests II-6, II-10 and II-13. Similar to test series I (Figure 4.31), The largest inertia force at resonant case results in a largest lateral pile deflections and give a smallest lateral soil stiffness and considerable damping. This is clearly demonstrated in Figure 4.36.

(D) Moderate Shaking Under High Soil Stress Condition

The third series of forced vibration tests were conducted using a relatively lower level shaking (compared to other two series) with an expected base input intensity of about 0.2 g under hydraulic gradient scale factor of 60. Data from these tests were used to determine whether approximately linear p-y response would occur when a pile is shaken in a dense sand deposit.

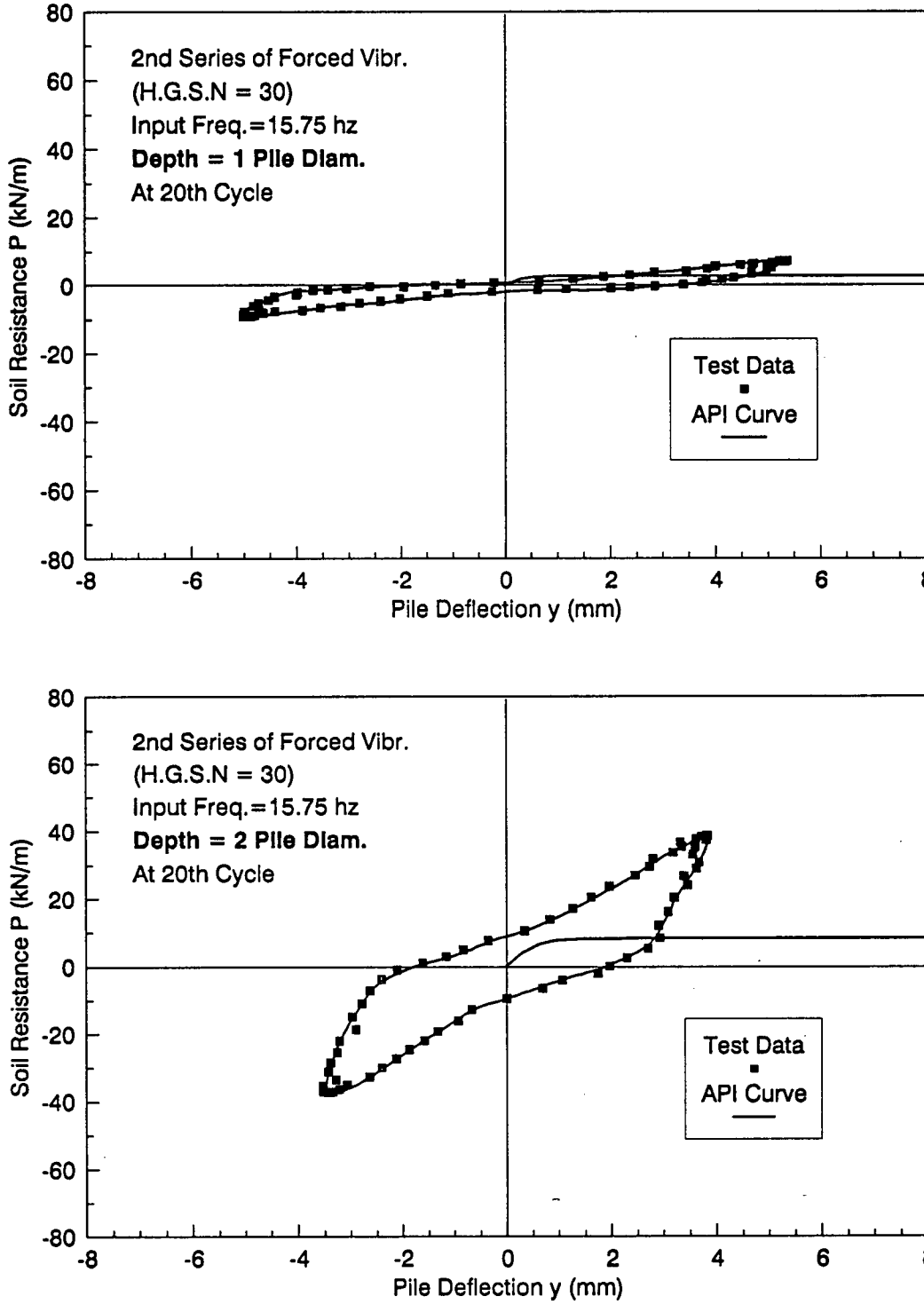

Figure 4.33: Cyclic p-y curves at 1 to 2 pile diameter depth during steady state shaking and comparison with API curves - test II-10

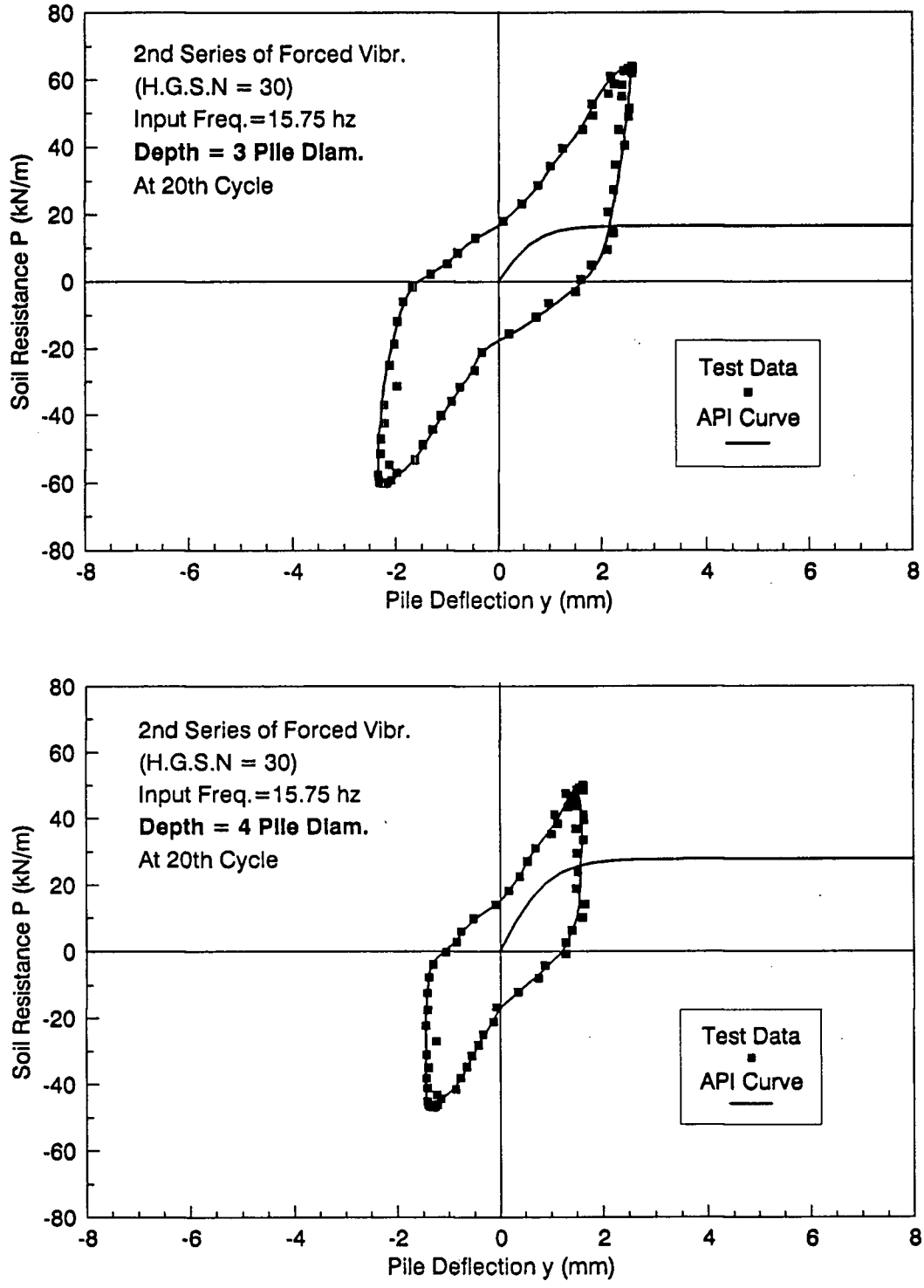

Figure 4.33: Cyclic p-y curves at 3 to 4 pile diameter depth during steady state shaking and comparison with API curves - test II-10

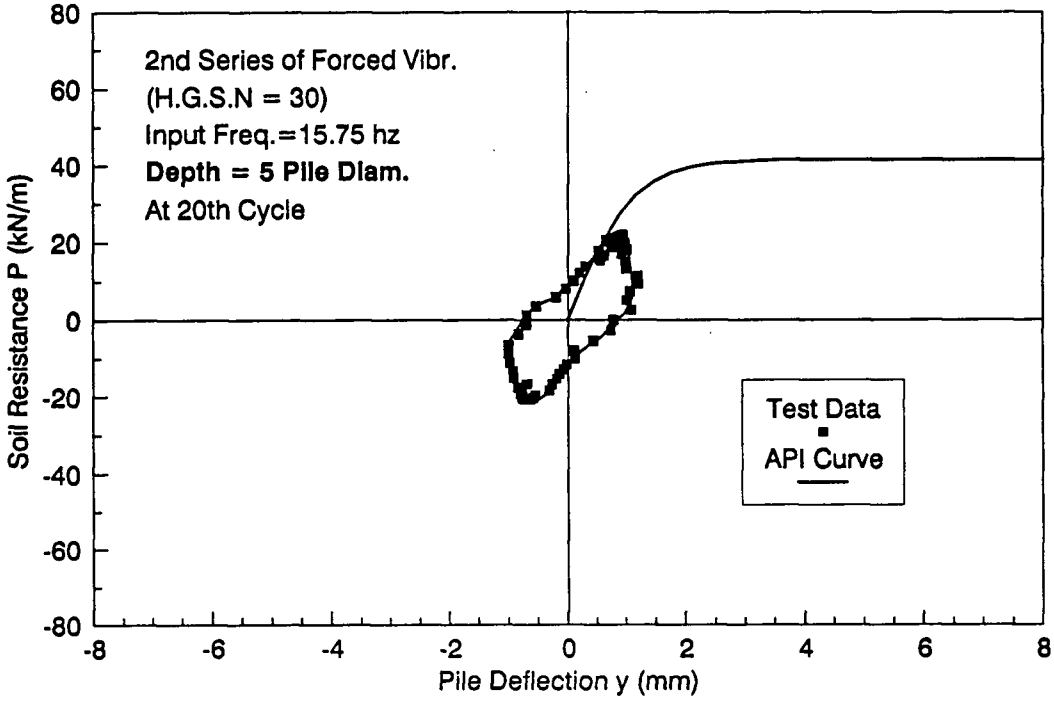

Figure 4.33: Cyclic p-y curves at 5 pile diameter depth during steady state shaking and comparison with API curves - test II-10

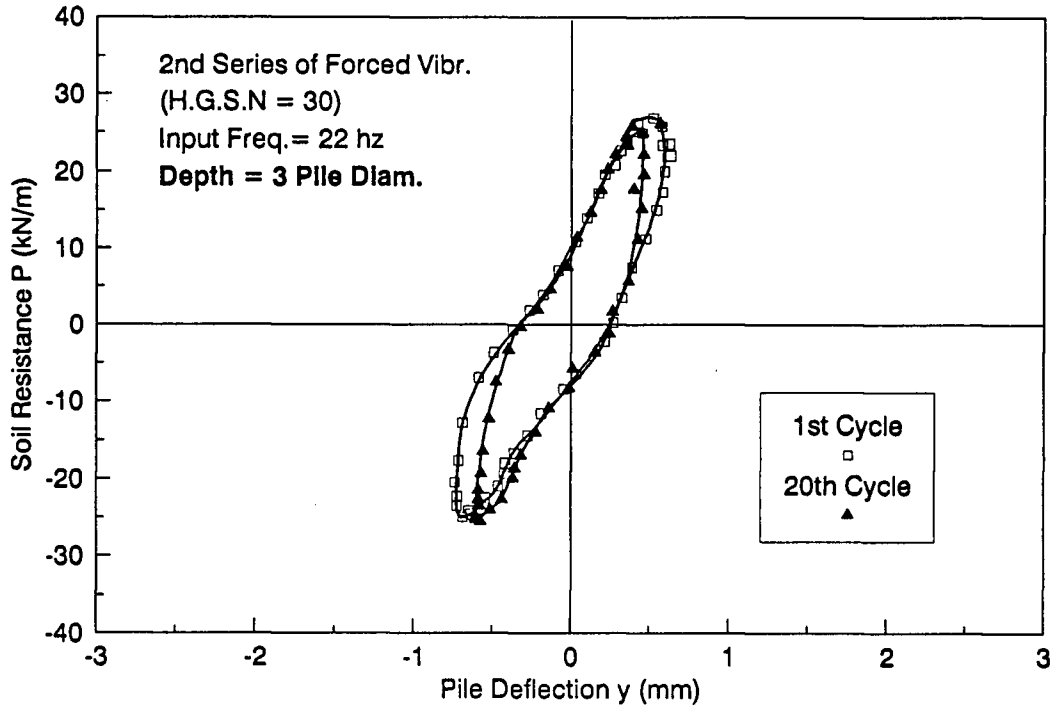

Figure 4.34: Cyclic p-y curves at different loading cycles at 3 pile diameter depth - test II-13

Figure 4.37 shows the cyclic p-y curves for two different loading cycles at the 3 pile diameter depth for test III-12 (input frequency of 30 Hz). It may be seen that the p-y behaviour for 1st and 20th cycles are consistent and linear. No significant change in secant soil stiffness was observed for the range of loading cycles. Cyclic p-y curves computed for test III-12 during steady state cycle are shown in Figure 4.38. The p-y curves have been computed up to the 4 pile diameter depth since below this depth lateral pile deflections could not be reliably discerned. The p-y data are seen to exhibit approximately linear elastic response over the range of depths. The use of elastic models to simulate soil-pile interaction would therefore appear to be reasonable. Apparently the lateral secant stiffness increases with depth, as was observed for the tests presented previously.

Cyclic p-y curves derived using the API procedures are also shown in Figure 4.38. It may be seen that the API curves at this test are in a relatively good agreement with the

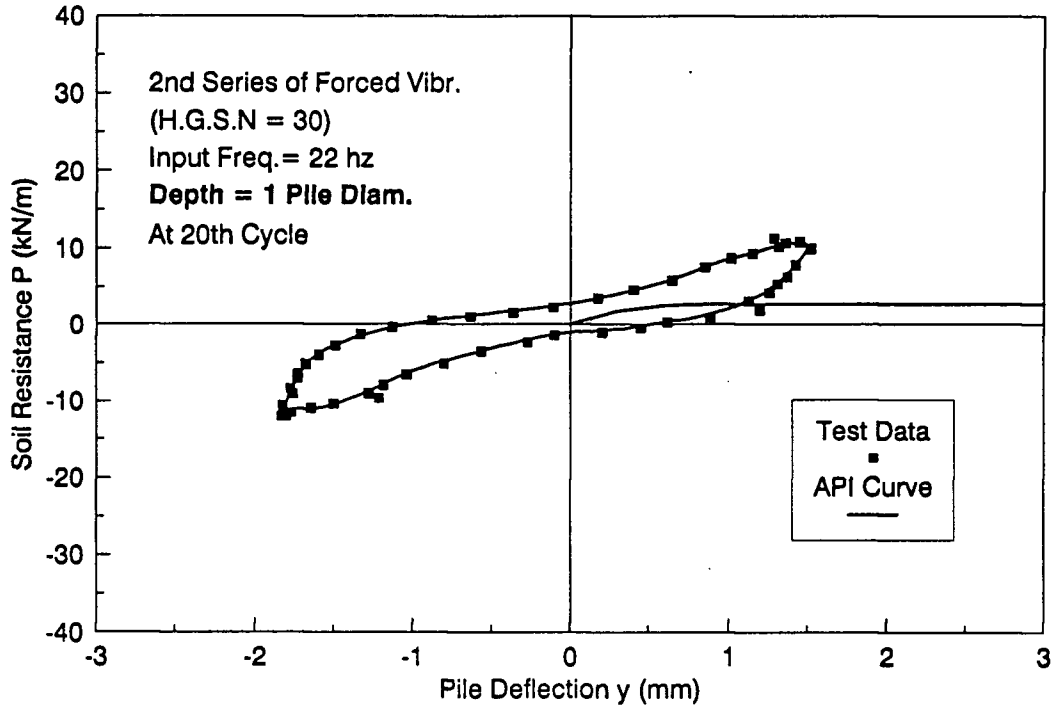

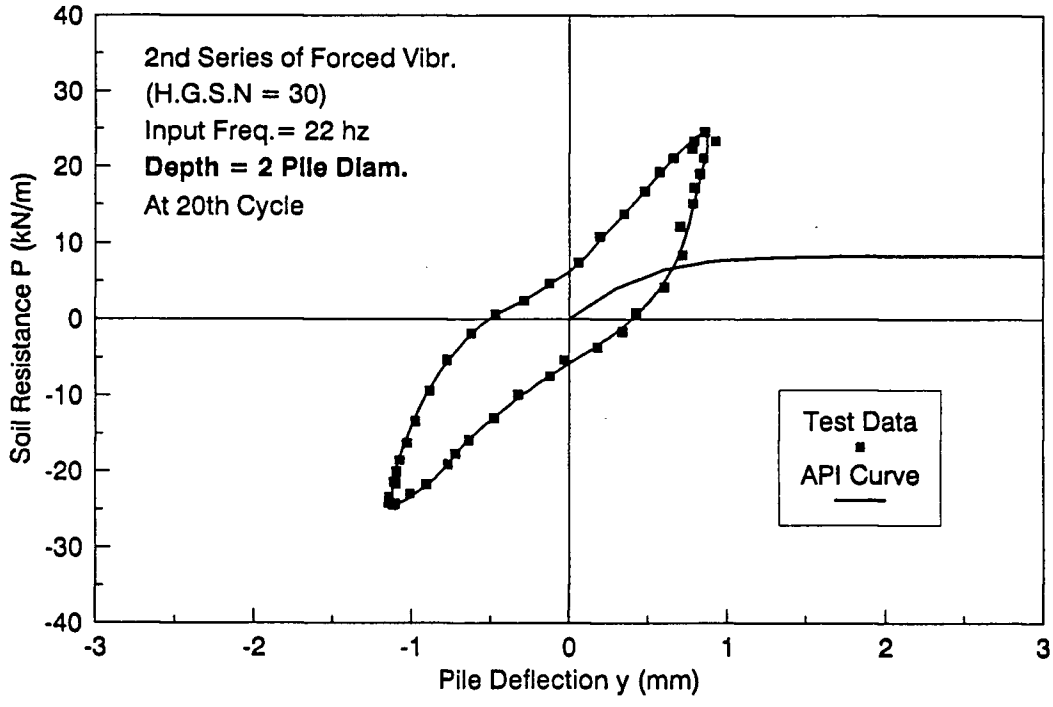

Figure 4.35: Cyclic p-y curves at 1 to 2 pile diameter depths during steady state shaking and comparison with API curves - test II-13

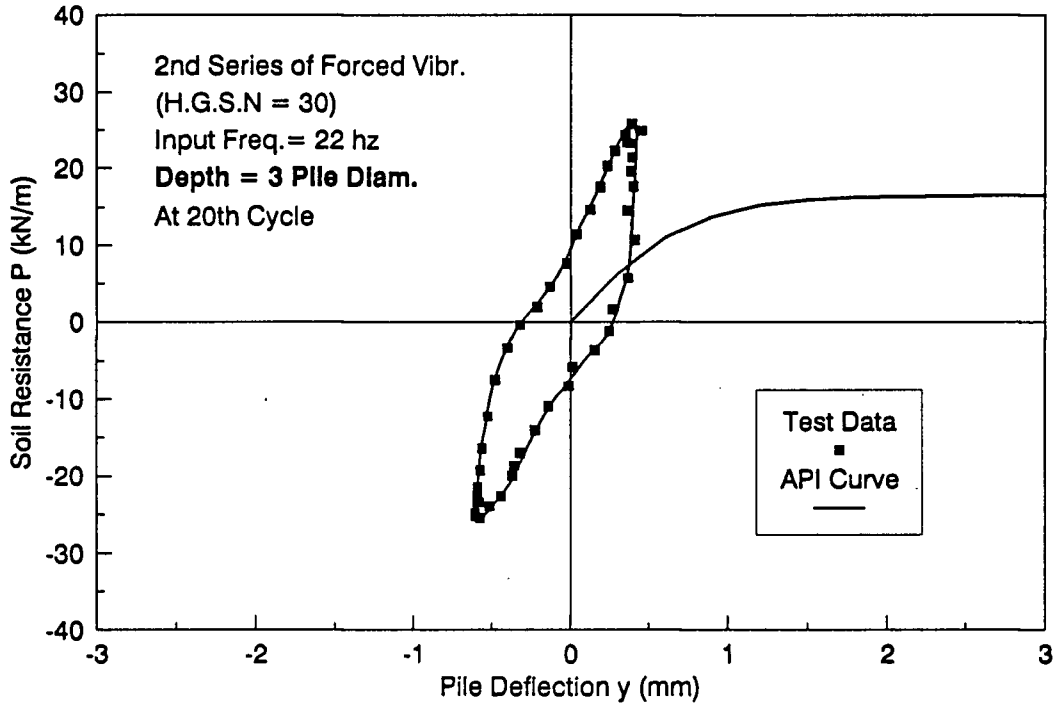

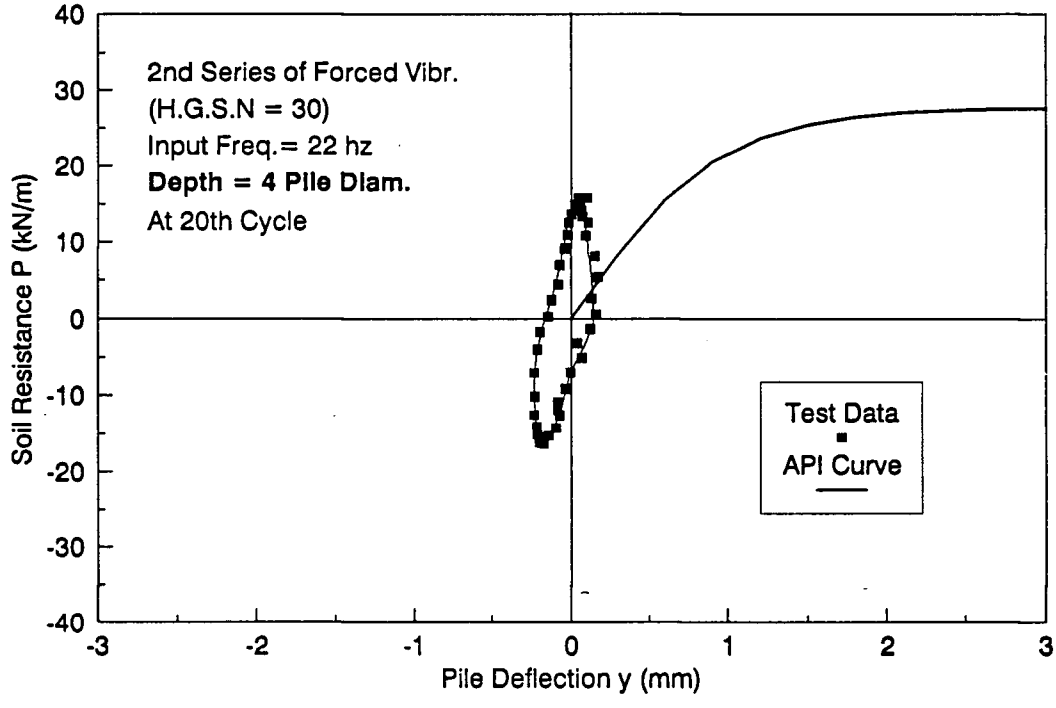

Figure 4.35: Cyclic p-y curves at 3 to 4 pile diameter depths during steady state shaking and comparison with API curves - test II-13

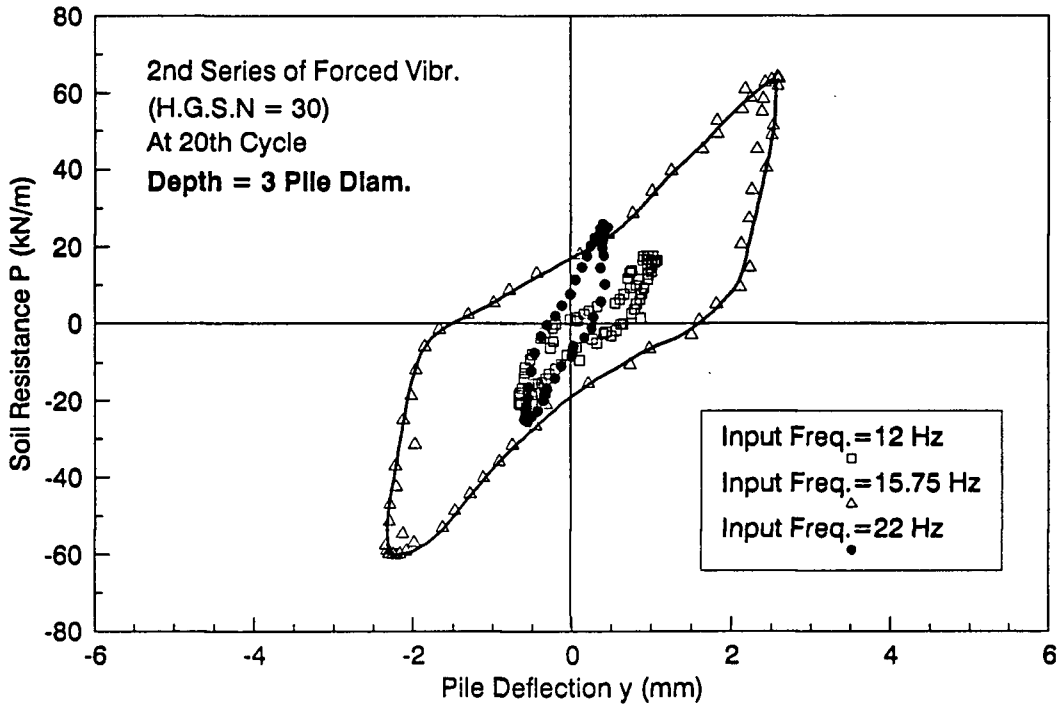

Figure 4.36: Comparison of p-y curves at different inertia loading level at 3 pile diameter depth - test Series II

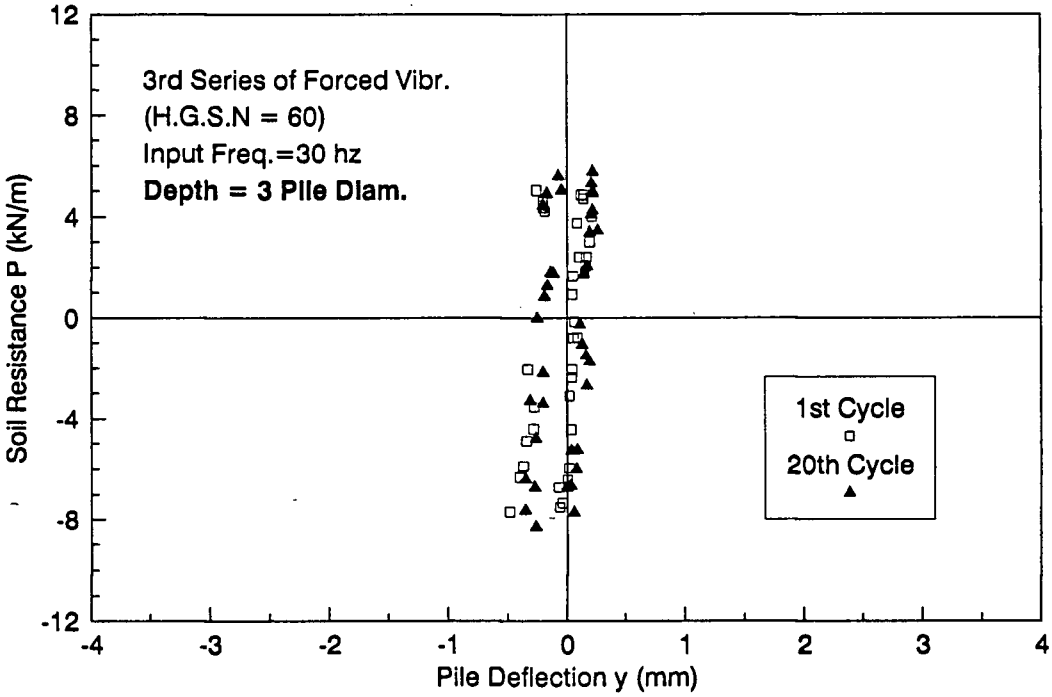

Figure 4.37: Cyclic p-y curves at different loading cycles at 3 pile diameter depth - test III-12

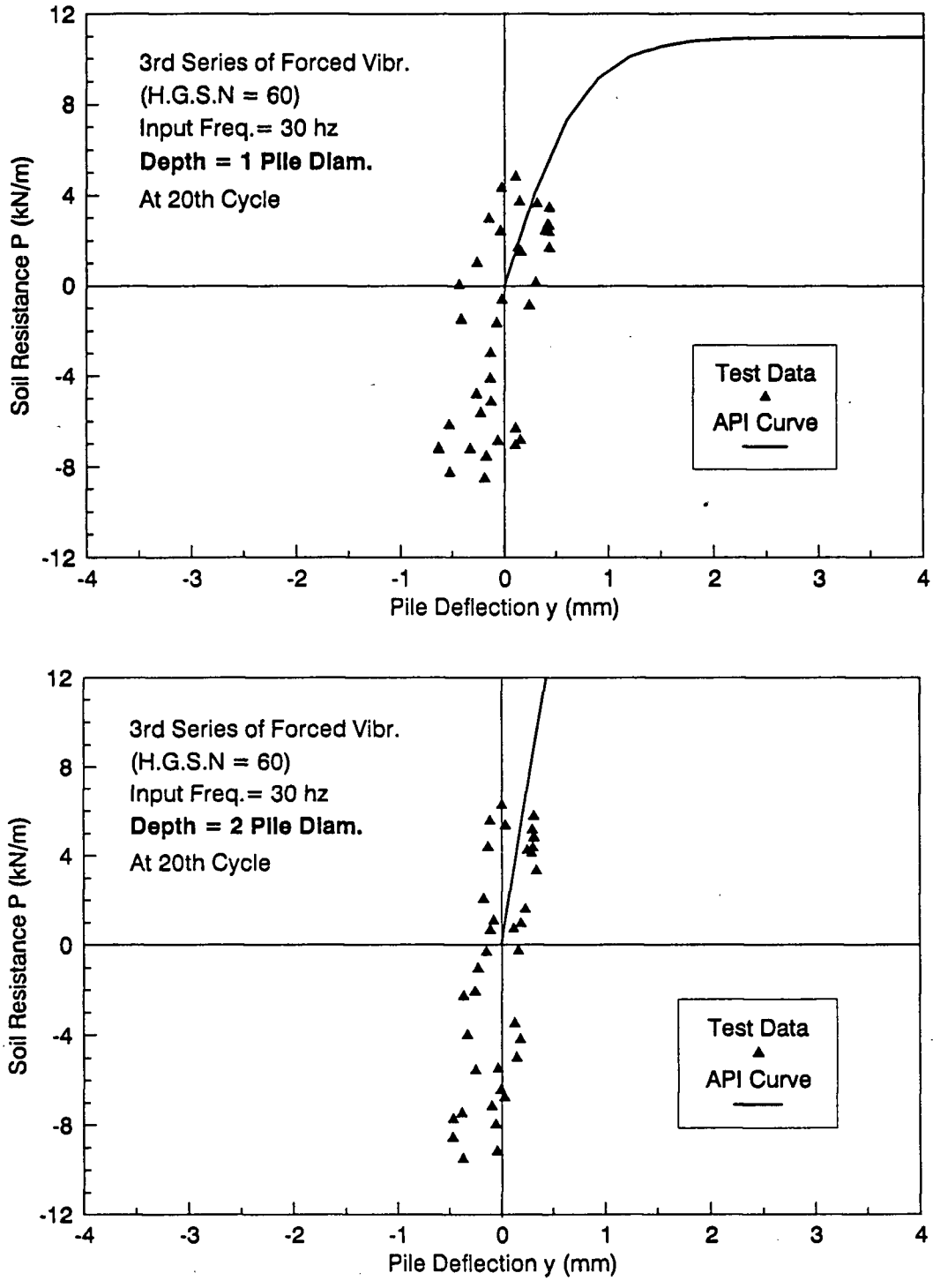

Figure 4.38: Cyclic p-y curves at 1 to 2 pile diameter depths during steady state shaking and comparison with the API curves - test III-12

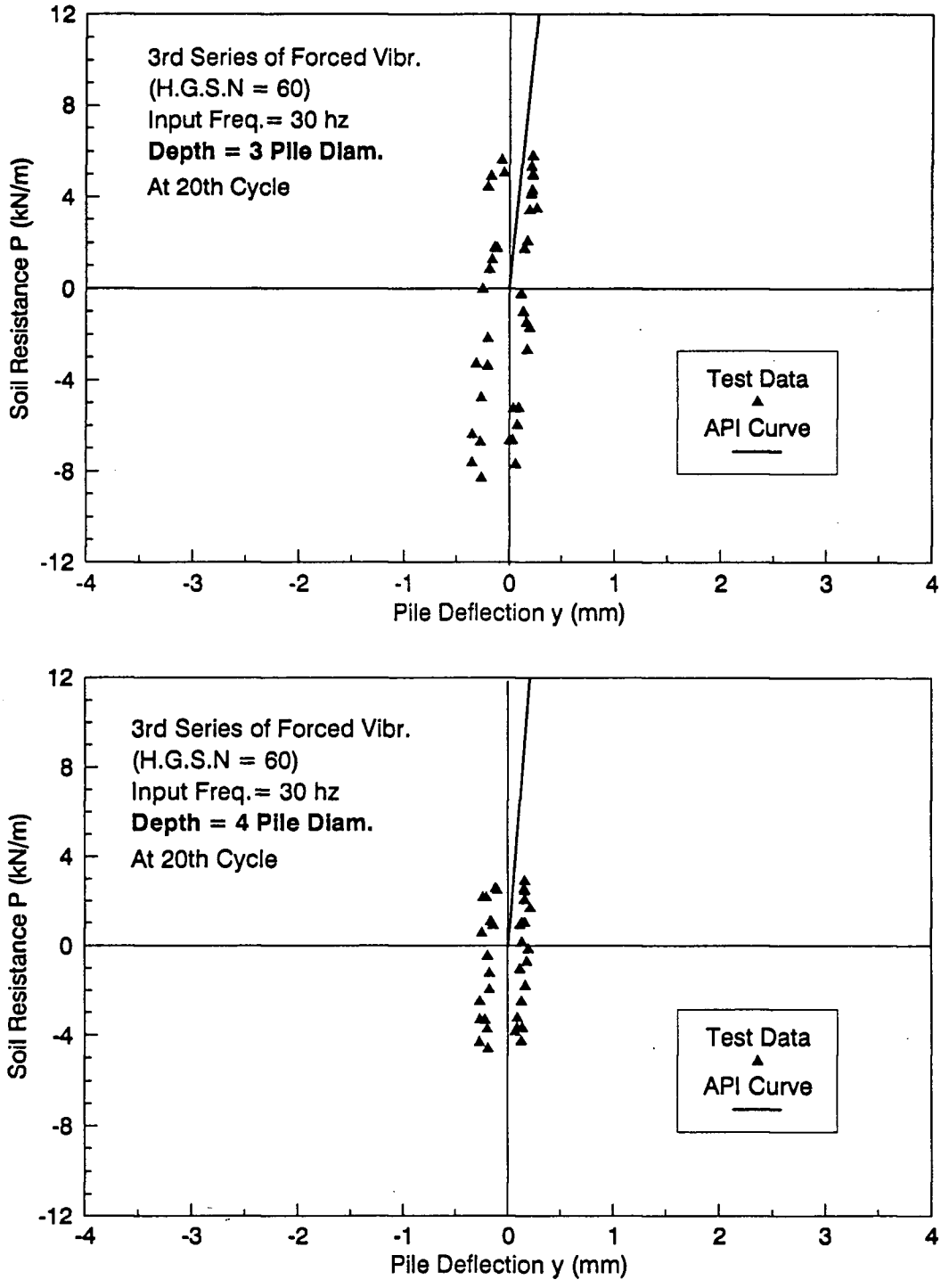

Figure 4.38: Cyclic p-y curves at 3 to 4 pile diameter depths during steady state shaking and comparison with API curves - test III-12

experimental data, in particular, at deep depths. This suggests that the API recommendations well predict the response soil-pile interaction under the condition that the soil resistance-pile deflection behaviour is in the linear elastic range of small pile deflection subjected to a moderate excitation in dense sand.

It appears that the general characteristics of soil-pile interaction at different depths and hydraulic gradients is quite alike and is stress level dependent. It will be very useful if the soil-pile interaction p-y curves can be normalized with regard to the soil stress levels and then for a given soil condition the p-y curves at various depths below the ground can be specified by a single equation.

As for static monotonic loading test on pile, the normalized p-y curves with maximum Young's modulus, E_{max}, are in the form of parabola (Yan, 1990), e.g. for dense sand ($D_r = 75\%$), the expression is given as:

$$\frac{p}{E_{max} D} = 0.15(\frac{y}{D})^{0.5} \tag{4.3}$$

where D refers to the diameter of pile. The advantage of this type of normalized p-y relationship is that the maximum soil Young's modulus, E_{max}, may be easily evaluated from the maximum shear modulus, G_{max} measured from insitu downhole and crosshole seismic tests.

Herein, for dynamic testing of pile, the endpoints of the hysteresis loop are used for Normalization of the p-y curves. Figure 4.39 shows the experimental p-y curves normalized by maximum Young's modulus E_{max} and pile diameter D. It is seen that all the normalized p-y data points fall into a band with a parabolic trend. Therefore, the average curve may be expressed by:

$$\frac{p}{E_{max}D} = \alpha[(1 + \frac{2}{\alpha}\frac{y}{D})^m - 1] \tag{4.4}$$

where α and m are curve fitting parameters that are determined from the normalized data. From these data $\alpha = 0.075$, and $m = 0.5$ for the dynamic test (Figure 4.39). Hence, the average curve become

$$\frac{p}{E_{max}D} = 0.075[(1 + 26.667\frac{y}{D})^{0.5} - 1] \tag{4.5}$$

Equation 4.4 gives a initial slope of 45 degrees which implies that the specific p-y curve at a certain depth start with a slope of E_{max} value corresponding to that depth. It also indicates that the stress level effects on p-y curves due to different depths below the ground can be reasonably taken into account by Equation 4.3.

Figure 4.40 gives comparison of normalized p-y curves from static, cyclic and dynamic loading tests. It is evident that the dynamic p-y curve is much stiffer than the static one, and the cyclic curve goes in between but nearly falls into the range of dynamic curve, resulting from increase of loading cycles and the soil densification around the pile. This postulates that the dynamic and cyclic pile loading tests resemble the unload-reload behaviour.

(E) Near Field Hysteretic Damping

The equivalent visco-elastic models are often used to approximate the previous non-linear, hysteretic p-y curves using a Kelvin-Voight model. Herein, a linear spring with stiffness k_h is placed in parallel with a viscous dashpot to represent frictional energy losses during one cycle of shaking within the near field soil (Seed and Idriss, 1970; Roesset, 1980).

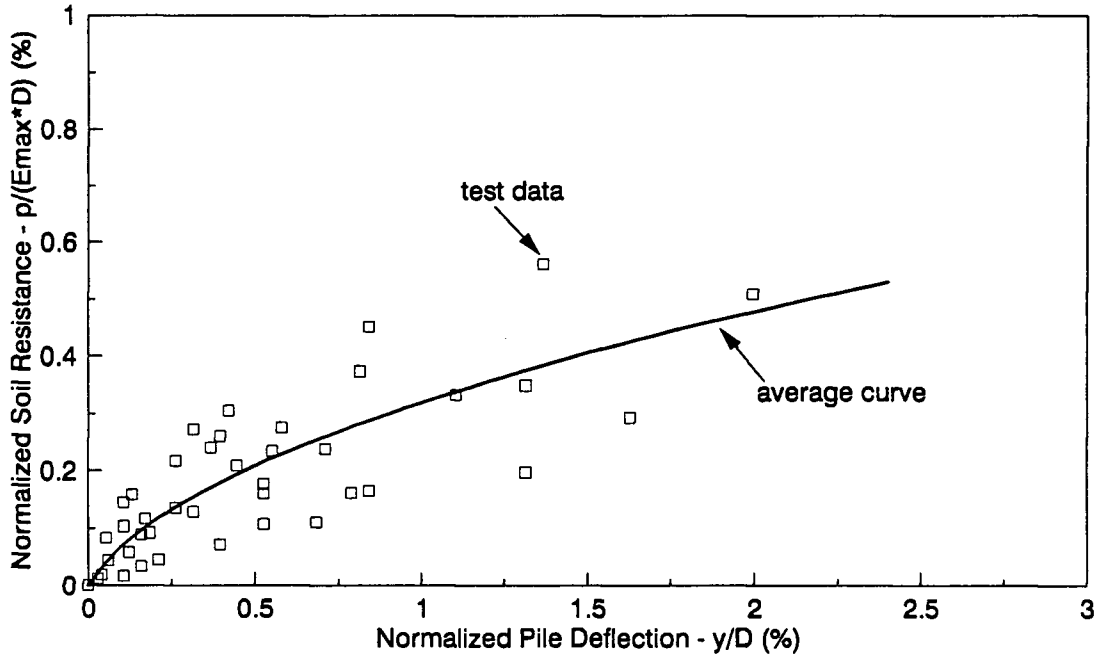

Figure 4.39: Normalized experimental p-y curves by maximum Young's modulus

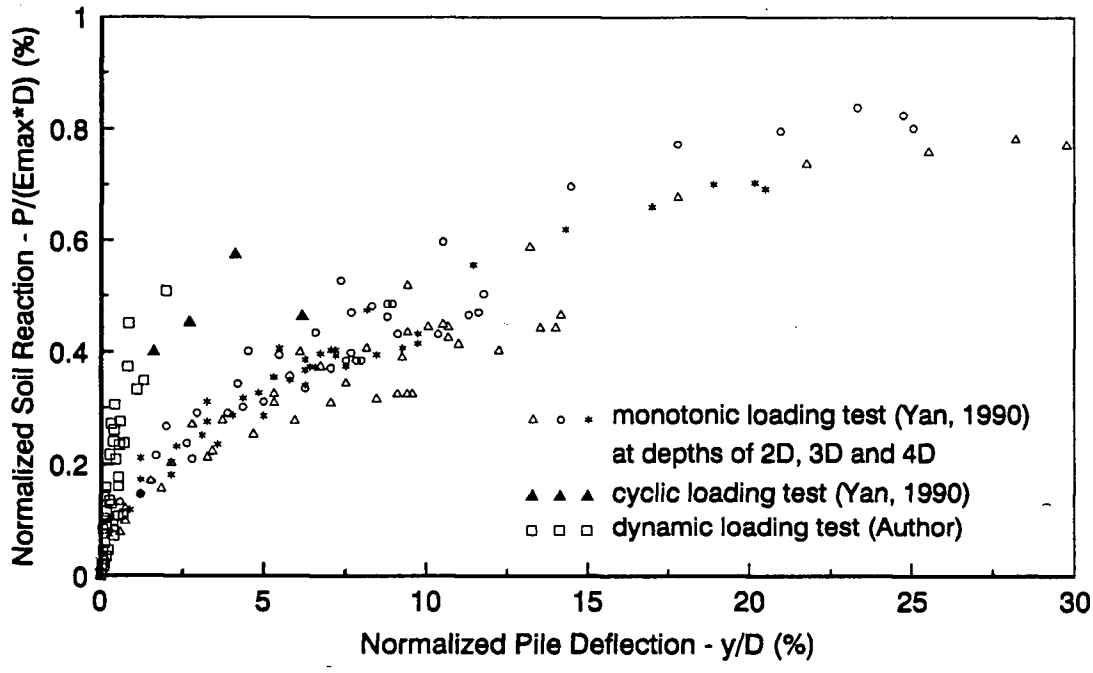

Figure 4.40: Comparison of normalized p-y curves for various natures of loadings

The area enclosed within a hysteretic loop of p-y curve for one cycle of shaking is equal to the energy lost due to frictional damping. For convenience of analysis, it is common to equate the work done by a frictional damping system over one load cycle, W_d, to the energy absorbed by a viscous damping system. Then, an equivalent viscous damping coefficient C_{eq}, or the fraction of critical damping D required to match the area within the p-y curves is defined. According to single degree of freedom vibration theory (Clough and Penzien, 1975) to define the damping characteristics of the near field soil, the work done by the damping forces over one cycle, W_d, is given as

$$W_d = \pi C_{eq} \omega y^2 \tag{4.6}$$

where ω is the angular frequency of vibration and y is the peak amplitude of lateral pile vibration relative to the free field ground motions. Substituting $c = 2D\omega_n m$ into Eq.4.5 yields

$$W_d = 2\pi D \omega \omega_n m y^2 \tag{4.7}$$

in which m is the mass and ω_n is the natural frequency of the idealized single degree of freedom system.

The elastic strain energy contained within the p-y curve over one load cycle is expressed by

$$W_s = \frac{1}{2} K_h y^2 \tag{4.8}$$

Then, the ratio of damping energy to elastic energy is

$$\frac{W_d}{W_s} = 4\pi D \frac{\omega}{\omega_n} \tag{4.9}$$

As the dynamic response of a single degree of freedom system is most sensitive to the damping at resonance, the damping ratio D is hence defined at $\omega = \omega_n$ and gives

$$D = \frac{W_d}{4\pi W_s} \tag{4.10}$$

As seen in Equation 4.9, the damping ratio can be defined by enclosed area W_d of the hysteresis loop and the elastic strain energy W_s. The damping ratio of sands is normally assumed to be independent of the frequency of cyclic shearing. Damping increases with the level of cyclic shear strain and decreases with the number of cycles of shaking (Hardin and Drnevich, 1972). Damping ratios of more than 30% are commonly adopted during large strain excitation of sand when shear strains exceed approximately 1%.

The strain in the soil in the vicinity of pile is related to the lateral pile displacement. Thus, hysteretic damping ratios are determined from the experimental p-y curves using Eq. 4.9 and plotted versus dimensionless displacement y/d for the depth under consideration. Here, y is the peak to peak lateral deflection divided by two and d is the pile diameter.

Damping ratios derived from strong shaking and moderate shaking tests in dense sand (D_r = 75%) during steady state vibration (at 20th cycle) for tests I-7, II-10 and III-7 are presented in Figure 4.41. In the case of strong vibration (Figures 4.41a and b), the computed damping ratios are in the range of 22 – 42% of critical damping, and the data at deep depths, the 1st and 2nd points in the figure, shows large strain damping ratios to be substantially higher than for shallower depths. This may suggest that as the amplitudes of pile vibration decrease with depth, cyclic densification and the reduction in maximum shear modulus G_{max} is not as pronounced.

The damping ratios obtained from test III-7 in moderate shaking are given in Figure 4.41c. Computed damping ratios are in the range of 15 to 25% which are obviously lower

than those for strong shaking by $30 - 40\%$. The damping ratios are not significantly different over the range of lateral pile deflections examined.

4.4 Summary and Conclusions

The dynamic behaviour of single pile response to simulated earthquake ground shaking were studied experimentally using hydraulic gradient similitude method. In order to better understand the fundamental characteristics of soil-pile interaction under lateral dynamic loading, a variety of free vibration and forced vibration tests were carried out at different shaking intensities and various soil stress levels. An extensive interpretation of test results were presented in this chapter and data base on dynamic pile foundation tests are thus further enriched.

Model studies of vertical single piles embedded in dense sand ($D_r = 75\%$) subjected to initial pile head perturbation as well as sinusoidal base excitation were performed and the dynamic properties were then measured. One major purpose of the study was to determine soil-pile interaction under simulated earthquake loading in a well controlled stress and soil condition so that the current understanding and analytical methods could be evaluated. On the other hand, this study also simultaneously assesses and demonstrates the successful application of the hydraulic gradient similitude technique to pile foundation investigations. The hydraulic gradient modelling laws for dynamic study of pile foundation have been verified experimentally using the indirect approach of modelling of models, similar to centrifuge testing observation, and found to be satisfied. In general, the technique appears to be suited to such experiments.

On the basis of an extensive series of free vibration tests on different piles, it is found that the experiments support the observation that the dynamic modulus of sand

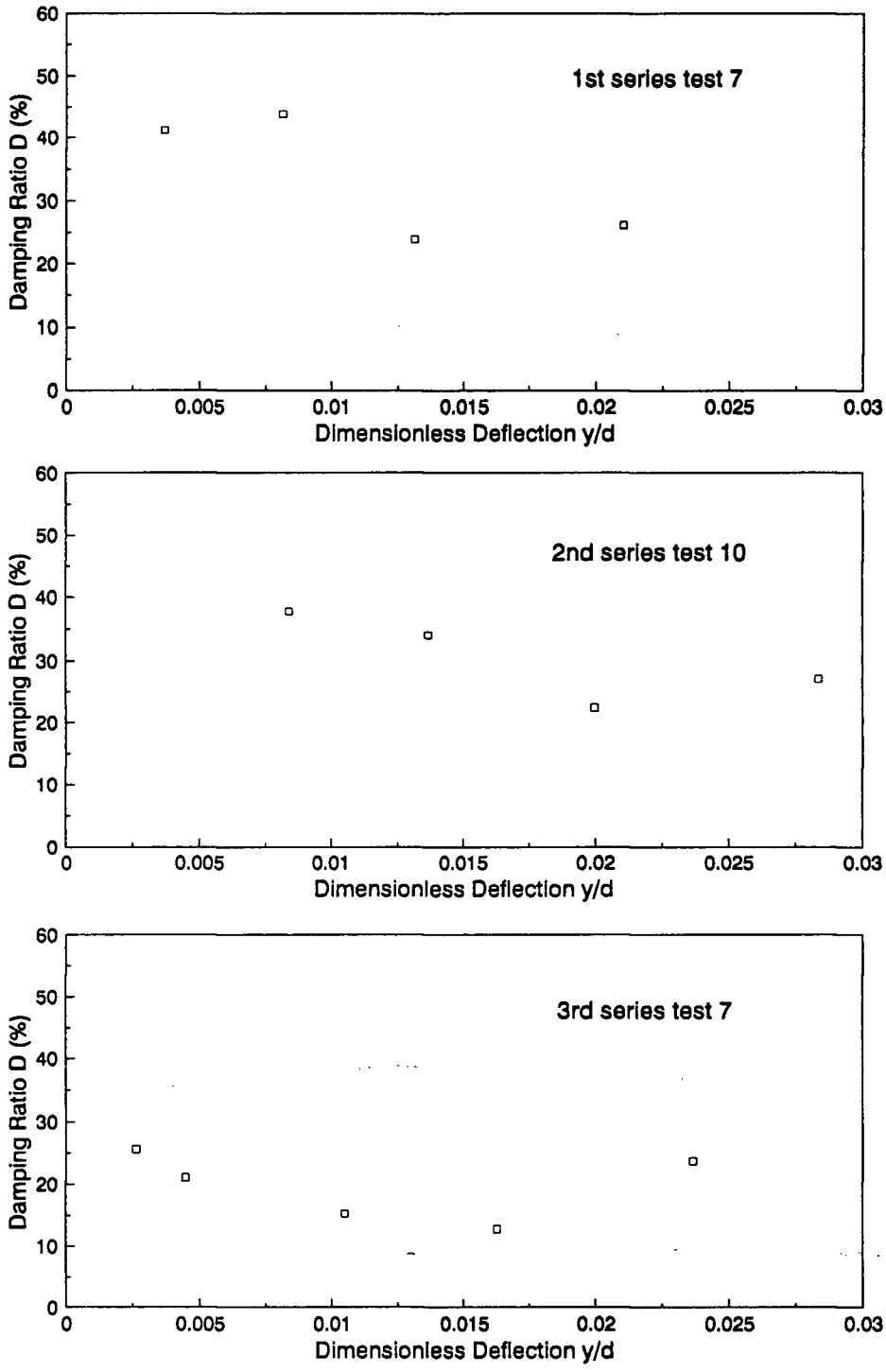

Figure 4.41: Hysteretic damping ratios versus dimensionless pile deflection y/d

is proportional to the square root of the confining stress. The soil-pile system stiffness is higher for the smaller strain of pile (deflection) than for the larger one. Also, the stiffer pile yields a higher stiffness of soil-pile system. An interesting finding is that, if the soil-pile system frequencies are normalized with regard to the fundamental frequency the normalized frequency of the system is constant regardless of soil stress level. It is also seen that the equivalent length of pile decreases with stress and reaches an asymptotic value.

The equivalent viscous damping of the soil-pile system is nearly independent of soil stress levels, depending upon the vibration amplitude (or strain level). Generally, larger amplitude causes an increase in the damping. It is also observed that the damping decreases with the number of vibration cycles.

For the piles subjected to simulated earthquake ground motion, the response is related to the shaking intensity, exciting frequency and soil stress level. The superstructure response appears to be not significantly different in terms of amplification to the free field motion for different hydraulic gradients under the same strong base shaking (about 0.5 g), whereas, under the same soil stress level the amplification of the superstructure is considerably higher for lower level shaking than for higher level shaking. The latter observation is in accord with the results of El Marsafawi et al. (1990). It can be seen that the resonant frequency increases with increasing soil stress level which confirms the free vibration results. The pile head stiffness is found to decrease with its increasing deflection.

Generally, soil densification did not occur. Under the dynamic base loading, the responses of pile deflection and bending moment were rationally symmetric. It seems that the number of the loading cycles do not make effect on the pile response except that initial transient phase occurs occasionally. The maximum bending moment in the model

pile is substantially greater for close to resonance frequency test because of higher inertia force than for the other tests. Also, the depth of maximum bending occurring appears to be greater at larger pile head load than at smaller one.

The soil-pile interaction under lateral dynamic loading were evaluated in terms of cyclic p-y curves. The cyclic p-y curves were found to be highly nonlinear and hysteretic under strong shaking but independent of number of loading cycles in dense sand. However the p-y response under moderate shaking is more linear elastic. Stiffer p-y curves are observed at deeper depths, and p-y responses are nearly linear elastic below about 5 pile diameter depth. The API recommended p-y curves for sand are also plotted together with test data. In general, the API procedure underpredict lateral soil stiffness or soil reaction under strong shaking intensity, especially at shallower depths, while in the range of linear p-y response (e.g. below 5 pile diameter depth), the API curves seems to well agree with experimental curves. However, in the tests of moderate shaking, the API procedures slightly overestimate the lateral soil stiffness, in particular, at shallower depths.

The dynamic normalized p-y curve by maximum Young's modulus are seen to have a parabolic trend with initial slope of 45°. Further, the p-y curves from dynamic tests is much stiffer than that from static tests, and the one from cyclic pile head loading lies in between but nearly falls into the dynamic range.

The near field hysteretic damping are also obtained and the damping under strong shaking intensity is higher than that for lower level shaking.

Chapter 5

Prediction of Pile Response to Dynamic Loading

In this chapter, the p-y curves constructed by different procedures are used to predict the observed responses of model pile and superstructure to pseudo dynamic and dynamic lateral loading at the pile head. These predictions are made using the finite difference computer program LATPILE (Reese, 1977) which incorporates the nonlinear subgrade reaction method. Analyses are made for selected tests and are presented in this chapter.

5.1 Construction of p-y Curves

The different procedures for constructing p-y curves are described herein, and compared with the API code, the empirically proposed model (Chapter 4), as well as experimental curves.

The construction procedure for p-y curves using API Code (1987) was described in Chapter 2. The p-y relationship is defined by Equation (2.1) as hyperbolic tangent function at a specific depth. The initial slope of the curve at a given depth is defined as "$n_h Z$", where n_h is determined from Figure 2.1. The ultimate lateral soil bearing capacity p_u is obtained from the smaller value of Equations 2.2 and 2.3 with the coefficients given in Figure 2.2. The factor A in Equation 2.1 is taken as 0.9 for cyclic loading. For the present test condition, the curve for saturated sand in Figure 2.1 is used to obtain the coefficient of subgrade reaction modulus, n_h. Both relative density and angle of internal friction can be used to enter the chart. Nevertheless, the stress level at which the friction angle is to be determined is not specified in the API design code (1987). Herein, the

peak friction angle of 39^0 obtained from conventional triaxial test data (see Table 3.4 in Chapter 3) are used for dense sand ($D_r = 75\%$) tested.

As proposed based on experimental data in Chapter 4 (Equation 4.4 and Figure 4.39), the initial slope of the p-y curves start with the maximum Young's modulus of soil, E_{max} at small strain level. In addition, Figure 4.40 suggests that the normalized dynamic p-y data fall into a narrow band with a approximate linear relationship in small strain range. Since the dynamic tests are carried out within a fairly small strain level, it may be reasonable to use a linear p-y relationship with a slope of E_{max} to predict the pile response. Therefore, the linear p-y curve will also be examined against the experimental data and compared with the API procedures.

Figure 5.1 shows comparison of the p-y curves from the API code (1987), linear model and proposed model with the test data. It is seen that the linear p-y curve is stiffer than the other procedures at any depth, and nearly the same as the API curves below 5 pile diameter depth. The API curves are softer than the test data and the proposed curves at shallow depths while slightly stiffer bellow about 4 pile diameter depth. It is also observed that the proposed average curve, in general, agree well with the test data in terms of lateral soil stiffness. It is worth noting that the API curves are essentially bilinear reaching ultimate soil resistance beyond a certain deflection and that the linear p-y curves coincide with the initial tangent of the proposed parabolic curves.

5.2 Prediction of Pile Response

The p-y curves constructed in the procedures described in Section 5.1 are applied to predict the response of single piles to pseudo dynamic loading at pile head. The computer program LATPILE are used to perform this analysis in which the soil resistances to the pile deflection are prescribed along the pile length at given depths starting from the

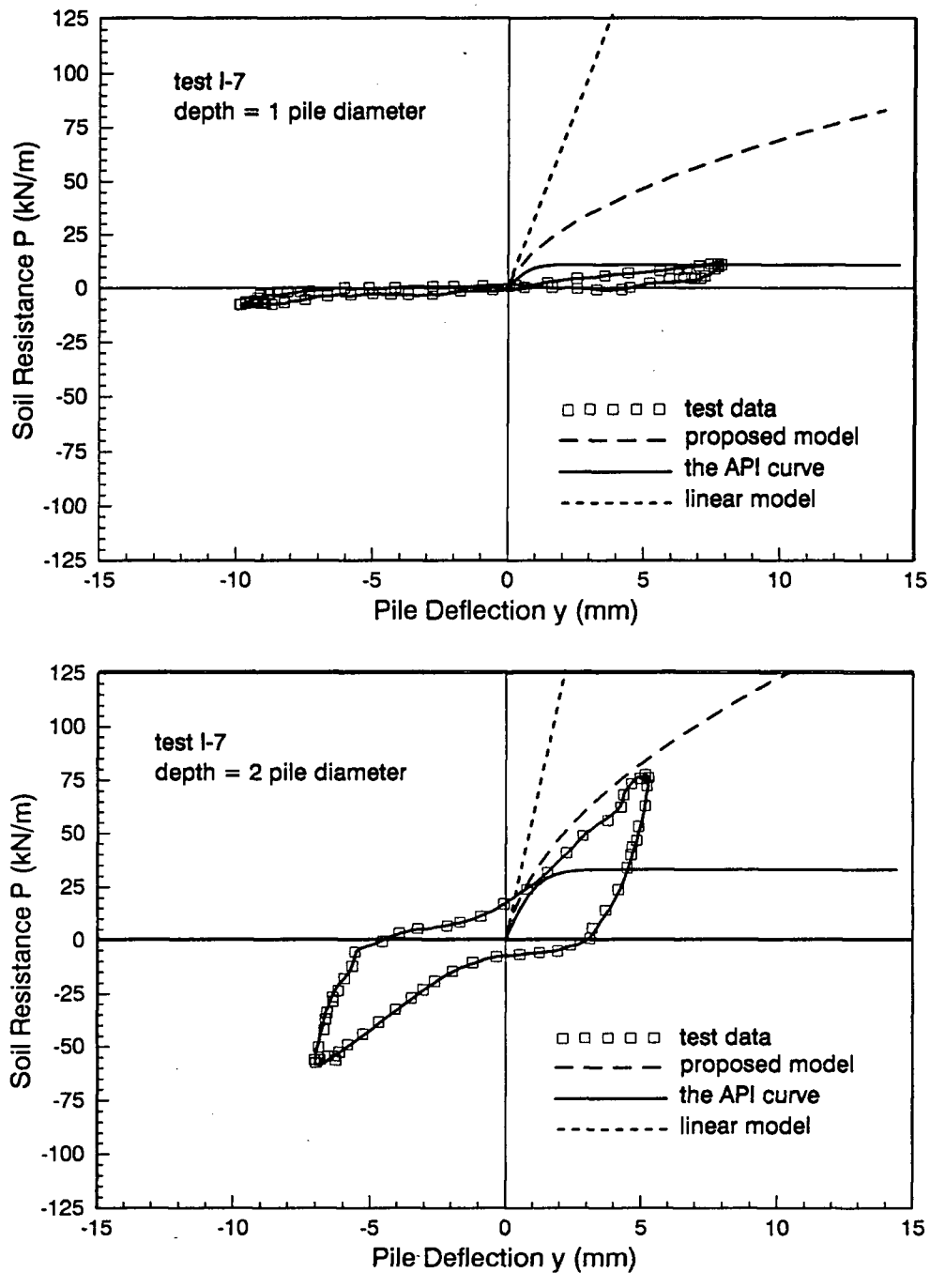

Figure 5.1: Comparison of p-y curves from the API code, linear model, proposed model and the test data at 1 to 2 pile diameter depth (prototype scale)

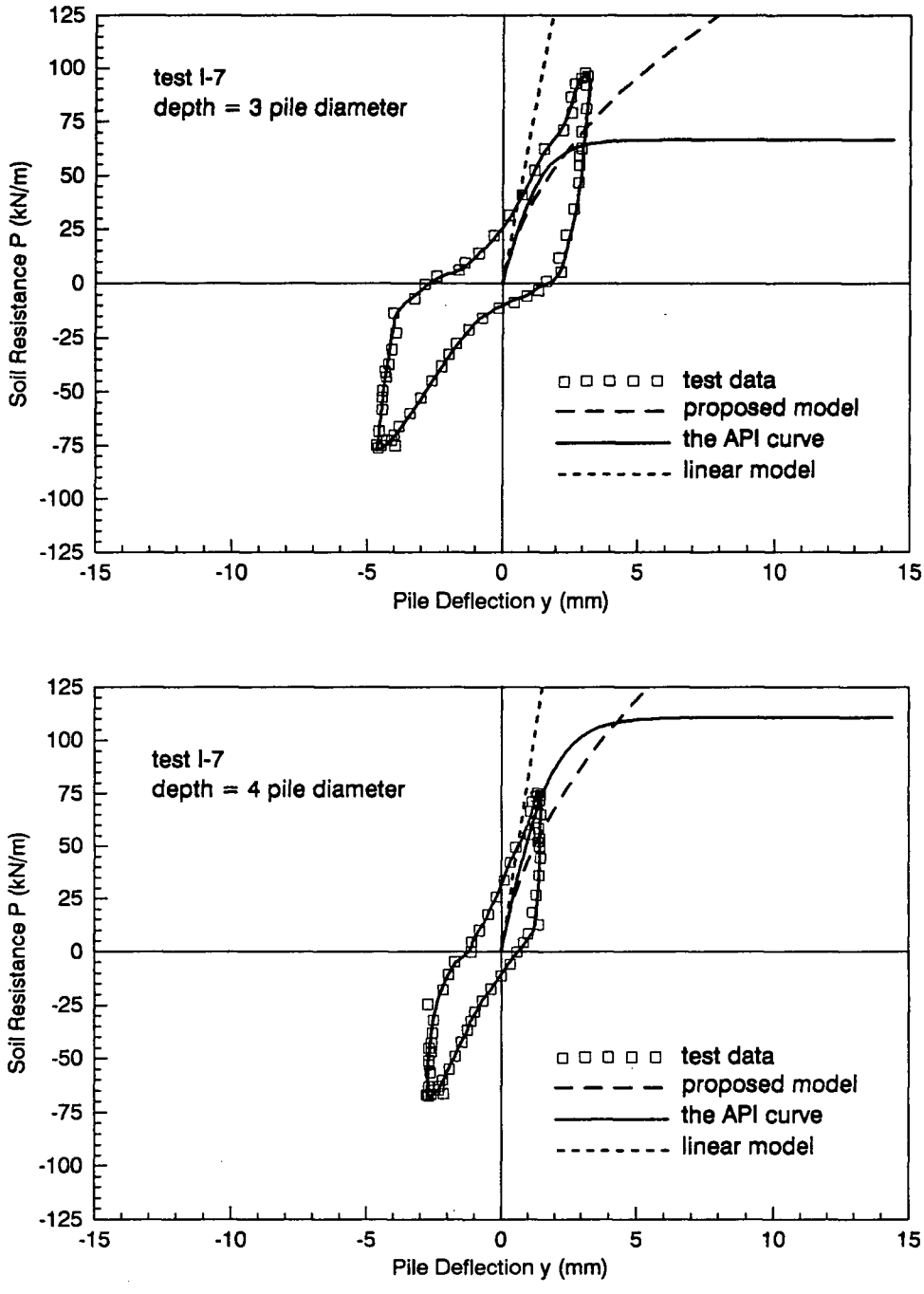

Figure 5.1: Comparison of p-y curves from the API code, linear model, proposed model and the test data at 3 to 4 pile diameter depth (prototype scale)

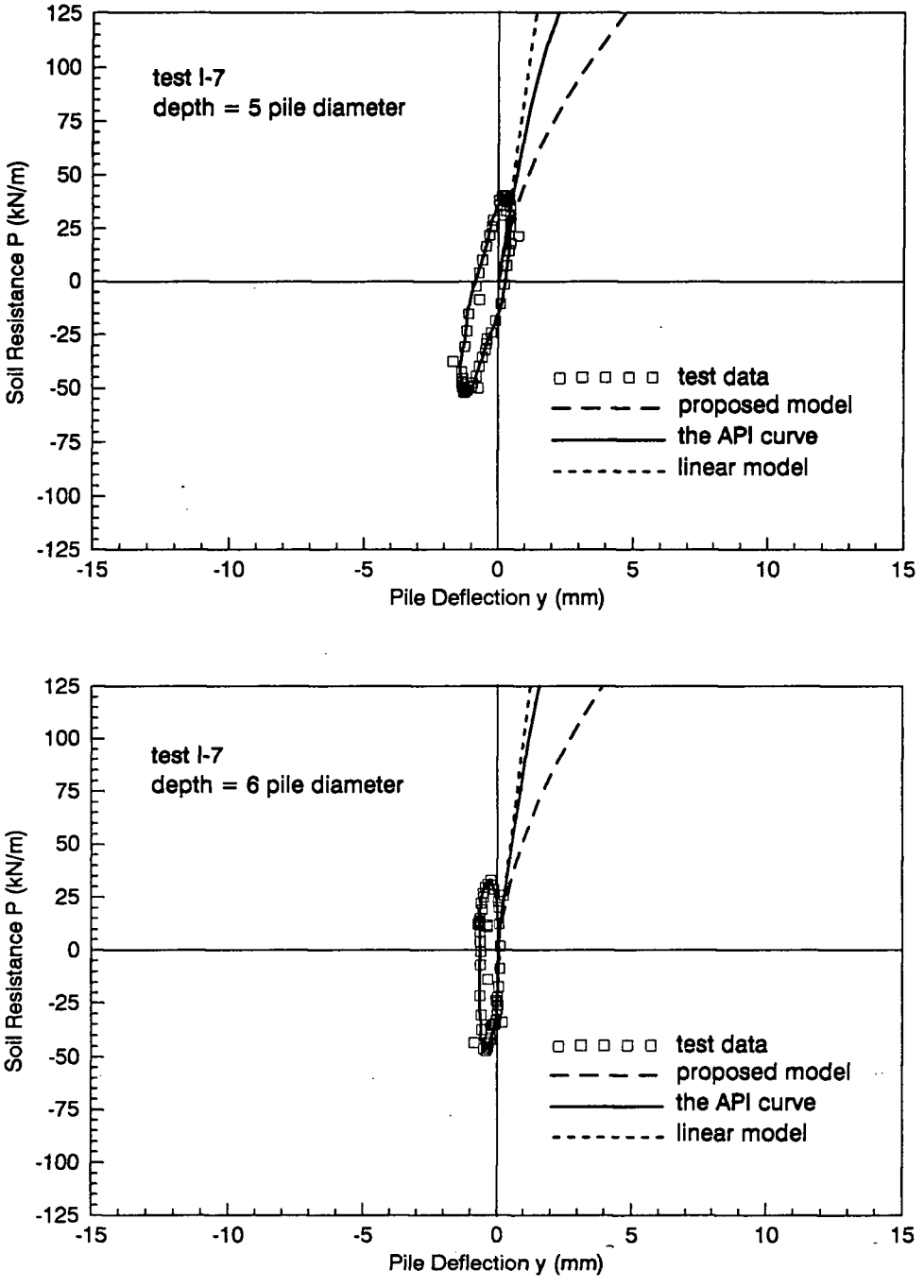

Figure 5.1: Comparison of p-y curves from the API code, linear model, proposed model and the test data at 5 to 6 pile diameter depth (prototype scale)

sand surface. A linear interpolated scheme is applied by the program to model the soil response between the p-y curves specified. Predictions are made on the basis of 1st series of forced vibration tests 4 and 7 (i.e. test I-4 and test I-7). It should be noted that all results discussed in this section are in prototype scale.

Figure 5.2 shows the prediction of pile bending moment distribution along the length of pile for tests I-7 and I-4 whose peak inertia forces are 43.485 kN and 25.487 kN, respectively. The analyses using the empirical model of p-y, the API procedure and linear model of p-y give the same results at shallow depth (1.5-2.0 pile diameters) and make negligible overprediction. Whereas at deep depth, the linear p-y model underestimates the bending moments for greater pile head load (Figure 5.2a), but exhibit a good agreement with test data for smaller load, which suggests that the soil behaviour may be modelled in a linear manner in small strain range . The API procedures overestimate bending moments at all depths, for the two tests concerned. The linear method yields a reasonable agreement with the test data on maximum bending moment but occurring at shallower depths than the measured.

In addition to pile bending moment distribution, other parameters such as pile deflection, soil reaction, shear force on the pile and the equivalent subgrade soil modulus used in the analysis can be determined from the computer program LATPILE. This information can be useful in evaluating the role of the p-y curves specified in the analyses by different methods. Since direct measurements of these quantities are not available, comparison is made against the predictions using the experiment-based p-y curves proposed in Chapter 4.

Figure 5.3 portrays the computed pile deflection profiles for tests I-7 and I-4. It is seen that in both tests, the API procedure produces slightly greater deflections, whereas the linear method yields smaller deflections, which is in accord with the overestimate and underestimate of bending moments from the API procedure and linear manner,

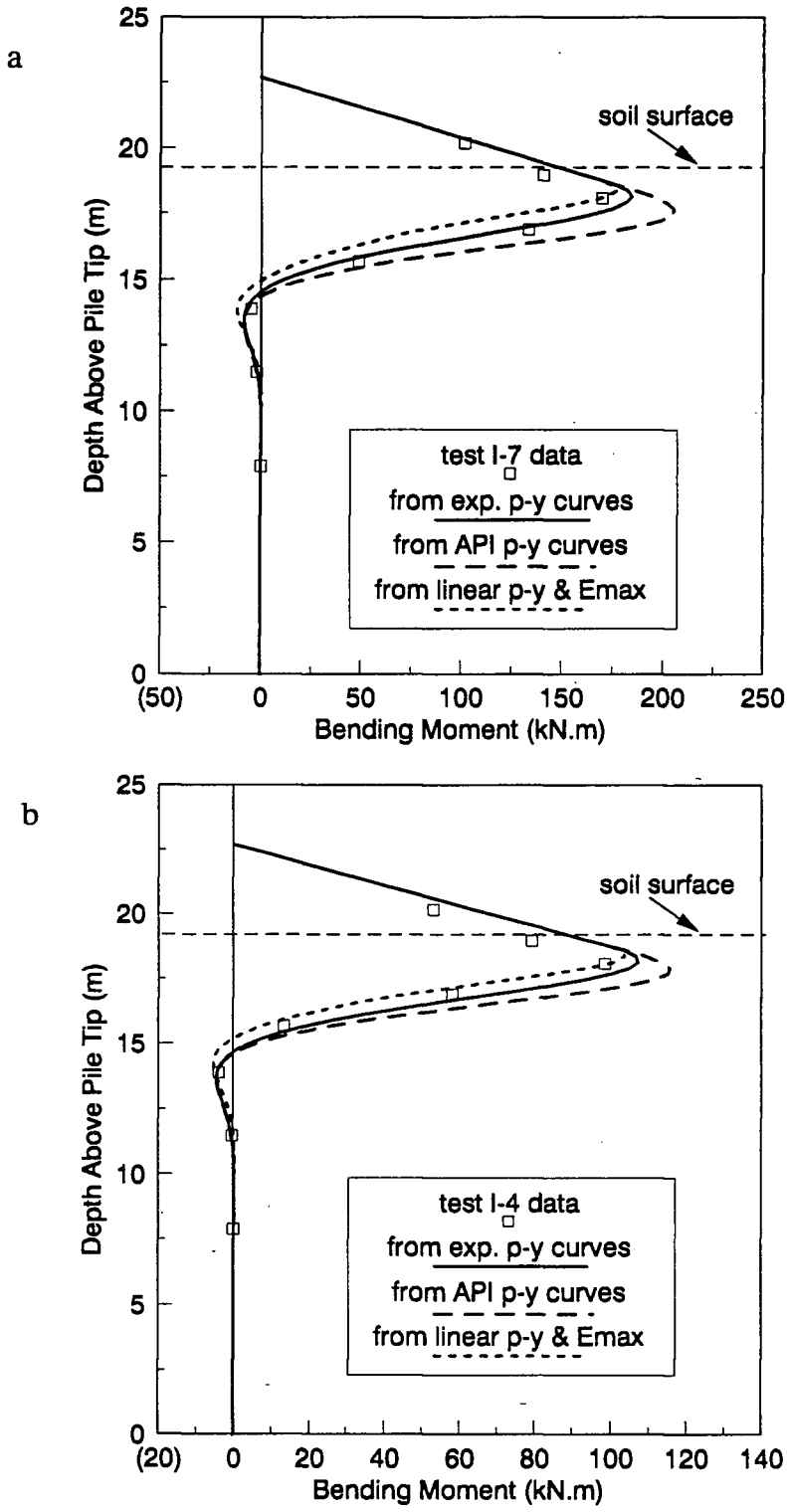

Figure 5.2: Computed bending moment distribution versus measured (a) test I-7; (b) test I-4

respectively.

The computed shear force and soil resistance distribution for the two tests are shown on Figures 5.4 and 5.5, respectively. It may be seen that greater maximum shear forces and soil resistances are predicted by the API procedure and linear method. The latter is more pronounced in its overprediction at shallow depths. The API recommendation gives smaller shear forces and soil resistances at shallow depths where pile deflection is large and the API p-y curves reach the ultimate values which are much less than the experimental data. At depths greater than 2.5 pile diameters, however, the API code procedure yields greater shear forces and soil resistances. The pile deflection is small and the API p-y curves are stiffer than the experimental ones at these depths.

5.3 Computed Superstructure Response

The motion of superstructure of model pile foundation are simulated by a single degree of freedom (SDOF) vibration system (Figure 5.6). The rotation mode is neglected since the vibration of the superstructure is dominated by translation mode. The prediction of the superstructure response is made based on SDOF amplification theory where the amplification to the base excitation is given as:

$$D = \frac{K}{\sqrt[2]{(K - m\omega^2)^2 + (C\omega)^2}} \tag{5.1}$$

in which m is the mass of structure, K is the pile head stiffness, C is the damping coefficient and ω is the forcing frequency of the excitation.

The API p-y curves and linear p-y curves are employed to compute the pile head cap (superstructure) response. A range of lateral loads at pile head were applied to cover the anticipated range of structural inertia forces acting at the pile for the considered shaking intensity. For each load level, the computer program LATPILE was used to compute

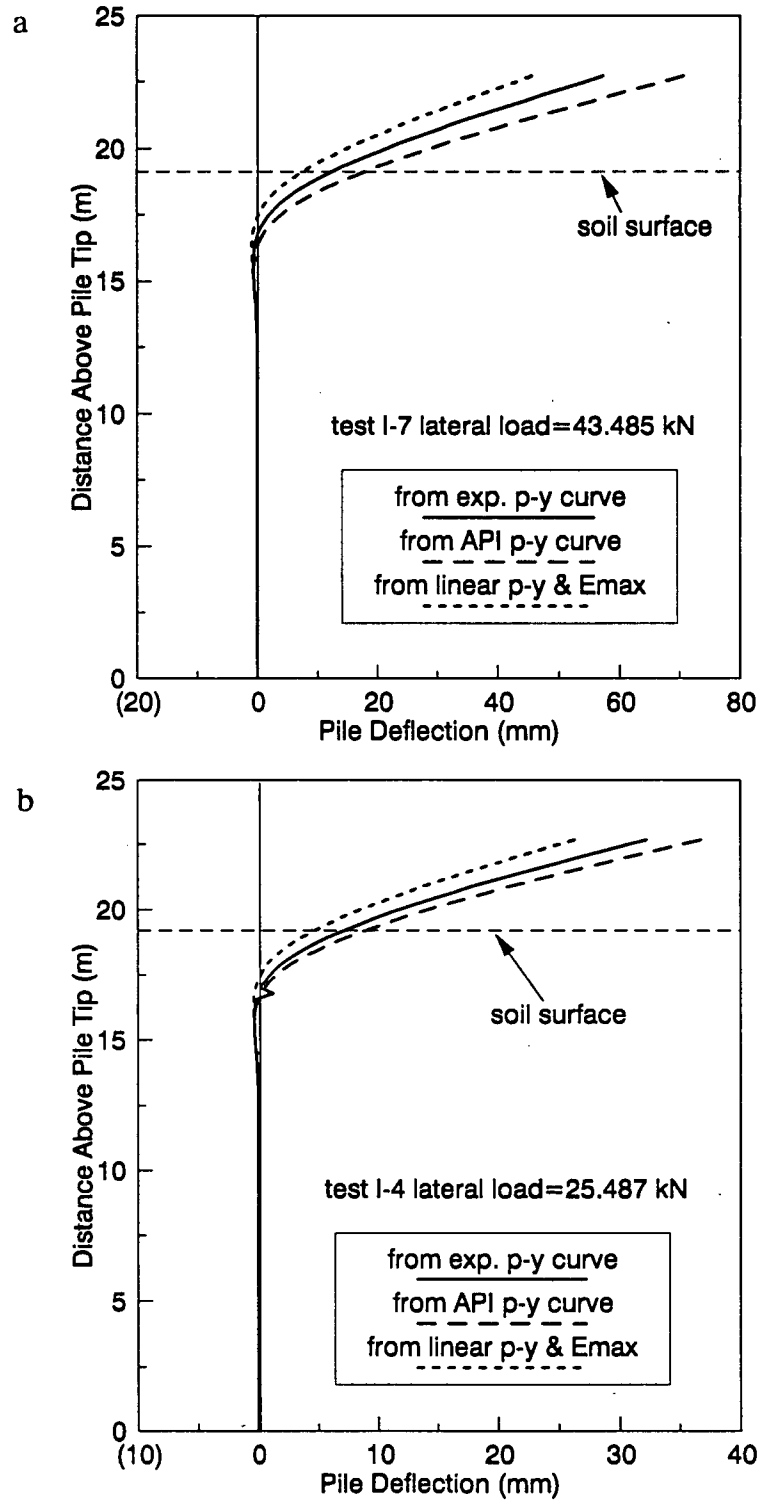

Figure 5.3: Computed pile deflections (a) test I-7; (b) test I-4

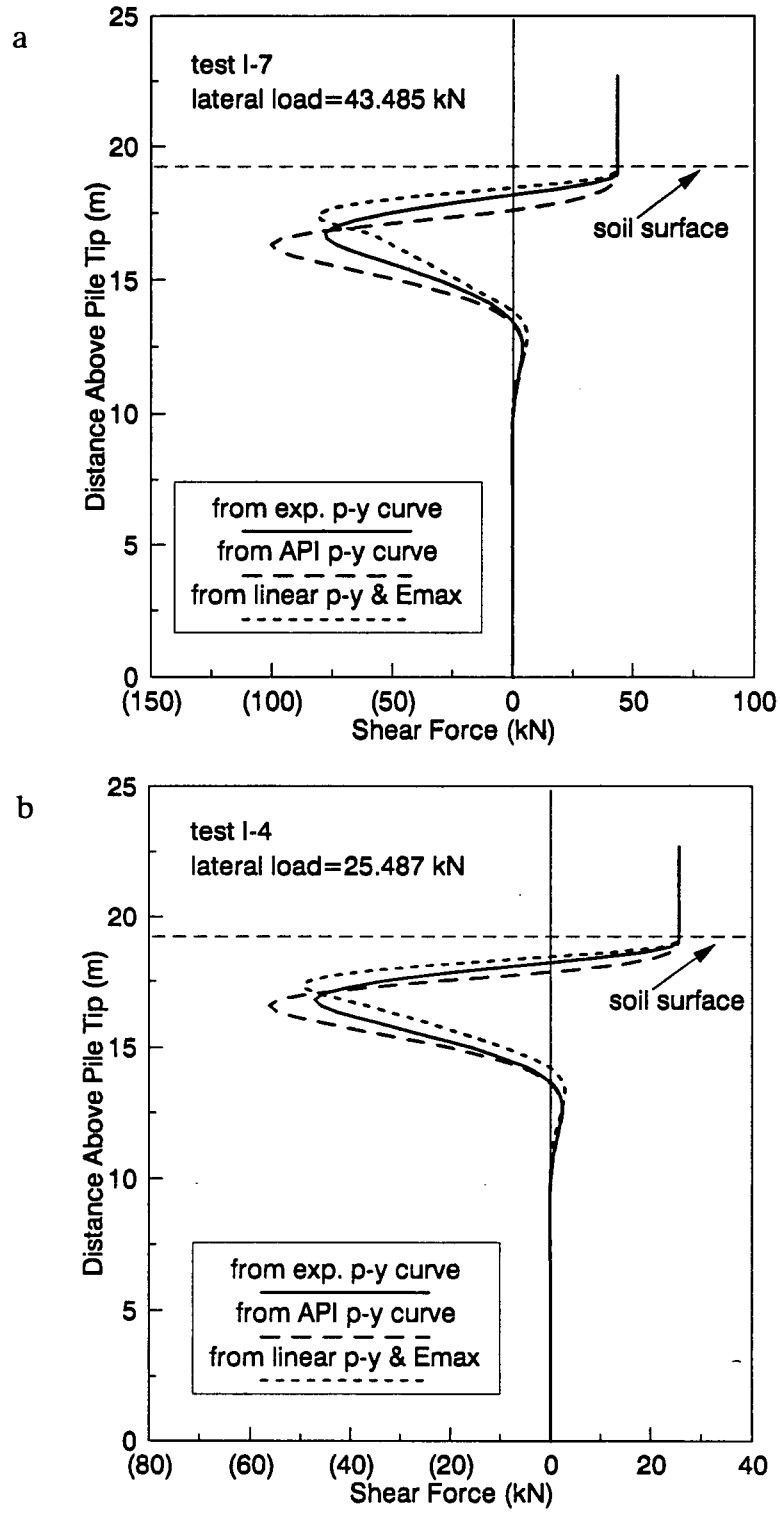

Figure 5.4: Computed shear force distribution (a) test I-7; (b) test I-4

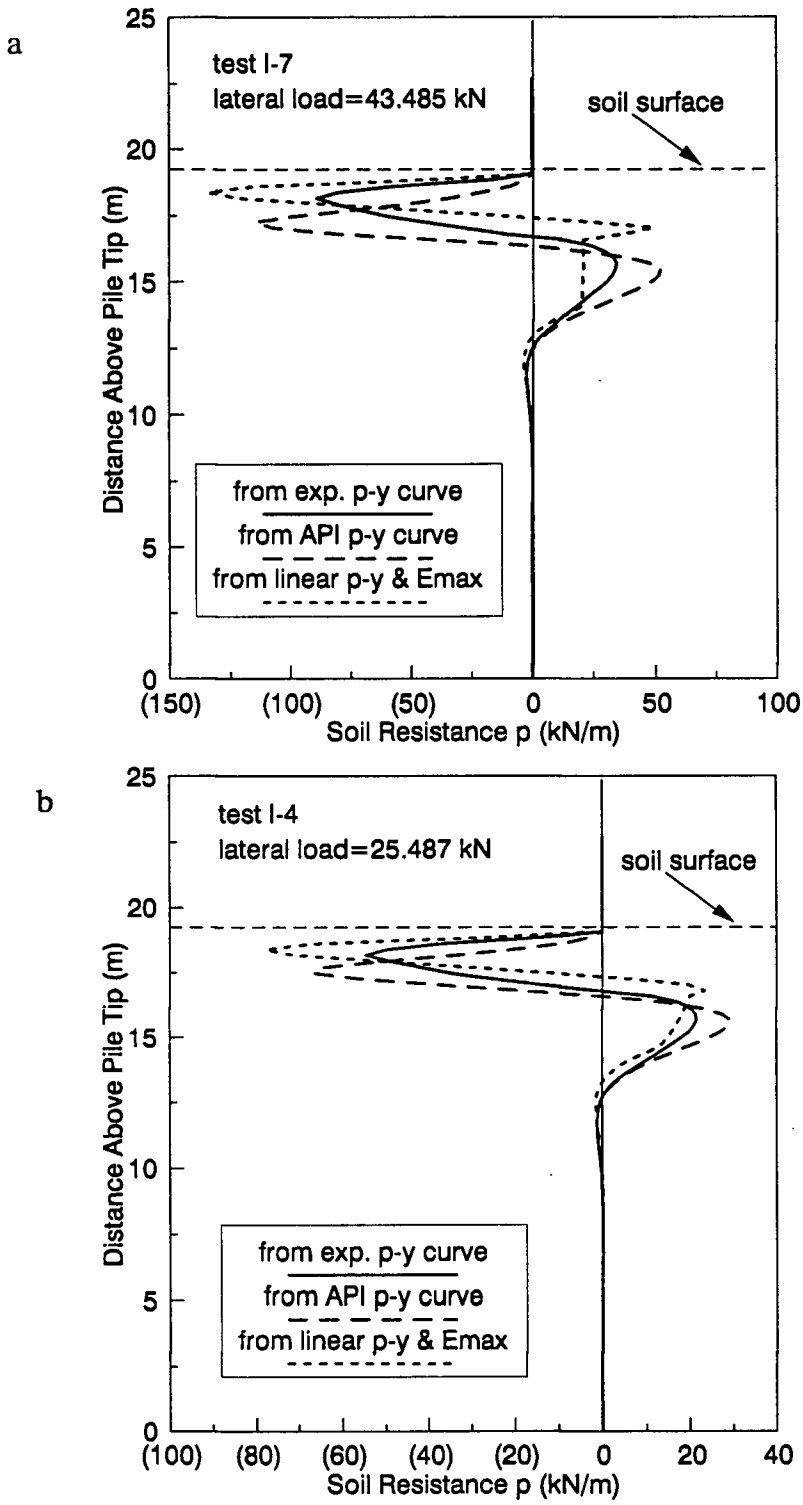

Figure 5.5: Computed soil resistance with depth (a) test I-7; (b) test I-4

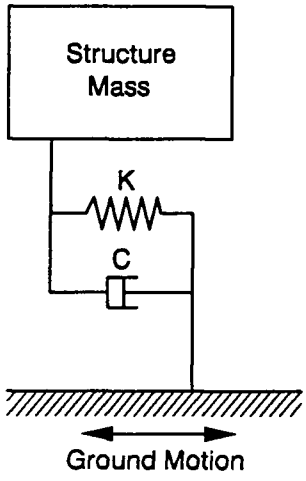

Figure 5.6: Model of superstructure motion

the deflected shape of the pile and the secant Winkler stiffness along the pile compatible with the pile deflection level. Therefore, the equivalent pile head stiffness is determined from the pile head load versus deflection relationships (Figure 5.7). It is shown that at small loading level the API procedure and linear method both give a good agreement with experimental p-y curves, while with increase of load, the load-deflection curve from API code become softer and the one from linear method stiffer. The pile head damping is obtained based on the force-displacement hysteresis loop measured at the cap. The damping used for computation are 16.4% and 12.5% for the first series of tests and the third series, respectively.

Using the model defined above, the dynamic response of the superstructure of pile foundation were computed under the conditions identical to first and third series of forced vibrations. Figure 5.8 shows the amplification factor at the cap computed for various frequencies and those observed in the tests. It is seen that all the methods can predict

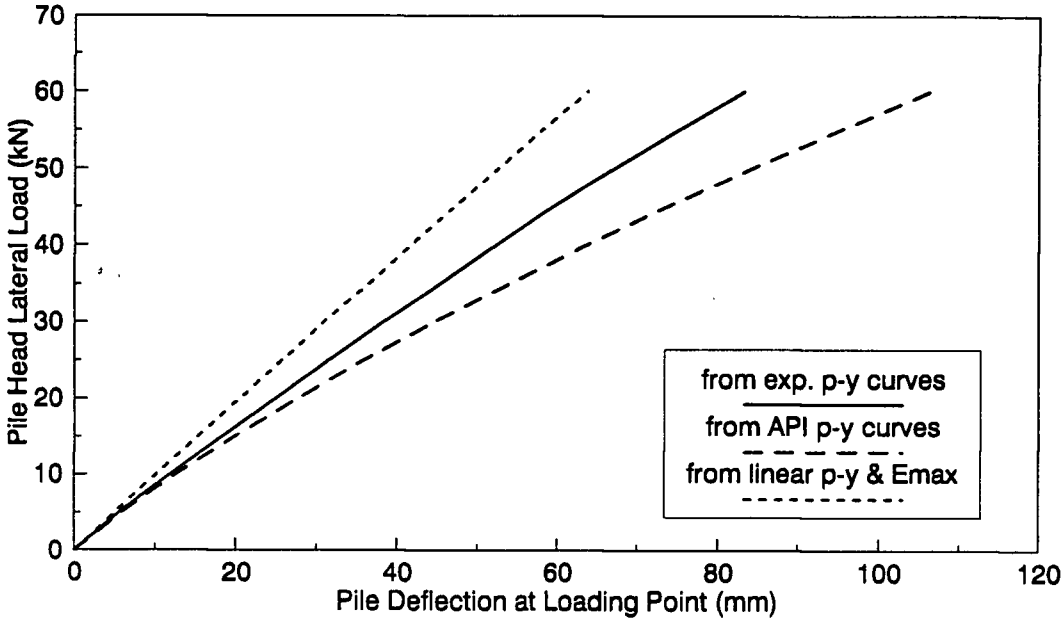

Figure 5.7: Computed pile head deflections versus lateral pile head load. (prototype scale)

the dynamic response of the superstructure reasonably well in terms of the shape and peak values. However, the frequencies peak values occur (resonant frequencies) move behind the test data except the case of the API p-y curve in first series of tests. It is also seen that under small intensity of shaking (Figure 5.8 b), all procedures nearly yield the same prediction because the pile head deflections fall into small range (Figure 5.7).

5.4 Summary and Conclusion

Nonlinear analyses of pile response to lateral pile load were made using the API recommendation of p-y relationship, linear relationship with slope of maximum Young's modulus and proposed p-y model. The computed results were then compared with experimental data if available in terms of bending moment, pile deflection, shear force, soil resistance, and dynamic response of superstructure. For the analyses of pile response,

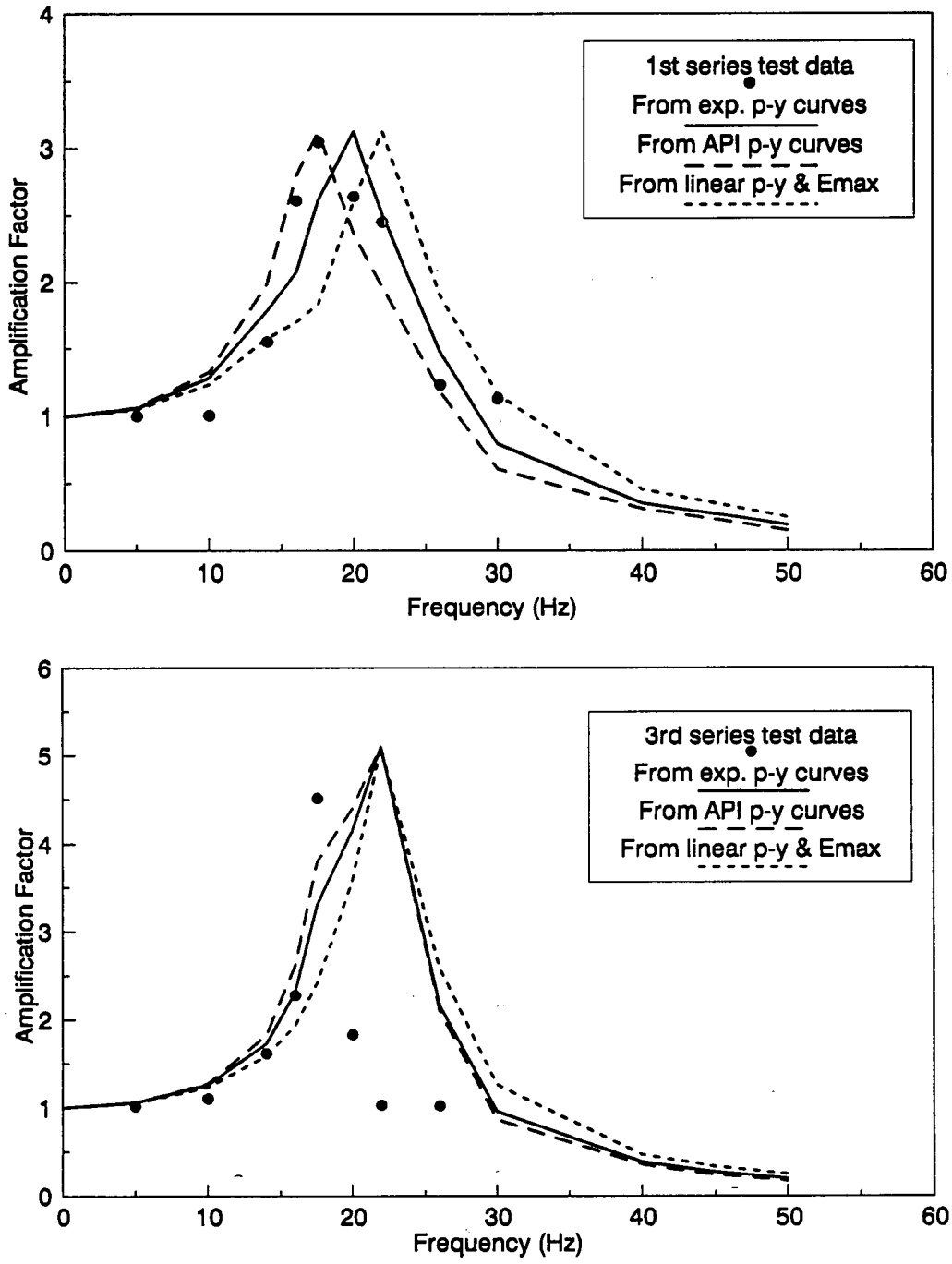

Figure 5.8: Amplification factor at various frequencies computed and measured at superstructure

the test conditions of tests I-7 and I-4 were simulated for the purpose of comparison between prediction and experiment. The theoretical prediction of dynamic response of superstructure were performed in the situations corresponding to the first and third series of forced vibrations.

Based on the analyses in present chapter, it is found that the API recommendation of soil resistance versus pile deflection relationship (p-y curves) generally overestimate pile bending moments, shear forces pile deflections and also slightly overpredict the pile head displacement. For the dynamic response of superstructure, it gives a reasonable agreement with the experimental data, especially for high intensity of shaking. The analyses indicate that the linear model of soil-pile interaction overall yields overprediction in bending moments ,shear forces and soil resistances at shallow depths, whereas underestimate them at deep depths. It underpredicts pile deflections and pile head displacements. In the analysis of superstructure, the linear model gives the resonant frequency for behind the experimental one in the case of high intensity of shaking which implies that this model result in a greater prediction of pile head stiffness than the test.

Chapter 6

Summary and Conclusions

Dynamic studies on model piles subjected to moderate to strong harmonic base excitation were presented in this thesis using the hydraulic gradient similitude testing technique. The method applies a high hydraulic gradient across the sand deposit and thus increase the body force in the model soil approaching the field condition. The testing principle is similar to that of the centrifuge technique where centripetal acceleration is applied to increase the model stress level. An extensive series of dynamic tests on single piles were carried out to examine the behaviour of pile response to simulated earthquake loading. The response characteristics of superstructure and soil-pile system were obtained from the test data. The soil-pile interaction p-y curves were also derived from the experiments and the lateral stiffness and damping behaviours of the near field soil were discussed and examined. The effect of boundary was also evaluated. Then, the experimental results are compared with the predictions from theoretical methods and numerical analyses.

Soil response in the HGS testing device was examined by experimental and analytical approaches with different boundary constraints. The results show that the soft material installed on the insides of the container wall is not efficient to simulate the infinite soil stratum response but causes active soil failure within the device under high hydraulic gradient. The accelerations at different locations on the soil surface in the rigid box are found to be reasonably uniform.

The modelling relations for the hydraulic gradient similitude technique were verified indirectly using the approach of modelling of models, and observed to be well satisfied.

The free vibration test results on the natural frequency of the soil-pile system are in accord with the observation that the dynamic modulus of sand is proportional to the square root of the confining stress, i.e., the fundamental frequency of soil-pile system is proportional to the 4th root of soil stress level. It was found that soil-pile system stiffness is dependent upon the deflection of the pile, rigidity of pile and soil stress level. However, the normalized frequency of the system by the soil deposit frequency is seen to be independent of soil stress level.

The equivalent viscous damping of the soil-pile system was derived from the logarithmic decrement method. It is observed that the damping is essentially constant regardless of soil stress levels, depending on the vibration amplitude and the number of oscillating cycles.

For the pile tests under simulated earthquake ground motion, the response is dependent upon the shaking intensities, exciting frequency and soil stress level under the same setup. The superstructure response is found to be insignificantly different in terms of amplification to the ground motion for different soil stress levels under the same strong base shaking. However, the amplification is substantially higher for lower level shaking than for the strong one at the case of same soil stress level. The study also shows that the resonant frequency of the soil-pile system increases with soil stress level, and pile head stiffness decrease with its increasing deflection.

In general, the soil densification did not occur for dense sand tested under dynamic loading. The pile bending moment and pile deflection responses were symmetric. The pile response appears not to be affected by the number of loading cycles with an exception of initial transient phase if any. The depth of maximum bending moment occurring in the pile is seen to move down with increasing load.

The dynamic soil-pile interaction p-y curves were derived from the measured bending moment distribution along the model pile using cubic spline fitting method. Commonly,

the computed p-y curves show nearly elastic response with small internal damping for piles tested in dense sand and subjected to moderate shaking. With increasing intensities of shaking greater non-linear and hysteretic response was observed. Linear elastic p-y response gradually develops as lateral pile deflections decrease with increasing depth. The backbone p-y curves recommended by the API for sand are compared with the test data, seen to be poorly predicted. In general, the API curves were softer than those induced from test results, in particular, at shallower depths for strong base shaking. On the contrary, under moderate shaking the slightly stiffer API curves than the test data are observed. It is seen that the stress level dependence of the p-y curves may be well normalized by the maximum Young's modulus of sand and the pile diameter. The normalized data shows essentially parabolic trend with dimensionless pile deflections in a initial slope of 45 degree, which implies that, as proposed in Chapter 4, the specific p-y curve has an initial slope of E_{max}. The normalized dynamic p-y curves are also compared with that static and cyclic curves, and found to be considerably stiffer than that from static testing.

Finally, the dynamic response of selected pile tests were computed using theoretical and analytical approaches. The finite difference program LATPILE was used to make nonlinear analyses of pile response to the pseudo dynamic loading. The different methods of constructing p-y curves, i.e. the API code, linear elastic model were described. Generally, the API method overpredict the maximum bending moment, shear force and pile head displacement as well. The linear elastic model appears to fairly well predict maximum bending moment and shear force, but overpredict pile head displacement. In the analysis of superstructure response, it was seen that all methods well estimate the amplification phenomena except the resonant frequencies.

The study in this thesis validates the hydraulic gradient similitude modelling for use

in examining soil-pile interaction behaviour under simulated earthquake loading. It has created a significant experimental data base related to the dynamic pile response. With those data, the existing analytical methods can be evaluated.

The data obtained in the thesis is on the single pile response, and limited to the pile foundation in the uniform sand deposit with good permeability. The further research using the HGS modelling should be carried out in order to make the model applicable to a wider range of soil conditions and earthquake loadings. The more studies may be performed using the present techniques such as vertical single piles under vertical static and dynamic loading, and pile group response to lateral and vertical static and cyclic pile head loading, and earthquake loading with direct measurement of pile-soil-pile interaction factors. Hence, the data base for dynamic response of single pile and pile group could be further enriched.

Appendix A

Instrumentation and Data Acquisition

A.1 Strain Gauges

The model pile of 6.35 mm outside diameter used for dynamic tests was instrumented with eight pair of 120Ω foil type strain gauges as shown in Figure 3.5. The gauges were mounted on opposite sides of the pile cross-section on an axis coincident with the direction of shaking so that one gauge registered compression and the other tension strain. This arrangement will reduce the adverse effects of temperature, and eliminate any axial strain effects at that level. Small holes are drilled on the tubing so that all the electrical lead wines come out from the inside of the tubing pile. All the strain gauges were coated with layers of M-coat which provide moisture protection and smooth the pile surface over the strain gauge areas.

Each pair of strain gauges in the model pile become the two active resistors in the Wheatstone bridge circuit. Normally, the half bridge circuit formed by each pair of the gauges is completed to make up a full bridge by another two dummy resistors, as illustrated in Figure A.1. Total of 16 dummy resistors and 32 lead wires are thus needed for this type of pile instrumentation scheme. It will lead to a great complication in the circuitry wiring and testing set-up. Complicated wiring may also create potential problems such as noisy signals.

For the present pile instrumentation, a simpler circuit has been adopted. The strain gauges were configured to share the same pair of dummy resistors as they all have the

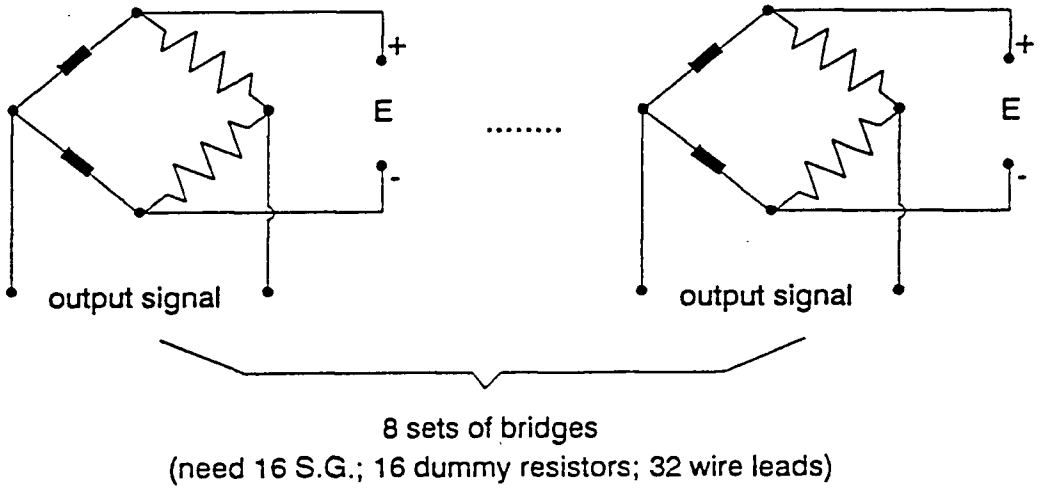

Figure A.1: Normal Wheatstone bridge connection

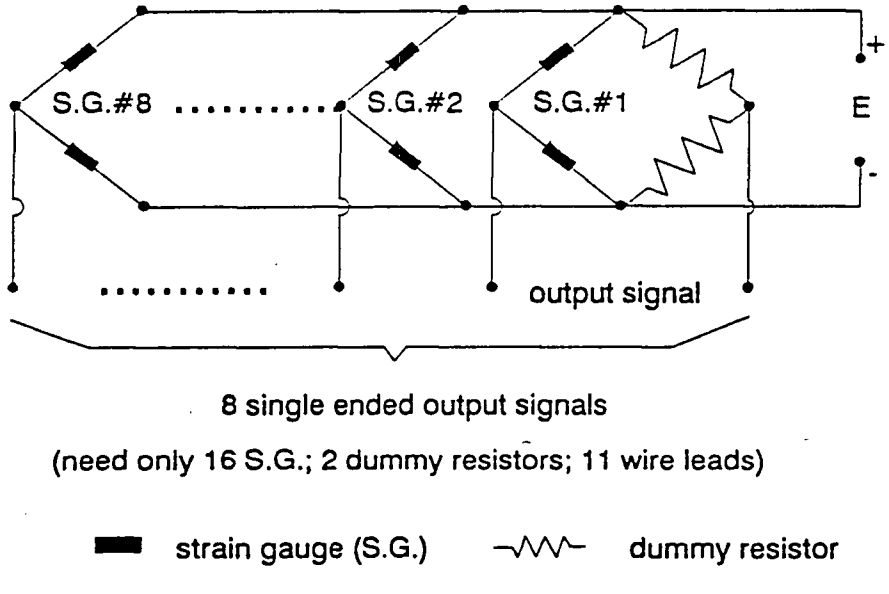

Figure A.2: Simpler Wheatstone bridge connection

same resistance (120Ω), as shown in Figure A.2. In addition, all the strain gauges are excited by the same power supply and their signal outputs are in common at one end whereas different at the other end giving single ended signals. This configuration greatly simplifies the wiring connection and experimental setup, and also reduces potential signal noise since only two dummy resistors and eleven lead wires are used to complete the pile instrumentation. With this strain gauge configuration, a Wheatstone bridge completion board using only two dummy precision resistors has been installed underneath the air chamber cap to complete all the strain gauge signals in a full bridge before they go out the air chamber.

The calibration of the bending strain gauge was carried out by clamping the pile at one end as a cantilever beam and various dead weights hung at the other end of the pile. Through knowing the distance to strain gauges from the dead weight, the strain gauge outputs were calibrated versus the known bending moments. The excellent linearity between the output and applied bending moment were, as expected, obtained.

A.2 Displacement Transducers

Two linear variable displacement transformers (LVDT's) were used to measure the displacements and rotations of the pile head mass supported by the model pile. The LVDT's have full scale displacements of $\pm 12.0mm$ and use a constant 6.0 volt DC input power supply. A DC-driven LVDT consists of a primary and secondary coil assembly and magnetic core which, when displaced along the axis and within the core of the coil assembly, produces a voltage output proportional to the displacement. A frictionless air leaking bearing system is used to provide axial guidance to the LVDT cores approaching the model pile to reduce the resistance to movement of the core. The mass of the core is small enough to neglect its dynamic inertia.

The LVDT's were calibrated statically using a micrometer with 0.025 mm divisions. The LVDT output was plotted versus displacement over the expected range of motions of the model pile. Excellent linearity and negligible hysteresis of the LVDT output was observed.

A.3 Accelerometers

Three accelerometers were used during testing. One was installed on the base of the soil container to measure the input shaking table motions, one embedded in the sand at the sand surface to measure free field surface accelerations, and another accelerometer mounted on the superstructure mass to measure pile head accelerations. These are piezoresistive type and are packaged on a ceramic substrate. The accelerometer consists of a micromachined silicon mass suspended by multiple beams to a silicon frame. Piezoresistors located in the beams change their resistance as the motion of the suspended mass changes the strain in the beams. Silicon caps on the top and the bottom of the device are added to provide over-range stops and prevent damage to the accelerometer. The accelerometer also feature a small dimension and low mass.

The weights and dimensions of the accelerometers used to measure free field and pile head accelerations were chosen to minimize the influence of the accelerometer on the dynamic response of the model. The accelerometer has a weight of 0.012 N, with a size of 15 $\times$ 15 $\times$ 4 mm cube. These weights are less than 0.2 percent of the weight of the object whose accelerations are being measured. Therefore, their effect on the dynamic response of the model is considered negligible.

The resonant frequency of the accelerometer measuring shake table are 1200 Hz. The resonant frequencies of the pile head and free field accelerometers are 1220 and 1080 Hz, respectively. The full scale range of table accelerometer is $\pm$50 g, $\pm$10 g and $\pm$5 g for pile

head and free field accelerometers, respectively. The accelerometers are damped to about 50 percent of critical and the dynamic response characteristics of the accelerometers are constant up to frequencies of 35 percent of their resonant frequencies. Therefore, the output of the accelerometers is not affected by dynamic resonance effects in the range of frequencies of interest.

Constant input excitation voltages were applied to the accelerometers and their output were amplified using variable gain amplifiers. The accelerometers were calibrated using static and dynamic loading procedures. During the static calibration, the sensitive axis of the accelerometer was rotated through various inclination angles. The outputs of accelerometers versus accelerations were found to be linear. During the dynamic calibrations, the free field and pile head accelerations were subjected to different accelerations using the shake table. Their outputs were measured using an oscilloscope and were compared with the table accelerometer output, which was assumed to accurately measure the table motions. This comparison led to calibration factors in good agreement with the static calibration results.

A.4 Data Acquisition System

A micro-computer based data acquisition system was used in this study. The system consists of three components, i.e. a multi-channel signal amplifier, a multi-channel analogue to digital (A/D) converter DT2801A card with 12 bit resolution, and an IBM-PC micro-computer. All the transducers were excited by a common power supply which was set to 6 volts.

A monitoring program was used to monitor all transducer readings, in particular the three pore pressure readings during the application of hydraulic gradient to the sand sample before start of dynamic tests on piles. Then, during the pile tests, total of 16

channels were monitored and 13 channels recorded on the disc during the test. The A/D convertor interfaces with the micro-computer using software which controls the rate of data acquisition per channel, Δt (second/sample), number of channels of analogue data, M, number of samples per channel, N, and the maximum voltage that can be input into the system.

Analogue to digital conversions carried on sequentially or multiplexed for each channel sampled and data stored on disc. The multiplexing procedure means that for one complete scan of all M channels there is a slight time shift between consecutive channels equal to $\Delta t/M$. A sampling rate of 0.001 sec per sample (1000 Hz) for each channel was used in the majority of H.G.S. tests, giving a maximum time shift of about 0.001 sec between the first and last sample for all 13 channels. This effect has not been corrected for the time shift,since it is insignificant relative to the duration of testing. Using the above sampling interval and storing 5000 samples per channel, which was limited by available buffer size on the microcomputer, a test duration of 5.0 seconds was achieved.

Appendix B

Computation of p-y Curves

The soil-pile interaction p-y curves are derived from the measured bending moment distribution along the pile. Based on the simple beam theory, the bending moment can be integrated or differentiated to obtain the pile inclination, θ, deflection, y, shear force, Q, and soil resistance, p, as follows (neglecting the sign):

$$\theta = \int \frac{M(z)}{EI} dz \tag{B.1}$$

$$y = \int\int \frac{M(z)}{EI} dz \tag{B.2}$$

$$Q = \frac{dM(z)}{dz} \tag{B.3}$$

$$p = \frac{d^2M(z)}{dz^2} \tag{B.4}$$

where EI is the flexural rigidity of the model pile, z is the distance along the pile.

Since the bending moments are only known at some discrete locations along the pile, a numerical curve fitting scheme is necessary to obtain the needed soil resistances and pile deflections along the pile length at each loading step. The desired p-y curve at a given depth can be obtained by repeating the curve fitting scheme at various loading stages. For the deflections, simple numerical integration suffices, as any slight errors in the bending moment data become smoothed in the integration process. However, for the soil resistance, any slight errors or deviations in the bending moment data become greatly magnified during double differentiation. To alleviate this problem, various curve fitting techniques have been proposed to process the bending moment data.

In contrast to most field test data, the application of curve fitting technique to model test data is possible as model tests usually are performed in a uniform soil condition, and the bending moment data can be represented by a smooth continuous curve. Erratic data such as those in the field due to alternating dense and loose soil layers do not present.

Scoot (1979) has reviewed various curve fitting functions which can be used for representing the bending moment data from centrifuge tests. Based on this study, he rejected the use of polynomial functions, as although these functions have the advantage of passing close to but not through the data points, they deviate widely from the known behaviour of the pile below the level of the last moment data points. The use of rational functions as fitting functions was also rejected as their use depends upon pre-assumption of soil-pile interaction. A fifth order spline curve fitting was recommended by Scott as it gave reasonable soil resistance distribution and required no pre-acknowledge about the soil-pile interaction.

Recently, Ting (1987) and Ting et al. (1987) proposed a curve fitting technique consisting of fitting a seventh degree polynomial to bending data below the soil surface and a linear function above the soil surface. The origin of the seventh degree polynomial was selected at an arbitrary point at which the pile deflection, slope, moment, shear, and net soil pressure were all zero. The coefficients of the seventh polynomial were obtained by subjecting them to the constraint that the net soil resistance was zero at the ground surface.

In this study, curve fitting techniques using both a cubic spline and the method proposed by Ting (1987) have been evaluated with present test data. The bending moment fitting by Ting's method was found to be very sensitive to the selection of the origin of the seventh order polynomial. it gave reasonable fitting at the low hydraulic gradient condition. However, at the higher stress level, the fitting on bending moment data was much worse than the obtained from the cubic spline.

Based on this experience, the cubic spline fitting is used in this study. This technique has been used by many researchers (Barton, 1982; Finn et al., 1984) with reasonable good results. In this procedure, a collection of cubic spline is fitted to the bending moment data, one between each two data points. Continuity of slope is assured at each point. Then the spline is differentiated to give the distributed shear force and soil resistance along the pile, and integrated to give the pile inclination and deflection. Boundary conditions are also applied to the fitted curves:

1. for the free-head piles, the bending moment is set to be zero at the loading point;
2. the shear force at the ground level is set equal to the applied load;
3. the soil resistance at ground level is set to zero; and
4. the moment, shear, soil resistance, deflection and pile inclination are all set to be zero at the pile tip.

Typical results using this procedure for the test data are shown in Figure B.1 and B.2 for free head pile test. The p-y curves at specific depths can be obtained from the computed soil resistances and pile deflections at different loading stages. The resulting p-y curves may be found in Chapter 4. The experimental p-y curves so obtained have been employed to back predict the pile response using the computer program LATPILE (Reese, 1977). As shown in Figure 5.2, good agreement with the measurement is obtained. this indicates that the numerical scheme used to derive the experimental p-y curves can provide reasonably good results.

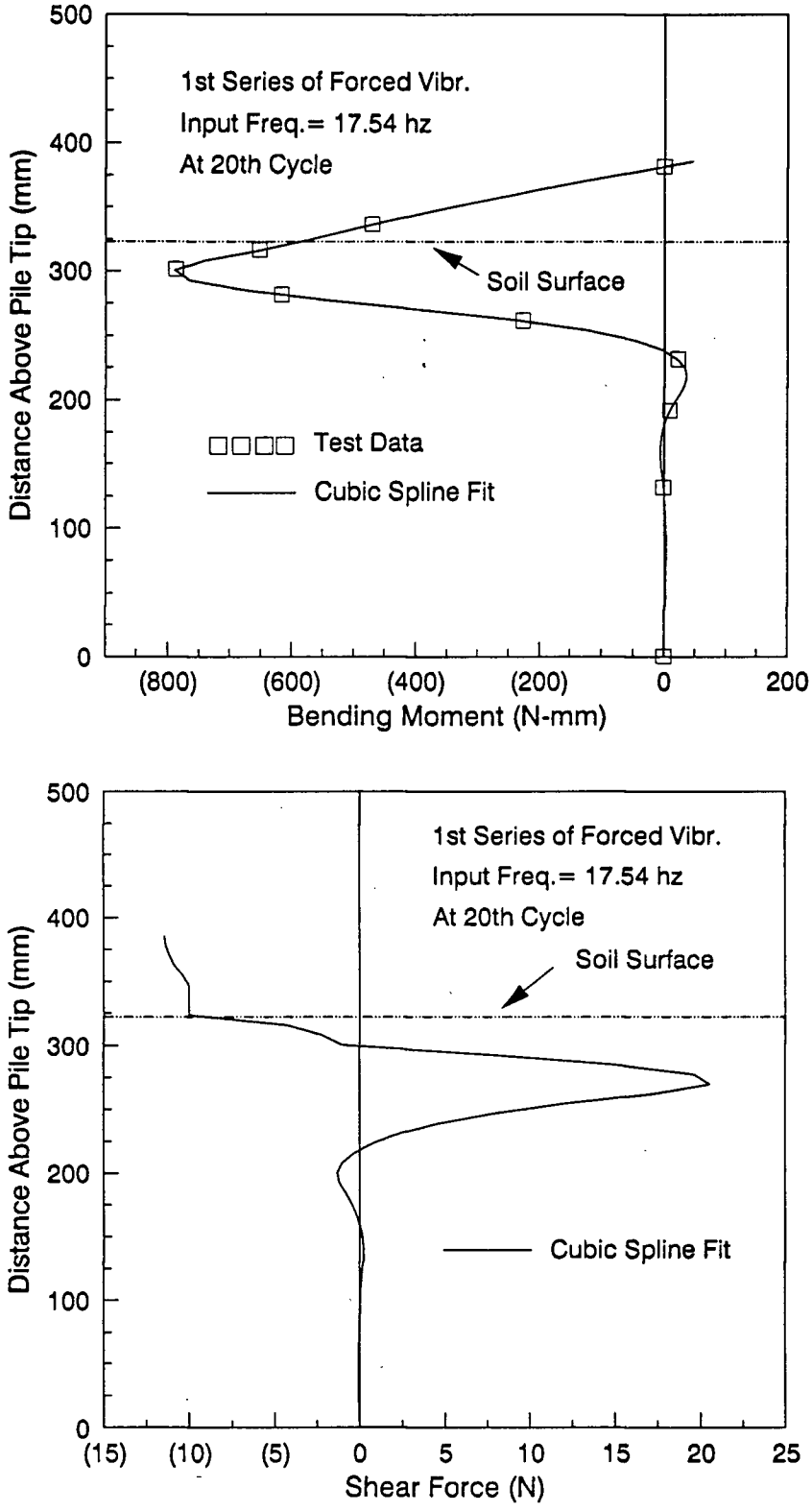

Figure B.1: Example of cubic spline fitting test data - bending moment and shear

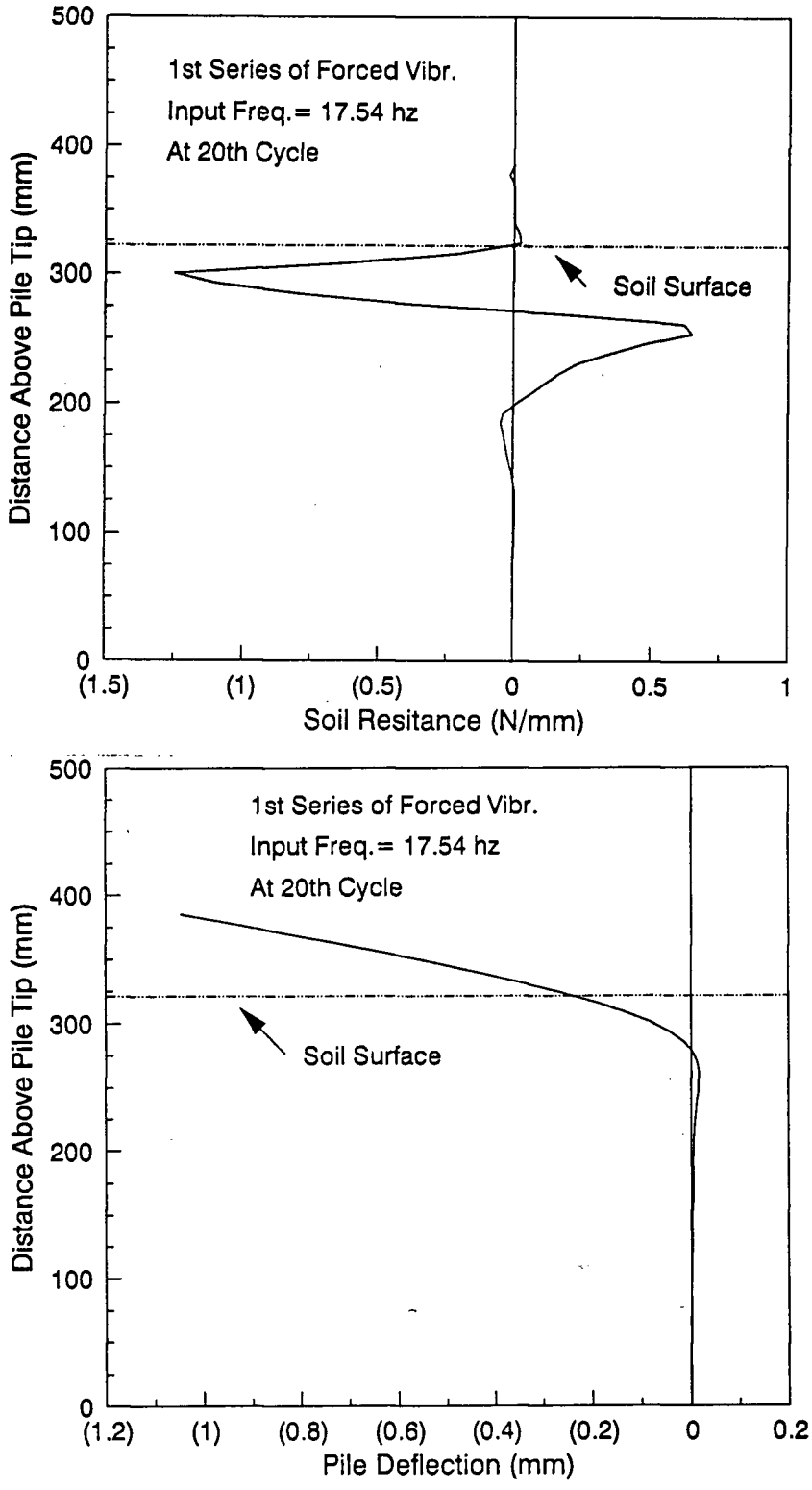

Figure B.2: Example of cubic spline fitting test data - soil resistance and pile deflection

Appendix C

Dynamic Response of Pile in Other Testing Cases

The response of pile foundation to simulated earthquake loading have been presented in Chapter 4 for several testing conditions. Herein, some more results under other exciting cases are presented.

C.1 Strong Shaking Under Low Soil Stress Level

Test #6 in series II was carried out suing strong base shaking at input frequency of 12 Hz under HGS sale factor of 30, referred to as low soil stress level in the thesis. The input shaking intensity is about 0.475 g. During sinusoidal shaking, the bending moment distribution is shown in Figure C.1 for 1st and 20th cycles. The p-y curves were computed for the initial cycle of transient excitation when maximum pile response occurred and were then compared with curves evaluated during steady state excitation, as shown in Figure C.2.

Figure C.1 shows that the bending moments at initial transient stronger excitation are much greater than those at steady state, especially at maximum value. The p-y curves have been computed up to the 6 pile diameter depth since below this depth lateral pile deflections could not be reliably discerned. During the initial transient excitation, relatively large lateral pile deflections occurred. The computed p-y curves are non-linear and exhibit hysteretic behaviour. Cyclic p-y curves computed during steady state excitation over the 20th cycle of shaking are also shown. The lateral pile deflections are less than those that occurred during the initial transient excitation, although similar non-linear

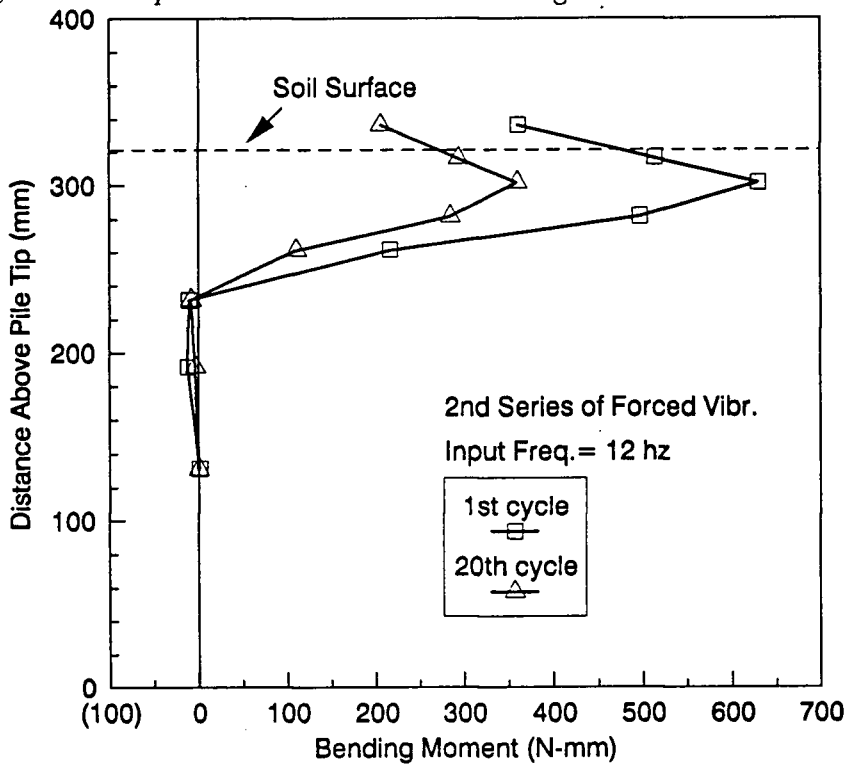

Figure C.1: Bending moment distribution for test II-6

p-y response was observed. The p-y response is approximately linear beyond the 5 pile diameter depth. The cyclic p-y curves computed using the API procedures are also shown on the figures. These again provide a poor match of the experimental p-y curves and underestimate the lateral soil stiffness especially at shallow depth.

C.2 Moderate Shaking under High Soil Stress Level

Cyclic p-y curves have also been computed for test 7 in series III where the pile was subjected to relatively low level sinusoidal shaking, compared to series I. The base input intensity is about 0.286 g. During the sinusoidal shaking, p-y curves were computed for steady state excitation (at 20th cycle) and shown in Figure C.3. Similar to test II-6, the p-y curves are non-linear and hysteretic up to 4 pile diameter depth. Beyond this depth, the p-y behaviour is essentially linear. The API curves are also shown on the figures and once more seems to be poorly in agreement with the test data.

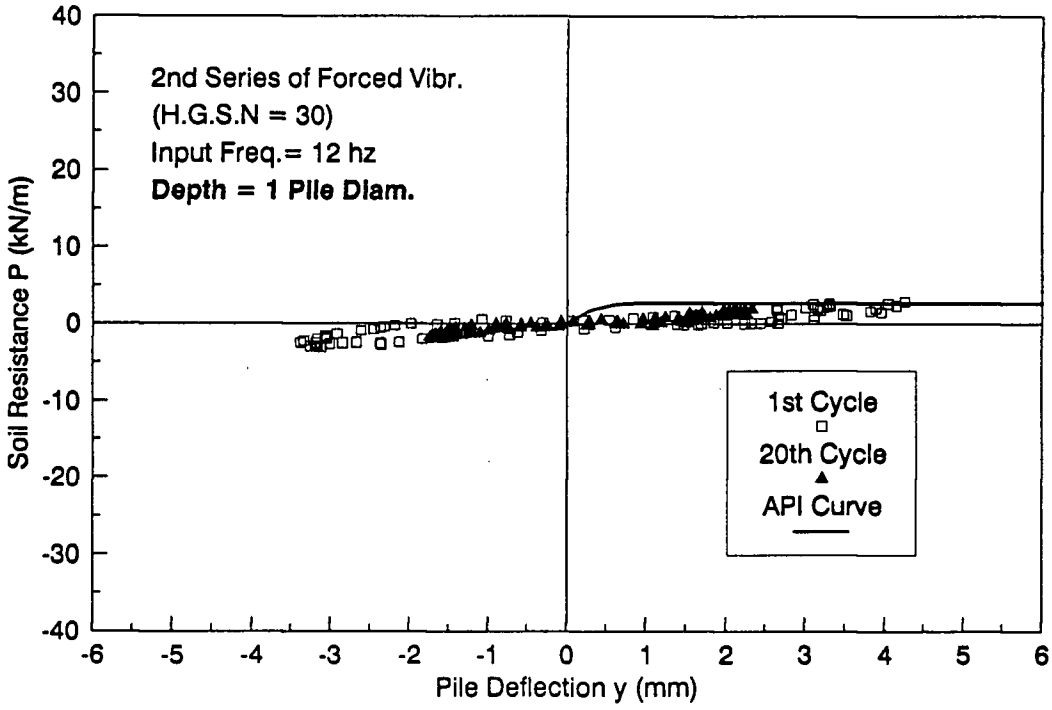

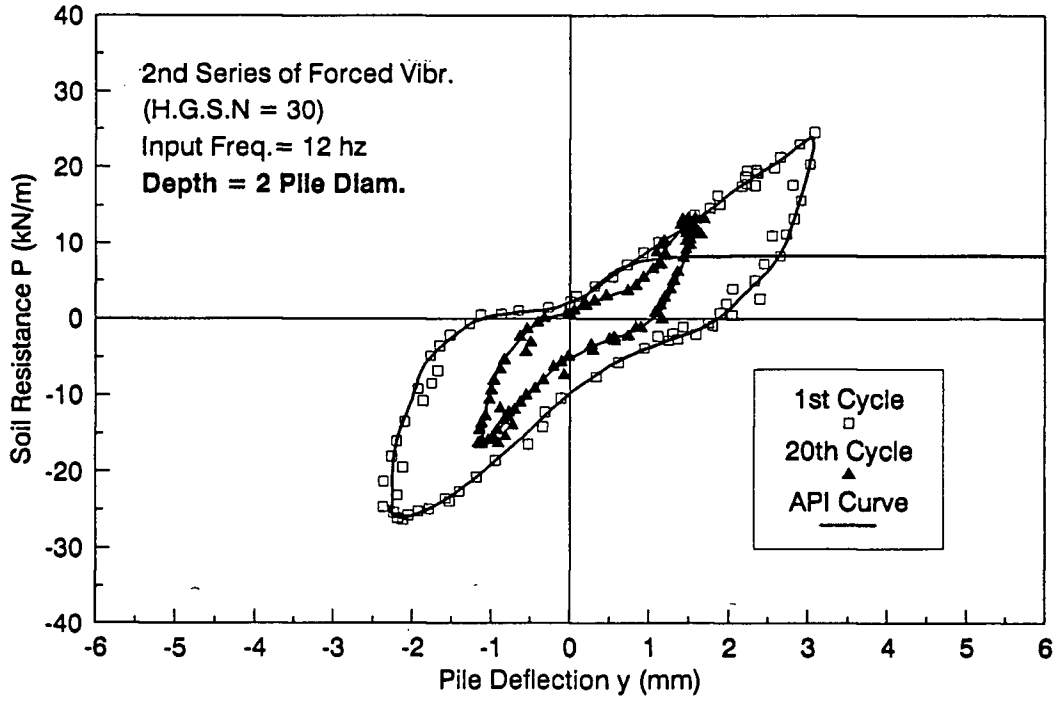

Figure C.2: Cyclic p-y curves at 1 to 2 pile diameter depth and comparison with API curves-test II-6

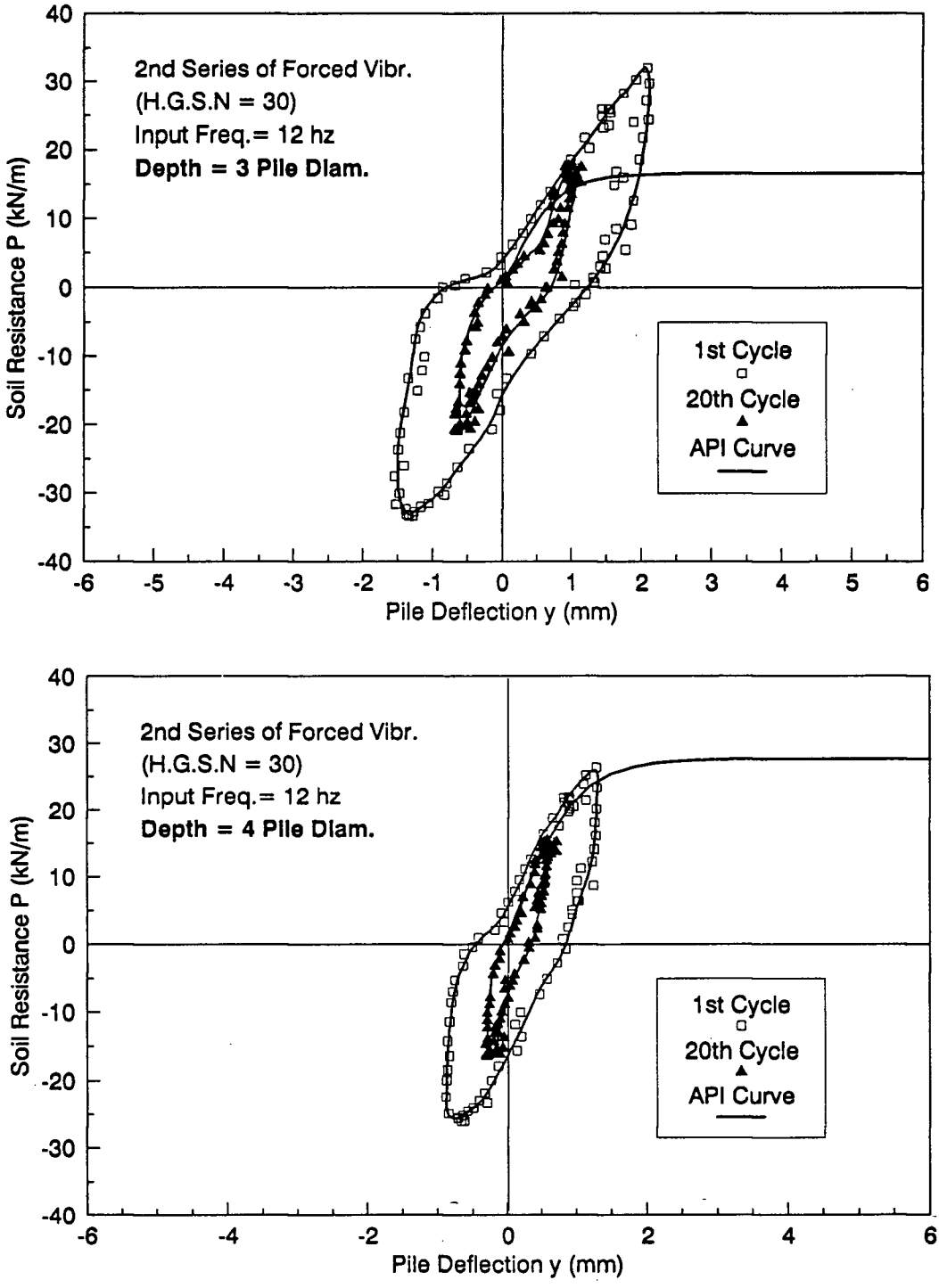

Figure C.2: Cyclic p-y curves at 3 to 4 pile diameter depth and comparison with API curves-test II-6

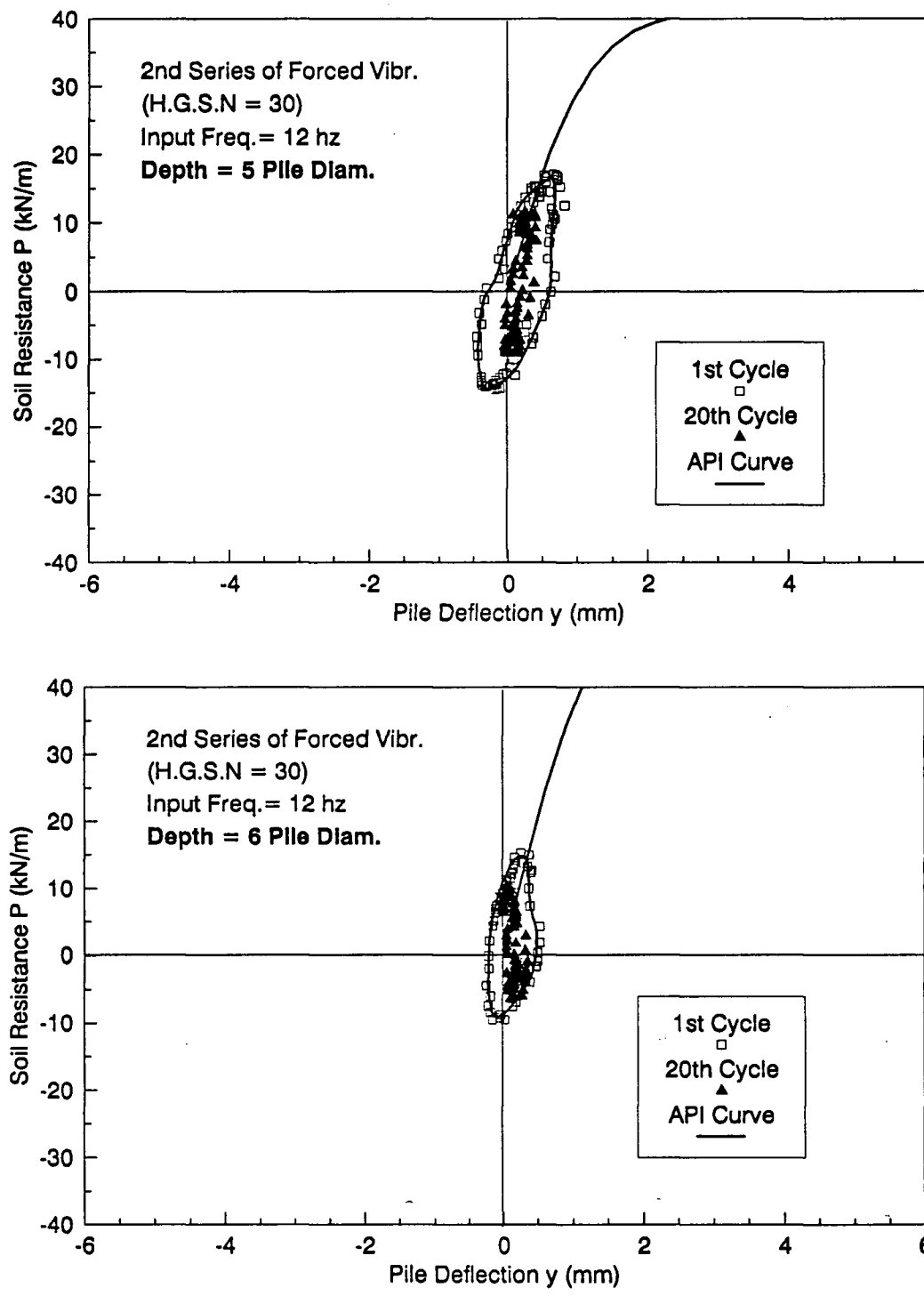

Figure C.2: Cyclic p-y curves at 5 to 6 pile diameter depth and comparison with API curves-test II-6

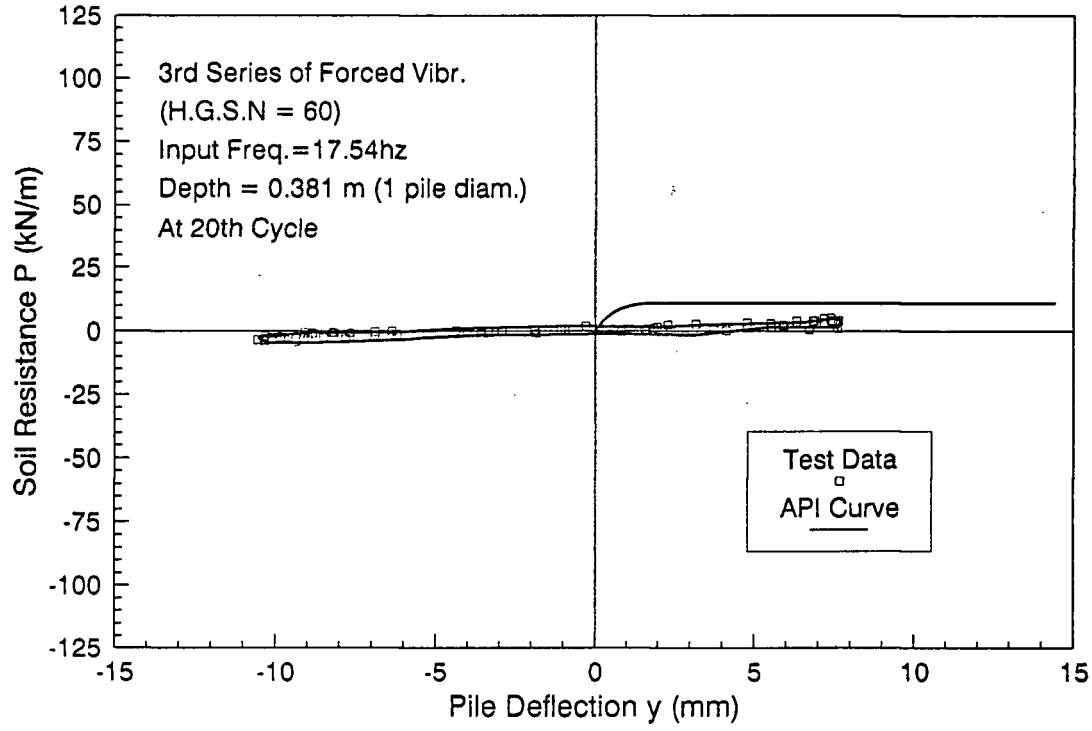

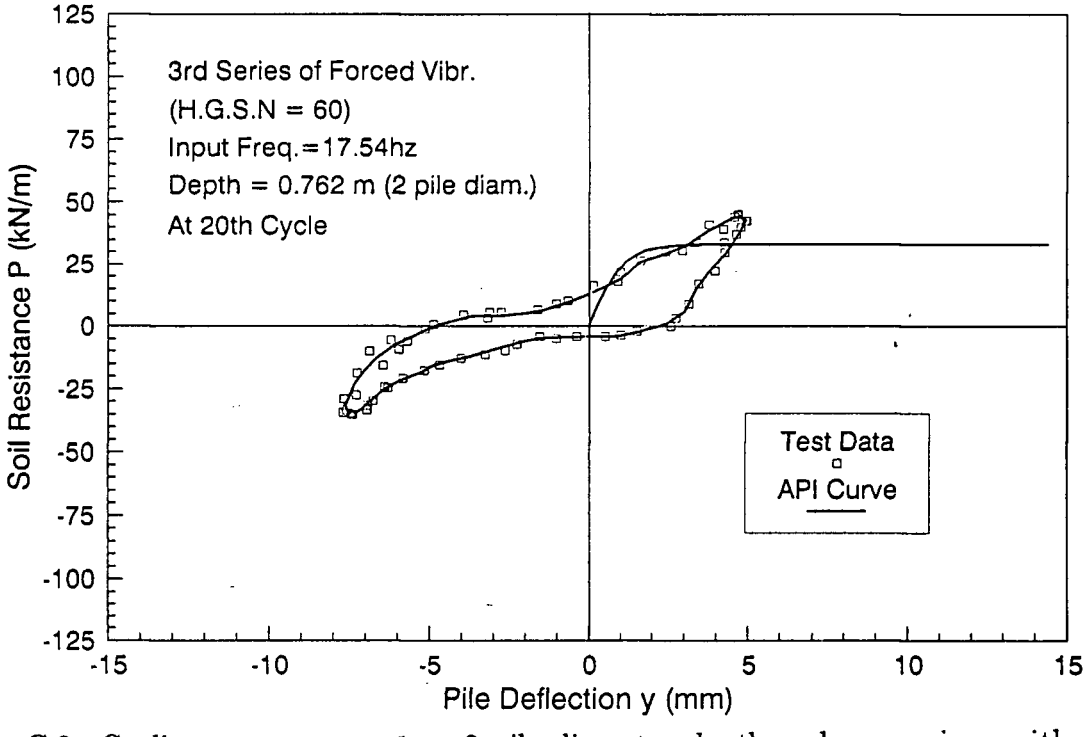

Figure C.3: Cyclic p-y curves at 1 to 2 pile diameter depth and comparison with API curves-test III-7

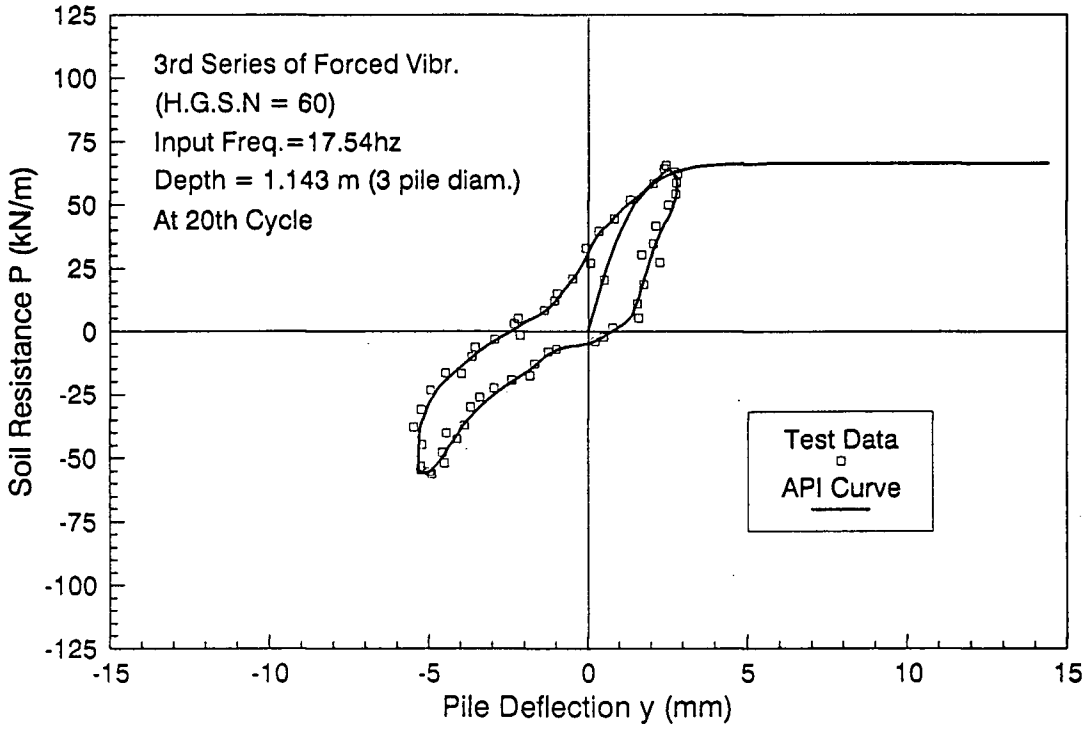

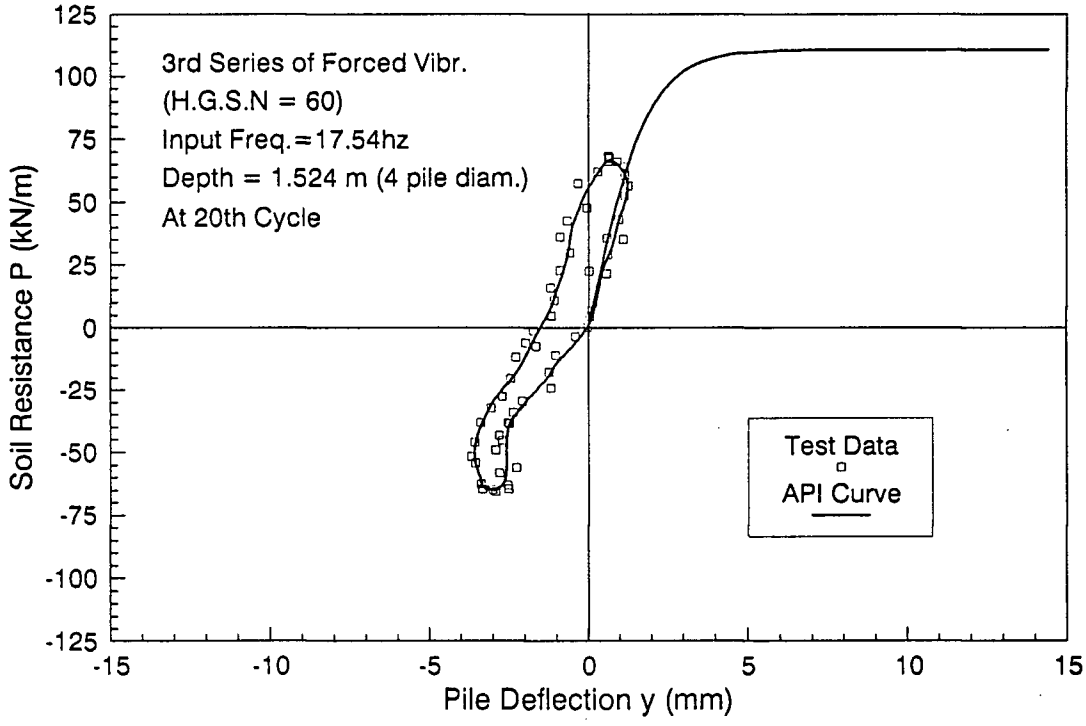

Figure C.3: Cyclic p-y curves at 3 to 4 pile-diameter depth and comparison with API curves-test III-7

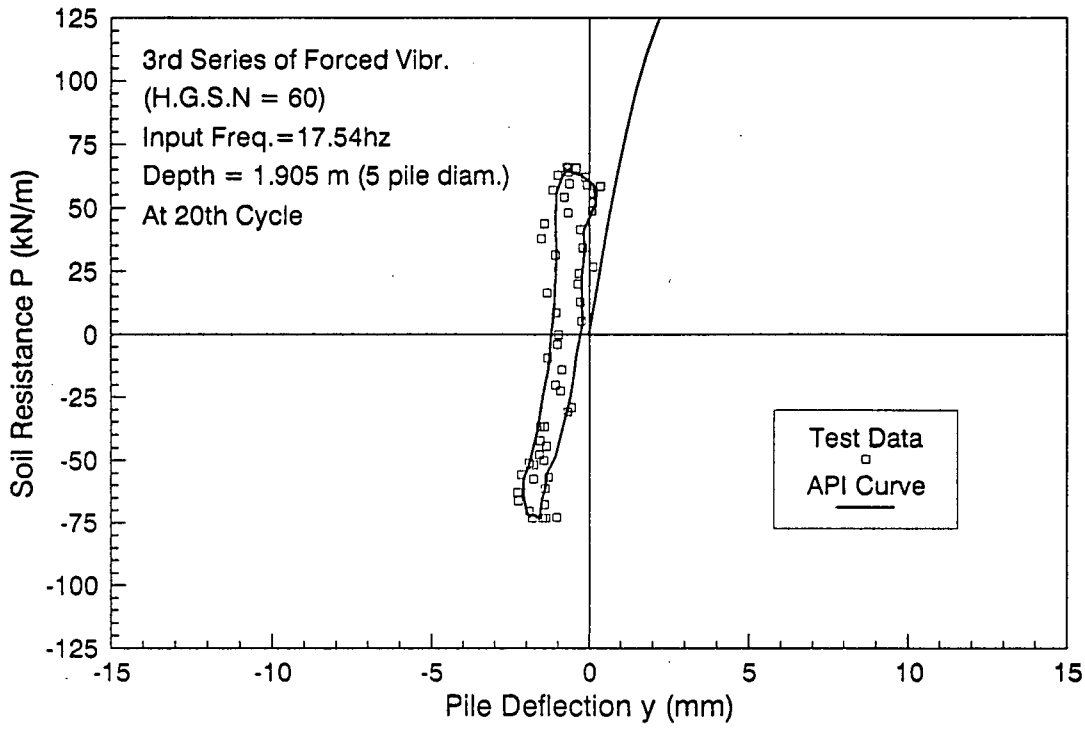

Figure C.3: Cyclic p-y curves at 5 pile diameter depth and comparison with API curves-test III-7

Bibliography

[1] Abe, Y., et al (1984), "Dynamic Behaviour of Pile Foundations During Earthquakes", Proc. 8th World Conf. on Earthquake Eng. Vol. 3, pp. 585-592

[2] American Petroleum Institute (1987), "Recommended Practice for Planning, Designing and Constructing Fixed Offshore Platforms", Washington, D.C. 17th Edition, April 1, 1987

[3] Arnold, P., Idriss, I.M., Reimer, R.B., Beebe, K.E. and Marshall, P.W. (1977), "A Study of Soil-pile-Structure Systems in Severe Earthquakes", 9th Offshore Technology Conference, No. OTC 2749, Houston, Texas, pp. 189-198

[4] ASTM Standard Method of Test for Relative Density of Cohesionless Soils, (1972), ASTM Designation: D 2049-69, American National Standard A 37-169

[5] Atukorala, U., Byrne, P.M. and She, J. (1986), "Prediction of P-Y Curves from Pressuremeter Tests and Finite Element Analyses", Department of civil Engineering, University of British Columbia, Soil Mechanics Series No. 108

[6] Barton, Y.O. (1982), "Laterally Loaded Model Piles in sand; Centrifuge Tests and Finite Element Analyses", PH.D. Thesis, Cambridge University, Engineering Department, June.

[7] Bea, R.G., Littom, R., Nour-Omid, S. and Chang, J.Y. (1984), "A Specialized Design and Research Tool for the Modelling of near-Field Soil Interactions", 16th Offshore Technology Conference, OTC 4806, Houston, Texas, pp. 249-252

[8] Blaney, G.W., kausel, E. and Roesset, J.M. (1976), "Dynamic Stiffness of Piles", Proc. 2nd Int. Conf. on Num. methods in Geomech., Blacksburg, Virginia, pp. 1001-1012

[9] Blaney, G.W. and O'Neill, M.W. (1986), "Measured Lateral Response of Mass on Single Pile in Clay", ASCE, Journal of the Geotechnical Engineering Division, Vol. 112, No. 4 pp. 443-457

[10] Bogard, D. and Matlock, H. (1980), "WSimplified Calculation of p-y Curves for Laterally Loaded Piles in Sand", Internal Report, The Earth Technology Corporation, Inc. Houston, Texas, April.

[11] Bolton, M.D., Steedman, R.S. (1982), "Centrifuge Testing of Microconcrete Retaining Wall Subjected to Base Shaking", Proceedings of the Conference on Soil dynamics and Earthquake Engineering, 13-25 july, Southampton, U.K., Vol. 1, pp. 311-329

[12] Bolton, M.D., Steedman, R.S. (1984), "The Behaviour of Fixed Cantilever Walls Subjected to Lateral Shaking", Proceedings of a Symposium on the Application of Centrifuge Modelling to geotechnical Design April 16-18, Manchester, U.K. pp. 301-313

[13] Cheney, J.A. (1985), "Physical Modelling in Geotechnical Engineering", Proc. from a Centrifugal Workshop Conducted During 12th Int. Conf. on SMFE, San Francisco

[14] Clough, R.W. and Penzien J. (1975), "Dynamics of Structures", McGraw Hill Book Company

[15] Coe, C.J. (1985), "On the Feasibility of Performing Dynamic Soil Tests in a Centrifuge", PH.D. Thesis, Princeton University, Princeton, N.J.

[16] Coe, C.J., Prevost, J.H., Scanlan, R.H. (1985), "Dynamic Stress Wave Reflections/Attenuation: Earthquake Simulation in Centrifuge Soil Models", International Journal of Earthquake Engineering and Structural Dynamics, Vol. 13, pp. 109-128

[17] Cox, W.R., Reese, L.C. and Grubbs, B.R. (1974), "Field Testing of laterally Loaded piles in Sand", Proc. 6th Annual OTC, Houston, Taxas, Vol. 2, Paper No. OTC 20, pp. 459-472

[18] Craig, W.H. (1984), "Installation Studies for Model Piles", Proc. of Symp. on the Application of Centrifuge Modelling to Geotechnical Design, ed. by Craig, W.H. Manchester, April 16-18

[19] Craig, W.H. (1985), "Modelling Pile Installation in Centrifuge Experiments", Proc. of 11th ICSMFE, San Francisco, Vol. 2, pp. 1101-1104

[20] Duncan, J.M., Byrne, P.M., Wong, K.S. and Mabry, P. (1980), "Strength, Stress-Strain and Bulk Modulus Parameters for Finite Element Analysis of Stresses and Movements in soil Masses", University of California, Berkeley, CA, Report No. UCBIGTI 80-01

[21] El Marsafawi, H., Han, Y. and Novak, M. (1990), "Dynamic Experiments on Two Pile Groups", Research Report GEOT-20-90, Dept. of Civil Eng., University of Western Ontario, Canada, August

[22] Esashi, Y. and Yoshida, Y. (1980), "Convenient Aseismic Design of Pile foundations", Proc. 7th World Conference on Earthquake Engineering, Istanbul, Vol. 3, pp. 419-426

[23] Finn, W.D.L., Barton, Y.O. and Towhata, I.(1984), "Dynamic Lateral Response of Pile Foundations: Centrifuge Data and Analyses", Proc. Symp.on the Application of Centrifuge Modelling to Goetechnical Design, ed. by W.H.Craig, Manchester, April 16-18

[24] Finn, W.D.L., Ledbetter, R.H. and Beratan, L.L. (1986), "Seismic Soil-Structure Interaction Analysis and Centrifuge Model Studies", Nuclear Engineering and Design, North Holland, Amsterdam, Vol. 94, pp. 53-66

[25] Finn, W.D.L. and Gohl, W.B. (1987), "Centrifuge model Studies of Piles Under Simulated Earthquake Lateral Loading", Geotechnical Special Publication, No. 11, ASCE Convention, Atlantic City, N.J., pp. 21-38

[26] Flores-Berrones, R. and Whitman, R.V. (1982), "Seismic Response of End-Bearing Piles", ASCE, Journal of the Geotechnical Engineering Division, Vol. 108, No. GT4, pp. 554-569

[27] Fukuoka, M. (1966), "Damage to Civil Engineering Structures", soils and Foundations, 6(2), pp. 45-52

[28] Fukushina, S. and Tatsuoka, F. (1984), "Strength and Deformation Characteristics of Saturated Sand at Extremely low Pressures", soils and Foundations, Vol. 24, No. 4, 30-48, Dec.

[29] Gazetas, G. (1984), "Seismic Response of End-Bering Single Piles", Soil Dynamics and Earthquake Engineering, Vol. 3, No. 2, pp. 82-94

[30] Gazioglu, S.M. and O'Neill, M.W. (1984), "Evaluation of p-y Relationships in Cohesive Soils", in Analysis and design of Pile Foundations, Proc. the Geotechnical Engineering Division, ASCE National Convention, San Francisco, California, Oct. 1 to 5, pp. 192-214

[31] Hamada, M. and Ishida, O. (1980), "Earthquake Observation and Numerical Analysis of Dynamic Strain of foundation Piles", Proc. 7th World Conference. on Earthquake Engineering, istanbul, Vol. 3, pp. 435-442

[32] Han, Y. and Novak, M. (1988), "Dynamic Behaviour of Single Piles Under Strong Harmonic Excitation", Canadian Geotechnical Journal, (Preprint)

[33] Hardin, B.O. and Drnevich, V.P. (1972), "Shear Modulus and Damping in Soils: Design Equations and Curves", J. of Soil Foundation Division, ASCE, Mechanics and Vol.98, No. SM7

[34] Kagawa, T. (1980), " Soil-Pile-Structure Interaction of Offshore Technology Conference, Houston, Texas, OTC 3820, pp. 235-240

[35] Kagawa, T. and Kraft, L.M. (1980) "Lateral Load-Deflection Relationships of Piles Subjected to Dynamic Loadings", Soils and Foundations, Vol. 20, No. 4, pp. 19-36

[36] Kagawa, T. and Kraft, L.M. (1980), "Seismic p-y Responses of Flexible Piles", J. Geotechnical Engineering Div., ASCE, GT8, pp. 899-918

[37] Kausel, E., Roesset, J.M. and Waas, G. (1975), "Dynamic Analysis of Footings on Layered Media", J. of Eng. Mech. Div., ASCE, Vol. 101, No. EM5, pp. 679-693

[38] Kishida, H. (1966), "Damage to Reinforced Buildings in Niigata city with Special Reference to Foundation Engineering", Soils and Foundations, Vol. 6, No. 1, pp. 71-88

[39] Ko, H.Y., Atkinson, R.H., Goble, G. and Ealy, C.D. (1984), "Centrifugal Modelling of Pile Foundations", Analysis and Design of Pile Foundations, Proceedings of a Symposium Sponsored by the ASCE Geotechnical Engineering Division, ASCE National Convention, San Francisco, California, Oct. 1st to 5th, 1984, pp. 21-41

[40] Kobori, T., Minai, R. and Baba, K. (1977), "Dynamic Behaviour of a Laterally Loaded Pile", Proc. of Specialty Session 10, 9th ICSMFE, Tokyo, July 14, pp. 175-180

[41] Krishana, R., Gazetas, G. and Veliz, A. (1983) "Static and Dynamic Lateral Deflection of Piles in Non-Homogeneous Soil Stratum", Geotechnique, Vol. 33, No. 3, pp. 307-325

[42] Kuerbis, R.H. (1988), "Effect of Gradation and Fines Content on the Undrained Response of Sand", M.A.Sc. Thesis, Department of Civil Engineering, The University of British Columbia, Canada

[43] Kuhlemeyer, R.L. (1979), "Static and Dynamic Laterally Loaded Floating Piles", ASCE, J. Geotech. Eng. Div. GT2, pp. 289-304

[44] Ayndon, A. and Schofield, A.N. (1978), "Centrifugal Model Tests of the Lodalen Landslide, Canadian Geotechnical Journal, 15 (1), pp. 1-13

[45] Margason, E. (1975), "Pile Bending During E/Q, Design, Construction and Performance of Deep Foundations", ASCE Continuing Education Committee, San Francisco, California

[46] Matlock, H. (1970), "Correlations for Design of Laterally Loaded Piles in Soft Clay", 2nd Offshore technology conference, Houston, Texas, OTC 1204, Vol. 1, pp. 577-594

[47] Matlock, H., Foo, S.H.C. and Bryant, L.M. (1978), " Simulation of Lateral Pile Behaviour under Earthquake Motion", Proc. Earthq. Eng. and Soil Dyn., ASCE Specialty Conference, Pasadena, CA, pp. 600-619

[48] Matlock, H., Foo, S.H.C. and Cheng, L.C. (1978), "Example of Soil Pile Coupling under Seismic Loading", Proc. 10th Annual Offshore Technology Conference, Houston, Texas, No. OTC 3310

[49] Mizuno, H. (1987), "Pile Damage During Earthquakes in Japan (1923-1983), Dynamic Response of Pile Foundations", ASCE, Geotech. Special Publications, No. 11 (Edited by T. Nogami), pp. 53-78

[50] Morris, D.V. (1981), "Dynamic Soil-Structure Interaction Modelled Experimentally on a Geotechnical Centrifuge", Canadian Geotechnical journal, Vol. 18, pp. 40-51

[51] Murchison, J.M. and O'Neill, M.W. (1984), "Evaluation of p-y Relationships in Cohesionless Soils", in Analysis and design of Pile Foundations, Proc. the Geotechnical Engineering Division, ASCE National Convention, San Francisco, CA, Oct 1-5, pp. 174-192

[52] Nogami, T. and Novak, M. (1977), "Resistance of Soil to a Horizontally Vibrating Pile", J. of Earthquake engineering and Structural Dynamics, Vol. 5, pp. 249-261

[53] Nogami, T. Chen, H.L. (1987), "Prediction of Dynamic Lateral Response of Non-Linear Single Pile Using a Winkler Soil Model", Dynamic Response of pile Foundations-Experiment, Analysis and Observation, Proc. of the Geotechnical Engineering Division, ASCE Convention, Atlantic City, N.J., Geotechnical Special Publication, No. 11, pp. 39-52

[54] Novak, M. (1974), "Dynamic Stiffness and Damping of Piles", Canadian Geotechnical journal, Vol. 11, No.4, pp. 574-598

[55] Novak, M. and Nogami, T. (1977), "Soil-Pile Interaction in Horizontal Vibration", J. of earthq. Eng. and Struct. Dyn. Vol. 5, pp. 263-282

[56] Novak, M. and Aboul-Ella, F. (1978), "Impedance Functions of Piles in Layered Media", J. Eng. Mech. Div., ASCE, June, Vol. 104, No. EM3, Proc. Paper 13847, pp. 643-661

[57] Novak, M. and Aboul-Ella, F. (1978), "Stiffness and Damping of Piles in Layered Media", Proc. Earthq. Eng. and Soil Dyn., ASCE Specialty Conf., Pasadena, CA, June 19-21, pp. 704-719

[58] Novak, M., Nogami, T. and Aboul-ella, F. (1978), "Dynamic Soil reaction for Plane Strain Case", J. Eng. Mech. Div. ASCE, Vol. 104, No.4, pp. 953-959

[59] Novak, M. and Sheta, M. (1980), "Approximate Approach to Contact Problems of Piles", Proc. Geotech. Eng. Div., ASCE National Convention, "Dynamic Response of Pile Foundations: Analytical Aspects", Florida, Oct. 30, pp.53-79

[60] Novak, M. and Sheta, M. (1982), "Dynamic Response of Piles and Pile Groups", Proc. 2nd Int. Conf. on Numerical Methods in Offshore Piling, U. of Texas at Austin, texas, April 29-30, pp. 489-507

[61] Novak, M and El Sharnouby, B. (1983), "Stiffness Constants of Single Piles", J. of Geotech. eng. Div. ASCE, Vol. 109, No. 7, pp. 961-974

[62] Oda, T., Uchiyama, S., Niwa, M. and Ueno, K. (1980), "Earthquake Response Characteristics of Structure with Pile Foundation on Soft Subsoil Layer and Its Simulation Analysis", Proc. 7th World conf. on Earthq. Eng., Istanbul, Turkey, Vol. 3, pp. 403-407

[63] Ohira, A., et al (1984), "Observations of earthquake Response Behaviours of Foundations Piles for road Bridges", Proc. 8th World Conf. on Earthq. Eng. San Francisco, Vol. 3, pp. 577-584

[64] Oldham, D.C.E. (1984), "Experiments with Lateral loading of Single Piles in Sand", Proc. Symp. on the Application of Centrifuge Modelling to Geotechnical Design, ed. by W.H. Graig, Manchester, April 16-18, pp. 121-142

[65] Ortiz, L.A., Scott, R.F. and Lee, J.(1983), "Dynamic centrifuge Testing of a Cantilever Retaining Wall", International Journal of Earthquake Engineering and Structural Dynamics, Vol. 11, pp. 251-268

[66] Pak, R.Y. and Jennings, P.C. (1987), "Elastodynamic Response of Pile under Transverse Excitations", J. Eng. Mech. Div., ASCE, Vol. 113, pp. 1101-1116

[67] Penzien, J. (1970), "Soil-Pile Foundation Interaction", Earthq. Eng. Ed. R.L. Wiegel, Prentice-Hall, Englewood Cliffs, New Jersey, pp. 349-381

[68] Poulos, H.G. and Davis, E.H. (1980), "Pile Foundation Analysis and Design", John Wiley and Sons, New York, Chapter 8

[69] Prevost, J.H. and Abdel-Ghaffar, A. (1982), "Centrifugal Modelling of the Dynamic Response of Piles", Proc. 2nd Int. Conf. on Numerical Methods in Offshore Piling, U. of Texas, Austin, Texas, April 29-30, pp. 533-541

[70] Rajapakse, R.K.N.D. and Shah, A.H. (1987), "On the Longitudinal Harmonic Motion of an Elastic Bar Embedded in an Elastic Half Space", Int. J. of Solids Structures, Vol. 23, pp. 267-285

[71] Rajapakse, R.K.N.D. and Shah, A.H. (1987), "On the lateral Harmonic Motion of an Elastic Bar Embedded in an Elastic Half Space", Int. J. of Solids Structures, Vol. 23, pp. 287-303

[72] Rajapakse, R.K.N.D. and Shah, A.H. (1989), "Impedance Curves for an Elastic Pile" J. Soil Dny. and Earthq. Eng. Vol. 8, No. 3, pp. 145-152

[73] Reese, L.C., (1977), "Laterally Loaded Piles: Program Documentation", J. of Geotech. Engrg. Division, Pro. of ASCE, Vol. 103, No. GT4, pp. 287-305

[74] Reese, L.C. (1979), "Design of Evaluation of Load Tests on Deep Foundations", Behaviour of Deep Foundations, ASTM STP 670

[75] Reese, L.C., Cox, W.R. and Koop, F.D. (1974), "Analysis of Laterally Loaded Pile in Sand", Proc. 6th Offshore Technology conference, Houston, Texas, Paper OTC 2080, pp. 473-483

[76] Robinsky, E.I., Morrison, C.E. (1964), "Sand Displacement and Compaction Around Model Friction Piles", Canadian Geotechnical Journal, Vol. 1, No. 2, pp. 81

[77] Roesset, J.M. and Angolides, D. (1979), "Dynamic Stiffness of Piles: Numerical Methods in Offshore Piling", Institute of Civil Engineers, London, pp. 75-82

[78] Roesset, J.M. (1980), "Stiffness and Damping Coefficients of Foundations", Proc. Dynamic Response of Pile Foundations: Analytical Aspects, ASCE National Convention, October 30, Ed. by M.W. O'Neill and R. Dobry.

[79] Roesset, J.M., Stokoe, K.H., Baka, J.E. and Kwok, S.T. (1983), "Dynamic response of Vertically Loaded Small-Scale Piles in Sand", Proc. 8th European Conf. Earthq. Eng., Lisbon, Vol. 2, 5.6 pp. 65-72

[80] Roscoe, K.H. (1968), "Soils and Model Tests", Journal of Strain Analysis, Vol. 3, No. 1, pp. 57-64

[81] Ross, G.A., Seed, H.B. and Migliceico, R. (1969), "Bridge Foundation Behaviour in Alaska Earthquake", J. Soil Mechanics and Foundations Division, ASCE, Vol. 95, SM4, pp. 1007-1036

[82] Schofield, A.N. (1981), "Cambridge Geotechnical Centrifuge Operations", Rankine Lecture, Geotechnique, Vol. 30, No. 3, pp. 227-268

[83] Schofield, A.N. (1981), "Dynamic and Earthquake Geotechnical Centrifuge Modelling", International conference on Recent Advances in Geotechnical Engineering and Soil Dynamics, St. Louis, USA, Vol. 3, pp. 1081-1097

[84] Scott, R.F. (1977), "Centrifuge Studies of Cyclic Lateral Load-Displacement Behaviour of Single Piles", Research Program for American Petroleum Institute, OS-APR Project 8

[85] Scott, R.F. (1978), "Summary Specialty Session 7-Modelling", Proceedings, Specialty Conference on Earthquake Engineering and Soil Dynamics, ASCE Vol. III, Pasadena, CA June 19-22

[86] Scott, R.F. (1979), "Cyclic and Static Model Pile Tests in a Centrifuge", 11th Offshore Technology Conference, Houston, Texas, OTC 3492, pp. 159-168

[87] Scott, R.F., Ting, J. and Lee, J. (1982), "Comparison of Centrifuge and Full Scale Dynamic Pile Tests", Proc. Soil Dynamics and Earthquake Engineering, ed. A.S. Cakmak, A. Abdel-Ghaffar, and C.A. Brebbia, Vol. 1, pp. 299-311

[88] Scott, R.F., Tsai, C.F., Steussy, D. and Ting, J.M. (1982), "Full-Scale Dynamic Lateral Pile Tests", 14th Offshore Technology Conference, Houston, Texas, OTC 4203, Vol. 1, pp. 435-450

[89] Seed, H.B. and Idriss, I.M. (1970), "Soil Moduli and Damping Factors for Dynamic Response Analyses", Earthquake Engineering Research Centre, University of California at Berkekey, Report No. EERC 70-10

[90] Sen, R., Davies, T.G. and Banerjee, P.K. (1985), "Dynamic Analysis of Piles and Pile Groups Embedded in Homogeneous Soils", J. of Earthq. Eng. and Struct. Dyn., Vol. 13, pp. 53-65

[91] Sugimura, Y. (1981), "Earthquake Damage and Design Method of Piles. Proc. 10th ICSMFE, Vol. 2, pp. 865-868

[92] Tajimi, H. (1966), "Earthquake Response of Foundation Structures", Rep. of Fac. Sci. Eng., Nihon University, 1966. 3, 1.1-3.5

[93] Tan, T.S. and Scott, R.F. (1985), "Centrifuge Scaling Considerations for Fluid-Particle System", Geotechnique, Vol. 35, No. 4, pp. 461-470

[94] Ting, J.M. (1987), "Full Scale Cyclic Dynamic Lateral Pile Response", ASCE, Journal of the Geotechnical Engineering Division, Vol. 113, No. 1, pp. 30-45

[95] Ting, J.M., Kauffman, C.R. and Lovicsek, M.(1987), "Centrifuge Static and Dynamic Lateral Pile Behavior", Canadian Geotech. Journal, Vol. 24, pp. 198-207

[96] Vaid, Y.P. and Negussey, D. (1986), "Preparation of Reconstituted Sand Specimens", Soil Mechanics Series No. 98, Department of Civil Engineering, University of British Columbia, Vancouver, Canada

[97] Waas, G. and Hartman, H.G. (1984), "Seismic Analysis of Pile Foundations Including Pile-Soil-Pile Interaction", 8th World Conference on Earthquake Engineering, San Francisco, Vol. 5, pp. 55-62

[98] Weissman, K. and Prevost, J.H. (1989), "Centrifugal Modelling of Dynamic Soil-Structure Interaction", Technical Report NCEER-89-0040, Department of Civil Engineering, Princeton University, Princeton, N.J.

[99] Whitman, R.V. (1984), "Experiments with Earthquake Ground Motion Simulation", Proc. Sym. on application of Centrifuge Modelling to Geotechnical design. Ed., W.H. Craig, Manchester, 281-300

[100] Whitman, R.V. and Arulanandan, K. (1985), "Centrifuge Model Testing with Dynamic and Cyclic Loads", Proc. on Advances in the Art of Testing Soils under Cyclic Conditions, Ed. by Vijay Khosia, Detroit, Michigan, Oct. 24, pp. 255-285

[101] Yan, L. and Byrne, P.M. (1989), "Application of Hydraulic Gradient Similitude Method to Small-Scale Footing Tests on Sand", Canadian Geotechnical Journal Vol. 26, No. 2, pp. 246-259

[102] Yan, L. (1990), "Hydraulic Gradient Similitude Method for Geotechnical Modelling Tests with Emphasis on Laterally Loaded Piles", Ph.D. Thesis, University of British Columbia, Canada

[103] Yan, L., Byrne, P.M. and Dou, H. (1991), "Model Studies of Dynamic Pile Response Using Hydraulic Gradient Shaking Table Tests", Proc. 6th Canadian Conf. on Earthq. Eng. 12-14, June, Toronto, pp. 335-342

[104] Zelikson, A. (1969), "Geotechnical Models Using the Hydraulic Gradient Similarity Methods", Geotechnique, Vol. 19, pp. 495-508

[105] Zelikson, A. (1978), "Rigid Piles in Sand under Inclined Forces; Model Tests Using the Hydraulic Gradient Similarity Method", Journal de Mecanique Applique, 2(2), 153-165

[106] Zelikson, A., Leguay, P. and Pascal, C. (1982), "Centrifugal Model Comparison of Pile and Raft Foundation Subjected to Earthquakes", 1st Intern. Conf. on Soil Dynamics and Earthquake Engineering, Southamption, England, 13-15 July, pp. 283-297

[107] Zelikson, A. and Leguay, P. (1986), "Some Basic Data on Piles Under Static and Dynamic Loading from Stress Conserving Models" Proc. 3rd Int. Conf. on Numerical Methods in Offshore Piling, Nantes, May, 21-22, pp. 105-124

[108] Zelikson, A. (1988), "Hydraulic Gradient Simulation of Sequences of Pile driving and Loading Tests", 3rd Int. Conf. on Application of Stress Wave Theory to Piles, Ottawa, Ontario, Edited by B.H. Fellenius, Preprint Vol. pp. 152-163